

UNCLASSIFIED

AD NUMBER
AD864555
NEW LIMITATION CHANGE
TO Approved for public release, distribution unlimited
FROM Distribution authorized to U.S. Gov't. agencies and their contractors; Administrative/Operational Use; NOV 1969. Other requests shall be referred to Air Force Flight Dynamics Lab., Wright-Patterson AFB, OH 45433.
AUTHORITY
AFFDL ltr, 6 Apr 1972

THIS PAGE IS UNCLASSIFIED

AD 864555

AFFDL-TR-68-161



**AIRCRAFT LOAD ALLEVIATION AND
MODE STABILIZATION (LAMS)
B-52 SYSTEM ANALYSIS, SYNTHESIS, AND DESIGN**

MR. P. M. BURRIS

The Boeing Co.

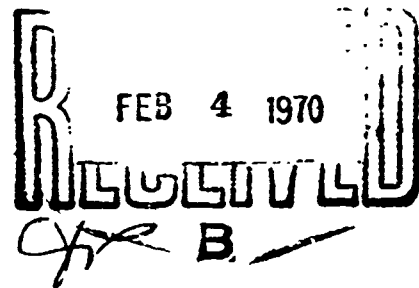
and

MR. M. A. BENDER

Honeywell, Inc.

TECHNICAL REPORT AFFDL-TR-68-161

NOVEMBER 1969



This document is subject to special export controls and each transmittal to foreign governments or foreign nationals may be made only with prior approval of Air Force Flight Dynamics Laboratory (FDCS), Wright-Patterson Air Force Base, Ohio 45433.

Reproduced by the
CLEARINGHOUSE
for Federal Scientific & Technical
Information Springfield Va. 22151

**AIR FORCE FLIGHT DYNAMICS LABORATORY
AIR FORCE SYSTEMS COMMAND
WRIGHT-PATTERSON AIR FORCE BASE, OHIO**

260

NOTICE

When Government drawings, specifications, or other data are used for any purpose other than in connection with a definitely related Government procurement operation, the United States Government thereby incurs no responsibility nor any obligation whatsoever; and the fact that the government may have formulated, furnished, or in any way supplied the said drawings, specifications, or other data, is not to be regarded by implication or otherwise as in any manner licensing the holder or any other person or corporation, or conveying any rights or permission to manufacture, use, or sell any patented invention that may in any way be related thereto.

This document is subject to special export controls and each transmittal to foreign governments or foreign nationals may be made only with prior approval of the Air Force Flight Dynamics Laboratory (FDCS), Wright-Patterson Air Force Base, Ohio 45433.

CFSTI	WHITE SECTION	<input type="checkbox"/>
EC	BUFF SECTION	<input checked="" type="checkbox"/>
UNCLASSIFIED		<input type="checkbox"/>
CLASSIFICATION		
REVISION AVAILABILITY CODE		
DISC.	AVAIL. and SPECIAL	

2

Copies of this report should not be returned unless return is required by security considerations, contractual obligations, or notice on a specific document.

AIRCRAFT LOAD ALLEVIATION AND MODE STABILIZATION (LAMS)

B-52 SYSTEM ANALYSIS, SYNTHESIS, AND DESIGN

MR. P. M. BURKIS

The Boeing Co.

and

MR. M. A. BENDER

Honeywell, Inc.

This document is subject to special export controls and each transmittal to foreign governments or foreign nationals may be made only with prior approval of Air Force Flight Dynamics Laboratory (FDCS), Wright-Patterson Air Force Base, Ohio 45433.

FOREWORD

This report was prepared for the Air Force Flight Dynamics Laboratory through joint effort of The Boeing Company, Wichita Division, Wichita, Kansas, and Honeywell, Inc., Aerospace Division, Minneapolis, Minnesota, in fulfillment of Contract AF33(615)-3753.

The work was administered and the program was conducted under the direction of Mr. R. F. Johannes (FDCS) during the period June 1966 through December 1968.

The program reported herein was made possible only through the dedicated and enthusiastic support of all those who participated which are too numerous to mention. The activity was directed by Mr. P. M. Burris, Boeing Engineering Manager, and Mr. M. A. Bender, Honeywell Project Manager. Mr. R. L. McDougal, Lockheed-Georgia Company, Marietta, Georgia, contributed significantly to the C-5A analyses.

The report is identified internally at The Boeing Company, Wichita Division, as D3-7901-1.

This technical report has been reviewed and is approved.



MORRIS A. OSTGAARD

Act'g Chief, Systems Integration and
Flight Experimentation Branch
Flight Control Division
Air Force Flight Dynamics Laboratory

ABSTRACT

➤ The Load Alleviation and Mode Stabilization (LAMS) program was conducted to demonstrate the capabilities of an advanced flight control system (FCS) to alleviate gust loads and control structural modes on a large flexible aircraft using existing aerodynamic control surfaces as force producers.

The analysis, design, and flight demonstration of the flight control system was directed toward three discrete flight conditions contained in a hypothetical mission profile of the B-52E test aircraft. The FCS was designed to alleviate structural loads while flying through atmospheric turbulence.

The LAMS-FCS was produced as hardware and installed on the test vehicle, B-52E AF56-632. Test vehicle modifications included the addition of hydraulically powered controls, a fly-by-wire (FBW) pilot station, associated electronics and analog computers at the test engineer's stations, instrumentation for system evaluation, and the LAMS flight controller.

Flight demonstration of the LAMS-FCS was conducted to provide a comparison of analytical and experimental data. The results obtained showed that the LAMS-FCS provided significant reduction in fatigue damage rates.

➤ In addition, a LAMS C-5A study was included in the program. This portion of the program was to analytically demonstrate that the technology developed for the B-52 could be applied to another aircraft. The C-5A study was conducted for one flight condition in the C-5A mission profile. Significant reductions in fatigue damage rates and fuselage accelerations were predicted by the LAMS C-5A analyses.

This Abstract is free for unlimited distribution

CONTENTS

	PAGE
1.0 INTRODUCTION	1
1.1 Purpose	1
1.2 Objectives	2
1.3 Criteria	2
1.4 Report Contents	3
2.0 SUMMARY	4
2.1 Introduction	4
2.2 Analysis Techniques	4
2.3 System Description	10
2.4 System Performance	12
2.5 Hardware Design	24
3.0 SYSTEM DEFINITION	28
3.1 Introduction	28
3.2 Mathematical Description of the LAMS B-52	28
3.3 Baseline SAS Design Analysis	39
3.4 Baseline SAS Description	39
3.5 LAMS-FCS Design Analysis	50
3.6 LAMS-FCS Description	50
3.7 Evaluation of Final Systems	54
4.0 SYSTEM PERFORMANCE	65
4.1 Introduction	65
4.2 Safety Analysis	65
4.3 Predicted LAMS Handling Qualities	101
4.4 Structural Performance Predictions	111
4.5 Performance Sensitivity Results	128
4.6 LAMS-FCS Longitudinal Design Modification Results	136
5.0 HARDWARE DESIGN	139
5.1 Introduction	139
5.2 Boeing Hardware Design	139
5.3 Honeywell Hardware Design	181
6.0 CONCLUSIONS	185
6.1 Conclusions, LAMS Program	185
6.2 Conclusions, LAMS B-52 System Analysis, Synthesis, and Design	185
7.0 REFERENCES	187
APPENDIX A	188
APPENDIX B	205
APPENDIX C	224

FIGURES

<u>FIGURE</u>		<u>PAGE</u>
1	LAMS Document Organization	xxi
2	B-52 Aircraft Geometry	5
3	LAMS-FCS Analysis Flow Diagram	7
4	LAMS Baseline Pitch SAS Block Diagram	11
5	LAMS Baseline Roll and Yaw SAS Block Diagram	13
6	LAMS Longitudinal Flight Control System Block Diagram	14
7	LAMS Lateral-Directional Flight Control System Block Diagram	15
8	Predicted Short Period Handling Qualities	17
9	Predicted Dutch Roll Handling Qualities	18
10	Fatigue Damage Rates	20
11	RMS Fuselage Vertical Acceleration	22
12	RMS Fuselage Side Acceleration	23
13	Limped Parametric Structural Idealization	30
14	Aerodynamic Panels	32
15	Longitudinal Free Aircraft Damage Calculations	42
16	Lateral Free Aircraft Damage Calculations	43
17	Longitudinal Artificial Damping Study	45
18	Open and Closed Loop System	46
19	Wing Symmetrical Modal Shapes	51
20	Fuselage Symmetrical Modal Shapes	52
21	LAMS Longitudinal, Lateral-Directional Sensor Locations	53
22	Performance Index Stress Locations	60
23	Longitudinal Baseline SAS Short Period Root Loci	66
24	Longitudinal Baseline SAS Sixth Structural Mode Root Loci	67

<u>FIGURE</u>		<u>PAGE</u>
25	Effects of Baseline Pitch SAS on Airplane Transient Response	68
26	Baseline Pitch SAS Frequency Response	69
27	Lateral-Directional Baseline SAS Dutch Roll Root Loci for Yaw SAS with Nominal Roll SAS	74
28	Lateral-Directional Baseline SAS First Structural Mode Root Loci for Yaw SAS with Nominal Roll SAS	75
29	Lateral-Directional Baseline SAS Roll Root Loci for Roll SAS with Nominal Yaw SAS	76
30	Effects of Baseline Yaw SAS on Airplane Transient Response	77
31	Effects of Baseline Roll SAS on Airplane Transient Response	78
32	Baseline Yaw SAS Frequency Response	79
33	Baseline Roll SAS Frequency Response	80
34	Open Loop Frequency Response - Spoiler	82
35	Open Loop Frequency Response - Elevator	86
36	Open Loop Frequency Response - Aileron	88
37	Open Loop Frequency Response - Spoiler	90
38	Open Loop Frequency Response - Rudder	95
39	Open Loop Frequency Response - Aileron	97
40	Baseline SAS Directional Axis Gain Variations	105
41	Baseline SAS - Longitudinal Axis Gain Variations	106
42	Baseline SAS - Lateral Axis Gain Variations	107
43	LAMS-FCS - Directional Axis Gain Variations	108
44	LAMS-FCS - Longitudinal Axis Gain Variations	109
45	LAMS-FCS - Lateral Axis Gain Variations	110
46	RMS Wing Vertical Bending Moment	113
47	RMS Wing Chordwise Bending Moment	114

<u>FIGURE</u>		<u>PAGE</u>
48	RMS Wing Torsional Moment	115
49	RMS Fuselage Vertical Bending Moment	116
50	RMS Fuselage Side Bending Moment	117
51	RMS Wing Vertical Acceleration	118
52	BS 172 Vertical Acceleration PSD	119
53	Peak Incremental Stress Comparison	123
54	Peak Incremental Stress Comparison	124
55	Peak Incremental Stress Comparison	125
56	Theoretical Closed Loop Frequency Response	141
57	Aileron Actuator Functional Diagram	142
58	Theoretical Auxiliary Actuator Open Loop Frequency Response	144
59	Spoiler Valve Functional Diagram	145
60	Theoretical Closed Loop Frequency Response, Spoiler	147
61	Theoretical Closed Loop Frequency Response, Rudder or Elevator	149
62	Rudder or Elevator Actuator Functional Diagram	150
63	Basic LAMS Test Vehicle Hydraulic Configuration	153
64	Basic LAMS Test Vehicle Hydraulic Configuration After LAMS Modification	154
65	Rudder - Elevator Hydraulic System	155
66	Sensor Locations	158
67	Forward Interface Electronics Rack	160
68	Aft Interface Electronics Rack	161
69	LAMS System Block Diagram	162
70	Auxiliary Auxiliary Actuator Open Loop Frequency Response	166
71	Auxiliary Actuator Closed Loop Frequency Response	167

<u>FIGURE</u>		<u>PAGE</u>
72	Test Engineer's Station	170
73	Cockpit Aisle Stand	172
74	Transient Function Generator	173
75	TR-48 Analog Computer Forward Installation	175
76	Rudder Pedal Travel Vs. Rudder Pedal Force, Evaluation Pilot	177
77	Column Force Vs. Column Displacement, Evaluation Pilot	178
78	Wheel Force Vs. Wheel Rotation, Evaluation Pilot	179
79	Aircraft Load Instrumentation Locations	181
80	LAMS-FCS Computer	183
81	LAMS-FCS Suitcase Tester	184
82	Open Loop Frequency Response, Elevator, FC-2	207
83	Open Loop Frequency Response, Aileron, FC-2	209
84	Open Loop Frequency Response, Spoiler, FC-2	211
85	Open Loop Frequency Response, Elevator, FC-3	213
86	Open Loop Frequency Response, Aileron, FC-3	215
87	Open Loop Frequency Response, Rudder, FC-2	217
88	Open Loop Frequency Response, Aileron, FC-2	219
89	Open Loop Frequency Response, Rudder, FC-3	221
90	Open Loop Frequency Response, Aileron, FC-2	223
91	Baseline SAS - Directional Axis Gain Variations	225
92	Baseline SAS - Longitudinal Axis Gain Variations	226
93	Baseline SAS - Lateral Axis Gain Variations	227
94	LAMS-FCS - Directional Axis Gain Variations	228
95	LAMS-FCS - Longitudinal Axis Gain Variations	229
96	LAMS-FCS - Lateral Axis Gain Variations	230

<u>FIGURE</u>		<u>PAGE</u>
97	Baseline SAS - Directional Axis Gain Variations	231
98	Baseline SAS - Longitudinal Axis Gain Variations	232
99	Baseline SAS - Lateral Axis Gain Variations	233
100	LAMS-FCS - Directional Axis Gain Variations	234
101	LAMS-FCS - Longitudinal Axis Gain Variations	235
102	LAMS-FCS - Lateral Axis Gain Variations	236

TABLES

<u>TABLE</u>		<u>PAGE</u>
I	LAMS Fatigue Damage Rates Due to Turbulence	21
II	Symmetric Analysis Degrees of Freedom	33
III	Symmetric Analysis Degress of Freedom	34
IV	Anti-Symmetric Analysis Degrees of Freedom	35
V	Anti-Symmetric Analysis Degrees of Freedom	36
VI	Baseline SAS Longitudinal Eigenvalues	70
VII	Baseline Yaw SAS Stability Margins	72
VIII	Baseline Roll SAS Stability Margins	73
IX	Baseline Lateral-Directional Eigenvalues	81
X	LAMS-FCS Spoiler Loop Margins - Longitudinal Axis	83
XI	LAMS-FCS Elevator Loop Margins - Longitudinal Axis	85
XII	LAMS-FCS Aileron Loop Margins - Longitudinal Axis	87
XIII	LAMS-FCS Spoiler Loop Margins - Longitudinal Axis	89
XIV	LAMS-FCS Longitudinal Eigenvalues - FC-1	91
XV	LAMS-FCS Longitudinal Eigenvalues - FC-2	92
XVI	LAMS-FCS Longitudinal Eigenvalues - FC-3	93
XVII	LAMS-FCS Rudder Loop Margins - Lateral-Directional Axis	94
XVIII	LAMS-FCS Aileron Loop Margins - Lateral-Directional Axis	96
XIX	LAMS-FCS Lateral-Directional Eigenvalues, FC-1	98
XX	LAMS-FCS Lateral-Directional Eigenvalues, FC-2	99
XXI	LAMS-FCS Lateral-Directional Eigenvalues, FC-3	100
XXII	LAMS Ultimate Stress Exceedances Due to Turbulence - No SAS	120
XXIII	LAMS Ultimate Stress Exceedances Due to Turbulence - Baseline SAS	121

<u>TABLE</u>		<u>PAGE</u>
XXIV	LAMS Ultimate Stress Exceedances Due to Turbulence - LAMS-FCS	122
XXV	LAMS Fatigue Damage Rates Due to Turbulence - No SAS	126
XXVI	LAMS Fatigue Damage Rates Due to Turbulence - Baseline SAS	127
XXVII	Effects of Parameter Variations on LAMS Performance, Longitudinal Axis, FC-1	129
XXVIII	Effects of Parameter Variations on LAMS Performance, Longitudinal Axis, FC-2	129
XXIX	Effect of Parameter Variations on LAMS Performance, Longitudinal Axis, FC-3	131
XXX	Effect of Hardover Actuator and Gyro Failures, Longitudinal Axis	132
XXXI	Effect of Parameter Variations on LAMS Performance, Lateral Axis, FC-1	133
XXXII	Effect of Parameter Variations on LAMS Performance, Lateral Axis, FC-2	134
XXXIII	Effect of Parameter Variations on LAMS Performance, Lateral Axis, FC-3	135
XXXIV	Revised LAMS Longitudinal FCS Eigenvalues, FC-1	137
XXXV	Revised LAMS Longitudinal FCS Eigenvalues, FC-3	138
XXXVI	Spoiler Actuation System Specifications	140
XXXVII	LAMS-FCS Spoiler Actuation System Specifications	146
XXXVIII	Rudder-Elevator Actuator Specifications	148
XXXIX	Electronic Sensors	157
XL	Monitor System Accelerometers	169
XLI	Optimal Control Law for Flight Condition 1 Longitudinal Axis	202
XLII	Optimal Controller Performance Longitudinal Axis	204
XLIII	Longitudinal Axis - Elevator Loop Margins, FC-2	206

<u>TABLE</u>		<u>PAGE</u>
XLIV	Longitudinal Axis - Aileron Loop Margins, FC-2	208
XLV	Longitudinal Axis - Spoiler Loop Margins, FC-2	210
XLVI	Longitudinal Axis - Elevator Loop Margins, FC-3	212
XLVII	Longitudinal Axis - Aileron Loop Margins, FC-3	214
XLVIII	Lateral-Directional Axis - Rudder Loop Margins, FC-2	216
XLIX	Lateral-Directional Axis - Aileron Loop Margins, FC-2	218
L	Lateral-Directional Axis - Rudder Loop Margins, FC-3	220
LI	Lateral-Directional Axis - Aileron Loop Margins, FC-3	222

NOMENCLATURE

SYMBOLS

Act	Actuator	
AF	Aft fuselage	
Aux Act	Auxiliary Actuator	
A_y	Normalized σ_y	
	$A_y = \left[\sigma_y^2 / \sigma_{gust}^2 \right]^{\frac{1}{2}}$	
B	Effective column damping	ft-lb/rad/sec
B/N	Bombardier/Navigator	
BS	Body station	
BWL	Body water line	
DVM	Digital volt meter	
ELEM	Matrix element	
FBW	Fly-by-wire	
F/B	Feedback	
FC	Flight condition	
FCS	Flight control system	
FF	Forward fuselage	
F_{c_w}	Compressibility factor	
F_p	Evaluation pilot's force	lbs
GW	Airplane gross weight	lbs
J_G	Column inertia about cg	slug ft ²
$K \left(\frac{V_T t}{b_r} \right)$	Wagner's lift growth function	
K_E	Effective feel spring	ft-lb/rad

SYMBOLS

M	Bending moment	in-lbs
MAC or \bar{c}	Mean aerodynamic chord	ft
M_L	Actuator load mass	lbs
$M_y(y_1)$	Number of times $y(t)$ crosses upward through the level y_1	
N	Structural acceleration	g's
$N(f_{a_i}, f_{\text{mean}})$	Number of cycles to failure at the i^{th} stress level	
N_{O_y}	Zero crossing of y	
	$N_{O_y} = \frac{1}{2\pi} \left[\frac{\sigma_{\dot{y}}^2}{\sigma_y^2} \right]^{\frac{1}{2}}$	cps
N_0	Stiffness matrix	
N_1	Damping matrix	
N_2	Mass matrix.	
P	Roll rate	rad/sec
PR	Pilot rating	
P_1, P_2, b_1, b_2	Empirical constants used to describe $\hat{f}(\sigma_w)$	
Q	Pitch rate	rad/sec
R	Yaw rate	rad/sec
RMS	Root mean square	
R_p	Moment arm to pilot's force	ft
R_2	Wagner damping matrix	
R_3	Wagner stiffness matrix	
SAS	Stability augmentation system	
T	Torsional moment	in - lbs
T_R	Roll time constant	sec

SYMBOLS

U_0	Equilibrium velocity along the X stability axis	ft/sec
V	Total velocity along Y stability axis	ft/sec
V_s	Shear	lbs
V_T	True airspeed	ft/sec
V_c	Calibrated airspeed	knots
V_e	Equivalent airspeed	knots
W	Total velocity along Z stability axis	ft/sec
WBL	Wing buttock line	
WS	Wing station	
W_c	Column weight	lb
XASLW	Longitudinal acceleration at left wing	
X_{cg}	Location of airplane cg aft of MAC leading edge	% MAC
Y	Side translation (+ right)	ft
\dot{Y}	Side velocity (+ right) Note: A dotted variable designates the first time derivative of the variable	ft/sec
\ddot{Y}	Side acceleration (+ right) Note: A double dotted variable designates the second time derivative of the variable	ft/sec
YAT	Lateral acceleration at tail	
YAFEA	Lateral acceleration at fin elastic axis	
Z	Vertical translation (+ down)	ft
ZACG	Vertical acceleration at center of gravity	

SYMBOLS

ZASLS	Vertical acceleration at left stabilizer	
ZASLW	Vertical acceleration at left wing	
ZASN	Vertical acceleration at nose	
b	Wing span	
b _r	Reference semi-chord length	ft
cg	Center of gravity	
db	Decibel	
f	Bending stress	psi
f _a	Alternating stress	psi
f _{mean}	Steady, level flight stress	psi
$f(\sigma_w)$	Probability density distribution of RMS vertical turbulence component	
h	Altitude	ft
m	Mach number	
n (f _{a_i})	Number of cycles of applied stress at the <u>i</u> th stress level	
p _g	Vertical gust velocity (asymmetrical)	rad/sec
p _{ss}	Steady state roll rate	rad/sec
p ₁	Upstream actuator pressure	psi
p ₂	Downstream actuator pressure	psi
q	Dynamic pressure	lbs/ft ²
q _i	Displacement of <u>i</u> th elastic freedom	
r	Distance to column cg	ft
s	Laplace operator	
st	Stabilizer position	units

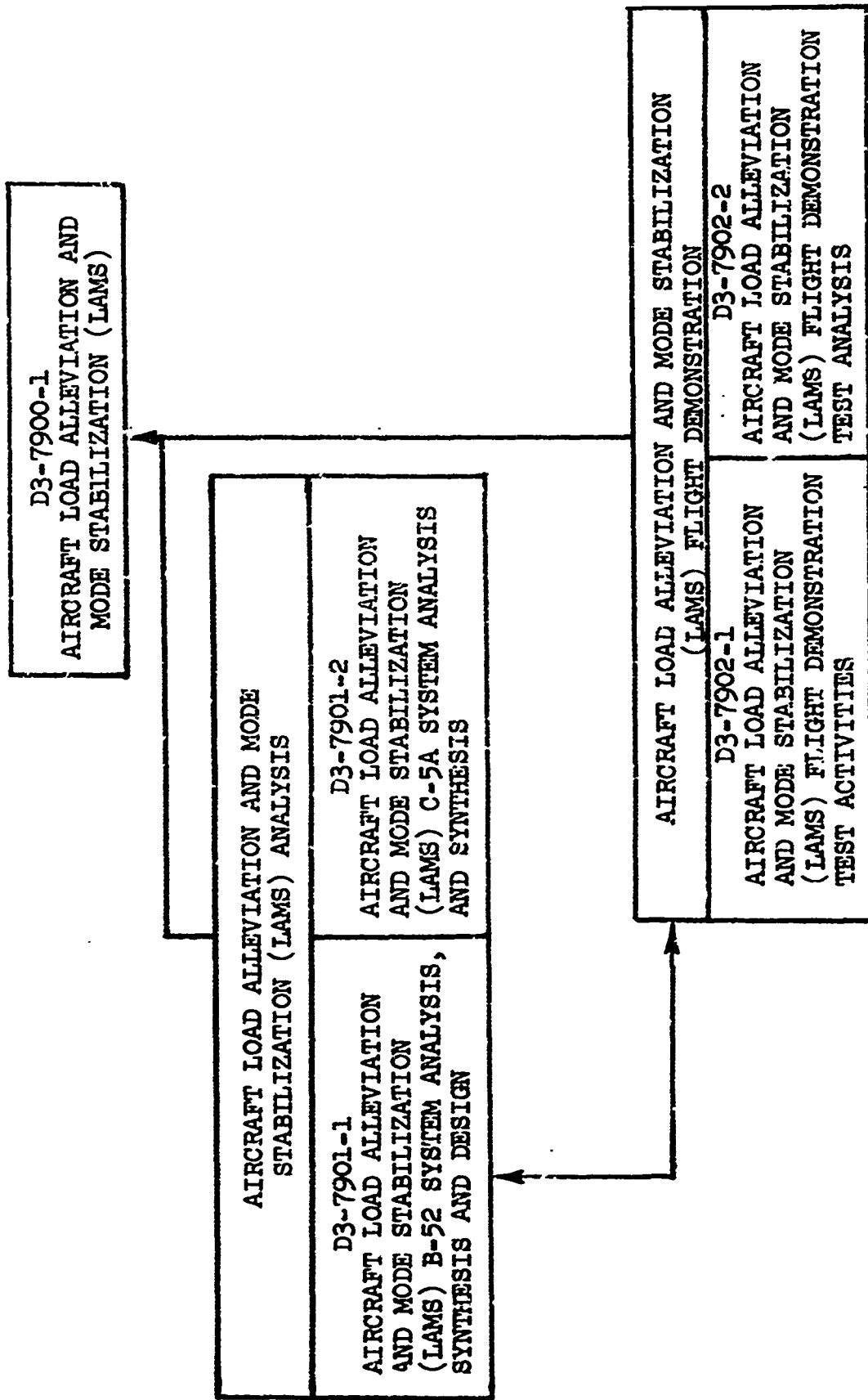
SYMBOLS

t	Time	sec
v	Volts	
v_g	Side gust velocity	ft/sec
w_g	Vertical gust velocity (symmetrical)	ft/sec
α	Angle of attack (+ nose up)	rad
α body	Airplane body angle of attack (+ nose up)	rad
α_{gust}	Angle of attack gust input	rad
β	Angle of sideslip (+ nose left)	rad
β_M	Bulk modulus for hydraulic fluid	
β_{gust}	Sideslip gust input	rad
γ	Airplane climb angle	rad
δ_c	Column displacement	deg
δ_{RP}	Rudder pedal displacement in	in
$\delta_{SP_{FBW}}$	Fly-by-wire spoiler deflection (+ up on right wing)	
$\delta_{SP_{LAMS}}$	LAMS spoiler deflection (+ up)	
δ_w	Wheel displacement	deg
δ_a	Aileron deflection (+ Trailing edge down on right wing) (asymmetrical)	
δ_e	Elevator deflection (+ Trailing edge down)	
δ_r	Rudder deflection (+ Trailing edge left)	
δ_t	Tab deflection	rad
e_{TGL}	Equivalent Thrust center line	ft
ζ	Damping ratio, fraction of critical damping	

SYMBOLS

ζ_{AL}	Air load damping ratio	
ζ_{SP}	Short period damping ratio	
ζ_{ST}	Structural damping ratio	
ζ_d	Dutch roll damping ratio	
θ	Pitch attitude	rad
θ_e	Angle of cg in equilibrium position	rad
θ_x	Roll angle (+ right wing down)	rad
θ_y	Pitch angle (+ nose up)	rad
θ_z	Heading angle (+ nose right) .	rad
σ_{p_g}	Root mean square of asymmetrical vertical gust input	rad
σ_{v_g}	Root mean square of lateral gust input	ft/sec
σ_{w_g}	Root mean square of vertical gust input	ft/sec
σ_y^2	Variance of $y(t)$	
$\sigma_{\dot{y}}^2$	Variance of $\dot{y}(t)$	
σ_α	Root mean square of incremental angle of attack	rad
σ_{β_g}	Root mean square of sideslip gust input	rad
σ_{β_o}	Root mean square of airplane sideslip output	rad
σ_{ϕ_o}	Root mean square of airplane roll angle	rad
Γ	Reaction time delay	sec
ϕ	Roll angle (+ right wing down)	rad
ψ	Airplane heading (+ nose right)	rad

ω	Frequency (radians/sec)	
ω_d	Dutch roll undamped frequency	rad/sec
ω_n	Undamped natural frequency	rad/sec
ω_{ϕ}	Undamped natural frequency of numerator oscillatory mode in ϕ/δ_a transfer function	rad/sec
ω_{ϕ}/ω_d	Oscillatory roll component Parameter	
Δs	Change in horizontal stabilizer position (+ leading edge up)	units
$\Delta \alpha$	Change in angle of attack	rad
$\phi_y(\omega)$	Power spectral density of $y(t)$	
$\psi \left(\frac{V_T t}{b_T} \right)$	Kussner's lift growth function	



LAMS DOCUMENT ORGANIZATION

FIGURE I

1.0 INTRODUCTION

This report presents the results of the analyses and design of a Baseline Stability Augmentation System for rigid body mode control and the Load Alleviation Mode Stabilization Flight Control System (LAMS-FCS) for rigid body and structural mode control on B-52E aircraft AF56-632. The Baseline SAS analysis, synthesis, and design were accomplished by The Boeing Company. The design criteria for the LAMS Flight Control System were established by Boeing; Honeywell accomplished system analysis, synthesis, and design. Boeing assisted in these analyses and accomplished additional checks on system stability and performance.

1.1 Purpose

The purpose of the LAMS B-52 analyses and design program was to provide a system which would provide structural mode stabilization and gust load alleviation at three discrete points in a typical B-52 mission profile.

The conditions selected for evaluation were:

- Flight Condition 1 (FC-1) which represents a 350,000 pound aircraft at 350 KIAS and 4000 feet altitude.
- Flight Condition 2 (FC-2) which represents a 350,000 pound aircraft at 240 KIAS and 4000 feet altitude.
- Flight Condition 3 (FC-3) which represents a 270,000 pound aircraft at .77 Mach (cruise) and 32,700 feet altitude.

The aircraft configuration used for this program, Figure 2 , was a basic B-52E with ECP-1128 structural modification to the aft fuselage and vertical tail. Also, the external tanks were removed to attain higher speed than required for Flight Condition 1. The basic B-52E control systems were modified to include hydraulically actuated control surfaces.

Initially, all spoiler segments were to accept the manual, fly-by-wire, and SAS signals. Because of difficulty with hardware design of the spoiler servo valves, the spoiler functions were altered. The final flight configuration consisted of manual and fly-by-wire operation through spoiler segments 3 through 12 and exclusive LAMS SAS operation through spoiler segments 1, 2, 13, and 14 biased at 15 degrees. Each of the remaining surface actuators (aileron, rudder, and elevator) is commanded by the monitor pilot (RH pilot) through the original control cable systems. With the electronics engaged, these surfaces respond with full authority to the electrical fly-by-wire (LH pilot) signals and with partial authority to the stability augmentation signals.

The Baseline SAS is a three axis (pitch, yaw, and roll) rigid body augmentation system designed to provide the benefits derived from a system representative of contemporary design and provide a basis for comparison with the LAMS-FCS performance data. The LAMS-FCS is a three axis system but addresses itself to stabilizing the significant load producing elastic

modes of vibration in addition to the rigid body modes. The SAS and associated electronics utilize two TR-48 analog computers installed at the navigator-bombadier station. These computers provide the flexibility required for system mechanization and expedite system changes identified during ground and flight testing.

1.2 Objectives

The objectives of the LAMS B-52 analysis program were:

- To validate techniques representative of contemporary practices for system analyses and design in the related technologies of Automatic Flight Controls, Aircraft Structures, and Aerodynamics.
- Analytically demonstrate gust load alleviation and structural mode stabilization using the conventional aerodynamic control surfaces.
- Analytically demonstrate the impact of airframe dynamic response control on significant vehicle attributes such as structural life, handling qualities, and ride quality.

1.3 Criteria

The LAMS B-52 analyses and design was based on the following criteria:

- The aircraft and control system will have an adequate flutter margin. The control system will possess a 10 db minimum gain margin and a 60 degree minimum phase margin as determined by open loop frequency response analyses.
- To provide adequate handling qualities with the LAMS-FCS engaged in turbulence, the short period damping ratio shall be equal to or greater than .40; for Dutch roll handling qualities, the product of the Dutch roll natural frequency times the Dutch roll damping ratio shall be equal to or greater than a value of .35 rad/sec. However, the Dutch roll characteristics for low speed conditions (FC-2) shall be acceptable with a value of the aforementioned product as low as .21 rad/sec. The roll time constant with the LAMS-FCS engaged shall be less than 2 seconds; if the roll time constant for the basic aircraft is greater than 2 seconds, the addition of LAMS-FCS shall not increase the constant. The spiral mode shall be positively damped, if possible. If the aircraft shows spiral divergent characteristics, the rate of divergence with controls fixed shall not result in doubling the bank angle in less than 20 seconds.
- Performance evaluation of the LAMS-FCS influence on such aircraft characteristics as peak loads, fatigue damage, and ride qualities will be based on comparisons of performance between the aircraft with the SAS engaged and disengaged. Fatigue damage rates and acceleration will be calculated at six locations using the equations of Section 3.0. These measurements will be calculated for atmospheric turbulence effects only. The effects of landing, takeoff, taxiing and maneuvering will

not be included except to the extent maneuvers are included in the atmospheric model. Fatigue damage evaluation will be accomplished by counting stress response level crossings normalized to a 1 ft/sec RMS random gust turbulence sample. Based on an arbitrary aircraft usage schedule, the fatigue damage rates will be combined in the following manner to determine a yearly damage accumulation:

25 hrs/year at FC-1

39 hrs/year at FC-2

511 hrs/year at FC-3

575 hrs/year total usage

The ride quality or acceleration performance will be based on the percent reduction of RMS aircraft accelerations along the fuselage due to a 1 ft/sec RMS random gust turbulence sample.

1.4 Report Contents

This report presents the comprehensive analyses, synthesis, and design of a Baseline SAS, and LAMS-FCS on B-52E test vehicle AF56-632.

Section 2.0 is a summary of the document contents.

Section 3.0 covers the control system definition for the Baseline SAS and LAMS-FCS. The analyses and analytical techniques leading to the final system configuration are discussed.

Section 4.0 presents the predicted performance characteristics of the Baseline SAS and the LAMS-FCS. Comparative data consisting of peak loads, response to step inputs, fatigue damage, ride qualities, and handling qualities are presented for the basic aircraft, Baseline SAS, and the LAMS-FCS design conditions. System stability evaluations are presented based on flutter and open loop frequency response analyses.

Section 5.0 discusses the system hardware design for the control surface hydraulic actuators, hydraulic power systems, interface electronics, fly-by-wire, instrumentation measurement requirements, and LAMS-FCS computer and ground test equipment.

Section 6.0 presents the general and specific conclusions reached during this program.

Section 7.0 contains all pertinent references contained herein.

2.0 SUMMARY

2.1 Introduction

The IAMS B-52 analyses, synthesis, and design has attained the program purpose and objectives by implementing a design to integrate advanced flight control hardware concepts and the existing flight control surfaces of B-52E AF56-632 into a versatile flight control system (FCS) test vehicle. The aircraft geometry used is shown on Figure 2. The design provides high bandpass hydraulic actuation systems and augmented hydraulic power supplies for the existing primary flight control surfaces. An electronic flight control equipment link from the controlling inputs (pilot commands and aircraft dynamics) to the actuators is also a part of the design.

The analysis resulted in two stability augmentation systems for the three flight conditions outlined in the Introduction. The Baseline SAS was designed to show the aircraft benefits derived from a system representative of contemporary design for comparison with the IAMS-FCS performance. The IAMS-FCS extended the state-of-the-art design and mechanization techniques to produce a SAS which would provide gust load alleviation and structural mode stabilization while flying through atmospheric turbulence.

2.2 Analysis Techniques

The Baseline SAS design emphasis was directed toward development of a control system representative of contemporary stability augmentation systems. Criteria limited the Baseline SAS performance to stability augmentation of the aircraft rigid body modes without significantly altering or controlling the aircraft structural modes.

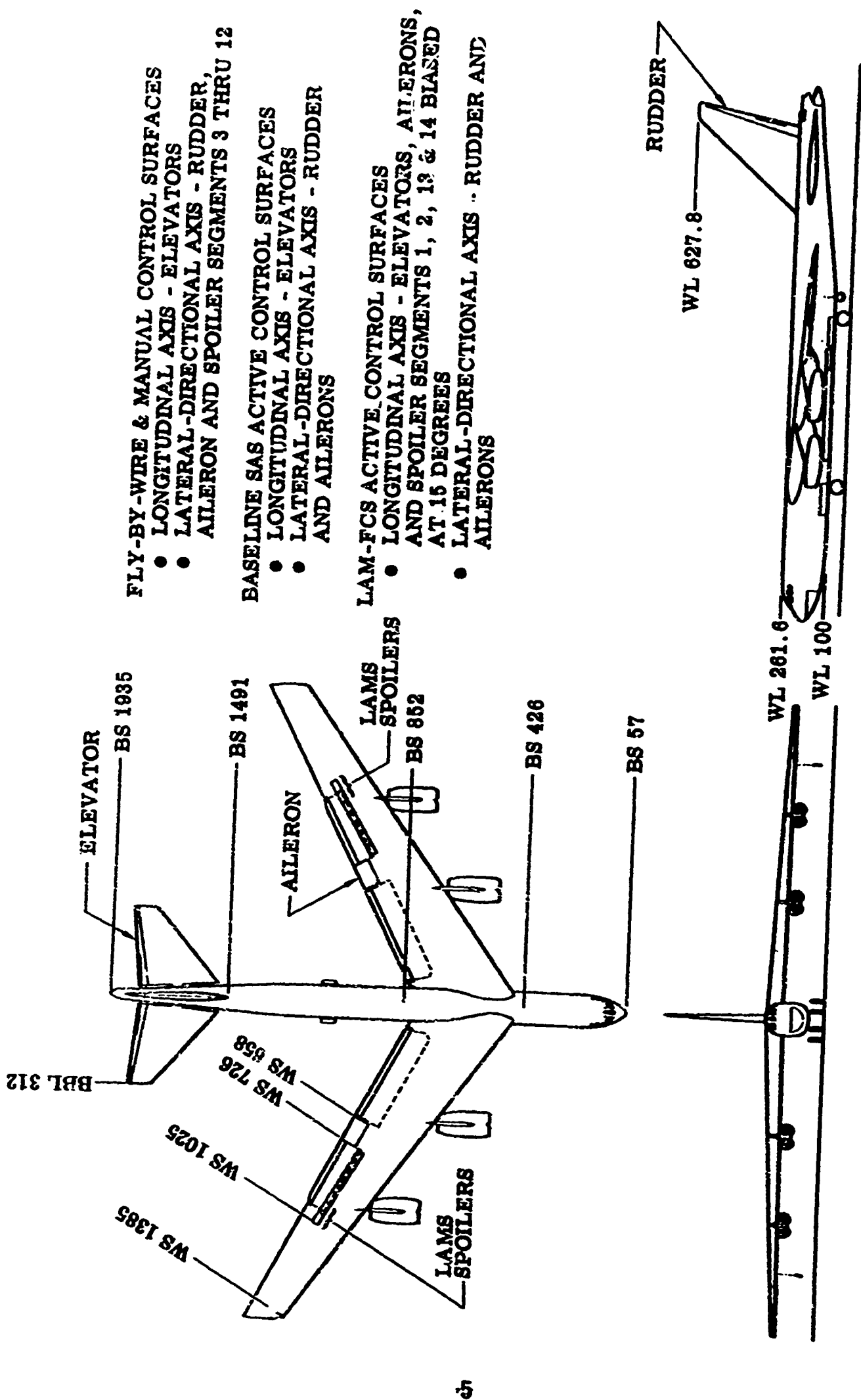
The IAMS Flight Control System design emphasis was directed toward development of a structural load alleviation system for flight through turbulence. The design criteria also required sufficient stability margins at all frequencies.

Design charters for both systems required retention or improvement of the basic aircraft handling qualities.

Analysis techniques for designing the two systems varied due to differences in design criteria and the fact that different companies designed the systems. Boeing-Michita designed the Baseline SAS and Honeywell Inc. had primary design responsibilities for the IAMS-FCS. Performance evaluation and analyses were comprehensive, in terms of mathematical model sizes and contents, and were nearly identical for the two systems.

2.2.1 Analyses Mathematical Model

Boeing developed a 65 degree-of-freedom mathematical model of the unique IAMS B-52 test vehicle for design synthesis, and evaluation of the IAMS flight control systems. The model included 33 symmetric (longitudinal) degrees-of-freedom, 32 antisymmetric (lateral-directional) degrees-of-freedom, Wagner and Kussner lift growth functions, gust penetration lags, and fourth order actuator and control surface dynamics. The symmetric and antisymmetric degrees-of-freedom were considered to be independent and were analyzed separately.



FLY-BY-WIRE & MANUAL CONTROL SURFACES

- LONGITUDINAL AXIS - ELEVATORS
- LATERAL-DIRECTIONAL AXIS - RUDDER, AILERON AND SPOILER SEGMENTS 3 THRU 12

BASELINE SAS ACTIVE CONTROL SURFACES

- LONGITUDINAL AXIS - ELEVATORS
- LATERAL-DIRECTIONAL AXIS - RUDDER AND AILERONS

LAM-FCS ACTIVE CONTROL SURFACES

- LONGITUDINAL AXIS - ELEVATORS, AILERONS, AND SPOILER SEGMENTS 1, 2, 13 & 14 BIASED AT 15 DEGREES
- LATERAL-DIRECTIONAL AXIS - RUDDER AND AILERONS

B-52E AIRCRAFT GEOMETRY

FIGURE 2

The complete mathematical model was used for structural performance evaluations and flutter boundary analyses. However, time and computer limitations dictated use of simplified mathematical models of various degrees for the majority of the IAMS program analyses.

2.2.2 Baseline SAS Analyses

Design synthesis for the Baseline SAS primarily utilized gain and phase root loci techniques and supporting design analyses used frequency response techniques. Handling qualities were initially evaluated from transient responses obtained from inverse Laplace calculations. All of the techniques described above were accomplished with digital computer programs. Final safety, structural performance, and handling qualities evaluations were similar to those conducted for the IAMS-FCS and are reviewed in Section 2.2.4.

2.2.3 IAMS-FCS Analyses

The IAMS-FCS design and synthesis were conducted by Honeywell Inc. under subcontract to The Boeing Company. Boeing furnished the aircraft mathematical model to Honeywell in the form of digital computer cards and provided engineering support throughout the IAMS-FCS design and synthesis segments of the IAMS program. Boeing-Wichita conducted the safety analyses and handling qualities evaluations of the IAMS-FCS while Honeywell conducted the performance sensitivity analyses. An analyses flow diagram is presented in Figure 3.

2.2.3.1 Initial Design Analyses

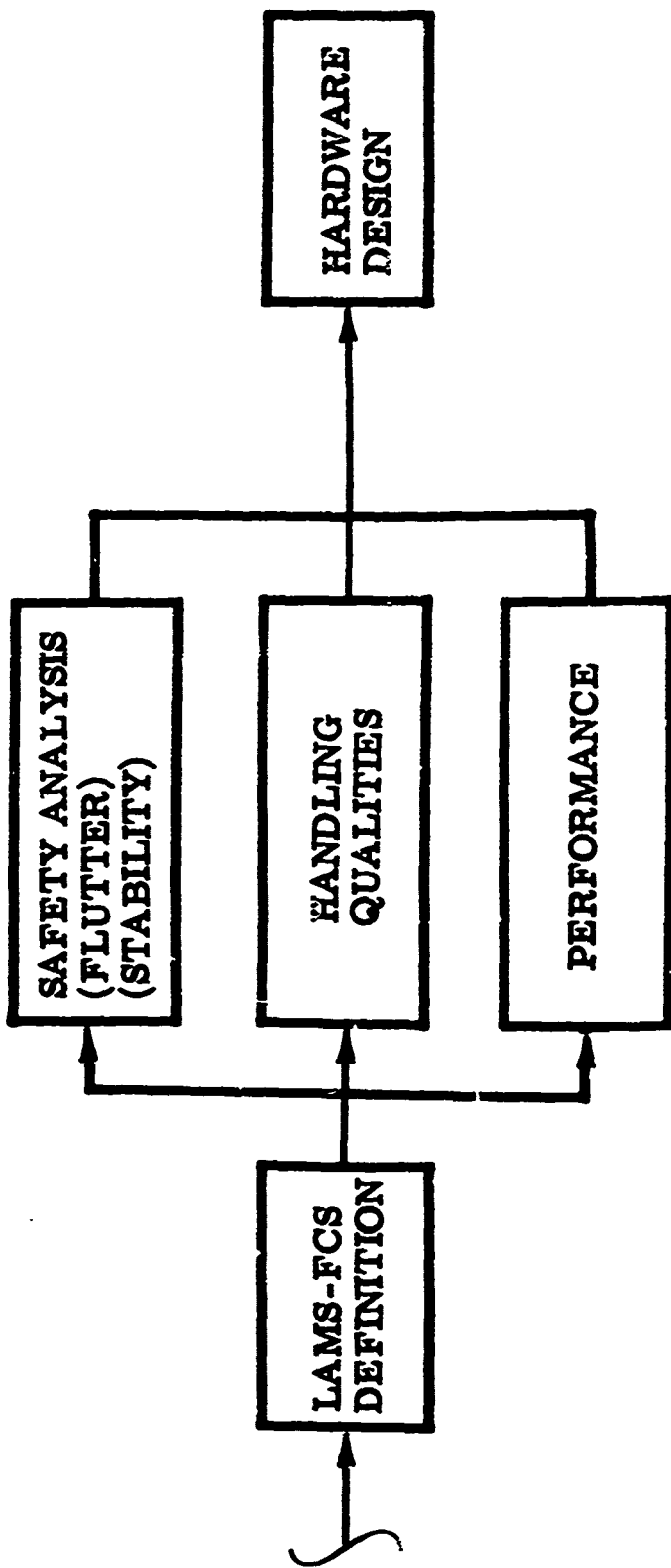
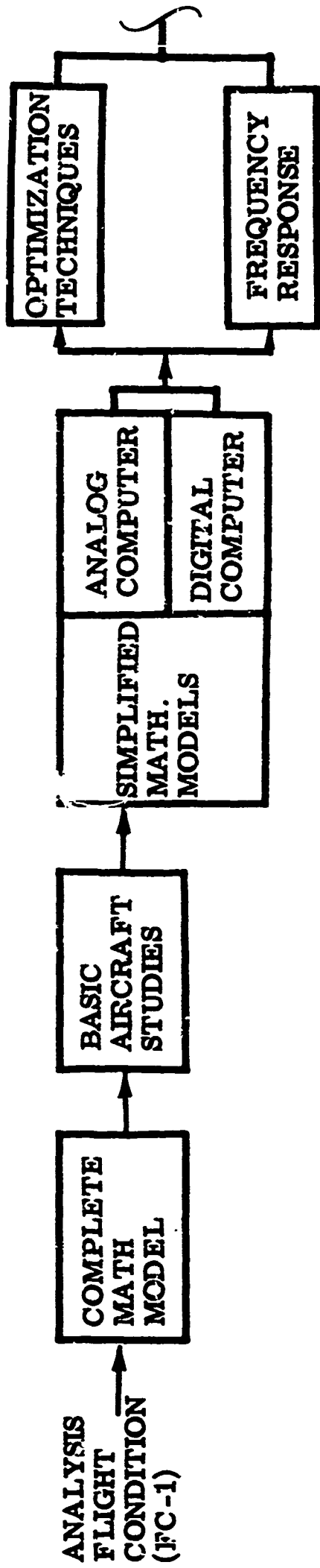
Initial design analyses objectives were twofold. The primary objective was to obtain an understanding of the relationship of rigid body and structural modes to fatigue damage and fuselage accelerations. Secondly, it was desired to verify the computation programs used for the IAMS-FCS design and synthesis by comparing Boeing and Honeywell basic aircraft data. These basic aircraft studies consisted of three segments; controls locked fatigue damage calculations, artificial mode damping studies, and an uncoupled mode investigation.

Three gust alleviation concepts were synthesized in the preliminary design analyses: stabilization of the rigid body motions; minimization of wing loads; and minimization of wing stresses and stress rates. These alleviation concepts were evaluated by inspection and by analog simulation. It became apparent from these and other IAMS studies that gust alleviation and mode stabilization problems should be solved simultaneously.

2.2.3.2 Design Synthesis

Optimal control theory was applied in an attempt to design an optimal gust load alleviation and structural mode stabilization system. The primary design goal was to reduce fatigue damage rates and a secondary goal was to provide improvement in ride qualities.

Two measures of structural integrity used during this program were; an estimate of the likelihood of a structural member exceeding its static



LAMS - FCS ANALYSIS FLOW DIAGRAM

FIGURE 3

ultimate strength and an estimate of its fatigue lifetime..

For the IAMS-FCS optimal program it was assumed that the event with the shorter expected time would define a structural performance measure for a single airframe member. The structural integrity measure for the entire aircraft was the minimum of all airframe members and the structural performance goal of the IAMS-FCS then was to increase that measure.

The maximum structural integrity measure was formulated as a minimum cost function and a controller minimizing the quadratic cost function was found by conventional Lagrange multiplier techniques. The performance index essentially minimized selected aircraft RMS stresses, stress rates, and accelerations at the pilot's station.

Optimal control programs designed a theoretical IAMS Flight Control System for each axis. The systems inherently contained an excessive number of feedbacks (81 for the symmetric axis and 90 for the antisymmetric axis) for practical implementation. However, the optimal control systems structural performance measures were used as a baseline for determining the merit of simplified or more practical systems. Also, the magnitude of the optimal control law gains generally indicated the relative importance of the feedback loops in terms of structural performance benefits.

Optimal control law simplification techniques were accomplished primarily by analog computer simulation. Supporting digital computer analyses evaluated the simplified systems stability and performance during the analog computer iterative processes.

The IAMS Longitudinal FCS was designed from optimal control techniques. Repeated difficulty encountered during attempts to simplify the lateral-directional optimal control law influenced a decision to design the IAMS Lateral-Directional FCS from "scratch" using analog computer techniques.

Design synthesis efforts defined system feedbacks assuming pure aircraft parametric signals were available. In reality, aircraft parameters normally cannot be sensed individually, that is, sensor signals are usually a function of several parameters. For the IAMS design synthesis, sensed signals at various aircraft locations were defined by modal coefficients. Matrix inversion techniques then defined sensor signal blending gains required to obtain the desired feedback parameters for the IAMS-FCS.

2.2.4 Final Systems Evaluation

The IAMS-FCS final design was evaluated at Boeing-Wichita with comprehensive safety, handling qualities, and structural performance analyses. The Baseline SAS design was evaluated in a similar manner and the general techniques applicable to both systems are discussed in this section. Honeywell also conducted a performance sensitivity analysis of the final IAMS-FCS design.

2.2.4.1. Safety Analyses

The safety analysis was conducted to assure that the systems had adequate stability margins. A flutter analysis segment evaluated structural stability as a function of airspeed. A stability analyses defined phase and gain margins as functions of feedback loop gains.

Flutter analyses were conducted to provide flutter clearance for the IAMS-FCS for flight conditions 1 and 3. The Baseline SAS and basic aircraft configurations were analyzed for flutter to provide flight clearance over the entire B-52 test vehicle flight envelope. Flutter boundaries were established for individual aircraft configurations by analyzing selected aircraft gross weight, airspeed, and altitude conditions.

The stability analyses provided closed loop gain and phase root loci plots and open loop frequency response data to determine the stability margins for selected aircraft flight conditions. Since the IAMS-FCS is a multiple feedback loop system, the individual feedback loops were opened and their gains varied with all other loops closed and at nominal gain (technique for frequency response analysis). Digital computer capabilities dictated the root loci technique math model size to be smaller than the comparable math model size for frequency response methods. Subsequently, a decision was made to utilize only frequency response techniques for the final stability analyses.

2.2.4.2 Handling Qualities Evaluation

A quasi-elastic six degree-of-freedom mathematical model was used to simulate the basic aircraft and evaluate the effects of the Baseline SAS and IAMS-FCS on basic aircraft handling qualities. The basic aircraft analog computer simulation was accurately checked by comparing pre-IAMS flight test data to analog computer response data. Baseline SAS dynamic characteristics were checked by comparing quasi-elastic model root loci data with the structural model root loci data. Accurate simulation of the IAMS-FCS was assured by comparison of response data with similar Honeywell analog simulation data.

The analog computer simulation of the aircraft and control system was used in conjunction with the point light source simulator facility to permit pilot evaluation of the aircraft handling qualities. Dutch roll and short period frequency and damping values were determined and qualitative data were obtained from test pilots in the form of Cooper ratings.

2.2.4.3 Structural Performance Evaluations

Selected aircraft parameters were used to evaluate the Baseline SAS and IAMS-FCS effects on structural performance during flight through turbulence. Fatigue damage rates, expected peak stresses, RMS stresses, and RMS accelerations were calculated at six significant stress points on the test vehicle. Acceleration power spectra were computed for the crew compartment. The six selected stress locations were chosen to be representative of sensitive areas of the wing, body, and empennage during flight through turbulence. The atmospheric turbulence model used for the structural performance studies assumed Gaussian random, stationary, isotropic turbulence represented by the

power spectral density function for vertical and lateral components. An antisymmetrical component of vertical turbulence was represented by a rolling gust acting on the wing as in NACA Report 1321, Reference 1. Rice's stress exceedance function was used in calculating the number of stress cycles of various amplitudes in response to the turbulence and Minor's hypothesis was utilized for calculations of fatigue damage.

2.2.4.4 Performance Sensitivity Analyses

Honeywell conducted a IAMS-FCS performance sensitivity analysis consisting of three segments; performance definition or initial handling qualities studies, sensitivity analysis, and failure analysis. The performance definition study provided an initial evaluation of the IAMS-FCS handling qualities. Aircraft transient responses to discrete gust inputs and pilot commands were compared with free aircraft data. Actuator hysteresis effects on various aircraft parameters were evaluated for random turbulence disturbances.

The sensitivity analysis evaluated the effects of aircraft and IAMS-FCS hardware parametric variations for random turbulence of 4 ft/sec RMS velocity.

Failure analyses consisted of two segments; hardware open failures and hardware hardover failures. The open failure analysis utilized a 4 ft/sec RMS random turbulence and the hardover failure analysis obviously needed no external excitation.

2.3 System Description

2.3.1 Baseline SAS

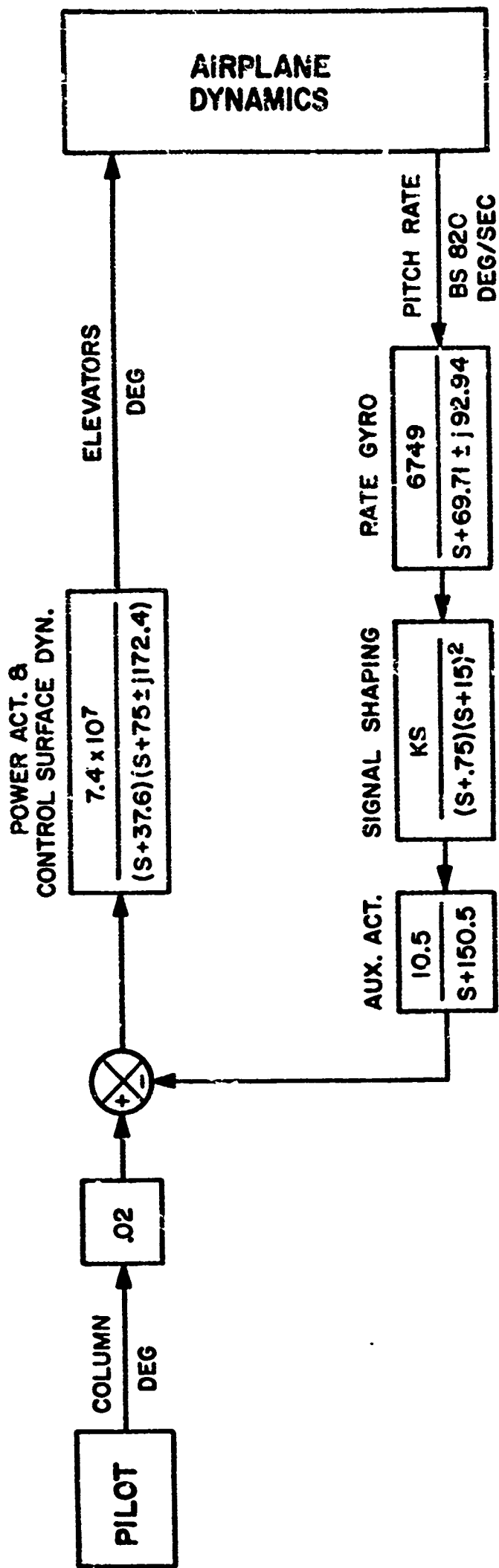
The Baseline SAS is a three axis flight control system. The system design accommodates operation of each axis independently or any combination of the three axes.

2.3.1.1 Longitudinal Axis

The primary function of the Baseline pitch SAS is to augment short period mode damping. The closed loop system provides a pitch rate feedback signal to drive a hydraulically powered elevator. The pitch rate signal is derived from a rate gyro located at Body Station 820 (near the aircraft cg, see Figure 2). Electronic filters in the feedback signal path shape the feedback signal to ensure stability and obtain desired handling qualities. Figure 4 shows a block diagram of the Baseline Pitch SAS.

2.3.1.2 Lateral-Directional Axis

The Baseline Roll SAS improves roll responsiveness of the aircraft to the pilot's wheel command without decreasing steady-state roll rate capability of the aircraft by more than 10 percent. A feedback loop decreases the roll time constant by sensing roll rate with a rate gyro located at Body Station 820 (approximately at the cg, see Figure 2) which is fed to the aileron actuator. Feedback loop electronic filters ensure system stability and desirable handling qualities.



LAMS FLIGHT CONDITION	FEEDBACK GAIN K VOLTS PER VOLT
1	40
2	50
3	45

LAMS BASELINE PITCH SAS BLOCK DIAGRAM

FIGURE 4

The Baseline Yaw SAS augments Dutch roll damping with a yaw rate feedback, utilizing a rate gyro located at Body Station 616 (forward of the cg, see Figure 2). The feedback signal is shaped for stability assurance and to obtain desirable handling qualities and then fed to the rudder actuator.

Coupling between the yaw and roll systems was not of major concern during the Baseline SAS design, but the SAS does reduce coupling effects.

A block diagram of the Baseline yaw-roll SAS design is presented in Figure 5.

2.3.2 LAMS-FCS

The LAMS-FCS is a three aircraft axis flight control system, but was designed as a longitudinal axis system and a lateral-directional axis system.

2.3.2.1 LAMS Longitudinal FCS

Figure 6 shows a block diagram of the LAMS Longitudinal FCS. Feedback signals are derived from four rate gyros; one located in the forward fuselage, one in the aft fuselage, and one in each wing. These gyro signals are blended to produce three parametric signals, rigid body pitch rate, mode one rate, and mode six rate. Pseudo integration of the structural mode rate signals gives approximate mode displacement signals. The signals are then gain adjusted as a function of the flight condition and then shaped with electronic filters. The filters are primarily for stability compensation and prevention of dc null offsets. The system operates the elevators, ailerons, and two outboard spoiler panels on each wing symmetrically. The spoiler panels operate from a 15 degree biased position.

Desirable handling qualities are obtained by adding a column-to-elevator feed forward signal path parallel to the existing path. System gains are a function of flight condition and are scheduled as tabulated in the table included in Figure 6.

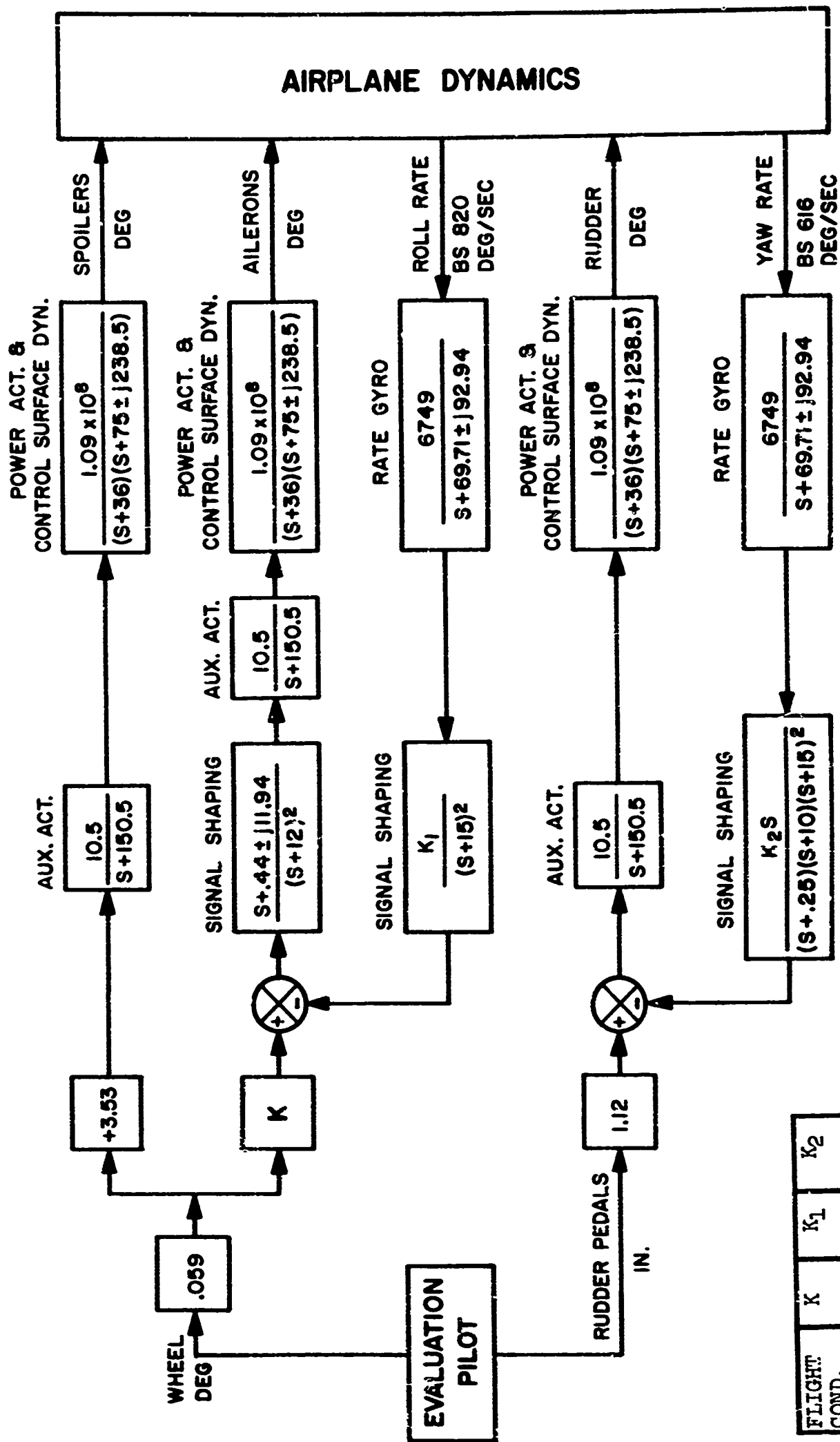
2.3.2.2 LAMS Lateral-Directional FCS

Figure 7 shows a block diagram of the LAMS Lateral-Directional FCS. Six fuselage mounted rate gyros are utilized to derive the raw feedback signals. The signals directly provide rigid body yaw rate and are blended to obtain rigid body roll rate and structural mode 9 rate. Filtering of the signals is required for appropriate stability margins. The system drives the rudder and ailerons asymmetrically. Handling qualities requirements were met by adding a wheel-to-aileron feedforward signal path parallel to the existing path. The system gains are scheduled as a function of flight condition as tabulated in the table in Figure 7.

2.4 System Performance

Systems performance criteria were defined in Reference 2.

The general LAMS Baseline SAS design criteria require that the Baseline SAS will:



LAMS BASELINE ROLL AND YAW SAS BLOCK DIAGRAM

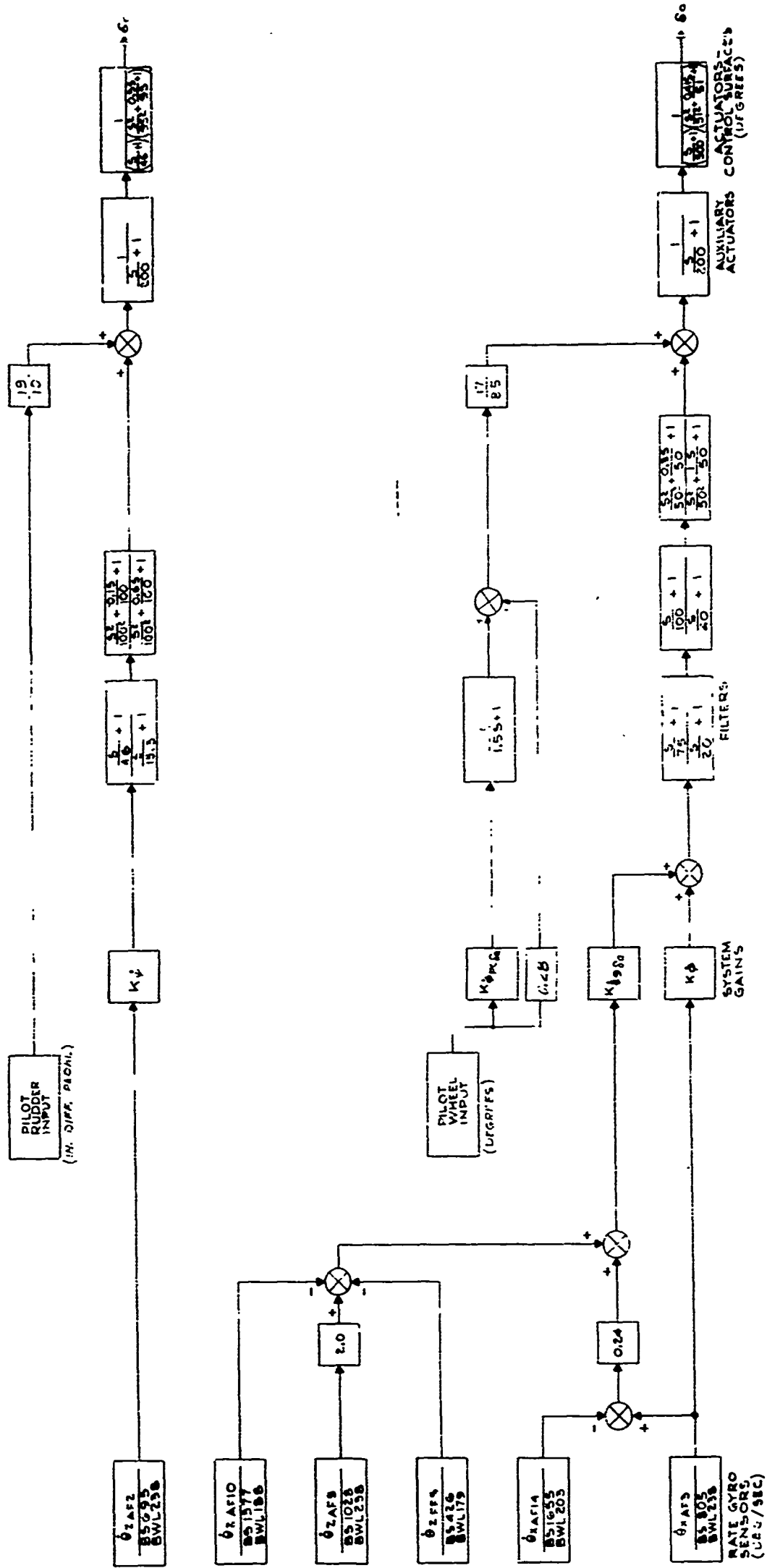
FIGURE 5



PLANT CONDITION	K ₂ O/PC	K ₂ O	K ₂ O/S ₂	K ₂ O/S ₂	K ₂ O/S ₂	K ₂ O/S ₂
FC1	0.79	0.81	0.20	0.25	1.47	0.219
FC2	1.16	1.12	0.45	0.80	1.39	0.207
FC3	0.70	0.78	0.26	0.73	1.63	0.340

LAMS LONGITUDINAL, FLIGHT CONTROL SYSTEM BLOCK DIAGRAM:

FIGURE 6



LATERAL FLIGHT CONTROL GAINS

FLIGHT CONDITION	K_p	K_d	K_f	$K_{p/f}$
FC1	1.025	0.950	4.060	1.17
FC2	2.160	0.850	4.060	1.93
FC3	1.820	0.970	9.300	2.72

LAMS LATERAL DIRECTIONAL FLIGHT CONTROL SYSTEM BLOCK DIAGRAM

FIGURE 7

- Be representative of conventional stability augmentation systems
- Not significantly disturb or control aircraft structural modes
- Provide stability augmentation to the three aircraft axes
- Retain or improve handling qualities
- Have a minimum of 10 db gain margin and 60 degree phase margin for all structural modes

The LAMS-FCS general design criteria require that the LAMS-FCS will:

- Have a minimum of 10 db gain margin and 60 degree phase margin for all rigid body and structural modes
- Retain or improve the existing aircraft handling qualities
- Provide measurable improvement in terms of fatigue damage and/or maximum expected loads

2.4.1 Safety Analysis

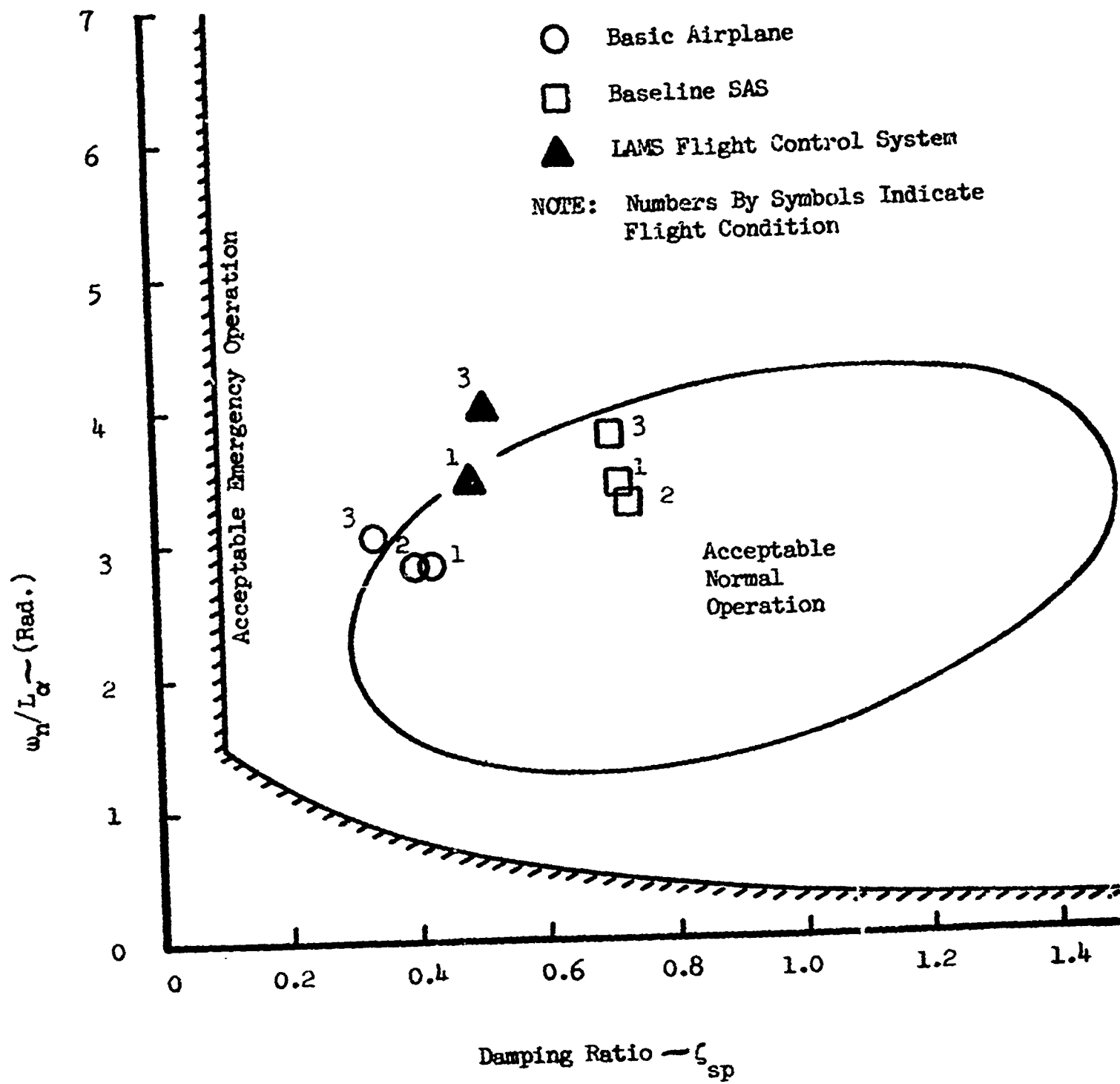
The Baseline pitch SAS is gain stabilized with all gain margins greater than 20 db. The Baseline Lateral-Directional SAS has a minimum gain margin of 14 db and a minimum phase margin of 70 degrees.

The LAMS Longitudinal FCS minimum gain margin is 10 db at 61.6 radians per second for the aileron loop at flight condition 1. The LAMS Lateral Directional FCS minimum gain margin is 17.7 db for the aileron loop at flight condition 1 and the minimum phase margin is 86 degrees for the rudder loop at flight conditions 2 and 3. The basic aircraft with hydraulically powered controls and the Baseline SAS have adequate flutter boundaries for all altitudes, gross weights, and airspeeds up to and including the maximum for straight and level flight (400 KEAS and .9 Mach number). The LAMS-FCS was flutter cleared only for the three LAMS flight conditions.

2.4.2 Handling Qualities Evaluations

Short period characteristics are indicated in Figure 8. Neither the Baseline SAS or the LAMS-FCS appreciably degraded the basic aircraft short period handling qualities. Handling qualities with the LAMS-FCS at flight condition 3 are not within the desired operating region, but are within the acceptable region. The Baseline SAS and LAMS-FCS pilot ratings obtained from simulator studies indicate both systems have acceptable longitudinal handling qualities. As would be expected, ratings degraded with increased RMS turbulence velocity.

Figure 9 shows the predicted Dutch roll handling qualities for the Baseline SAS and LAMS-FCS compared to the basic aircraft. Both systems improve the Dutch roll handling qualities to be within the satisfactory



PREDICTED SHORT PERIOD HANDLING QUALITIES

FIGURE 8

operating region. Predicted roll time constants and spiral time constants were within the criteria requirements for both systems. The Baseline SAS and IAMS-FCS pilot ratings obtained from simulator studies indicate both systems have acceptable lateral and directional handling qualities but ratings degraded with increased RMS turbulence velocity.

2.4.3 Structural Performance Predictions

Figure 10 presents the predicted Baseline SAS and IAMS-FCS effects on turbulence induced fatigue damage for a hypothetical annual mission composed of the three IAMS flight conditions. The data includes effects of vertical, lateral, and rolling gusts. Table I shows the contribution to total fatigue damage of each of the three analyzed flight conditions for the IAMS-FCS.

The IAMS-FCS provides significant reductions over the Baseline SAS in fatigue damage rates caused by turbulence for the wing stations and mid fuselage stations. The IAMS Longitudinal FCS is primarily credited for the major segments of improvement in structural performance at those stations. That performance is attained through control of the rigid body short period mode, the first symmetric structural mode, and the sixth symmetric structural mode.

Preliminary design studies indicated the primary contributor to fatigue damage rate at the aft fuselage stations and the vertical fin station to be the Dutch roll mode, see Section 3.5.1.2. Based on that data, the IAMS Lateral-Directional FCS was designed to control only the Dutch roll mode for fatigue damage rate reduction. Therefore, the Baseline SAS and the IAMS-FCS have approximately equal effects on structural performance for aft fuselage stations and the vertical fin station. Both systems show significant improvement over the basic aircraft configuration. It should be noted that contributions to fatigue damage by asymmetrical structural modes were considered insignificant at the three flight conditions analyzed during this program for the specific IAMS test vehicle configuration. The validity of similar conclusions for other flight conditions or other aircraft configurations would be questionable in the absence of additional analyses.

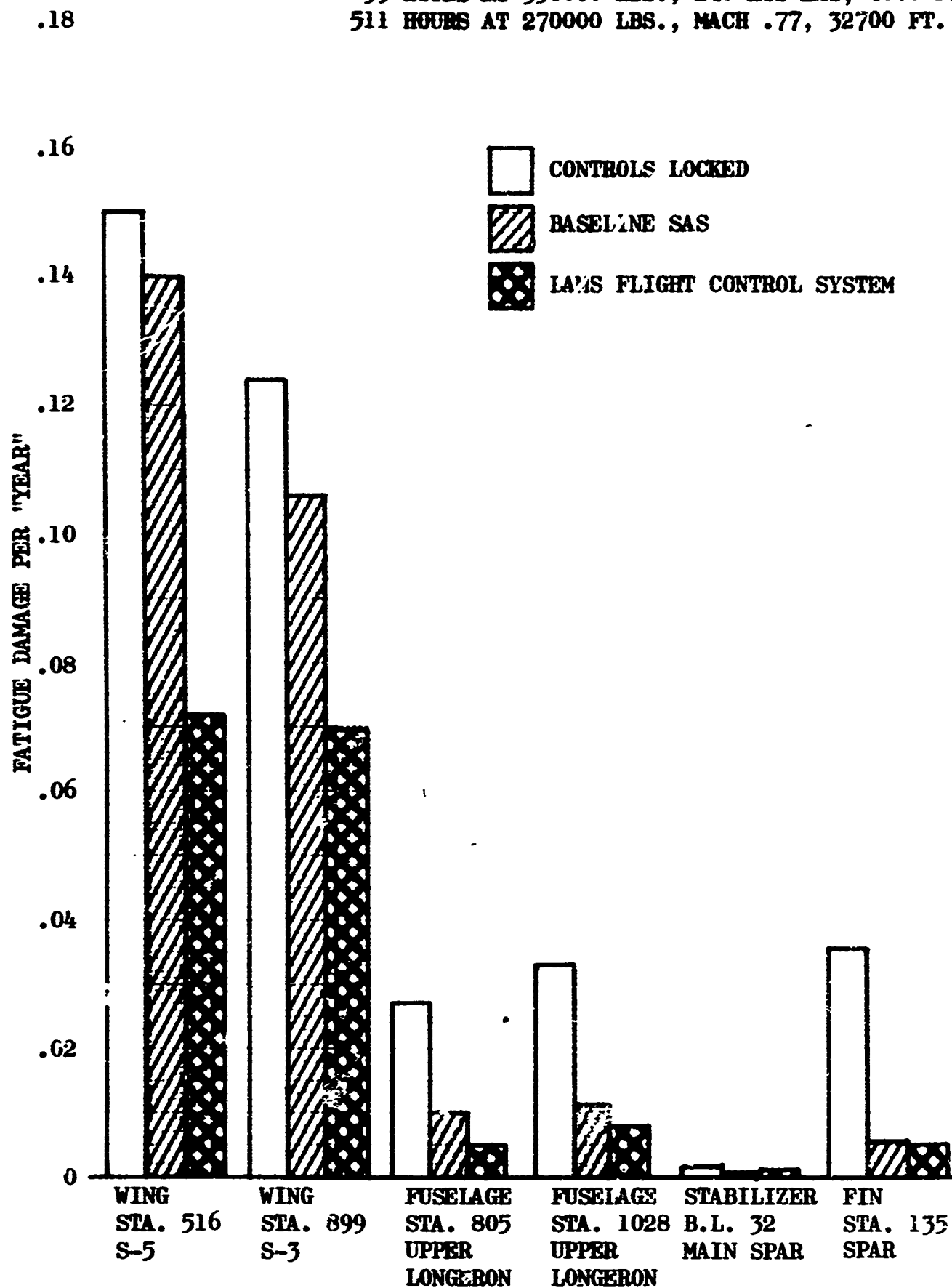
Both the Baseline SAS and the IAMS-FCS provide reduced RMS accelerations at the pilot's station and along the entire fuselage, as presented in Figures 11 and 12. Reductions in RMS accelerations along the wing were also provided by both systems. Control of the sixth symmetric structural mode and ninth asymmetric structural mode was intended to afford the IAMS-FCS minor ride qualities improvement over the Baseline SAS.

2.4.4 Performance Sensitivity Results

The performance definition studies data indicated that the IAMS-FCS would operate satisfactorily for all levels, frequencies, and types of inputs considered in the study. The sensitivity analyses indicated that the IAMS-FCS would in general provide acceptable operation for the aircraft parametric variations studied. In one case, a 25 percent variation in the rigid body pitch rate modal coefficient, a statically unstable condition was indicated. Since that coefficient is a function of the aircraft rigid body motion it was not expected to vary from predicted values. The failure

**LAMS B-52 FATIGUE DAMAGE RATES DUE TO TURBULENCE
COMBINED VERTICAL, LATERAL, AND ROLLING GUSTS**

"ANNUAL USAGE" = 25 HOURS AT 350000 LBS., 350 KTS EAS, 4000 FT.
39 HOURS AT 350000 LBS., 240 KTS EAS, 4000 FT.
511 HOURS AT 270000 LBS., MACH .77, 32700 FT.



FATIGUE DAMAGE RATES

FIGURE 10

TABLE I
LAMS FATIGUE DAMAGE RATES DUE TO TURBULENCE
LAMS - FCS SAS (ROLL, PITCH, AND YAW)
2 OUTBD. SPOILERS UP 15°
COMBINED VERTICAL, LATERAL, & ROLLING GUSTS
CONTOUR LOW LEVEL & CRUISE ENVIRONMENTS
ARE FROM ECP 1128 (B-52 DATA)

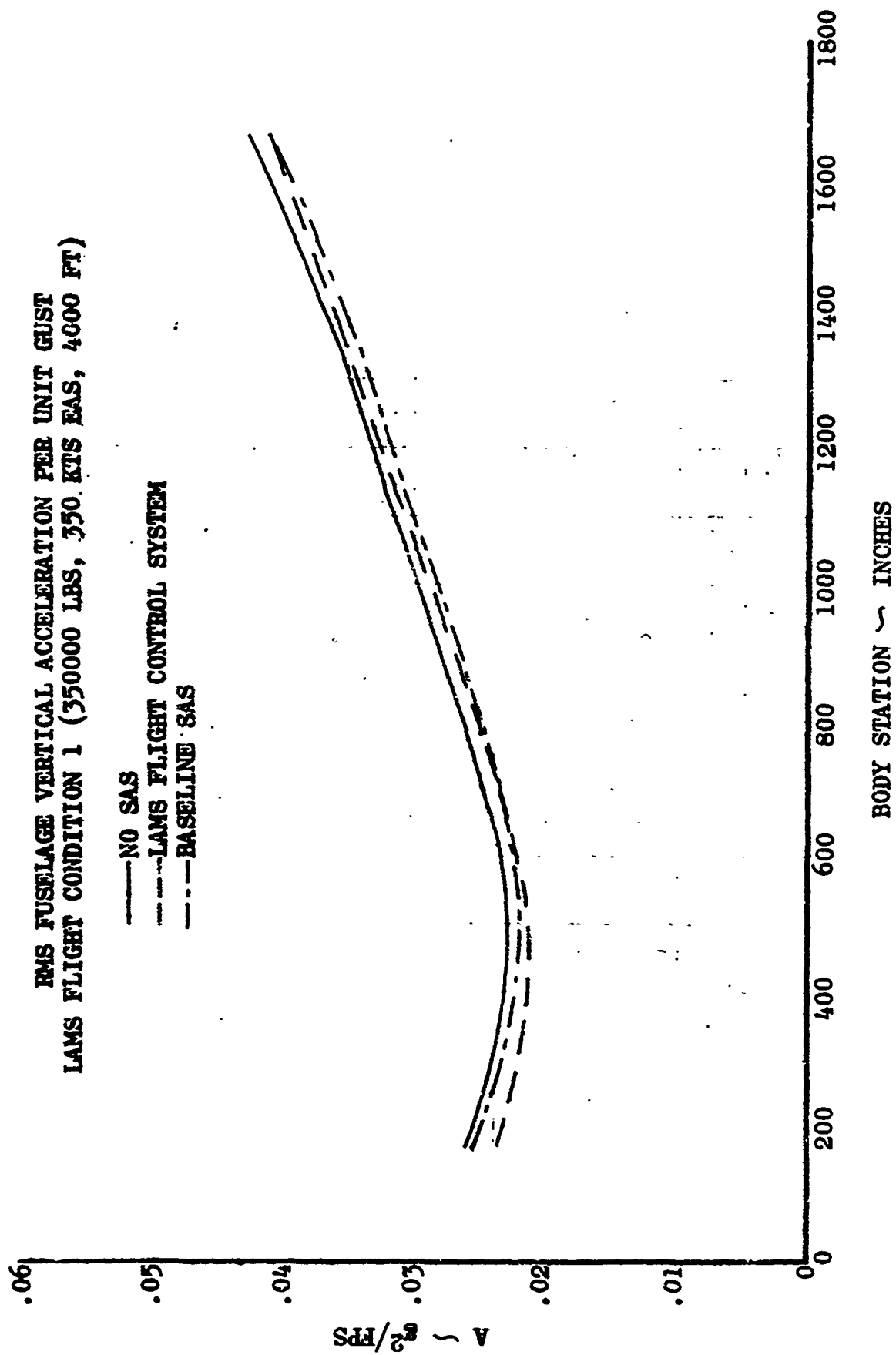
STRESS LOCATION	COND. 1	DAMAGE PER HOUR COND. 2	COND. 3	DAMAGE PER YEAR*
W.S. 282 S-7	1.66×10^{-3}	$.846 \times 10^{-3}$	$.0025 \times 10^{-3}$.0758
W.S. 516 S-5	1.45×10^{-3}	$.847 \times 10^{-3}$	$.0049 \times 10^{-3}$.0718
W.S. 899 S-3	1.323×10^{-3}	$.731 \times 10^{-3}$	$.0154 \times 10^{-3}$.0695
B.S. 805 U.L.	$.1589 \times 10^{-3}$	$.0114 \times 10^{-3}$	$.0005 \times 10^{-3}$.0047
B.S. 1028 U.L.	$.2821 \times 10^{-3}$	$.0142 \times 10^{-3}$	$.0010 \times 10^{-3}$.0081
S.B.L. 32 SPAR	$.0290 \times 10^{-3}$	$.0006 \times 10^{-3}$	$.00005 \times 10^{-3}$.0008
F.S. 135 SPAR	$.186 \times 10^{-3}$	$.0093 \times 10^{-3}$	$.0004 \times 10^{-3}$.0052

COND. 1 = CONTOUR LOW-LEVEL, 350,000 LBS., 350 KEAS, 4000 FT. ALT.

COND. 2 = CONTOUR LOW-LEVEL, 350,000 LBS., 240 KEAS, 4000 FT. ALT.

COND. 3 = CRUISE, 270,000 LBS., MACH. .77, 32,700 FT. ALT.

*ANNUAL USAGE = 25 HOURS @ COND. 1
 +39 HOURS @ COND. 2
 +511 HOURS @ COND. 3



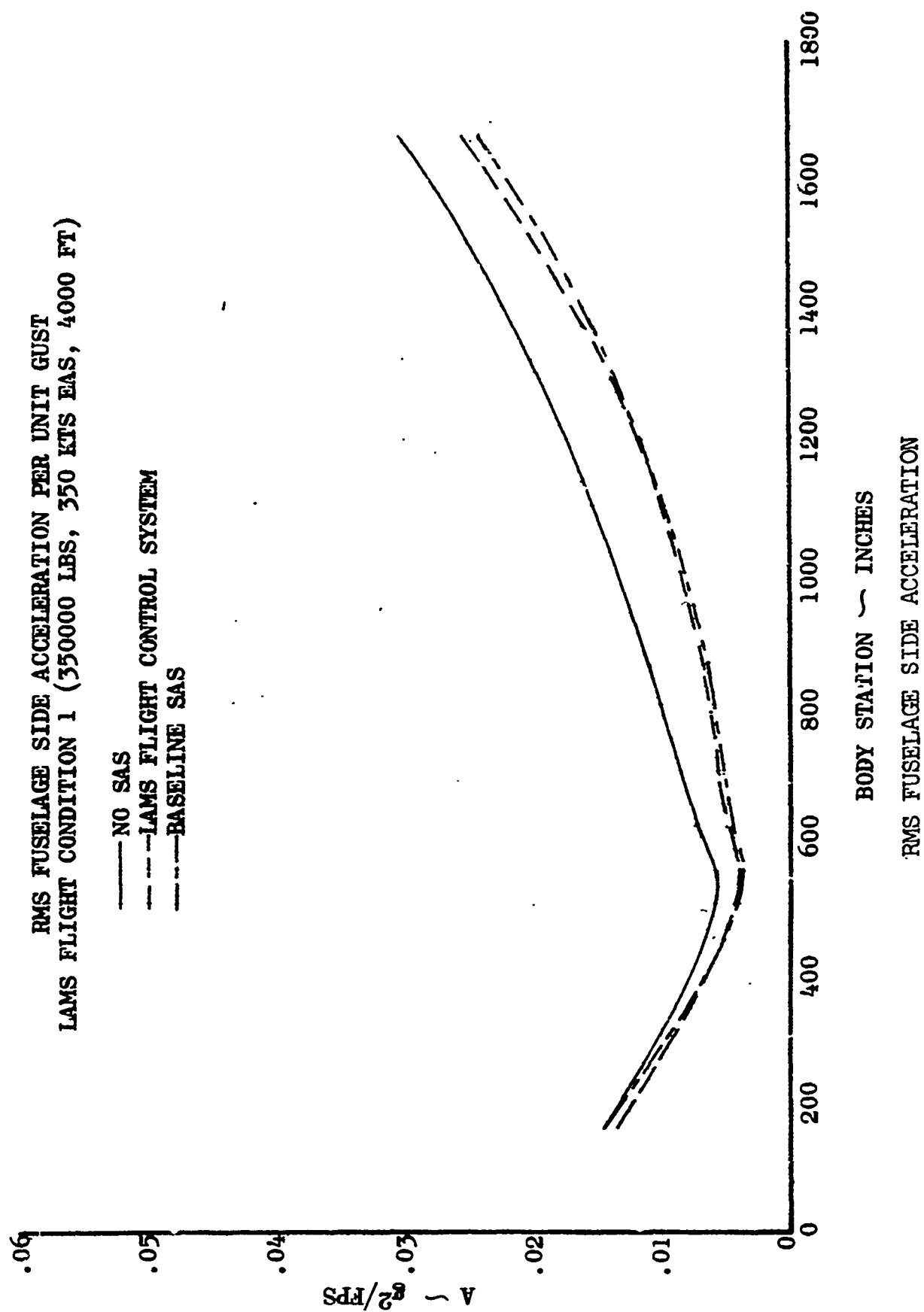


FIGURE 12

analyses results predicted that LAMS-FCS hardware open or hardover failures would not result in an uncontrollable flight condition.

2.5 Hardware Design

2.5.1 Aileron Actuator

The aileron hydraulic actuator positions the aileron in response to inputs transmitted from the control wheel, electrical signals from the stability augmentation system, electrical trim inputs or simultaneous combinations of all inputs. Aileron position feedback is obtained from the actuator piston rod.

The aileron actuator contains a force feedback piston that provides the compensation necessary to achieve the required closed-loop response and a delay valve that limits the actuator centering rate to 60 degrees-of-aileron travel per second upon electrical shutdown of the stability augmentation system.

The aileron actuator was designed for an open loop gain of 45 deg/sec/deg, a no-load rate of 120 deg/sec, and a maximum force capability of 6250 pounds.

2.5.2 Spoiler Actuation

The five inboard spoiler panels on each wing are divided into groups of three panels and two panels. Metered hydraulic flow is supplied to the spoiler segment actuators by an integrated servo-valve.

The integrated spoiler valve responds to electrical fly-by-wire inputs, electrical airbrake commands, mechanical pilot input commands, or simultaneous combinations of all command inputs. Mechanical position feedback commands are provided by the existing aircraft follow-up linkage system.

The integrated spoiler servo valve actuation system had the following design requirements:

TWO PANEL CONFIGURATION

Open Loop Gain	40 deg/sec/deg
No Load Rate	220 deg/sec
Force Capability Per Panel Up	5,700 lbs

THREE PANEL CONFIGURATION

Open Loop Gain	27 deg/sec/deg
No Load Rate	140 deg/sec
Force Capability Per Panel Up	5,700 lbs

The two outboard spoiler panels are used for the IAMS Longitudinal FCS. Each spoiler panel actuator is fitted with a special manifold which adapts an electro-hydraulic flow control valve to the unit. Position feedback is provided by a transducer fitted to the actuator piston rod. The IAMS-FCS spoiler panels operate from a 15 degree bias point.

Design requirements of the IAMS-FCS spoiler actuation were as follows:

Gain Margin	10 db
Phase Margin	70 deg
Open Loop Gain	43 sec ⁻¹
Force Capability - Per Panel Up	5,700 lbs

2.5.3 Rudder and Elevator Actuators

The hydraulic actuators used for control of the rudder and elevators are essentially the same as those used for the B-52 G and H fleet installation of ECP 1195.

The rudder and elevator actuators are mechanically similar and differ only in envelope dimension, stroke, and force output. Maximum actuator force output is limited by differential pressure limiters incorporated in the actuator package. The actuators position the surfaces in response to mechanical inputs, electrical inputs, or combinations of both. Surface position feedback is obtained from the actuator piston rod position.

The actuator characteristics are as follows:

	Rudder	Elevator
Open Loop Gain	45 deg/sec/deg	45 deg/sec/deg
Actuator No Load Rate	80 deg/sec	80 deg/sec
Stroke	±1.30 inch	±1.47 inch
Force Capability	7,320 lbs	10,530 lbs

2.5.4 Hydraulic Power

The wing hydraulic power is provided by six engine driven hydraulic pumps, each augmented with an electric motor driven pump and accumulator.

The rudder and elevator hydraulic power is provided by two electric motor driven pumps. Two separate systems are used and each system has a self-pressurizing reservoir. A standby source of hydraulic power is furnished by a hydraulic motor driven pump (transformer) powered by the number 5 engine driven system.

2.5.5 Electronics

Three types of sensors are used in the control system; position, rate, and acceleration. The position sensors consist of both a.c. and d.c. types. The d.c. sensors are conductive plastic potentiometers used for indication of evaluation pilot's control position and control surface position. The a.c. position sensor is a Linear Variable Differential Transformer used for sensing auxiliary actuator position in the control actuators.

The rate sensors are miniature rate gyros in two ranges: 0-20 deg/sec and 40 deg/sec. The high range gyros were used for sensing aircraft roll rates.

The acceleration sensors are linear accelerometers used for monitoring aircraft structural and normal accelerations.

The interface electronics comprise the major portion of the control system electrical/electronics installation. All control signal paths pass through some segment of this system. Safety monitor, system engagement control functions, and inflight data monitoring are all part of the interface electronics.

An interpatch panel, consisting of a removable patchboard and a mating base panel, receives all flight control loop input and output signals and allows desired routing of these signals.

The safety monitor system detects deviation in output signals with preset signal levels and disengages the control system when the preset signal levels are exceeded. In addition, the safety monitor provides a visual warning indicator panel for the test engineer to monitor the cause of the system disengagement.

An engage control panel allows the pilot to select the control mode desired for a particular flight condition. A slow turn on system is incorporated in the engage system to prevent large engage transients. Lamp indicators are available to the pilot, co-pilot, and test engineer for monitoring system status.

The test engineer's station has a direct writing oscillograph and associated switching panel, an oscilloscope, and aileron and spoiler position indicators for inflight data monitoring. The pilot is provided seven special instruments for in-flight data monitoring. Included in these are rudder and elevator position and normal acceleration at the cg.

The fly-by-wire system is a three axis system using electrical input capabilities of the hydraulic actuator packages.

The evaluation pilot's column, wheel, and rudder pedals are disconnected from the normal control cables and connected to springs for centering and force gradient control. Position transmitters are installed to electrically indicate the position of the controls. The position transmitter output signals are conditioned in the interface electronics and used for control surface actuator electrical inputs.

Two analog computers are installed in the test engineer's station. These units are slaved together and used for control signal conditions and to allow control system flexibility.

The LAMS computer is the main component in the LAMS-FCS. The function of the LAMS computer is to provide analog signal blending and filtering of control system signals.

3.0 SYSTEM DEFINITION

3.1 Introduction

This section of the report contains the analyses conducted in defining and synthesizing the Baseline SAS and LAMS-FCS. A description of the B-52 mathematical model utilized in the LAMS program analyses is presented in Section 3.2. Simplified math models used for individual design, synthesis, and evaluation studies are also presented. The LAMS Baseline SAS design analyses and the Baseline SAS description are presented in Sections 3.3 and 3.4, respectively. The LAMS-FCS design analyses are discussed in Section 3.5 and the resulting LAMS-FCS design is presented in Section 3.6. Several final system design evaluation studies were conducted for the basic aircraft, Baseline SAS, and LAMS-FCS configurations and are described in Section 3.7. The LAMS-FCS spoiler loop was modified when flight demonstration data indicated the initial design had less than optimum performance. The design modifications techniques are outlined in Section 3.8.

3.2 Mathematical Description of the LAMS B-52

The design and theoretical performance analysis of the LAMS-FCS were based upon the mathematical model of the LAMS B-52 described in this section. The mathematical form of the equations of motion and the idealizations required to describe the structure and aerodynamic loading are presented. Simplifications and approximations made to expedite specialized analyses are noted.

3.2.1 Aircraft Equations of Motion

The aircraft equations of motion were written in the following form:

$$\begin{aligned} & [C_1] \left[\ddot{q}(t) \right] + [C_2] \left[\dot{q}(t) \right] + [C_3] \left[q(t) \right] + [C_4] \left[\dot{K}(t) * \dot{q}(t) \right] \\ & + [C_5] \left[\dot{K}(t) * q(t) \right] + [C_6] \left[\dot{\psi}(t) * v_g(t-\tau_1) \right] \\ & + [C_7] \left[\dot{\psi}(t) * w_g(t-\tau_1) \right] + [C_8] \left[\dot{\psi}(t) * p_g(t-\tau_1) \right] = [0] \end{aligned}$$

where:

$[q(t)]$ are the generalized coordinates representing rigid body motions, control surface motion, and elastic modes (actuator and SAS freedoms were added as required).

$K(t)$ is Wagner's lift growth function.

$\psi(t)$ is Kussner's lift growth function.

$v_g(t)$ is the lateral gust velocity at the gust probe.

$w_g(t)$ is the vertical gust velocity at the gust probe.

$p_g(t)$ is the roll gust angular velocity at the gust probe.

τ_i is the gradual penetration time lag for each aerodynamic panel.

$[C_1] \dots [C_8]$ are coefficient matrices, constant for a specified fuel loading, speed and altitude.

For convenience in taking the Laplace transform of the equations of motion, the following Wagner and Kussner lift growth function approximations were used:

$$K(t) \approx 1 - .165 \exp\left(-.0455 \frac{Vt}{b_r}\right) - .335 \exp\left(-.3 \frac{Vt}{b_r}\right)$$

$$\psi(t) \approx 1 - .5 \exp\left(-.13 \frac{Vt}{b_r}\right) - .5 \exp\left(-1.0 \frac{Vt}{b_r}\right)$$

where:

V = aircraft velocity

b_r = reference semi-chord (130 inches).

The equations of motion shown above include both the symmetric (longitudinal) and the antisymmetric (lateral-directional) degrees-of-freedom. However, the symmetric and antisymmetric degrees-of-freedom were considered independently and were analyzed separately.

Structural bending and torsional moments and shears were found after solution of the equations of motion by adding the airload panel contributions to the mass panel inertia loads (load summation method).

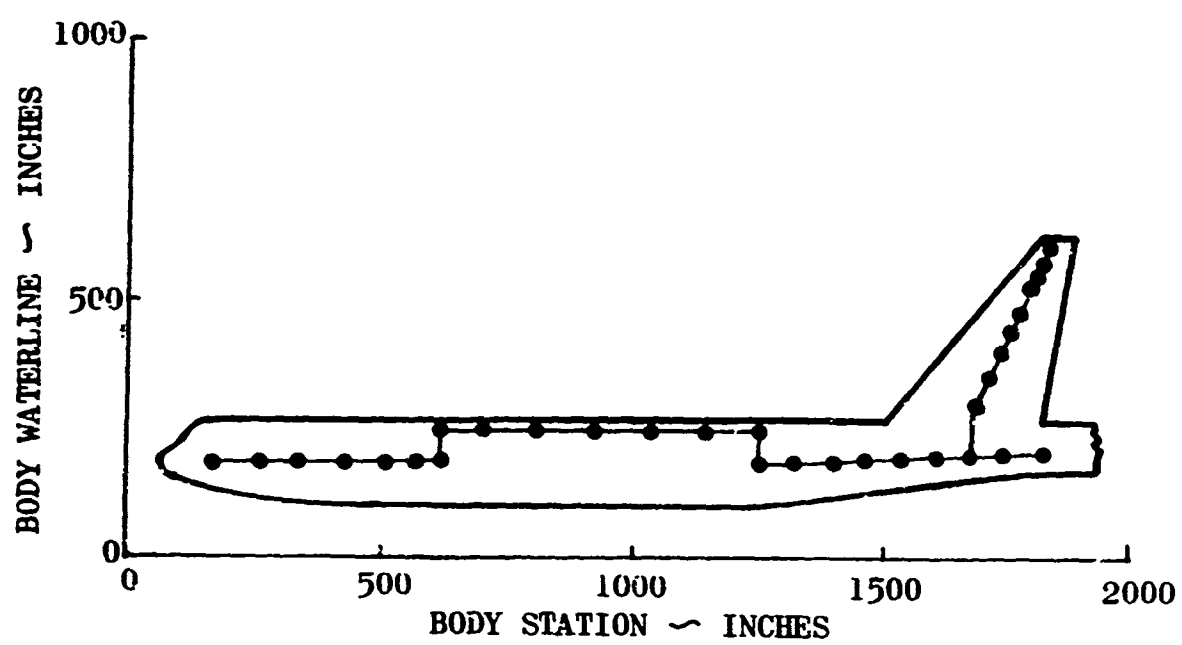
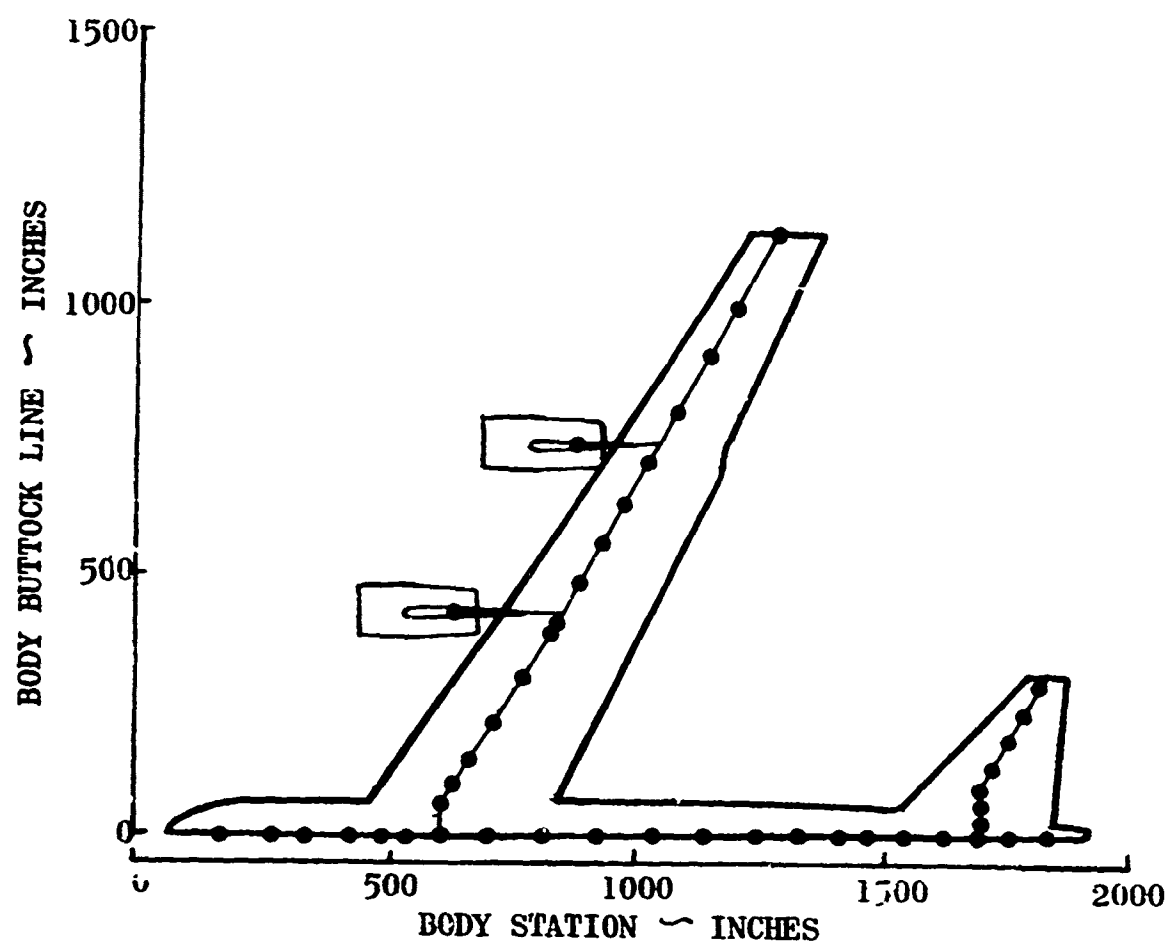
Descriptions of the structural model and aerodynamic assumptions used to obtain the equations of motion are given in the following paragraphs.

3.2.2 Structural Idealization

The B-52 elastic and inertia characteristics were idealized in two stages:

- Lumped parameter idealization
- Free vibration mode idealization

The lumped parameter idealization resulted in a model as shown in Figure 13. Inertia properties (mass, static moments, moments of inertia) were lumped at the structural nodes shown. The nodes were connected by one dimensional (elastic axis) members. Each node on the wing, fuselage, or nacelle struts had five degrees-of-freedom in its local axis system; the segments were assumed rigid only for axial loading. Each node on the horizontal or vertical tail had three degrees-of-freedom. These segments were assumed rigid for fore and aft loading and axial loading.



LUMPED PARAMETRIC STRUCTURAL IDEALIZATION

FIGURE 13

Vibration modes were then computed for the unrestrained aircraft using the lumped parameter model. The modal idealization of the structure restricted the elastic motions of the aircraft to those which could be obtained from linear superposition of the selected vibration mode shapes. Fifty-nine vibration modes (30 symmetric and 29 antisymmetric) were selected as elastic degrees-of-freedom for the basic equations of aircraft motion. Natural frequencies for those modes ranged from 0.8 cps to 33 cps.

3.2.3 Aerodynamic Loading

The airloads on the aircraft were idealized in terms of finite area aerodynamic panels, as shown in Figure 14. A preliminary calculation gave the unsteady aerodynamic loads on each panel from two-dimensional incompressible theory. Then the circulatory part of the airloads was modified to account for coupling of the aerodynamic panels using an aerodynamic influence matrix. That matrix was computed, assuming a static Weissinger discrete vortex sheet, with modifications to the section lift curve slope to account for experimentally measured pressure fluctuations near the fuselage and engine nacelles. Fuselage panel airloads were based on experimental data and were not coupled. Experimental compressibility (Mach number) correction factors were applied separately to the wing, body, stabilizer, fin, and each control surface. Control surface aerodynamics were further modified to match test data for hinge-moments and center of pressure.

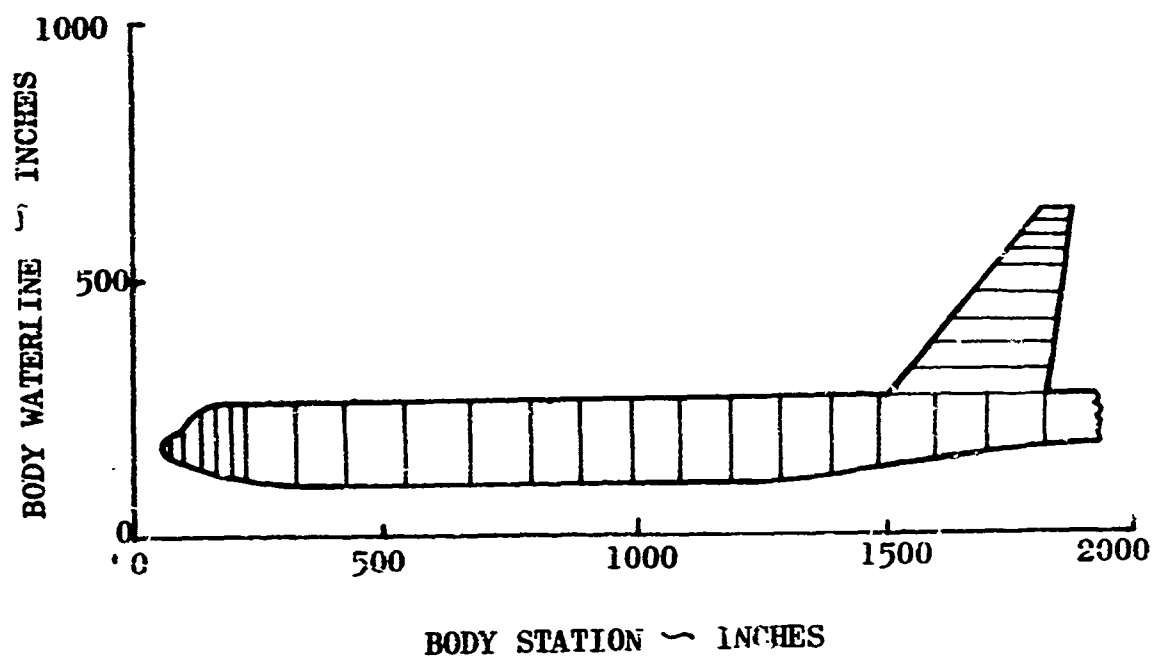
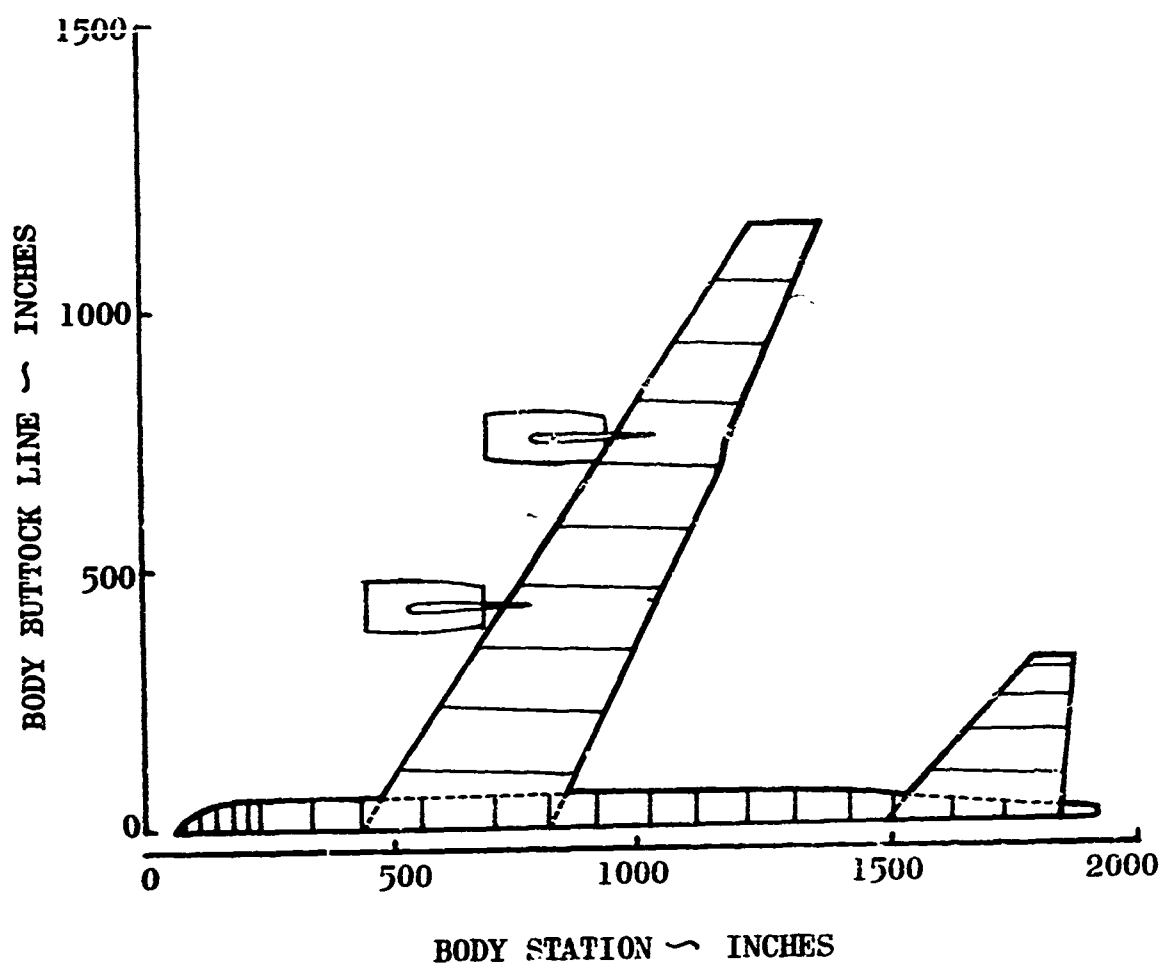
Additional modifications were made to the lateral-directional parts of the equations of motion to assure correct Dutch roll performance of the mathematical model. The most important change of this type was the addition of lift on the wing due to sideslip which provides the primary contribution to " $C_{l\beta}$ " (rolling moment due to sideslip) for the B-52.

The above "experimental corrections" were small with the exceptions of control surface effectiveness at high Mach numbers, hinge moment data, and lateral derivatives depending upon symmetric angle of attack. A purely theoretical aerodynamic analysis with conventional lateral derivative corrections would yield essentially the same results.

The panel airloads were used directly for computing structural loads. For the equations of motion, generalized airloads were found from a matrix expression of the external work done on the aircraft by the airloads using vibration mode shapes as elastic degrees-of-freedom.

3.2.4 Simplified Mathematical Model

The complete mathematical model, 30 symmetric and 29 antisymmetric elastic modes, as shown in Table II through V, was used for structural performance evaluation and stability margin analyses. Smaller, simplified mathematical models, which contained fewer elastic modes, were used advantageously throughout the program. Their use not only reduced computer requirements, but provided the designer with a convenient tool for specialized analyses.



AERODYNAMIC PANELS

FIGURE 14

TABLE II
SYMMETRIC ANALYSIS DEGREES OF FREEDOM

MODE NO.	350 KIP		270 KIP		
	FREQ. Hz	MODE DESCRIPTION	FREQ. Hz	MODE DESCRIPTION	
	-	Rigid Body Vert.	-	Rigid Body Vert.	
	-	Rigid Body Pitch	-	Rigid Body Pitch	
1	.85	WG	.89	WG	
2	1.80	ON-WG	1.82	ON-WG	
3	2.01	IN	2.01	IN	
4	2.19	ON-WG	2.21	ON-WG	
5	2.34	WG-AB	2.41	WG-AB	
6	2.62	AB-WG	2.76	AB-WG	
7	3.13	WG-IN-AB	3.13	WG-IN-AB	
8	3.45	WG-AB	3.85	WG-AB	
9	5.35	WG-FB	5.55	WG-ON	
10	5.80	ON	5.98	IN-ON	
11	5.99	IN	6.01	IN-ON	
12	6.44	WG-ON	6.80	WG-ON-FB	
13	7.55	HT	7.59	HT	
14	9.09	WG	9.25	WG	
15	9.61	AB-WG	10.28	WG	
16	10.11	WG	10.41	AB-WG-FB	
17	10.71	ON-WG	11.10	WG-AB-ON	
18	13.53	AB-WG	14.02	WG-AB	
19	14.52	WG	14.72	WG	
20	15.13	WG-HT	15.76	HT	
21	16.21	HT	17.09	HT-WG	
22	18.20	HT-AB-WG	18.74	WG	
23	18.94	WG	19.43	WG	
24	19.51	WG	20.50	HT-WG-AB	
25	21.58	HT	21.70	HT	
26	22.20	WT-WG	23.21	HT-WG	
27	24.39	HT	24.40	HT	
28	24.57	HT	27.86	AB	
29	31.34	WG	31.78	WG	
30	31.92	WG	32.88	HT	

Actuator and Control Surface Dynamics
SAS degrees-of-freedom
Wagner and Kussner lift growth

Component Abbreviations: AB - Aft Body
FB - Forward Body
WG - Wing
HT - Horizontal Tail
VT - Vertical Tail
IN - Inboard Nacelle
ON - Outboard Nacelle

TABLE III

SYMMETRIC ANALYSIS DEGREES OF FREEDOM

241 KIP			222 KIP	
MODE NO.	FREQ. Hz	MODE DESCRIPTION	FREQ. Hz	MODE DESCRIPTION
-	-	Rigid Body Vert.	-	Rigid Body Vert.
-	-	Rigid Body Pitch	-	Rigid Body Pitch
1	1.00	WG	1.04	WG
2	1.86	WG-ON	1.88	WG
3	2.02	IN	2.02	WG-ON
4	2.24	WG-ON	2.25	WG-IN
5	2.67	AB-WG	2.77	WG-AB
6	2.90	WG-AB	3.02	AB-WG
7	3.14	WG-IN-AB	3.15	WG-AB
8	3.98	WG-AB	4.25	WG-AB
9	5.80	ON-WG	5.82	ON
10	6.00	IN	6.00	IN
11	6.15	ON-WG-HT	6.23	WG-AB
12	7.22	WG-HT	7.35	WG-AB-HT
13	7.61	HT	7.62	HT-AB
14	9.65	WG	10.18	WG
15	10.57	WG-AB	10.76	AB-WG
16	10.99	WG-AB-FB	11.44	WG-AB-FB
17	11.52	WG-ON-AB	12.13	WG
18	14.44	WG-AB	14.47	WG-AB-FB
19	15.41	HT	15.58	WG-AB-HT
20	16.08	HT-WG	16.42	HT-WG
21	17.42	HT-WG	17.98	WG-HT
22	19.83	WG	20.14	WG-AB-HT
23	20.31	WG	21.13	WG-HT
24	21.06	HT-WG	21.50	HT-WG
25	21.98	HT	22.28	HT

Actuator and Control Surface Dynamics
SAS Degrees-of-Freedom

Component Abbreviations: AB - Aft Body
FB - Forward Body
WG - Wing
HT - Horizontal Tail
VT - Vertical Tail
IN - Inboard Nacelle
ON - Outboard Nacelle

TABLE IV

ANTI-SYMMETRIC ANALYSIS DEGREES OF FREEDOM

350 KIP			270 KIP	
MODE NO.	FREQ. Hz	MODE DESCRIPTION	FREQ. Hz	MODE DESCRIPTION
	-	Rigid Body Lateral	-	Rigid Body Lateral
	-	Rigid Body Roll	-	Rigid Body Roll
	-	Rigid Body Yaw	-	Rigid Body Yaw
1	1.18	AB	1.19	AB
2	1.57	WG	1.58	WG
3	1.95	ON-WG	1.96	ON-WG
4	2.05	IN	2.06	IN
5	2.54	VT-WG	2.61	WG-VT
6	2.68	WG-VT	2.80	VT-WG
7	3.15	WG	3.16	WG
8	3.43	VT-WG	3.67	WG-FB
9	4.09	VT-FB	4.35	VT-FB
10	5.02	WG-VT	5.06	WG-VT
11	5.85	IN-VT	5.87	IN-VT
12	5.92	VT	5.93	VT
13	5.95	VT-ON	5.96	ON-VT
14	6.29	VT-IN	6.60	VT-IN
15	6.92	HT-VT	7.30	VT-HT
16	7.97	WG	8.32	WG
17	9.37	HT-VT	10.65	ON-WG
18	10.64	ON-WG	10.90	VT
19	11.17	VT	11.59	VT-WG
20	11.61	WG-FB	12.92	VT-AB
21	13.11	VT	13.68	WG
22	13.46	AB-HT	14.28	VT
23	13.63	WG-FB	14.46	VT-WG
24	14.42	WG	14.86	VT
25	15.63	VT	16.20	VT
26	15.95	VT	16.75	VT-HT
27	16.66	VT-HT	18.18	VT
28	18.22	VT	18.42	VT
29	18.26	VT	19.21	VT-HT

Actuator and control surface dynamics

SAS degrees-of-freedom

Wagner and Kussner lift growth

Airplane Components are abbreviated as follows:

FB - Forward Body

AB - Aft Body

WG - Wing

HT - Horizontal Tail

VT - Vertical Tail

IN - Inboard Nacelle

ON - Outboard Nacelle

TABLE V
ANTI-SYMMETRIC ANALYSIS DEGREES OF FREEDOM

241 KIP			222 KIP	
MODE NO.	FREQ. Hz	MODE DESCRIPTION	FREQ. Hz	MODE DESCRIPTION
	-	Rigid Body Yaw	-	Rigid Body Yaw
1	1.23	AB	1.26	AB
2	1.72	WG	1.73	WG
3	1.99	ON-WG	2.02	IN
4	2.07	IN	2.08	IN
5	2.64	WG-VT	2.65	WG-VT
6	2.81	VT-WG	2.82	VT
7	3.22	WG	3.39	WG
8	3.75	WG-FB	3.77	FB-VT-WG
9	4.39	VT-FB	4.42	VT-FB
10	5.50	WG	5.71	VT-WG
11	5.93	VT	5.94	VT
12	5.95	VT	5.98	ON
13	5.97	ON	6.01	VT
14	6.87	VT-HT	6.94	VT-HT
15	7.50	VT-HT	7.63	VT-HT
16	9.25	WG	9.89	WG
17	10.95	VT	11.02	VT-HT
18	11.10	WG-VT	11.48	WG
19	11.96	VT-FB	12.31	FB
20	12.93	VT-AB	12.94	VT
21	14.29	VT	14.34	VT
22	14.74	WG-VT	14.91	WG
23	15.14	VT-WG	15.80	VT
24	15.56	WG-VT-HT	16.10	VT-HT-WG
25	16.23	VT-HT	16.29	VT
26	16.77	VT-HT	16.80	VT
27	18.23	VT	18.24	VT

Actuator and control surface dynamics
SAS degrees-of-freedom

Component Abbreviations: AB - Aft Body
FB - Forward Body
WG - Wing
HT - Horizontal Tail
VT - Vertical Tail
IN - Inboard Nacelle
ON - Outboard Nacelle

The simplified models are derivatives of the complete models and are summarized below. In general, all of the simplified model gust penetration lags were reduced to three. The three lags consisted of: one for the in-board wing and forward fuselage, the second for the outboard wing and aft fuselage, and the third for the empennage. The simplified models used are as follows:

Baseline SAS Design and Stability Analysis Model

- 14 degrees-of-freedom longitudinal axis (2 rigid body and first 12 structural modes)
- 14 degrees-of-freedom lateral-directional axes (3 rigid body and first 11 structural modes)
- 4th order actuator model
- Wagner lift growth functions

IAMS-FCS Basic Aircraft Studies Model

- 16 degrees-of-freedom longitudinal axis (2 rigid body and first 14 structural modes)
- 14 degrees-of-freedom lateral-directional axes (3 rigid body and first 11 structural modes)

IAMS-FCS Gust Alleviation Studies Model

- 2 degrees-of-freedom longitudinal axis (rigid body modes)
- 1st order actuator dynamics

IAMS-FCS Optimal Control Derivation Model

- 5 degrees-of-freedom longitudinal axis (2 rigid body and first, second, and sixth structural modes)
- 5 degrees-of-freedom lateral-directional axes (3 rigid body and first, eighth, and ninth structural modes)
- First order actuator dynamics
- Wagner lift growth functions

IAMS-FCS Controller Synthesis and Performance Sensitivity (Analog Computer Model)

- 8 degrees-of-freedom longitudinal axis (2 rigid body and first, second, fourth, fifth, sixth, and eighth structural modes)
- 8 degrees-of-freedom lateral-directional axes (3 rigid body and first, second, fifth, eighth, and ninth structural modes)

- Second order actuator dynamics
- Wagner lift growth functions

In addition to the above, the sensitivity analysis included:

- Gyro limits, actuator limits, and internal system signal path limits
- Actuator hysteresis

IAMS-FCS Initial Structural Performance and Stability Analysis Model

- 16 degrees-of-freedom longitudinal axis (2 rigid body and first 14 structural modes)
- 14 degrees-of-freedom lateral-directional axes (3 rigid body and first 11 structural modes)
- 3rd order actuator dynamics

(stability analysis only)

- Wagner lift growth functions

Handling Qualities Studies (Analog Computer Simulation)

- 3 degrees-of-freedom longitudinal axis (rigid body quasi-elastic)
- 3 degrees-of-freedom lateral-directional axes (rigid body quasi-elastic)
- 3rd order actuator dynamics
- Actuator and control input limits
- Spoiler nonlinear gains

IAMS-FCS Final Stability Analysis

- 24 degrees-of-freedom longitudinal axis (2 rigid body and first 22 structural modes)
- 24 degrees-of-freedom lateral-directional axes (3 rigid body and first 21 structural modes)
- 4th order actuator dynamics
- 2nd order sensor dynamics
- Wagner lift growth function

Flutter Analysis Models

- These analyses used the mathematical models described in Section 3.7.1.2 based on the degrees-of-freedom contained in Tables II through V.

Final Systems Structural Performance Evaluation Model

(Used entire math model as described in Section 3.2.1)

3.3 Baseline SAS Design Analysis

The general Baseline SAS design criteria states that the Baseline SAS will:

- Be representative of conventional stability augmentation systems
- Not significantly disturb or control aircraft structural modes
- Provide stability augmentation to the three aircraft axes
- Retain or improve handling qualities
- Have a minimum of 10 db gain margin and 60 degree phase margin for all structural modes

Design synthesis for the Baseline SAS primarily utilized gain and phase root loci techniques; supporting design analyses used frequency response techniques.

Stability analyses were conducted using gain and phase root loci as well as frequency response techniques. Handling qualities were evaluated using time history response of the rigid body dynamics. All of the techniques described above are accomplished with digital computer programs.

The initial LAMS B-52 test vehicle configuration included spoilers flown in the zero airbrake position. Subsequently, the configuration was modified to fly the outboard two spoiler panels on each wing at a 15 degree biased position to accommodate the LAMS-FCS design. The Baseline SAS was designed for the initial test vehicle configuration and was not modified as a function of the altered test vehicle configuration since the biased spoiler configuration would not materially affect the results.

Stability margins for the 15 degree bias spoiler configuration were calculated for flight condition 1 and no significant effects were observed.

3.4 Baseline SAS Description

The Baseline SAS is a three axes aircraft flight control system. The system design accommodates operation of each axis independently or any combination of the three axes. The system is described in the following paragraphs as a longitudinal axis system and a lateral-directional axis system.

3.4.1 Longitudinal Axis (Symmetric)

The primary function of the Baseline longitudinal SAS is to augment damping of the short period mode. Figure 4 shows the system block diagram and contains the gain schedule for the three LAMS flight conditions. The SAS augments short period damping with a pitch rate feedback signal driving a hydraulically powered elevator. Pitch rate is obtained from a rate gyro located at Body Station 820. An electronic filter shapes the feedback signal to ensure stability and obtain desired handling qualities. This filter includes two networks. The washout network $\frac{s}{(s + .75)}$, reduces the SAS re-

sponse to low frequency pilot commands and the rolloff network $\frac{1}{(s + 15)^2}$, attenuates structural mode feedback. Thus, the electronic filter rejects feedback signals generated by the pilot or the structural modes and accepts only the signal generated by the aircraft short period mode.

3.4.2 Lateral-Directional Axis (Antisymmetric)

The Baseline Lateral-Directional SAS design and gain schedule are presented in the block diagram of Figure 5. This block diagram includes a Baseline roll SAS, a Baseline yaw SAS, and an aircraft dynamics block which includes coupling effects between the roll and yaw systems. Also included are spoiler contributions to the system and the evaluation pilot's inputs.

This Baseline roll SAS design improves roll response of the aircraft to the evaluation pilot's wheel command without decreasing steady-state roll rate capability of the aircraft by more than 10 percent. A feedback loop decreases the roll time constant by sensing roll rate with a rate gyro located at Body Station 820. The gyro signal, with proper shaping and gain (K_1), is fed into the aileron acutators.

Signal shaping is made up of two electronic filters. A notch filter placed in the forward path keeps the evaluation pilot's wheel command from exciting the second structural mode, which consists primarily of the wing vertical bending. A filter in the feedback path provides high frequency attenuation. This prevents the feedback signal from operating on the structural vibration modes. A forward gain (K) is also included in the Baseline roll SAS design to maintain the required steady-state roll rate level.

The Baseline roll SAS was designed to be used with the evaluation pilot only. No provisions were made to implement the change in forward gain (K) other than by electrical amplification of the fly-by-wire signal generated by the evaluation pilot's wheel command.

Improvement in roll response is obtained by aileron overshoot and therefore is not attainable for wheel commands large enough to saturate the ailerons. The minimum fraction of full wheel command that can begin to saturate the ailerons is equal to the reciprocal of the forward gain (K).

The Baseline yaw SAS increased Dutch roll damping with yaw rate feedback, utilizing a rate gyro located at Body Station 616. The rate gyro signal is shaped and fed to the rudder actuator. A washout term is included in the shaping network to prevent the rudder from opposing the evaluation pilot and monitor pilot commands during turns. High frequencies are attenuated with a roll off term to eliminate structural mode feedback.

Coupling between the roll and yaw systems was not of major concern during the Baseline SAS design, but the SAS does reduce coupling effects. Roll rate response resulting from a wheel command contains a Dutch roll component which the Baseline SAS damps; thus, the roll rate component attributable to aircraft sideslip is reduced.

3.5 IAMS-FCS Design Analysis

The suggested general design criteria for the IAMS-FCS require that the system:

- Retain or improve the existing aircraft handling qualities.
- Have a minimum of 10 db gain margin and 60 degree phase margin for all rigid body and structural modes.
- Provide measurable improvement in terms of fatigue damage or maximum expected loads.

The segments of the design process were categorized as basic aircraft studies, gust alleviation studies, optimal control theory design, and system simplification synthesis. These analyses used the math models described in Section 3.2.4.

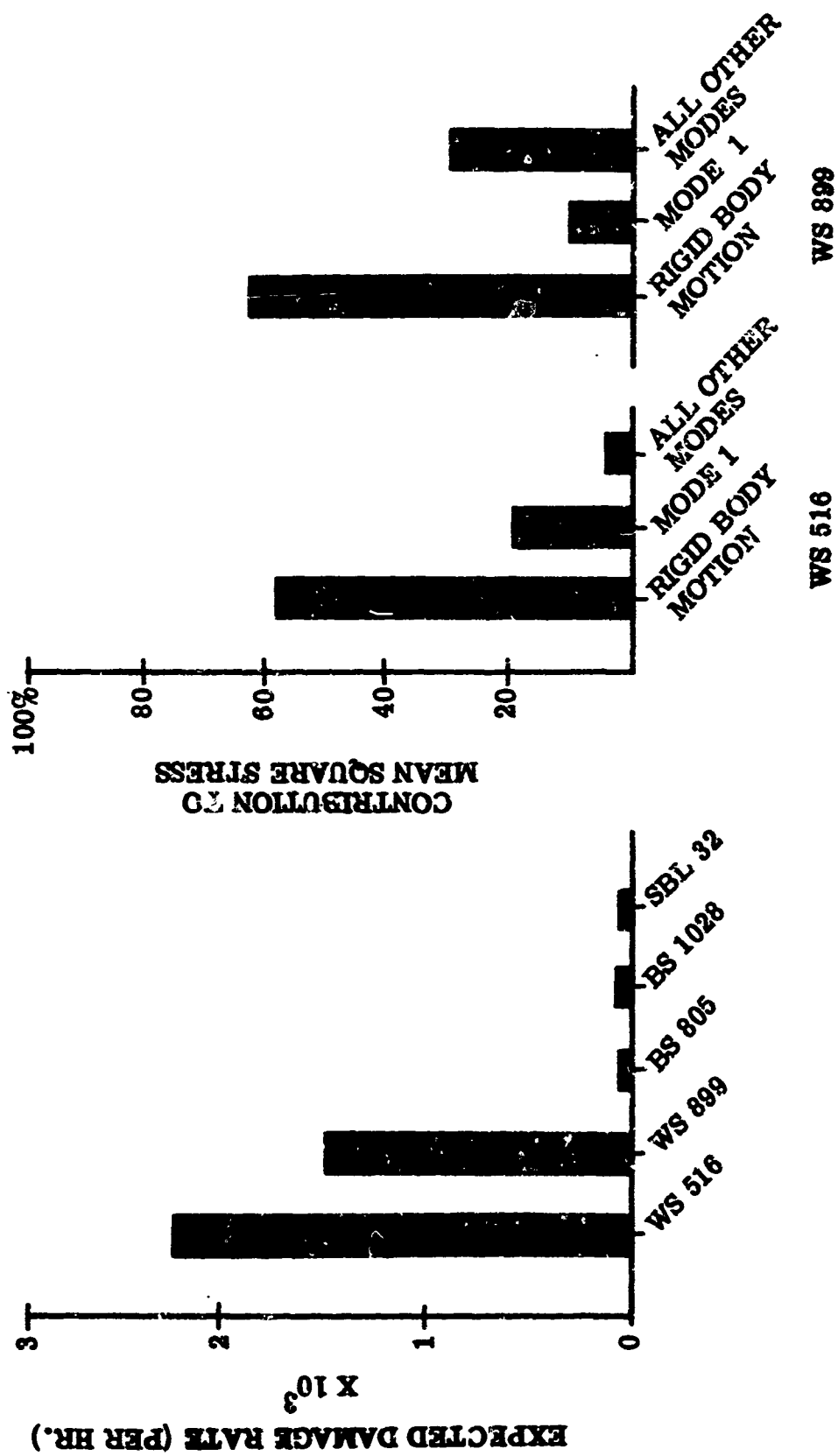
3.5.1 Basic Aircraft Studies

The basic aircraft study validated the computational program used by Boeing and Honeywell. This was accomplished by comparing free aircraft data. In addition, this study suggested the relationship of both rigid body and structural modes to fatigue damage rate and to local accelerations at the pilot's station.

3.5.1.1 Controls Locked Fatigue Damage Calculations

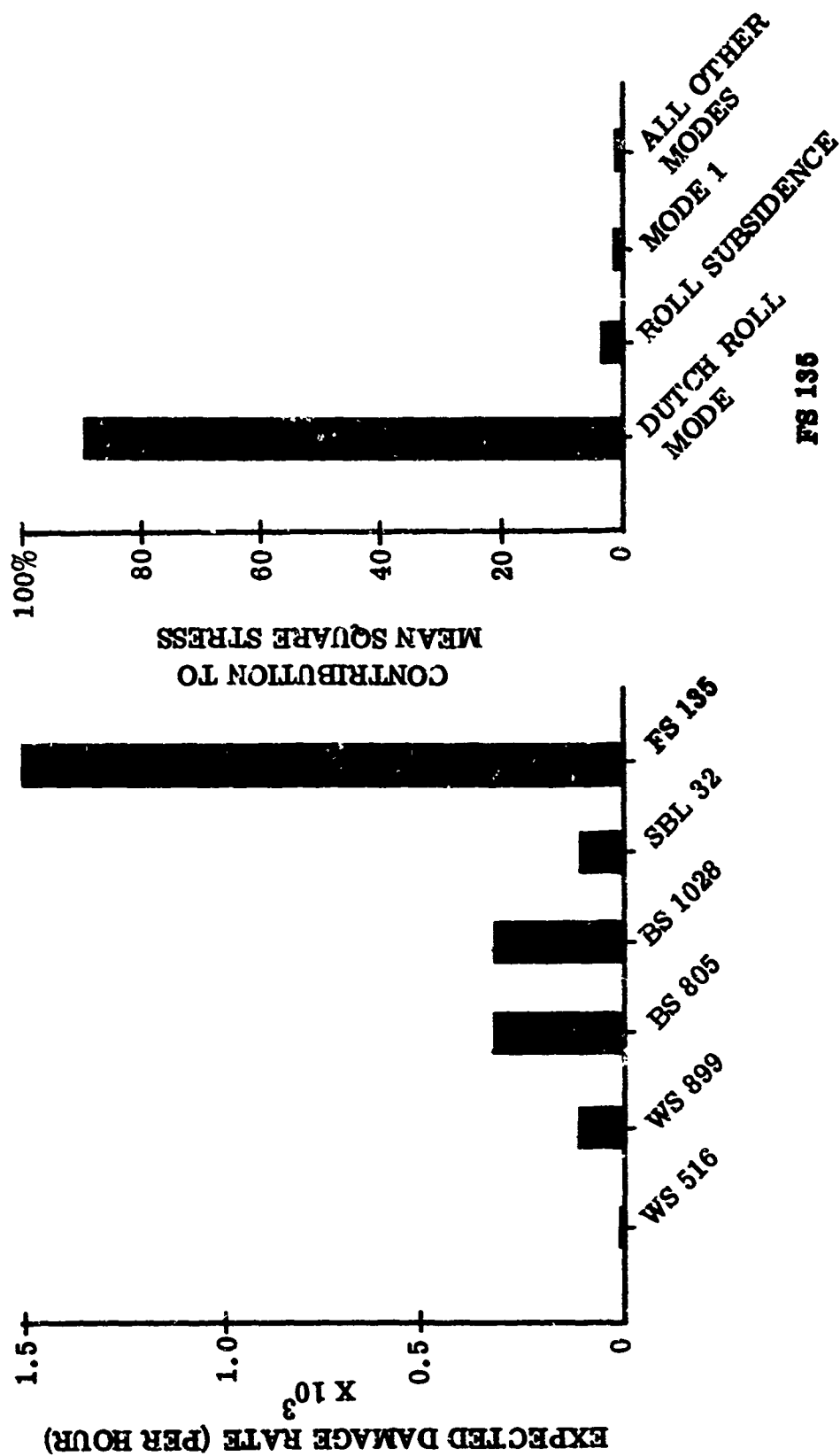
RMS stress and stress rate calculations are based on the application of residue theory to the stress or stress rate per RMS gust transfer functions. These transfer functions are formed from a linear combination of moment to RMS gust transfer functions and appended with the turbulence model transfer function. Fatigue damage rate calculations are derived from the Minor hypothesis.

The computer programs for calculating RMS stresses, RMS stress rates, RMS accelerations, and fatigue damage rates were verified by Honeywell by computing check data for the free aircraft configuration to compare with similar data computed at Boeing-Wichita. Figures 15 and 16 present the relative mode contribution to the total mean square stress and the relative expected fatigue damage rates at each of the critical stress



LONGITUDINAL FREE AIRCRAFT DAMAGE CALCULATIONS

FIGURE 15



LATERAL FREE AIRCRAFT DAMAGE CALCULATIONS

FIGURE 16

locations that were evaluated. The relative mode contributions were based on ranking of the residues associated with the second order complex structural mode roots.

3.5.1.2 Artificial Damping Studies

The objective of this study was to determine how damping the structural modes altered the damage rate. Mode damping was accomplished by altering the uncoupled mode damping ratio. The modal pole and zero both undergo translation, since modifying the free vibration mode damping values will effect the numerator and denominator roots of the stress and stress rate per RMS gust transfer functions. The study used flight condition 1 longitudinal and lateral data without transport delays.

For the longitudinal axis, uncoupled damping was increased by a factor of two and then four over nominal for structural modes 1 through 6. The only significant change in damage rate results from a modification of structural mode 1 damping. Doubling the uncoupled damping of structural mode 1 decreases the damage rate of Wing Station 516 by 26 percent while increasing the damage rate at Wing Station 899 by 23 percent. Additional structural mode 1 damping increases the damage at Wing Station 516. The only significant reduction in RMS acceleration resulted when structural mode 6 damping was increased to four times nominal. For this condition, the acceleration decreased from 0.0156 g to 0.0125 g RMS. Figure 17 shows results of the artificial damping study for the longitudinal axis.

Similarly, for the lateral axis, the uncoupled damping ratio was first doubled and then increased by a factor of four. The first five structural modes were artificially damped for this axis. The results indicate that only by damping structural mode 5 can any appreciable improvement in location FS 135 fatigue damage be obtained. Increasing the damping of structural mode 1 by a factor of four reduced the pilot's lateral acceleration from 0.0082 g RMS to 0.0051 g RMS.

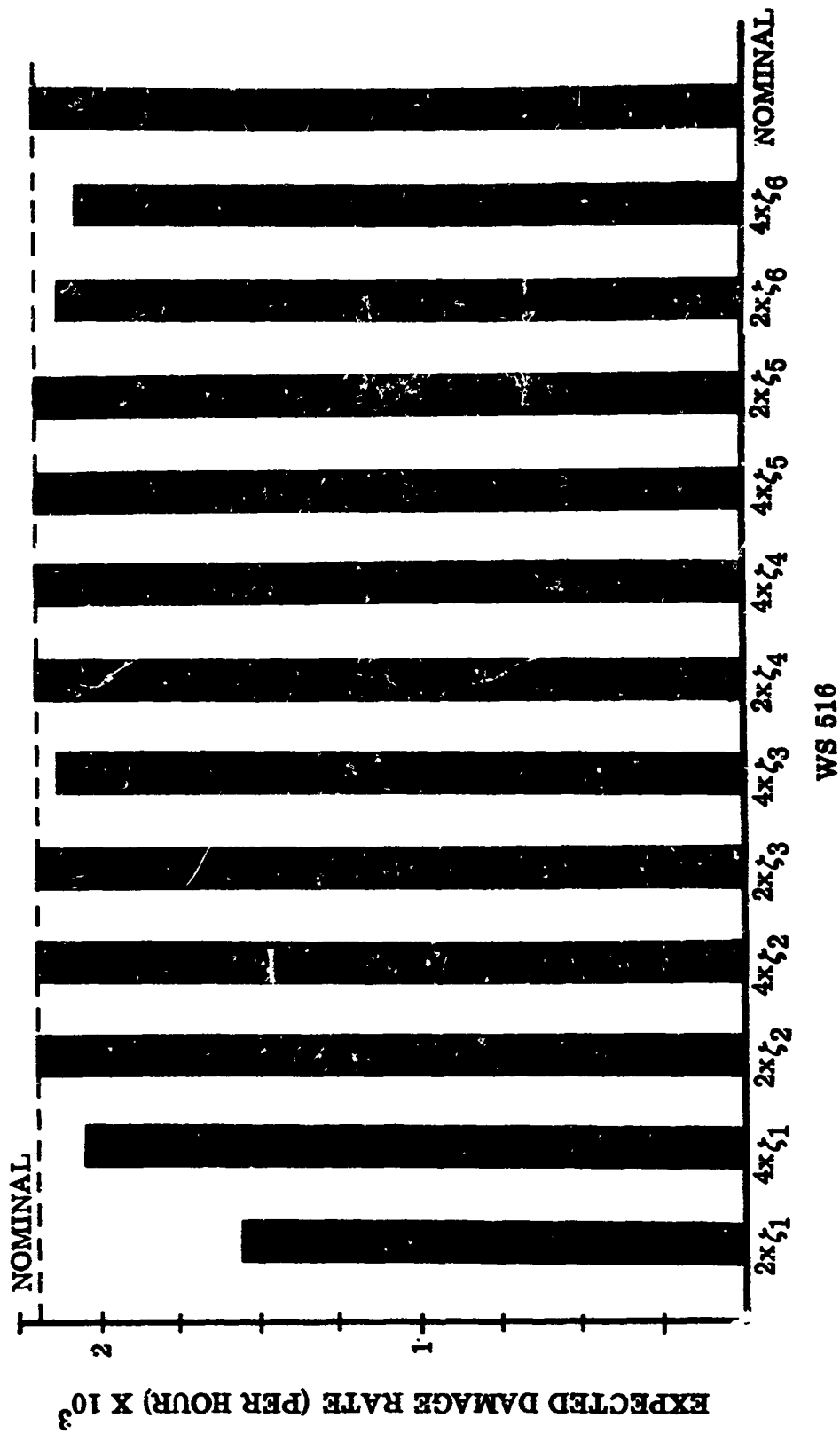
3.5.1.3 Uncoupled Mode Investigation

By uncoupling the equations of motion, the natural frequencies, damping ratios, and importance of forcing functions may easily be determined. The uncoupled natural frequency and damping ratio of all symmetric and unsymmetric elastic modes were calculated and tabulated for flight condition 1.

The ratio of the control surface response to the gust response of a given elastic mode demonstrates to what extent the effects of the total response may be alleviated. From the uncoupled equations of motion, this ratio can be calculated for steady-state conditions.

3.5.2 Gust Alleviation Studies

Three preliminary gust alleviation concepts were synthesized. The first concept stabilizes rigid-body motion, the second concerns loads, and the third attempts to minimize wing fatigue. These alleviation concepts were evaluated by inspection and analog simulation. It became apparent from the other IAMS studies that the IAMS type problem had to be solved as an entirety which suggested the application of the optimal control theory.



LONGITUDINAL ARTIFICIAL DAMPING STUDY

FIGURE 17

Although it was apparent that they would not be used in the IAMS-FCS, the three gust alleviation concepts were evaluated to provide background information and insight to the system designer.

3.5.2.1 Center of Gravity Disturbance Alleviation

This concept attempts algebraic cancellation of gust forces with aileron and elevator controls. The required elevator and aileron gains are as follows:

$$\frac{\delta_e}{\dot{w}_g} = -.0735 \text{ deg/fps}$$

$$\frac{\delta_a}{\dot{w}_g} = +2.78 \text{ deg/fps}$$

A problem arises from this approach if vertical turbulence is sensed with a vane or gust probe. The system is destined to sense α feedback, as shown in Figure 18.

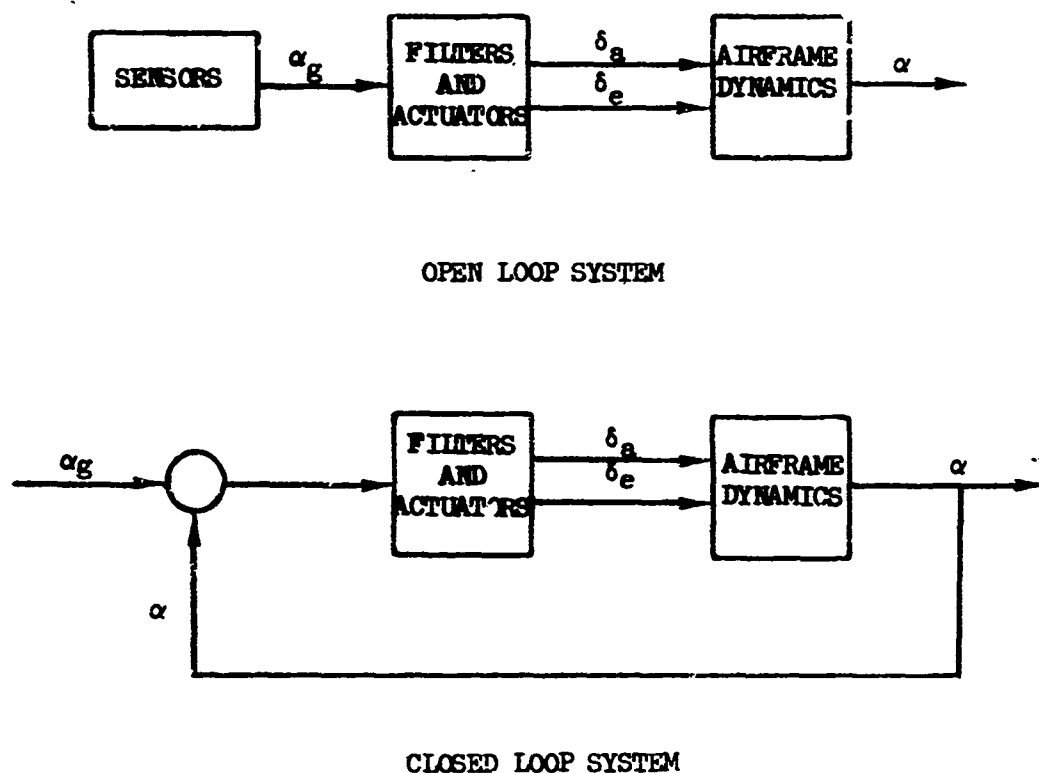


FIGURE 18

This closed loop system can be effective only if the feedback is high-pass filtered for frequencies above the short period natural frequency. This filtering though omits the most important portion of the gust spectrum for load alleviation. If filtering is neglected, airframe dynamics will be severely altered to the point of unacceptable handling qualities. Initially, this concept was considered to have the most promise for the B-52; however improved filtering and a scheme for deriving α_g would be needed for implementation. Had this concept been pursued, considerable design emphasis would have had to have been placed on handling qualities and aircraft structural mode stability.

3.5.2.2 Wing Stress Disturbance Alleviation Concept

This concept considered cancellation of loads with control surface activity to maintain minimum wing stress levels. This method calls for control surface activity far beyond realistic amplitude and rate values as noted below:

$$\frac{\delta_e}{\omega_g} = 8.47 \text{ deg/fps}$$

$$\frac{\delta_a}{\omega_g} = 17.55 \text{ deg/fps}$$

A supplementary approach which feeds back aircraft rigid-body motions and sensed turbulence also required unrealistic control surface activity. This method gives rise to undesirable handling qualities caused by exceptionally large pitch short-period natural frequency.

3.5.2.3 Wing Fatigue Disturbance Alleviation Concept

This concept attempts to hold wing stress rates at a minimum via cancellation of gust and gust rate induced loads with the aileron and elevator control surfaces. The required control surface activity was found to be:

$$\begin{bmatrix} \dot{\delta}_e \\ \dot{\delta}_a \end{bmatrix} = \begin{bmatrix} -27.1 & -5.03 \\ -54.1 & -11.82 \end{bmatrix} \begin{bmatrix} \delta_e \\ \delta_a \end{bmatrix} + \begin{bmatrix} -140 \\ -298.5 \end{bmatrix} \alpha_g + \begin{bmatrix} 91.6 \\ 191.6 \end{bmatrix} \dot{\alpha}_g$$

A supplemental system fed back aircraft rigid body motions as well. The controller equation was then:

$$\begin{bmatrix} \dot{\delta}_e \\ \dot{\delta}_a \end{bmatrix} = \begin{bmatrix} -140.0 & 77.1 \\ -298.5 & 160.0 \end{bmatrix} \begin{bmatrix} \alpha \\ \dot{\theta} \end{bmatrix} + \begin{bmatrix} -25.85 \\ -57.0 \end{bmatrix} \delta_e + \begin{bmatrix} -140.0 \\ -298.5 \end{bmatrix} \alpha_g + \begin{bmatrix} 91.6 \\ 191.6 \end{bmatrix} \dot{\alpha}_g$$

Both approaches created sluggish aircraft responses and the systems were marginally stable.

3.5.3 Optimal Control Theory

One goal of the LAMS study was to reduce fatigue damage rate and acceleration at the pilot's station through the use of automatic control. One technique for accomplishment of this goal is the use of optimal control theory. In this, the quadratic control problem was determining the linear feedback controller which minimized a scalar performance index of fatigue damage and acceleration.

Two measures of structural integrity were used in this program: an estimate of the likelihood of exceeding static ultimate strength and an estimate of fatigue lifetime. The lifetime of a single structural member is determined by the minimum value for this pair of measures. Since the aircraft is a multimember structure, its lifetime is the minimum of all members. Therefore, the structural performance goal of the control system is to increase this measure.

A mathematical property of optimal controllers permitted exclusion of handling qualities from initial design efforts. The property is that the quadratic-optimum controller, which minimizes the effects of disturbances, consists of a linear feedback controller and a linear feedforward controller (from the disturbance input), and the feedback controller is independent of the statistics of the disturbing input. This independence implies that one could initially design a feedback controller for structural integrity and ride qualities in gusts, and later design an input filter (for pilot stick commands) for good handling qualities. Therefore, handling qualities were not considered in the optimization formulation. The maximum structural integrity measure was formulated as a minimum cost function and the controller minimizing the quadratic cost function was found by a conventional Lagrange multiplier manipulation.

Digital programs were used in the iteration process necessary for obtaining final results. Detailed derivations of the performance measure and the optimal control law are presented in Appendix A and a description of the mathematical model used for the optimal control program is presented in Section 3.2.4.

3.5.4 Optimal Control Law Simplification

Optimization techniques resulted in control laws containing 81 gains in the longitudinal axis and 90 gains in the lateral-directional axis. Therefore, the control laws had to be simplified to lend themselves to a practical system design for implementation aboard the B-52 flight test vehicle.

The simplification techniques primarily utilized the analog computer simulation described in Section 3.2.4. The simplification procedure was an iterative method:

- Start with the free aircraft simulation
- Add one feedback from the control law
- Retain that feedback if the performance was beneficial
- If the performance was not beneficial, change the feedback sign and retain if beneficial
- If the performance was still not beneficial, discard that feedback
- Add another feedback and iterate the above procedure

After a simplified set of feedbacks were determined in this manner, additional iterations were accomplished for variations in feedback gains in an attempt to duplicate the original optimal control law performance.

Supporting digital computer analyses evaluated the simplified system stability and performance during the analog computer relative processes. Descriptions of the mathematical models used for the digital computer programs are presented in Section 3.2.4..

The LAMS longitudinal FCS was designed with the foregoing technique but repeated difficulty in attempts to simplify the Lateral-Directional optimal control law required a "start from scratch" analog computer design synthesis for the LAMS Lateral-Directional FCS. That procedure was similar to the one described above with the exception of having a control law as a guideline.

3.5.5. Sensor Blending Technique

The controller synthesis efforts determined the appropriate aircraft parameters to be used as feedbacks to the available control surfaces. Application of matrix inversion techniques then defined the sensor signal blending gains required to obtain the desired feedback parameters. As an example, the LAMS Longitudinal FCS required feedback signals of rigid body pitch rate ($\dot{\theta}$), structural mode 1 rate (\dot{q}_1) and structural mode 6 rate (\dot{q}_6). Three rate gyros were selected to derive the three rate feedback terms. Their location was chosen by judiciously observing the mode shape slopes of the fuselage and wing, see Figures 19 and 20. Observe that the sensor locations tend to maximize desired sensed parameters and minimize undesired sensed parameters within the constraints of required polarities.

Considering the rate gyro output signals to be functions of only the three desired parameters, $\dot{\theta}$, \dot{q}_1 , and \dot{q}_6 , the output signals may be expressed:

$$\begin{bmatrix} \text{rate gyro 1 output} \\ \text{rate gyro 2 output} \\ \text{rate gyro 3 output} \end{bmatrix} = \begin{bmatrix} a_{11} & a_{12} & a_{13} \\ a_{21} & a_{22} & a_{23} \\ a_{31} & a_{32} & a_{33} \end{bmatrix} \begin{bmatrix} \dot{\theta} \\ \dot{q}_1 \\ \dot{q}_6 \end{bmatrix}$$

$$\begin{bmatrix} \text{rate gyro 1 output} \\ \text{rate gyro 2 output} \\ \text{rate gyro 3 output} \end{bmatrix} = \begin{bmatrix} a \end{bmatrix} \begin{bmatrix} \dot{\theta} \\ \dot{q}_1 \\ \dot{q}_6 \end{bmatrix}$$

where a_{11} , a_{12} , etc. are the numerical modal coefficients from the mode shape curves. After pre-multiplying by the inverse of the matrix $\begin{bmatrix} a \end{bmatrix}$ the equation above becomes:

$$\begin{bmatrix} \dot{\theta} \\ \dot{q}_1 \\ \dot{q}_6 \end{bmatrix} = \begin{bmatrix} a \end{bmatrix}^{-1} \begin{bmatrix} \text{rate gyro 1 output} \\ \text{rate gyro 2 output} \\ \text{rate gyro 3 output} \end{bmatrix}$$

and the elements of $\begin{bmatrix} a \end{bmatrix}^{-1}$ are the required blender gains.

3.6 IAMS-FCS Description

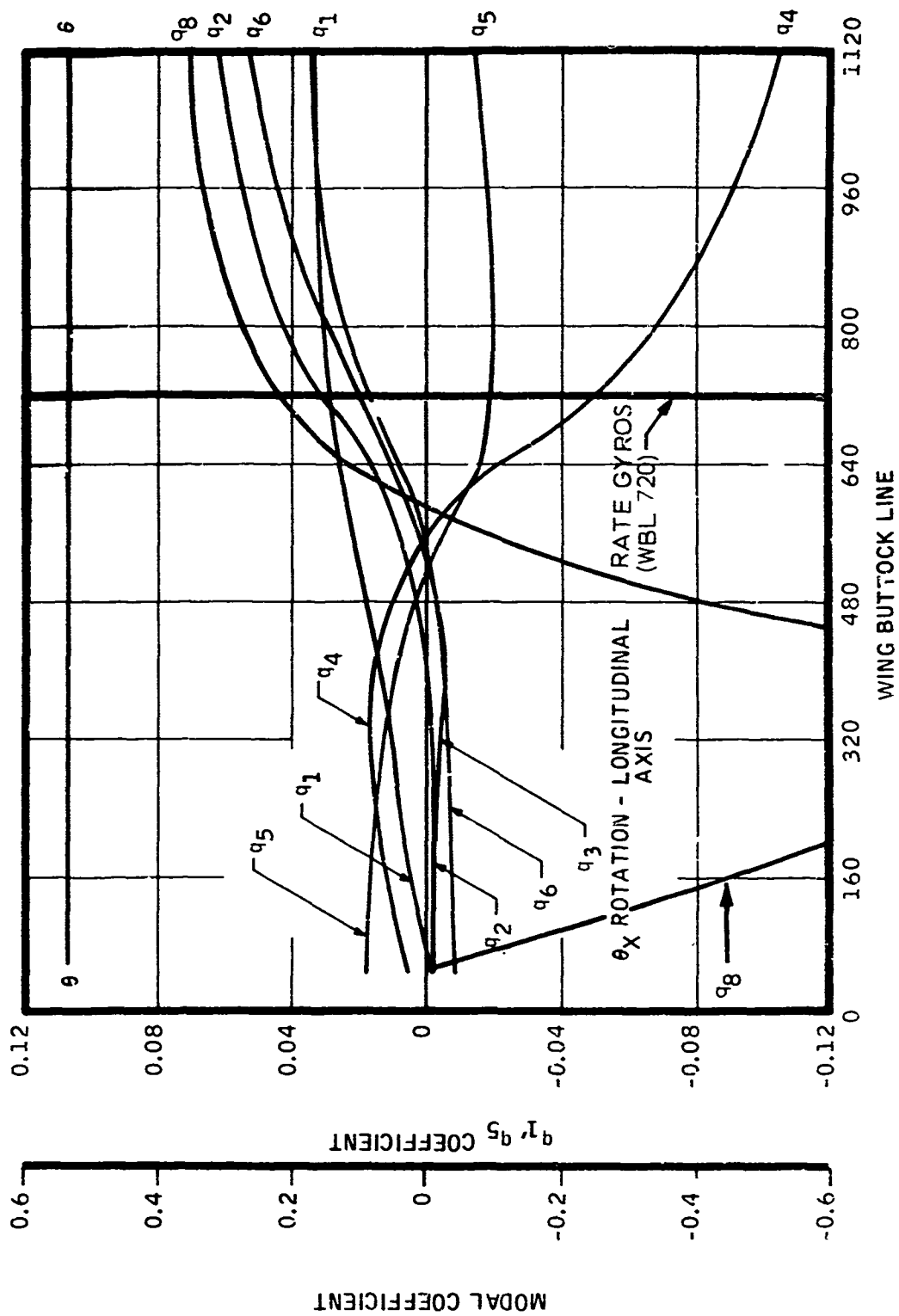
The preceding analyses resulted in the design of the IAMS Flight Control System. The Longitudinal-Axis is defined in paragraph 3.6.1 and the Lateral-Directional Axis in paragraph 3.6.2. The location of the 10 rate gyros used in the IAMS-FCS is shown in Figure 21.

3.6.1 Longitudinal Axis

Figure 6 shows the block diagram of the longitudinal axis FCS and the system gains for each flight condition. The $25/(25s+1)$ pseudo integrations of the sensed rate signals provide displacement signals for blending and shaping. The 25 second time constant was based on analog studies. A smaller time constant made the command response overdamped, whereas a larger time constant gave rise to extremely large settling times on command signal release.

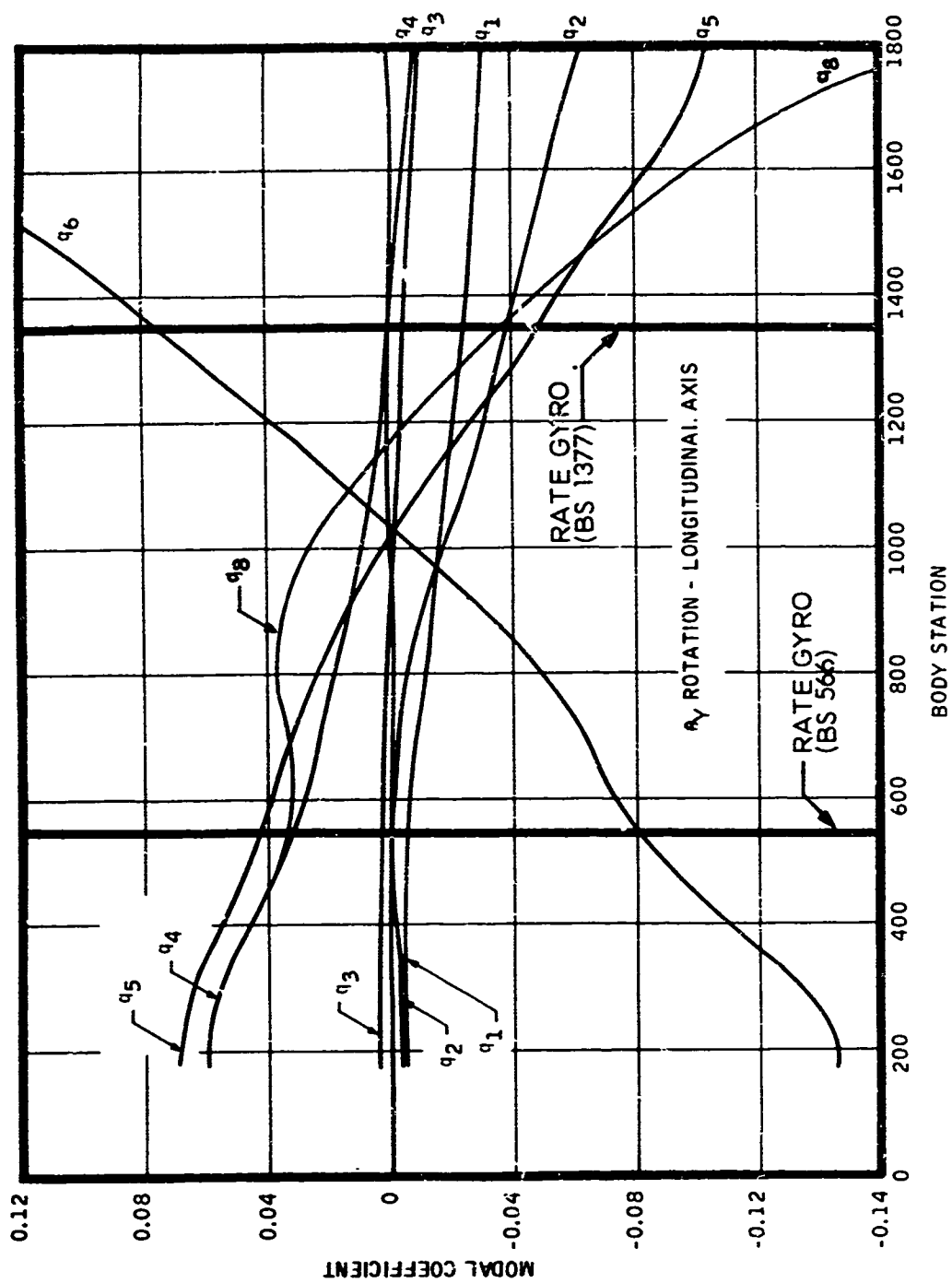
The elevator control loop lag-lead filter $(S/45+1)/(S/20+1)$ was selected to modify the elevator actuator-control surface dynamics to conform with the dynamics associated with the derivation of the optimal feedbacks. The ideal system had actuator-control surface dynamics which corresponded to a lag at 20 radians per second. Hence, cancellation of the pole at 46 radians per second, and the addition of a pole at 20 radians per second combined with the actual actuator-control surface dynamics, yields a reasonable approximation to the ideal dynamics. The 100 radians per second notch filter is used to offset the peaking at 102 radians per second caused by the elevator control surface. This notch filter provides approximately 16 db attenuation at 100 radians per second.

The aileron loop lead-lag network $(S/10+1)/(S/100+1)$ provides lead compensation for structural mode 6. The 100 radians per second notch is functionally identical to the elevator notch filter.



WING SYMMETRICAL MODAL SHAPES
FLIGHT CONDITION 1

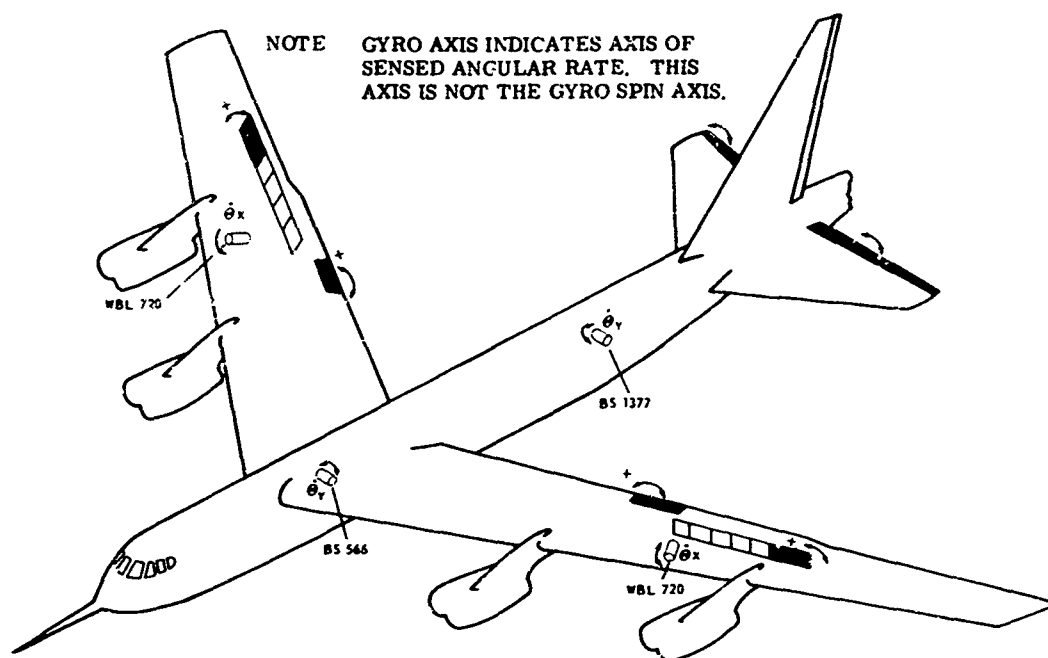
FIGURE 19



FUSELAGE SYMMETRICAL MODEL SHAPES
FLIGHT CONDITION 1

FIGURE 20

LAMS LONGITUDINAL AXIS SENSOR LOCATIONS



LAMS LATERAL - DIRECTIONAL SENSOR LOCATIONS

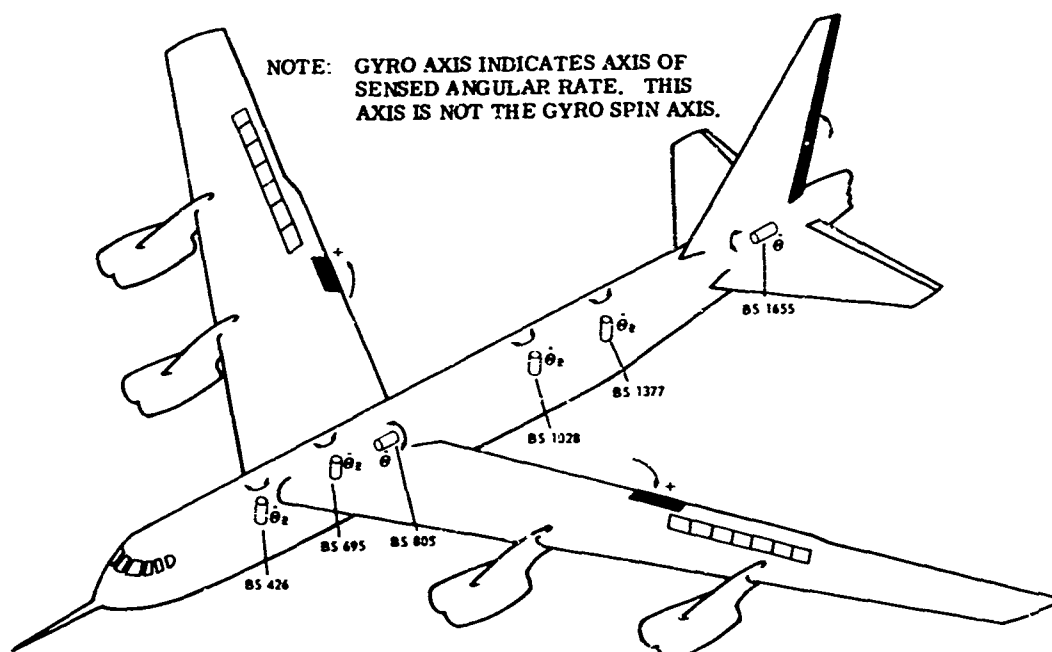


FIGURE 21

The high-pass filters $10s/(10s+1)$ in the elevator, aileron, and spoiler loops prevent D.C. null offsets in the loops.

The pilot input command drives an electromechanical servo in parallel with a direct low-pass input to the elevator servo. The gain, K_p , is a function of flight condition and is selected to give a fixed pitch rate response per control column deflection for each of the three flight conditions.

3.6.2 Lateral-Directional Axis

Figure 7 shows the block diagram of the Lateral-Directional Axis FCS and the system gains for each flight condition.

Rudder control loop actuation dynamics are altered to approximate ideal system actuator dynamic with the lag-lead network $(s/46+1)/(s/15.3+1)$. The 100 radians per second notch filter attenuates the peaking of the rudder actuator-control surface dynamics at 100 radians per second.

Aileron loop filters $(s/75 + 1)(s/100 + 1) / (s/20 + 1)(s/40 + 1)$ modify the aileron actuator-control surface dynamics to approximate actuator dynamics of the optimal system.

The lateral-directional axis pilot command inputs drive the rudder directly for yaw control and command the ailerons and spoilers to obtain sufficient roll rate. The gain, K_p , is selected to achieve a constant roll rate per control wheel deflection for all flight conditions.

3.7 Evaluation of Final Systems

Upon completion of the Baseline SAS and IAMS-FCS design synthesis programs, several detailed evaluation analyses of the system designs were conducted. Boeing-Wichita evaluated the systems stability, handling qualities, and structural performance and Honeywell conducted a performance sensitivity study. These analyses and studies were more comprehensive and detailed than those accomplished during the systems design and development stages. The analyses served two distinct functions:

- Assured theoretical compliance with the suggested criteria presented in Section 1.0
- Produced theoretical performance data for comparison with flight demonstration data

3.7.1 Safety Analysis

The safety analyses were conducted to assure the systems had adequate stability margins. The stability analysis segment calculated phase and gain margins as a function of the feedback loop gains and the flutter analysis segment calculated aircraft structural stability as a function of test vehicle airspeed.

3.7.1.1 Stability Analyses

Stability analyses were conducted for the Baseline SAS and IAMS-FCS. System bandwidth differences required that the IAMS-FCS stability analysis be conducted using a larger mathematical model than was used for Baseline SAS. The mathematical model descriptions are presented in Section 3.2.4.

3.7.1.1.1 Baseline SAS

The Baseline SAS stability analysis utilized closed loop gain and phase root loci plots and open loop frequency response plots to determine the theoretical system gain and phase margins. Digital computer programs were used exclusively to calculate the required data.

3.7.1.1.2 IAMS-FCS

Initially the IAMS-FCS stability analysis utilized closed loop gain and phase root loci plots and open loop frequency response plots to determine the theoretical system gain and phase margins for the three IAMS flight conditions. The root loci programs varied the gain of each feedback loop of the multiloop system while all other loops remained at nominal gains. Open loop frequency response plots were obtained for the multiple feedback loop system by assuming one loop open with all others closed at nominal gain. Digital computer programs calculated the frequency response and root loci data. Digital computer capabilities limited the number of degrees-of-freedom used for root loci techniques to be less than the number of degrees-of-freedom utilized for frequency response programs. Subsequently, only frequency response programs were used for final calculations of the IAMS-FCS stability analysis.

3.7.1.2 Flutter Analyses

Flutter analyses of the IAMS aircraft were conducted for the basic hydraulically powered aircraft (with SAS), the Baseline SAS, and the IAMS-FCS Stability Augmentation System.

3.7.1.2.1 Basic Aircraft and Baseline SAS

The basic aircraft and Baseline SAS analyses were conducted to provide flutter clearance for all altitudes and gross weights used throughout the IAMS test bed mission profile up to and including the maximum airspeed for straight and level flight (400 KEAS and .90 Mach). These analyses consisted of analyzing three altitudes (10,000, 22,000, and 32,700 feet) and four gross weights (350, 270, 241, and 222 KIPS). To attain the high airspeed at low altitude, the B-52E 3000 gallon external tanks were removed as tabulated in T.O. 1B-52E-1 handbook, Section V, Flutter Limitations.

The analyses required to provide adequate evaluation of the aircraft flutter boundary for the above conditions are as follows:

Gross Weight	Altitude	Analyses	
KIPS	1000 feet	Symmetric	Antisymmetric
350	10, 22 & 32.7	Included 2 RB & Elastic DOF's 4 thru 22, 27 & 28. (Section 3.2.4, Table II)	Included RB Yaw & Elastic DOF's 4 thru 18, 20, 22, 30 & 31. (Section 3.2.4, Table IV)
270	10, 22 & 32.7	Included 2 RB & Elastic DOF's 4 thru 16, 18 thru 22, 26 & 28. (Section 3.2.4, Table II)	Included RB Yaw & Elastic DOF's 4 thru 18, 21, 22, 29 & 30. (Section 3.2.4, Table IV)
241	10, 22 & 32.7	Included 2 RB & Elastic DOF's 4 thru 16, 18 thru 22, 26 & 28. (Section 3.2.4, Table III)	Included RB Yaw & Elastic DOF's 4 thru 18, 20, 22, 29 & 30. (Section 3.2.4, Table V)
222	10, 22 & 32.7	Included 2 RB & Elastic DOF's 4 thru 16, 18 thru 22, 26 & 28. (Section 3.2.4, Table III)	Included RB Yaw & Elastic DOF's 4 thru 18, 20, 22, 29 & 30. (Section 3.2.4, Table V)

The basic aircraft analyses included control surface and actuator dynamics and the Baseline SAS analyses added the SAS dynamics presented in Section 3.4. Inputs by Kussner and Schwarz two-dimensional strip theory, corrected for finite span and compressibility effects, was used in the aerodynamic portion of the analyzer.

3.7.1.2.2 IAMS-FCS

The IAMS-FCS flutter analyses were conducted to provide flutter clearance for IAMS flight conditions one and three as discussed in the Introduction. However, the following analyses were conducted to provide adequate clearance for the flight test program with respect to airspeed, gross weights, and IAMS flight conditions:

Gross Weight	Altitude	Flight Condition	Analyses	
KIPS	1000 feet		Symmetric	Antisymmetric
350	10	1	Included 2 RB & the first 26 elastic modes from Table II.	Included 2 RB & the first 28 elastic modes from Table IV.
270	10	1	Included same number of modes as above from Table II.	Included same number of modes as above from Table IV.
270	32.7	3	Used same as 10,000 foot, 270 KIPS configuration	Used same as 10,000 foot 270 KIPS configuration
241	32.7	3	Included 2 RB & the first 26 elastic modes from Table IV.	Included 2 RB & the first 28 elastic modes from Table V.

All analyses included the hydraulic actuator and control surface dynamics in addition to the IAMS-FCS dynamics presented in Section 3.6. As noted above, Kussner and Schwarz two-dimensional strip theory, corrected for finite span and compressibility effects, was used in the analysis.

In addition to the above primary analyses, parametric variations in the longitudinal, lateral and direction control system stiffness, the aileron and rudder actuator dynamics, and the nonlinear effects of the aileron hinge moment were accomplished to identify the sensitivity of these parameters to the aircraft flutter boundary.

The above IAMS-FCS flutter analyses were conducted with the initial IAMS spoiler configuration which used all seven spoiler panels per wing as discussed in the Introduction and Section 5.2.2. However, when the IAMS spoiler configuration was changed to using only panels 1, 2, 13, and 14, the 270 KIP symmetric and antisymmetric analyses were rerun for FC-1 and 3 respectively. No further analyses were accomplished since no apparent flutter problems existed up to and including the intended test airspeeds for either flight condition.

3.7.2 Handling Qualities Evaluation

To evaluate the effect of the Baseline JAS and IAMS-FCS on the aircraft handling qualities, the basic aircraft was simulated using a six degree-of-freedom, quasi-elastic model. To assure that the simulated aircraft model was an adequate representation, the simulated aircraft response

was compared to that of past flight test data.

The dynamic characteristics of the simulated model including the Baseline SAS were checked by comparing root loci plots from the quasi-elastic model analysis and a 24 degree-of-freedom model analysis. To check the response of the quasi-elastic model with the LAMS flight control system in the loop, time history responses were obtained from Honeywell analog simulations for various types of inputs and compared to the Boeing quasi-elastic responses.

When it was assured that the aircraft and both SAS systems were being simulated accurately, the analog computer was coupled to the Boeing-Wichita print light simulator facility to evaluate the aircraft handling qualities.

Several different tasks were assigned during each test run so that the pilot could judge the maneuvering qualities of the aircraft for various control inputs. The first task was to fly the aircraft straight and level maintaining constant airspeed and altitude. The different maneuvers performed for each run included a constant altitude turn into a specified bank angle and then a return to the original heading. After this task was accomplished the pilot did a climbing turn using the same procedure as for the level turn except that he maintained a fixed rate-of-climb throughout the turn. The descending turn was then accomplished and a given rate-of-descent was maintained throughout the maneuver. After completing the turns, the pilot accomplished a visual tracking task to further evaluate the aircraft flying qualities.

The runs were five minutes in duration and the pilot was allowed to fly longer if required for a proper evaluation.

The runs were scheduled in a random sequence to minimize the learning effects and to ensure that each configuration was evaluated on its own merits. Pilots were briefed on the purpose of the tests and the flight condition being evaluated prior to the start of any testing. The pilot was also allowed a warm up period before each testing session. Total test times were limited to two hours maximum with a short break at the end of the first hour to avoid biasing the data by pilot fatigue.

The rating system utilized was typical for handling qualities evaluation. Although the data is essentially subjective, it was quantified by the use of Cooper ratings. A questionnaire was also utilized to obtain a reason for the pilot rating, i.e., problems in holding heading, or difficulty due to a longitudinal stability characteristic. Also measured were the root mean square angles of attack and sideslip and the pilot's control activity in terms of wheel, pedal, and column rates.

3.7.3 Structural Performance Analysis

Selected aircraft parameters were used to evaluate the Baseline SAS and LAMS-FCS effects on structural performance for flight through turbulence. The parametric evaluations utilized the entire mathematical model described in Section 3.2. The evaluation parameters and analysis procedures and methods are discussed in the following sections.

3.7.3.1 Selected Evaluation Parameters

The structural performance of the LAMS-FCS was evaluated for flight through random atmospheric turbulence. Fatigue damage rates, expected peak stresses, RMS stresses, and RMS accelerations were calculated at selected aircraft stations. Acceleration power spectra were computed for the crew compartment.

The structural performance parameters were used as performance indices in the design of the LAMS Flight Control System. Available performance gains were subject to handling qualities, flutter, control authority, and other restraints. The same parameters, plus RMS loads at many additional aircraft stations, were used to evaluate and compare the performance of the final LAMS Flight Control System design with the Baseline SAS and basic aircraft.

The following paragraphs describe the selected stress stations, the atmospheric turbulence description and the relationships of turbulence, the B-52 mathematical model, and predicted structural performance.

3.7.3.2 Stresses for Performance Index

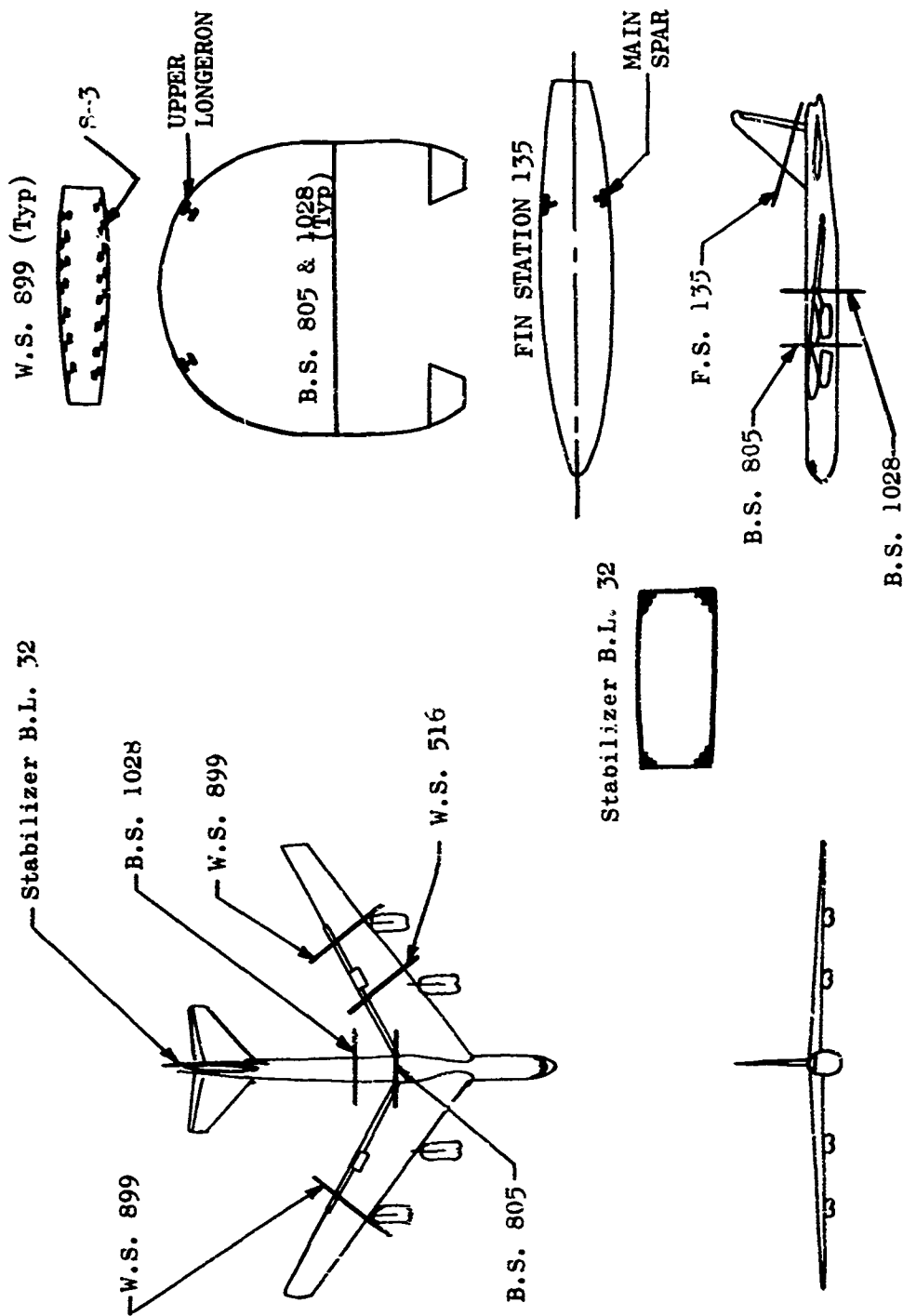
Bending stresses at six points in the B-52 structure shown in Figure 22 were selected as the basis of fatigue damage rate performance index calculations. The stress locations were chosen to be representative of the most sensitive areas of the wing, body, and empennage during flight through turbulence. Other important contributions to B-52 accumulated fatigue damage such as takeoff, landing, and aerial refueling were not considered.

The selected stiffeners, longerons, and spar caps are each in tension during steady, level flight. Stiffener 5 at Wing Station 516 accumulates damage at about the same rate as the other critical areas of the in-board part of the wing. Stiffener 3 at Wing Station 899 is typical of the susceptible parts of the mid-wing. The cyclic nature of main spar cap stresses at Fin Station 135 and Stabilizer Buttock Line 32 is typical of that for the upper longeron in the aft fuselage.

3.7.3.3 Atmospheric Turbulence Model

The atmospheric turbulence model used for the LAMS B-52 structural performance studies assumed Gaussian random, stationary, isotropic turbulence with the Dryden power spectral density for vertical and lateral components. The equation for this turbulence model is as follows:

$$\Phi(f) = \frac{2\sigma_g^2 L}{V} \frac{\left[1 + 3 \left(\frac{2\pi f L}{V}\right)^2\right]}{1 + \frac{2\pi f L}{V} \cdot 2} \frac{(Ft/Sec)^2}{CPS}$$



PERFORMANCE INDEX STRESS LOCATIONS

FIGURE 22

Both σ_f and σ_f^2 can be calculated from the gust power spectral density and the stress frequency response function to gusts. The frequency response functions for this analysis were calculated numerically from the B-52 mathematical model.

The exceedance function was computed at:

$$M(f_i) = \int_0^{\infty} [M(f_i)]_{\sigma_g = \text{CONST.}} \times \hat{f}(\sigma_g) d\sigma_g$$

where $\hat{f}(\sigma_g)$ is the probability density distribution of the appropriate RMS turbulence component and where Rice's exceedance is

$$[M(f_i)]_{\sigma_g = \text{CONST.}} = \frac{(\sigma_f^2/\sigma_g)}{2\pi(\sigma_f/\sigma_g)} \exp \left[\frac{-f_i^2}{2(\sigma_f/\sigma_g)^2 \sigma_g^2} \right]$$

The adaptation of stress exceedance data to fatigue damage calculations requires further assumptions. The linear cumulative theory of fatigue states that:

$$\text{Damage} = \sum_{i=1}^M \frac{n_i}{N(f_i, f_{\text{mean}})}$$

where f_i = alternating stress amplitude

f_{mean} = steady level flight stress

$N(f_i, f_{\text{mean}})$ = experimental number of alternating cycles at the i th stress level before fatigue cracks appear

n_i = number of cycles of applied stress at the i th stress level

Fatigue cracks will theoretically appear when Damage = 1.0.

For random stress variations, an equivalent n_i is defined for the stress level $(f_i - \frac{\Delta f}{2}) < f \leq (f_i + \frac{\Delta f}{2})$ as:

$$n_i = \left[M(f_i - \frac{\Delta f}{2}) - M(f_i + \frac{\Delta f}{2}) \right] \times (\text{flight time})$$

The final equation for fatigue damage accumulation rate in terms of the exceedance function is then:

where

- $\phi(f)$ = power spectral density for vertical or lateral turbulence component
- σ_g = RMS gust component velocity
- V = airplane speed
- L = "Scale of Turbulence", 1000 ft was used
- f = frequency in cps

The antisymmetrical component of vertical turbulence was represented by a rolling gust acting on the wing as in NACS Report 1321, Reference 1. The power spectral density of the rolling gust was given by:

$$\phi_{\text{ROLL}}(f) = \frac{8\sigma_g^2 (2.1 - \frac{b}{L})}{VL (1 + 7\pi^2 f^2)^3} \frac{(\text{Rad/Sec})^2}{\text{CPS}}$$

where b is the wing span and the other parameters are the same as for the vertical gust spectrum. The assumed probability density distribution of RMS gust velocity, σ_g is defined by:

$$f(\sigma_g) = \frac{P_1}{b_1} \sqrt{\frac{2}{\pi}} \exp \left(-\frac{\sigma_g^2}{2b_1^2} \right) + \frac{P_2}{b_2} \sqrt{\frac{2}{\pi}} \exp \left(-\frac{\sigma_g^2}{2b_2^2} \right)$$

The turbulence parameters used for the B-52 study were:

Altitude	P_1	P_2	b_1	b_2
Counter Low Level	.80	.20	3.6	4.2
Cruise (30-40,000 Ft)	.13	.01	1.8	4.8

3.7.3.4 Stress Exceedances and Fatigue Damage

In the random turbulence environment, stresses are described statistically. A useful description is the stress exceedance function $M(f_1)$ which is the number of times (per unit time) the random stress f will rise above the level $f = f_1 + f_{\text{mean}}$. For Gaussian random stresses, only two parameters are required to calculate $M(f)$. These are σ_f/σ_g (RMS variation of stress, f , from its mean value for unit RMS gusts) and $\sigma_{\dot{f}}/\sigma_g$ (RMS variation of $\frac{df}{dt}$ for unit RMS gusts).

$$\frac{\text{Damage}}{\text{Flight Time}} = \int_C^{(f_{\text{ult}} - f_{\text{mean}})} - \frac{\frac{d}{df} M(f)}{N(f, f_{\text{mean}})} df$$

This equation was evaluated numerically for the LAMS B-52 analysis.

3.7.4 Performance Sensitivity Analysis

The LAMS-FCS performance sensitivity analysis consisted of three segments; performance definition or initial handling qualities studies, sensitivity analysis, and failure analysis. The total analysis was conducted with the analog computer mathematical model simulation described in Section 3.2.4. The longitudinal and lateral-directional axes systems were studied independently at the three LAMS flight conditions.

3.7.4.1 Performance Definition Study

The performance definition study was an initial evaluation of the LAMS-FCS handling qualities. Aircraft transient responses were recorded for discrete gust inputs and step and sinusoidal pilot commands. Parametric RMS and exceedance count data were obtained for actuator hysteresis variations and RMS random gust variations. The random turbulence data was furnished to Honeywell by Boeing, on magnetic tapes. The data included Kussner lift growth effects and transport delays.

3.7.4.2 Sensitivity Analysis

The sensitivity analysis utilized one basic forcing function: a 4 ft/sec random gust. Variations were made in modal coefficients, mode natural frequencies, and LAMS-FCS filter time constants to determine the sensitivity of RMS stresses, RMS accelerations and exceedance data at selected aircraft locations to the variations.

3.7.4.3 Failure Analysis

The failure analysis consisted of two segments: open failures and hardover failures of actuators and sensors. The open failure analysis was conducted with a 4 ft/sec random gust disturbance; no external disturbances were included in the hardover failure analysis. Open failures were evaluated by observing effects on the RMS stresses and RMS pilot station attitudes and stability from time history data.

3.8 LAMS Longitudinal FCS Design Modification

Initial flight test data indicated that the LAMS Longitudinal FCS was not functioning properly since the stability margins for the first and sixth structural modes were considerably lower than predicted. The B-52 mathematical model was upgraded to include: spoiler lift growth functions; and modified free vibration mode damping values to that equivalent to the aircraft as obtained from ground vibration testing.

Stability data was recalculated using the revised math model for the free aircraft and the nominal gains LAMS-FCS configuration. Predicted first and sixth structural mode damping values were similar to the experimental data. The LAMS-FCS design was then modified to obtain the required predicted stability margins and new data was calculated to assure that the structural performance was not degraded. Design modifications were restricted to the spoiler loop rate and displacement gains.

4.0 SYSTEM PERFORMANCE

4.1 Introduction

Section 4.0 contains the theoretically evaluated performance of the Baseline SAS and the LAMS-FCS. Predicted safety analysis data is given in Section 4.2, handling qualities data in Section 4.3, structural performance data in Section 4.4, analog computer sensitivity studies in Section 4.5, and the revised LAMS-FCS predicted stability data in Section 4.6.

4.2 Safety Analysis

4.2.1 Results of Stability Analysis

The objective of the stability analysis was to insure that the Baseline SAS and the LAMS-FCS meet the stability requirements of at least 10 db gain margin and 60 degree phase margin.

4.2.1.1 Baseline SAS

The Baseline SAS provides augmentation to the longitudinal, lateral, and directional axes. The Baseline longitudinal SAS increases short period damping, the Baseline yaw SAS increases Dutch roll damping, and the Baseline roll SAS improves aircraft roll response for fly-by-wire pilot commands. The Baseline SAS meets all stability and handling quality requirements.

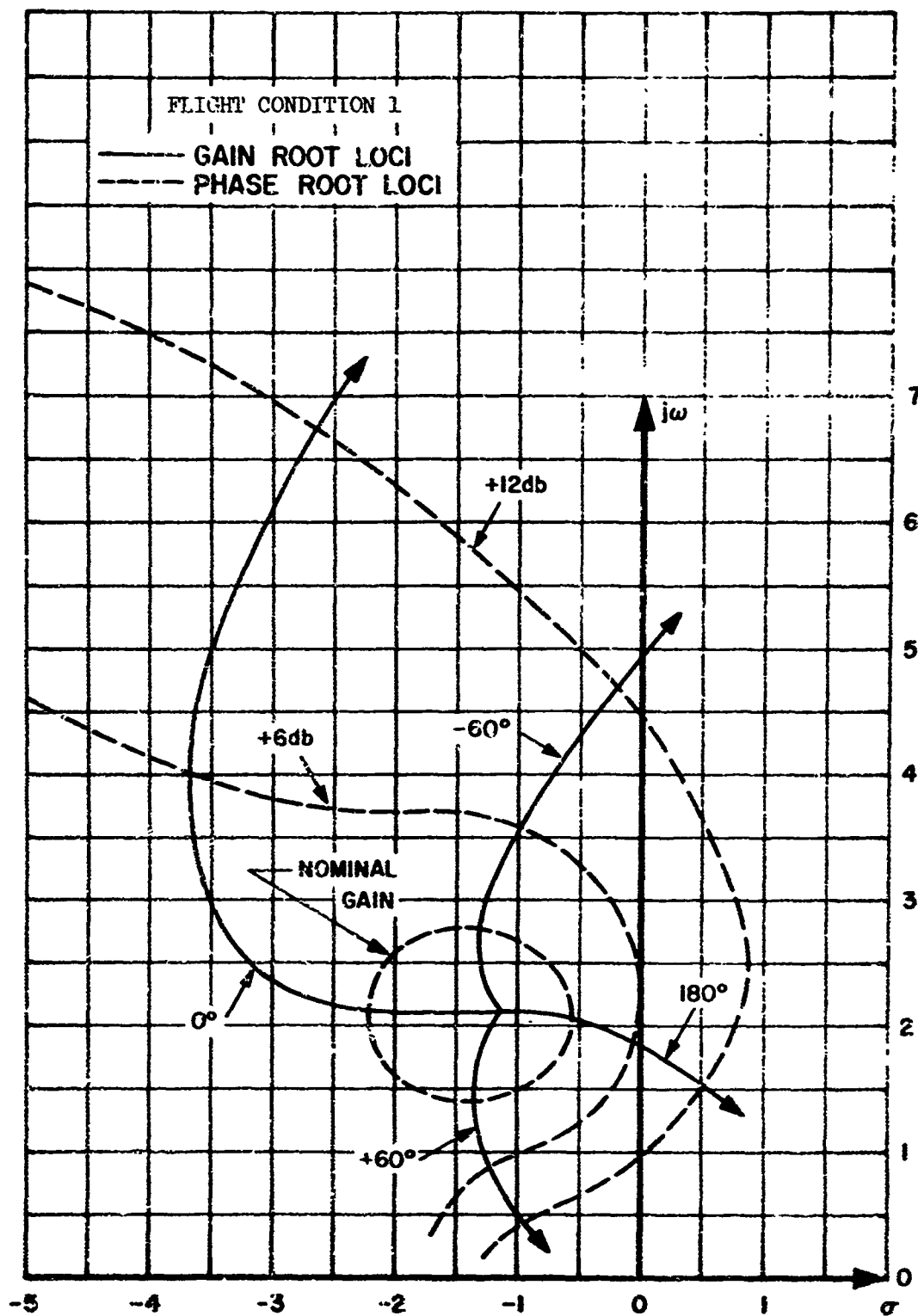
4.2.1.1.1 Longitudinal Axis (Symmetric)

The Baseline longitudinal SAS is gain stabilized with all gain margins greater than 20 db. These stability margins exceed the specified minimum requirement of 10 db gain margin and ± 60 degree phase margin. Minimum gain margins at worst phase conditions are 6 db for the short period mode and greater than 20 db for the structural modes.

Figure 23 shows gain and phase root loci for the short period mode and Figure 24 shows root loci for the sixth structural mode that is most strongly coupled with the Baseline pitch SAS. Other structural modes are not shown since they show little movement. The root loci shown pertain to Flight Condition 1 but are typical of all three flight conditions.

Figure 25 shows the effects of the Baseline SAS on aircraft transient response to a control column step input for Flight Condition 1. This curve shows the elevator deflection due to SAS feedback and the resulting increased damping of the short period oscillation. The pitch rate and normal acceleration responses shown are at Body Station 820.

Figure 26 shows the frequency responses and Table VI the eigenvalues of the Baseline pitch SAS for the three flight conditions analyzed.



LONGITUDINAL BASELINE SAS
SHORT PERIOD ROOT LOCI

FIGURE 23

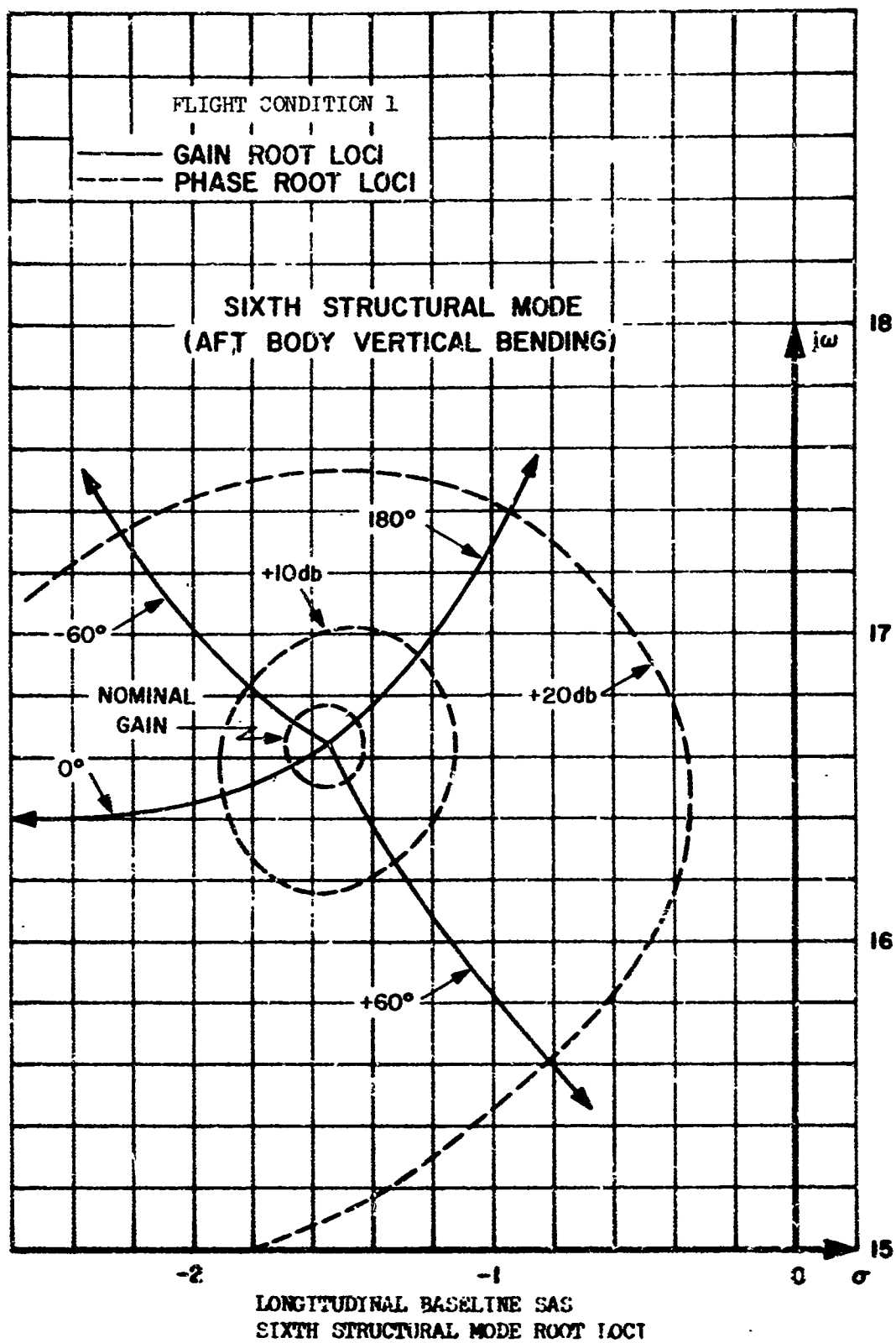
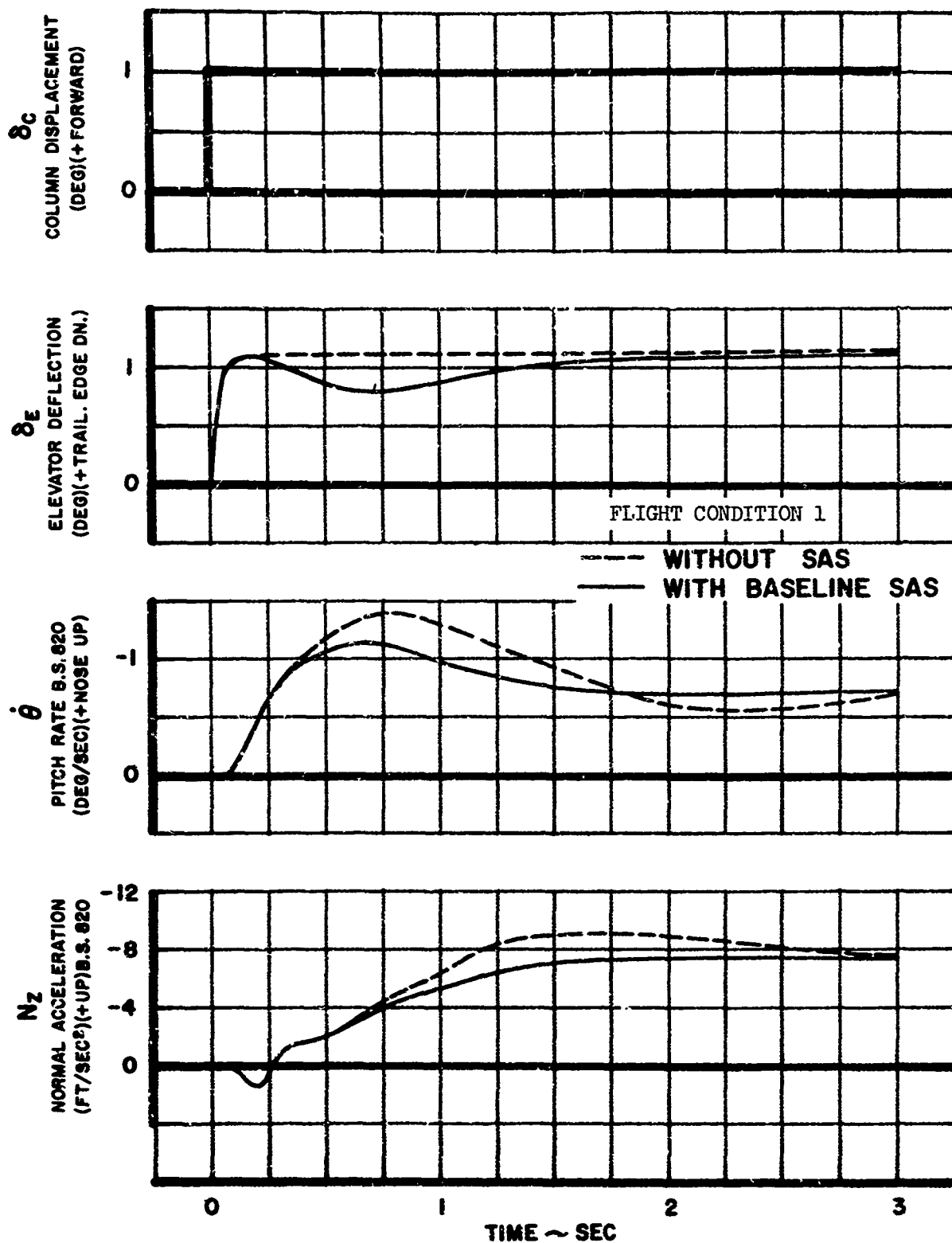
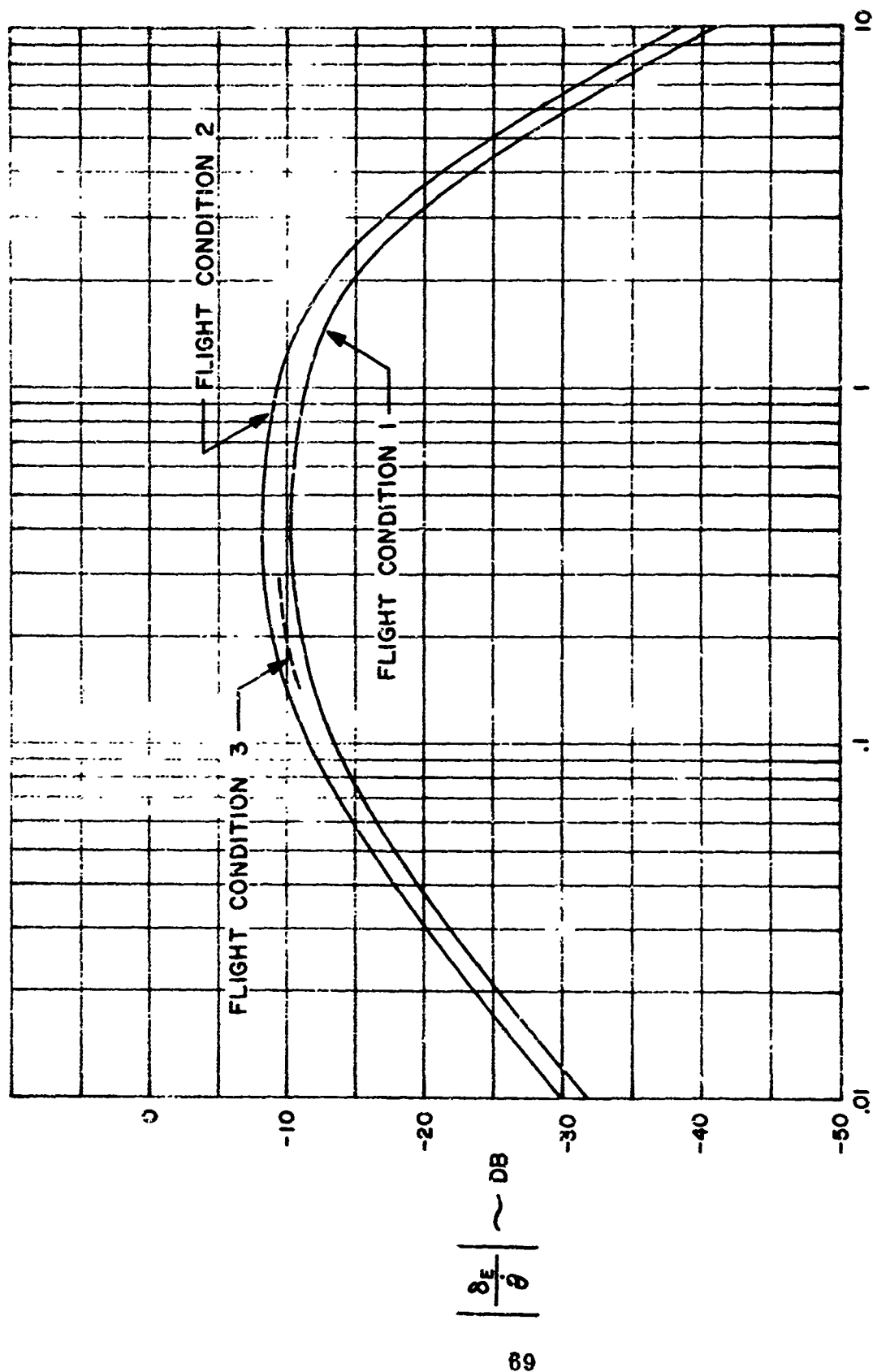


FIGURE 24



EFFECTS OF BASELINE PITCH SAS
ON AIRPLANE TRANSIENT RESPONSE

FIGURE 25.



FREQUENCY ~ CPS
BASELINE PITCH SAS FREQUENCY RESPONSES

FIGURE 26

TABLE VI
BASELINE SAS LONGITUDINAL EIGENVALUES

FREE AIRPLANE DATA				AUGMENTED AIRPLANE DATA		
Mode	Root Locations	ζ	ω_n f_n	Root Locations	ζ	ω_n f_n

FLIGHT CONDITION 1

SP	$-1.08 \pm j 2.28$.428	2.52 .401	$-2.16 \pm j 2.08$.72	3.0 .477
1	$-.98 \pm j 6.65$.146	6.71 1.07	$-.98 \pm j 6.64$.146	6.7 1.07

FLIGHT CONDITION 2

SP	$-.76 \pm j 1.65$.415	1.83 .291	$-1.53 \pm j 1.43$.73	2.1 .334
1	$-.82 \pm j 6.00$.135	6.05 .962	$-.83 \pm j 6.05$.136	6.1 .97

FLIGHT CONDITION 3

SP	$-.74 \pm j 2.06$.338	2.19 .348	$-1.94 \pm j 1.83$.71	2.6 .414
1	$-.70 \pm j 6.62$.105	6.65 1.06	$-.70 \pm j 6.65$.105	6.7 1.07

4.2.1.1.2 Lateral Axis (Antisymmetric)

Yaw SAS and roll SAS gain and phase margins at the three flight conditions exceed minimum requirements of 10 db and ± 60 degrees. Specific stability margins for the various modes are tabulated in Tables VII and VIII. The Dutch roll mode has a minimum gain margin of 14 db and a minimum phase margin of 70 degrees. These margins occur at Flight Condition 1. Each of the first 11 antisymmetrical structural modes has at least a 30 db gain margin and 180 degree phase margin. At the worst phase condition each structural mode has at least a 12 db gain margin.

Figures 27 and 28 show gain and phase root loci for the Dutch roll and first structural modes, respectively. Other modes are not shown since their coupling with the Baseline yaw SAS is insignificant. Root loci shown for Flight Condition 1 are typical of all three flight conditions.

Figure 29 contains the Flight Condition 1 gain and phase root loci of the roll mode for the roll SAS with nominal yaw SAS. Movement of structural modes is insignificant.

Rudder, yaw rate, and side acceleration responses to a step displacement of the rudder pedals are shown in Figure 30. Increased damping of the Dutch roll mode and the corresponding rudder activity are the significant SAS effects shown by these curves.

Figure 31 shows the effects of the Baseline SAS on aileron deflection, roll rate, and bank angle responses to a step rotation of the evaluation pilot's wheel. Significant aileron activity is required to attain only small improvements in roll rate rise time and bank angle. This results from the fact that the spoilers, which overshadow the ailerons in roll authority, are not included in the Baseline SAS loop.

Figures 32 and 33 show Baseline Yaw and Roll SAS frequency responses for Flights Conditions 1, 2, and 3. The Yaw SAS contains both washout and rolloff filters and the roll SAS contains a rolloff term and a 1.9 cps notch filter in the forward loop. The notch filter reduces the pilot's wheel command gain at the second antisymmetric (wing bending) mode frequency. The eigenvalues for the lateral axes are shown in Table IX.

4.2.1.2 LAMS Flight Control System

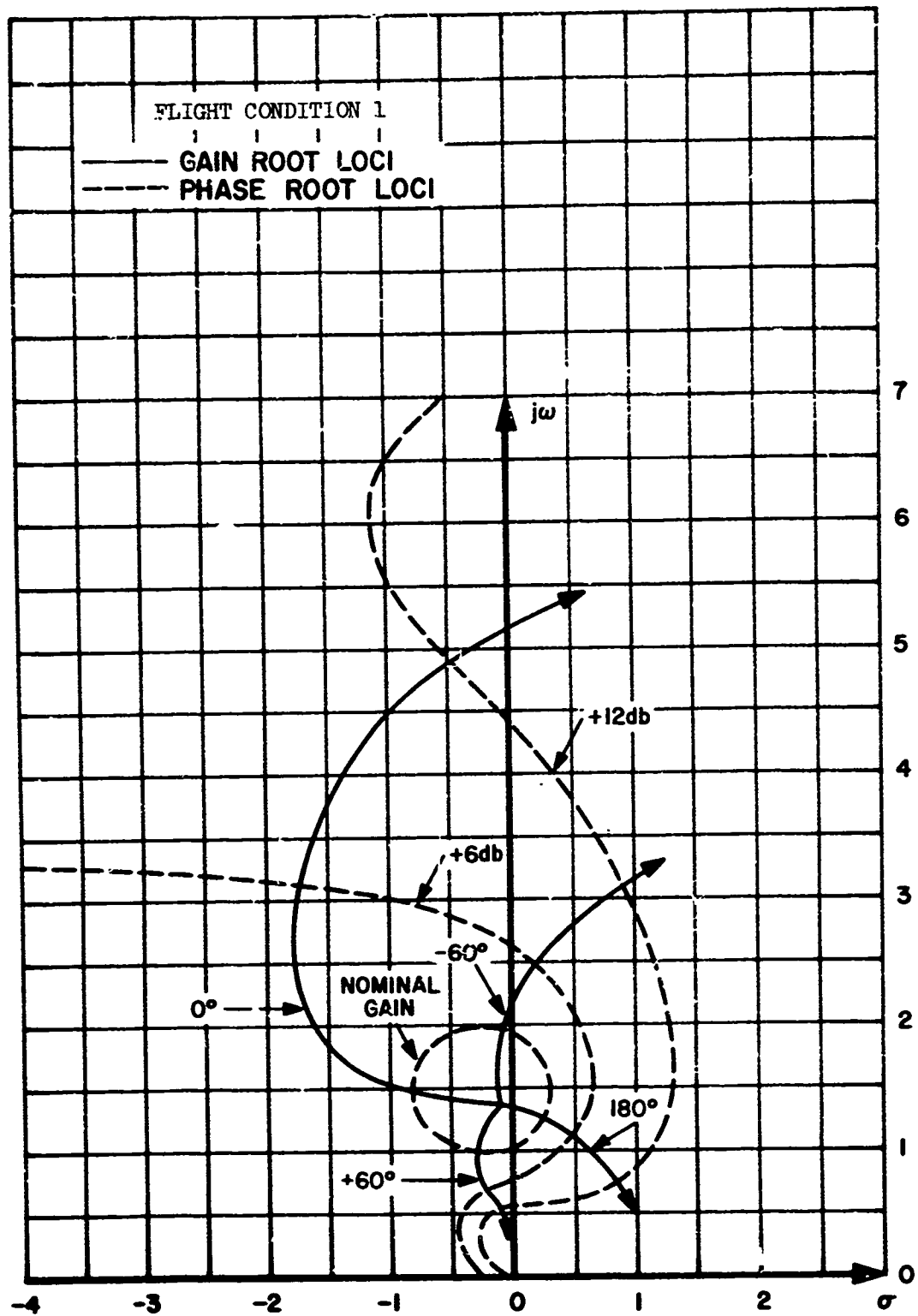
The LAMS-FCS provides augmentation to the longitudinal, lateral, and directional axes. The system was designed to increase the damping for rigid body motion as well as alleviate aircraft structural loads. The LAMS-FCS meets the stability requirement with one exception. The spoiler loop at Flight Condition 3 for the longitudinal axis exhibits a 52 degree phase margin at 7.7 radians per second, as noted in Figure 34 and Table X.

TABLE VII
BASELINE
YAW SAS STABILITY MARGINS

LAMS FLIGHT CONDITION	MODE	GAIN MARGIN (10 db REQUIRED)	PHASE MARGIN ($\pm 60^\circ$ REQUIRED)	MINIMUM GAIN MARGIN AT WORST PHASE CONDITION (STRUCTURAL MODES ONLY)
1	Dutch Roll	14 db		---
1	1st Struct.	> 30 db	$\pm 180^\circ$	12 db
1	Struct. 2-11	> 30 db	$\pm 180^\circ$	> 18 db
2	Dutch Roll	16 db		---
2	1st Struct.	> 30 db	$\pm 180^\circ$	12 db
2	Struct. 2-11	> 30 db	$\pm 180^\circ$	> 18 db
3	Dutch Roll	16 db		---
3	1st Struct.	> 30 db	$\pm 180^\circ$	12 db
3	Struct. 2-11	> 30 db	$\pm 180^\circ$	> 18 db

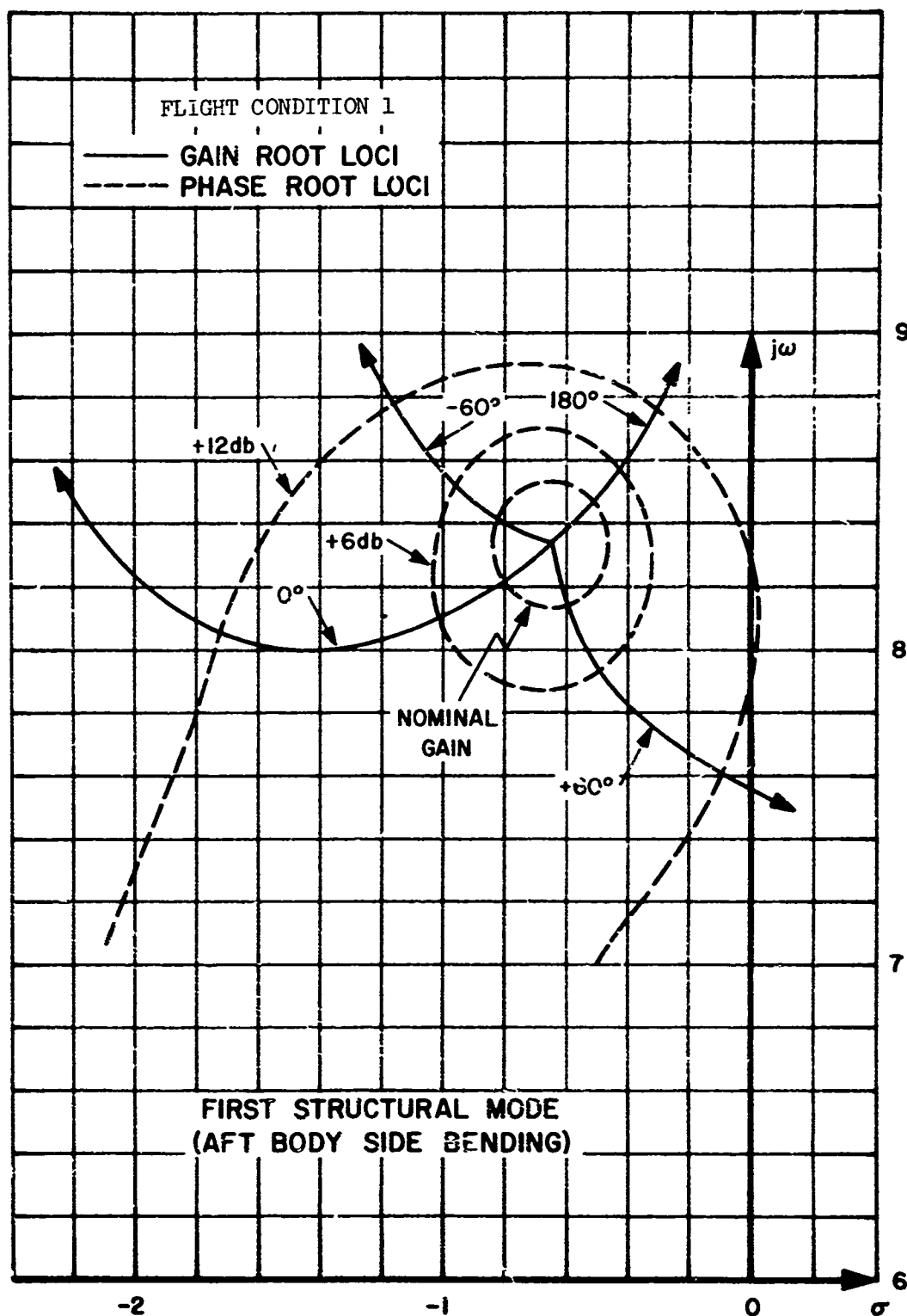
TABLE VIII
BASELINE
ROLL SAS STABILITY MARGINS

IAMS FLIGHT CONDITION	MODE	GAIN MARGIN (10 db REQUIRED)	PHASE MARGIN ($\pm 60^\circ$ REQUIRED)	MINIMUM GAIN MARGIN AT WORST PHASE CONDITION (STRUCTURAL MODES ONLY)
1	Roll	31 db	$\pm 180^\circ$	---
1	Struct. 1-11	> 45 db	$\pm 180^\circ$	> 36 db
2	Roll	36 db	$\pm 180^\circ$	---
2	Struct. 1-11	> 45 db	$\pm 180^\circ$	> 36 db
3	Roll	33 db	$\pm 180^\circ$	---
3	Struct. 1-11	> 45 db	$\pm 180^\circ$	> 36 db



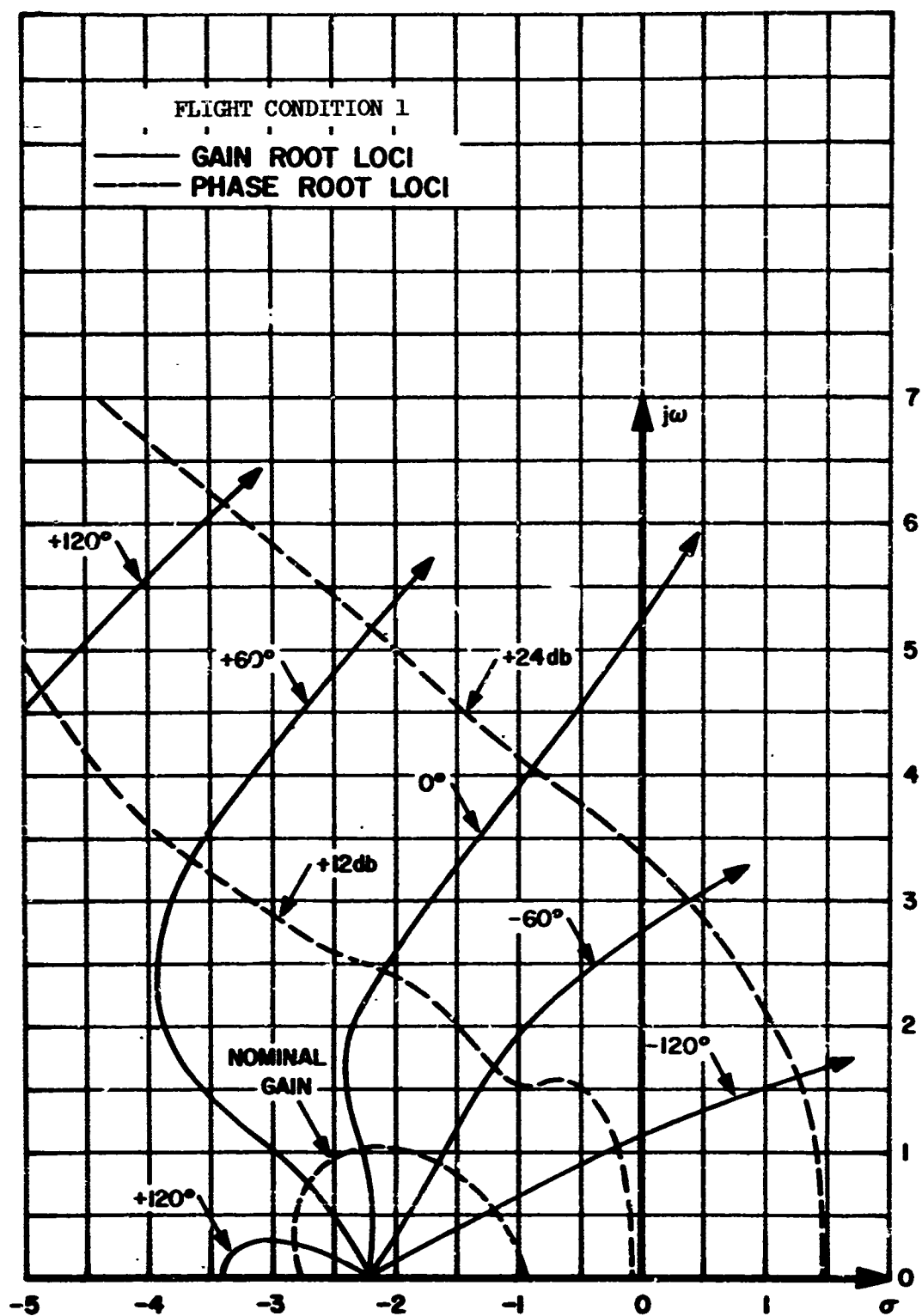
LATERAL-DIRECTIONAL BASELINE SAS DUTCH ROLL
 ROOT LOCI FOR YAW SAS WITH NOMINAL ROLL SAS

FIGURE 27



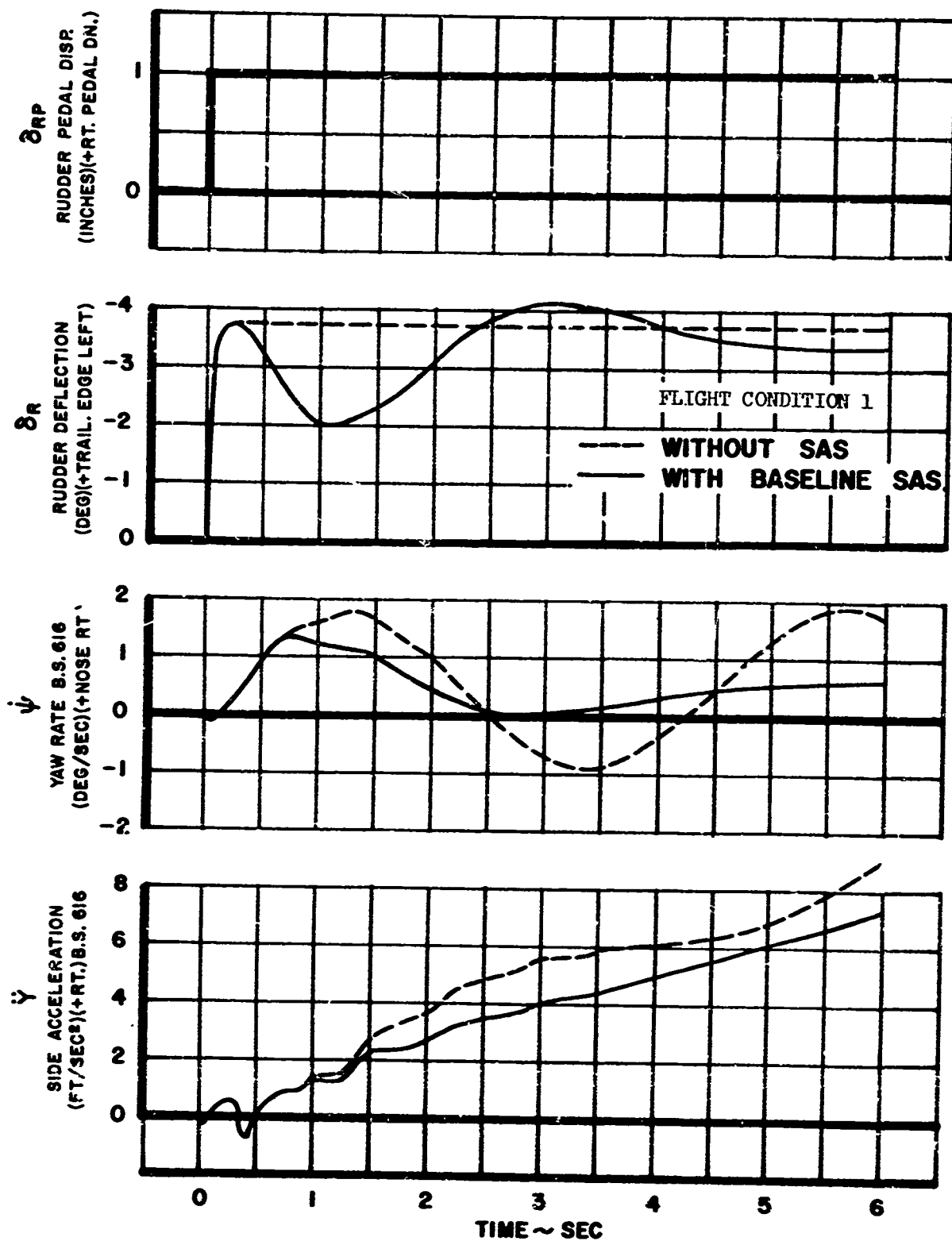
LATERAL-DIRECTIONAL BASELINE SAS FIRST STRUCTURAL
 MODE ROOT LOCI FOR YAW SAS WITH NOMINAL ROLL SAS

FIGURE 26



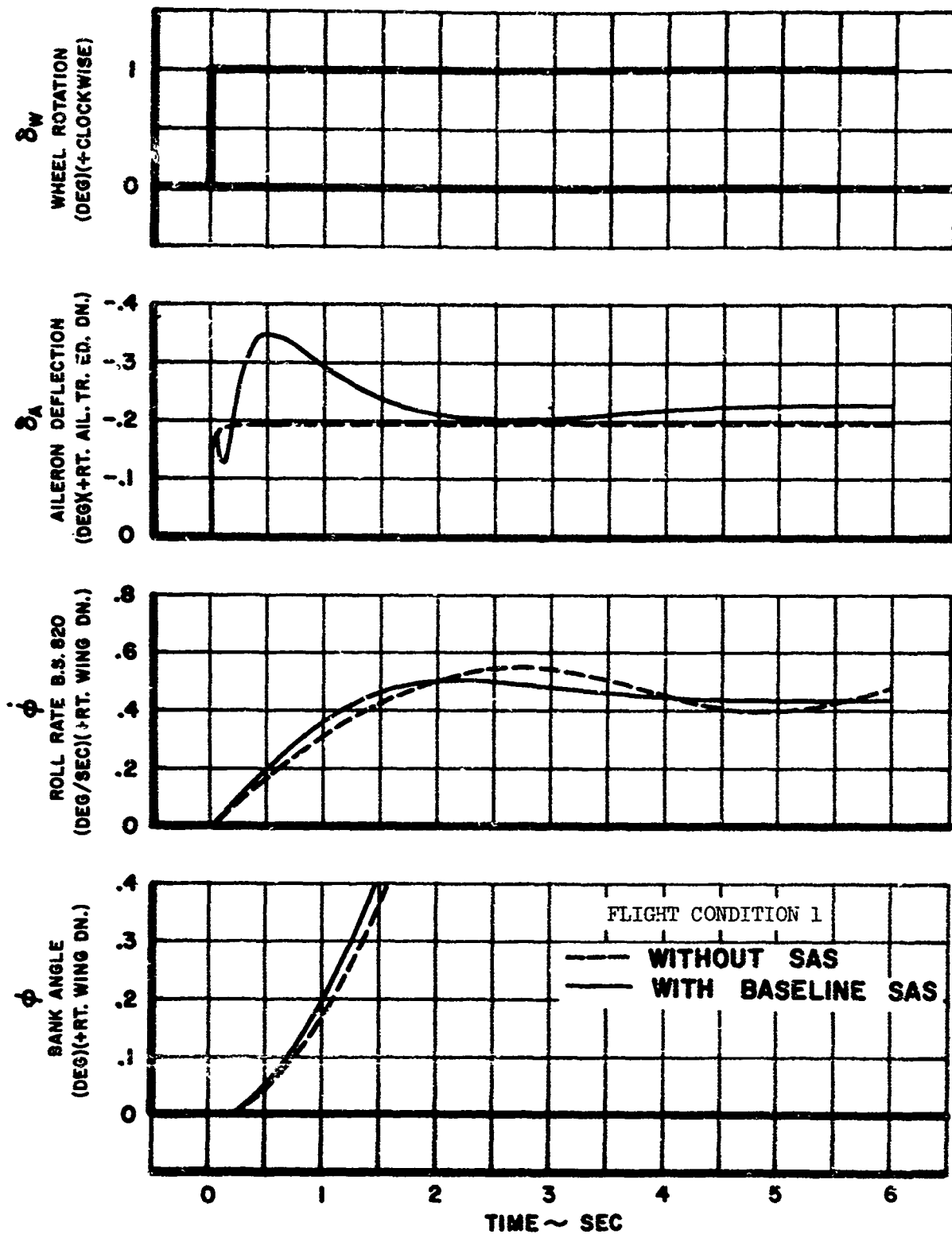
LATERAL-DIRECTIONAL BASELINE SAS ROLL ROOT LOCI
FOR ROLL SAS WITH NOMINAL YAW SAS

FIGURE 29



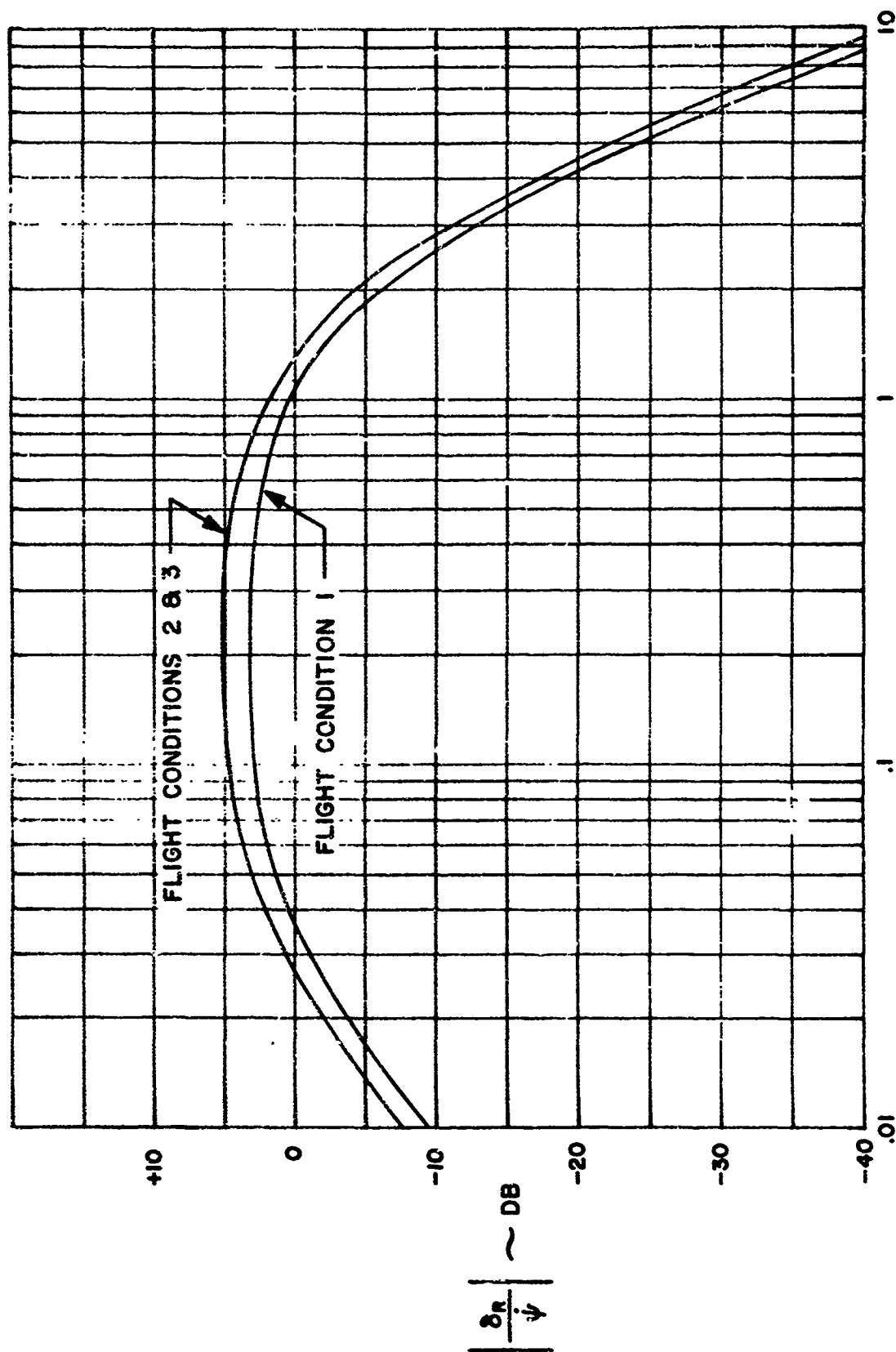
EFFECTS OF BASELINE YAW SAS ON
AIRPLANE TRANSIENT RESPONSE

FIGURE 30.



EFFECTS OF BASELINE ROLL SAS
ON AIRPLANE TRANSIENT RESPONSE

FIGURE 31.



FREQUENCY ~ CPS
 BASELINE YAW SAS FREQUENCY RESPONSES

FIGURE 32

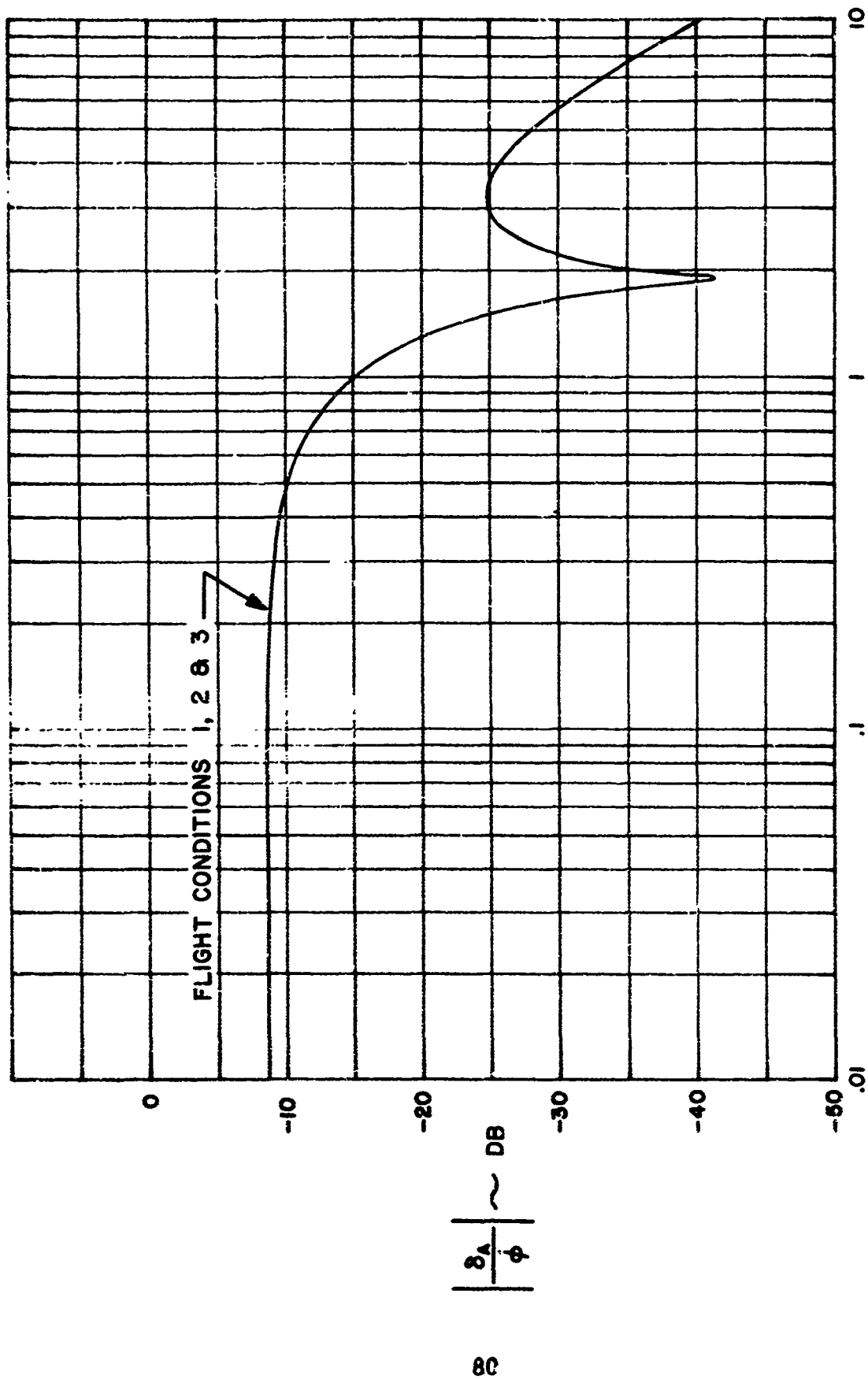


FIGURE 33

TABLE IX
BASELINE LATERAL-DIRECTIONAL EIGENVALUES

FREE AIRPLANE DATA				AUGMENTED AIRPLANE DATA		
Mode	Root Locations	ζ	ω_n f_n	Root Locations	ζ	ω_n f_n
FLIGHT CONDITION 1						
DR	$-.072 \pm j 1.37$.053	1.37 .218	$-.86 \pm j 1.58$.48	1.8 .287
1	$-.63 \pm j 8.33$.076	8.33 1.33	$-.80 \pm j 8.2$.098	8.2 1.30
FLIGHT CONDITION 2						
DR	$-.044 \pm j 1.08$.041	1.08 .172	$-.52 \pm j 1.08$.43	1.2 .191
1	$-.54 \pm j 7.82$.069	7.82 1.24	$-.70 \pm j 7.7$.091	7.7 1.23
FLIGHT CONDITION 3						
DR	$-.048 \pm j 1.24$.039	1.24 .197	$-.66 \pm j 1.24$.47	1.4 .223
1	$-.47 \pm j 3.18$.057	3.18 1.30	$-.66 \pm j 3.0$.082	3.0 1.27

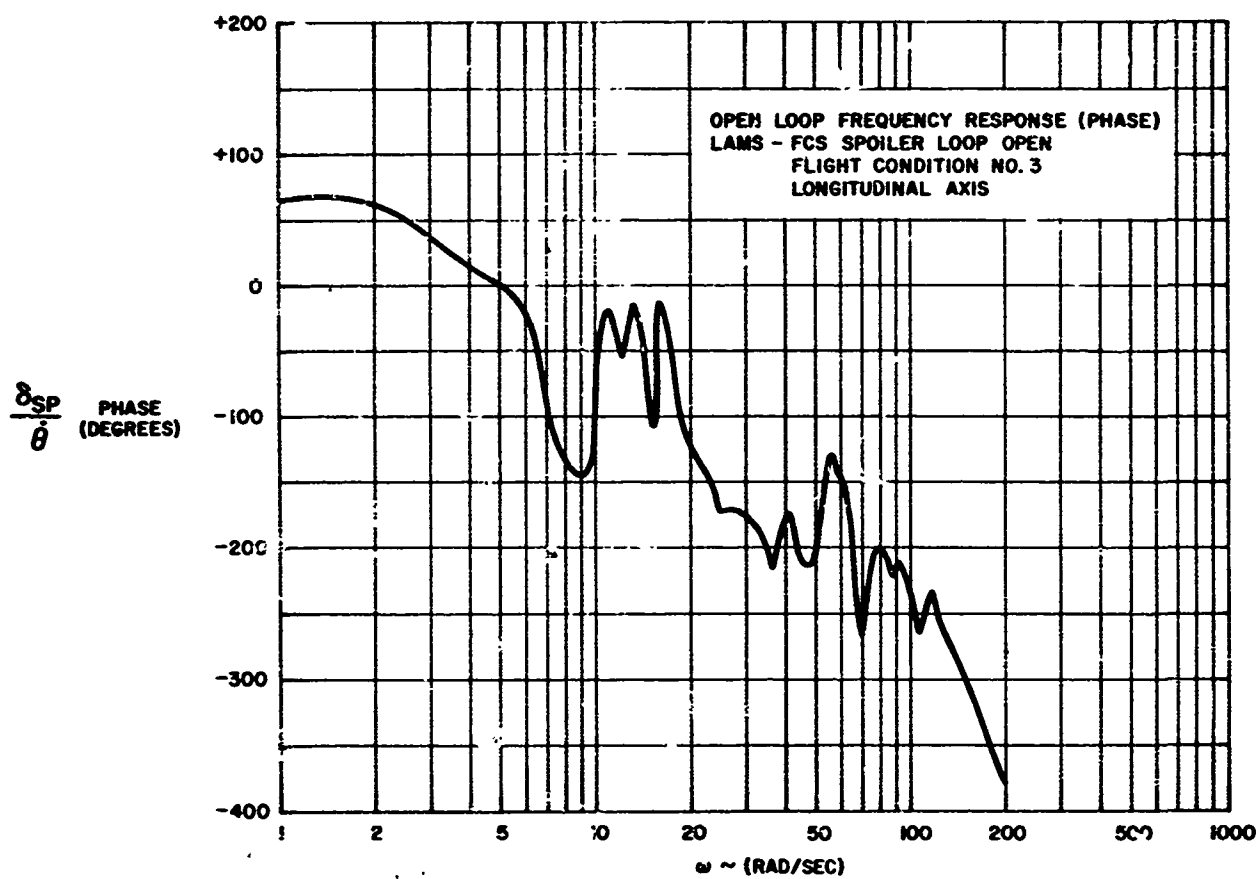
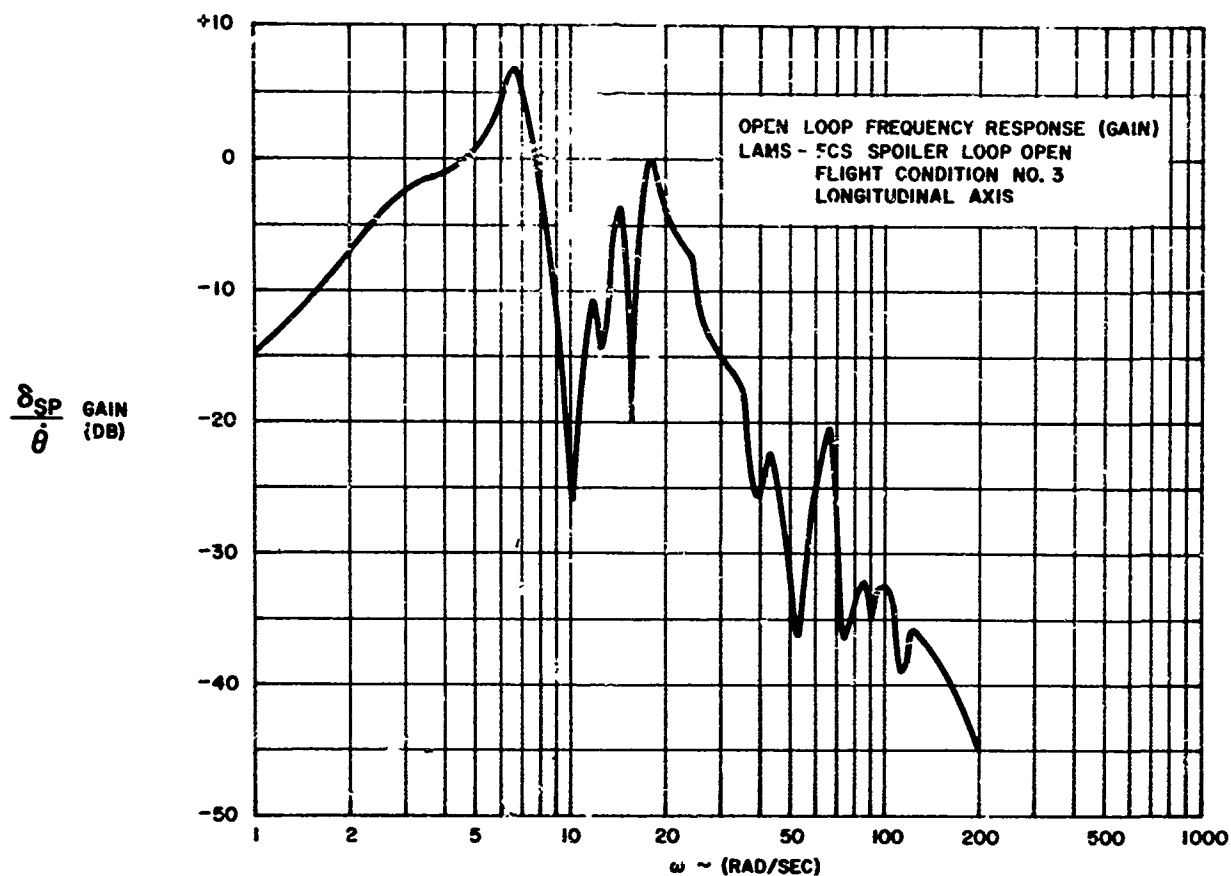


FIGURE 34

TABLE X
LAMS-FCS
SPOILER LOOP MARGINS - LONGITUDINAL AXIS
FLIGHT CONDITION 3

CRITICAL FREQUENCY (RAD/SEC)	GAIN MARGIN AT NOMINAL PHASE (DB)	PHASE MARGIN AT NOMINAL GAIN (DEG)	GAIN MARGIN AT WORST PHASE (DB)
4.5		173	
6.7			Unstable 7.0
7.7		52	
11.7			10.6
14.3			3.4
17.9			0.0
31.4	15.8		
39.4	25.5		
42.2	22.5		
42.8			22.3
51.6	36.1		
64.0	20.8		
65.7			20.3
85.0			32.5
96.3			32.5
121.5			35.8

4.2.1.2.1 Longitudinal Axis (Symmetric)

The stability analysis results for the spoiler loops are not for the final spoiler configuration. The equations used included LAMS spoilers but did not include the spoiler loop gain changes to provide proper surface to structural mode phasing as discussed in Section 3.8. This improper phasing was the result of an incomplete math model with respect to spoiler aerodynamics. The revised math model and final system configuration had adequate predicted eigenvalue equations presented in Section 4.6 and would yield similar results to that presented in Tables through XIII.

Figures 35 through 37 are the Bode plots for Flight Condition 1. The plots are typical of Flight Conditions 2 and 3 except for the spoiler loop of FC-3 noted above, and are presented in Appendix B. The minimum gain margin is 10 db at 61.6 radians per second for Flight Condition 1 aileron loop. The longitudinal axis FCS has at least 10 db gain margin at worst phase for all modes above 69 radians per second.

Eigenvalue comparisons of the free aircraft and LAMS-FCS configurations are presented in Tables XIV through XVI and show frequency and damping for each of the analysis roots.

4.2.1.2.2 Lateral Axis (Antisymmetric)

The stability analyses conducted indicated that the lateral axis met the minimum flight control system design criteria. Typical results are presented in Tables XVII and XVIII, and Figures 38 and 39 for Flight Condition 1. The results for Flight Conditions 2 and 3 are presented in Appendix B.

The data shows that the minimum phase margin at nominal gain is 86 degrees for the rudder loop of FC-2 and 3, and the minimum gain margin at nominal phase is 17.7 db for the aileron loop of FC-1. Also, the system has greater than 10 db gain margin at worst phase for frequencies above 28 radians per second, and all structural modes are gain stabilized.

Eigenvalue comparisons of the free aircraft and LAMS-FCS configurations are presented in Tables XIX through XXI and show frequency and damping for each of the analysis roots.

TABLE XI
LAMS-FCS
ELEVATOR LOOP MARGINS - LONGITUDINAL AXIS

FLIGHT CONDITION 1

CRITICAL FREQUENCY (RAD/SEC)	GAIN MARGIN AT NOMINAL PHASE (DB)	PHASE MARGIN AT NOMINAL GAIN (DEG)	GAIN MARGIN AT WORST PHASE (DB)
1.8		110	
7.6			11.1
11.8			17.6
12.6			18.3
14.4			15.5
18.9	19.3		
19.2			19.0
20.3	25.0		
21.0	20.0		
21.7			17.7
29.4			30.4
37.5			29.0
43.3			28.5
60.2			22.9
84.5			22.7
112.0			29.9
113.4	30.3		

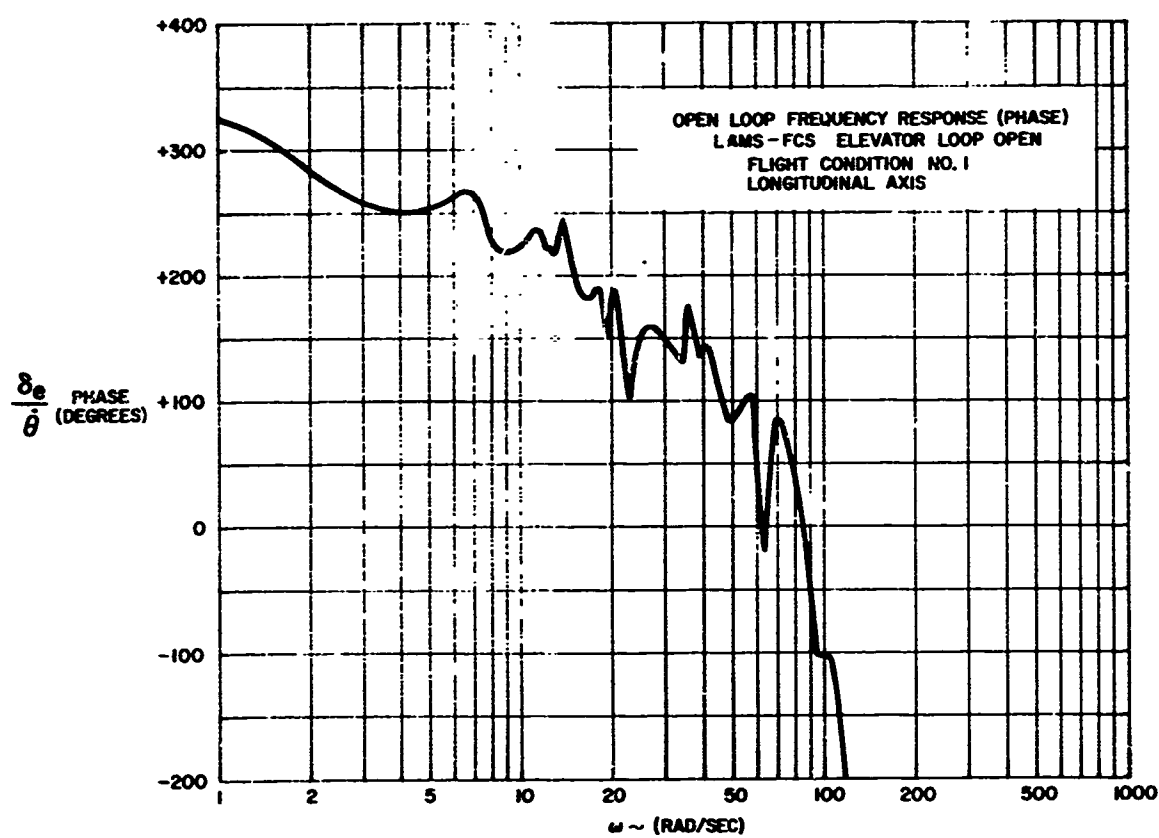
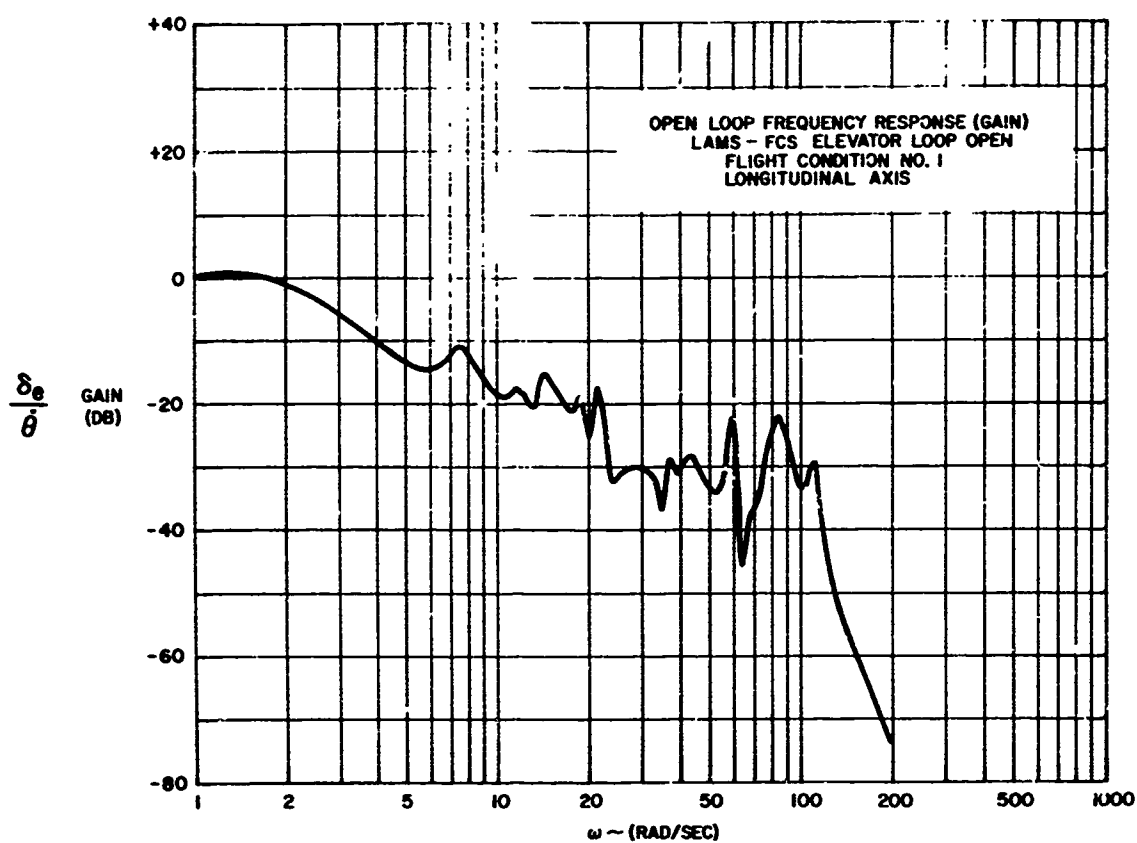


FIGURE 35

TABLE XII
LAMS-FCS
AILERON LOOP MARGINS - LONGITUDINAL AXIS
FLIGHT CONDITION 1

CRITICAL FREQUENCY (RAD/SEC)	GAIN MARGIN AT NOMINAL PHASE (DB)	PHASE MARGIN* AT NOMINAL GAIN (DEG)	GAIN MARGIN AT WORST PHASE (DB)
11.8			14.3
12.6			16.2
14.4			7.2
18.8			14.7
21.4			10.9
22.3	13.8		
31.2			41.2
36.2			28.4
40.3			22.0
59.4			6.1
61.6	10.0		
86.3			18.4
117.0	40.0		

*System is Gain Stabilized

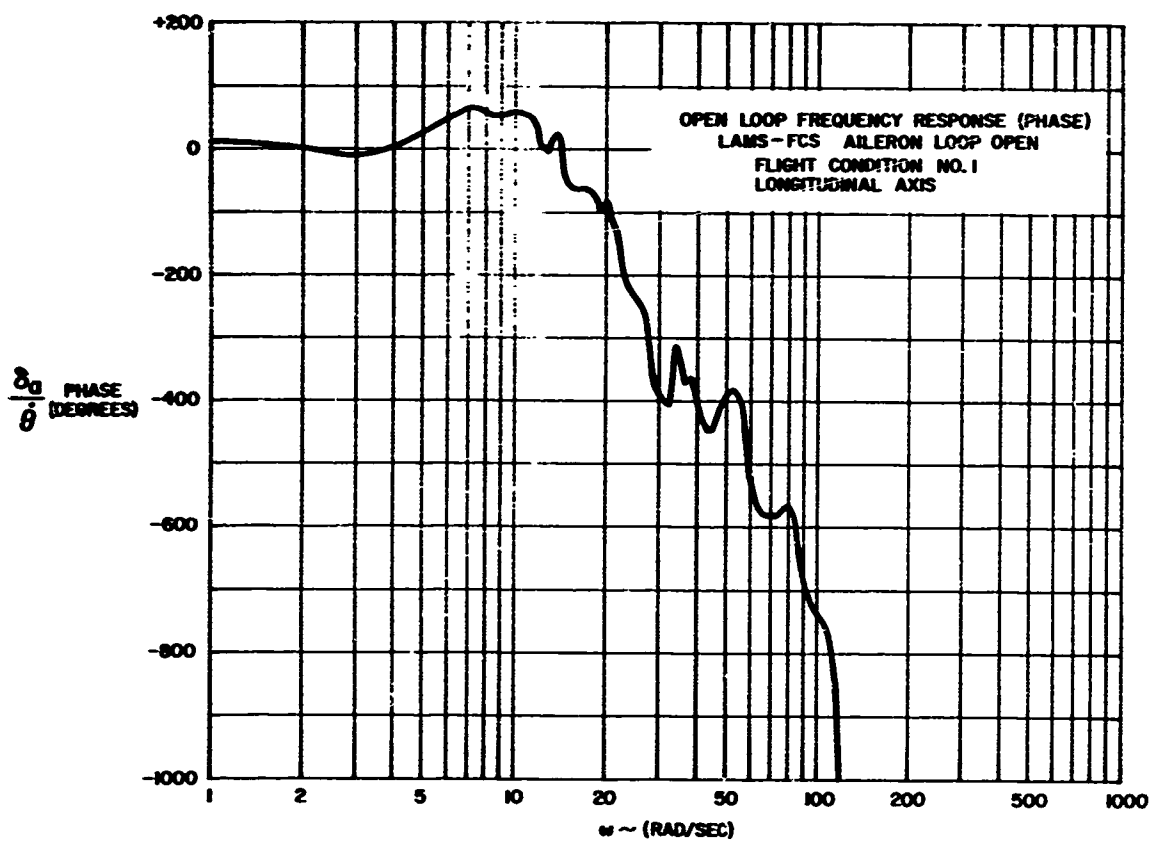
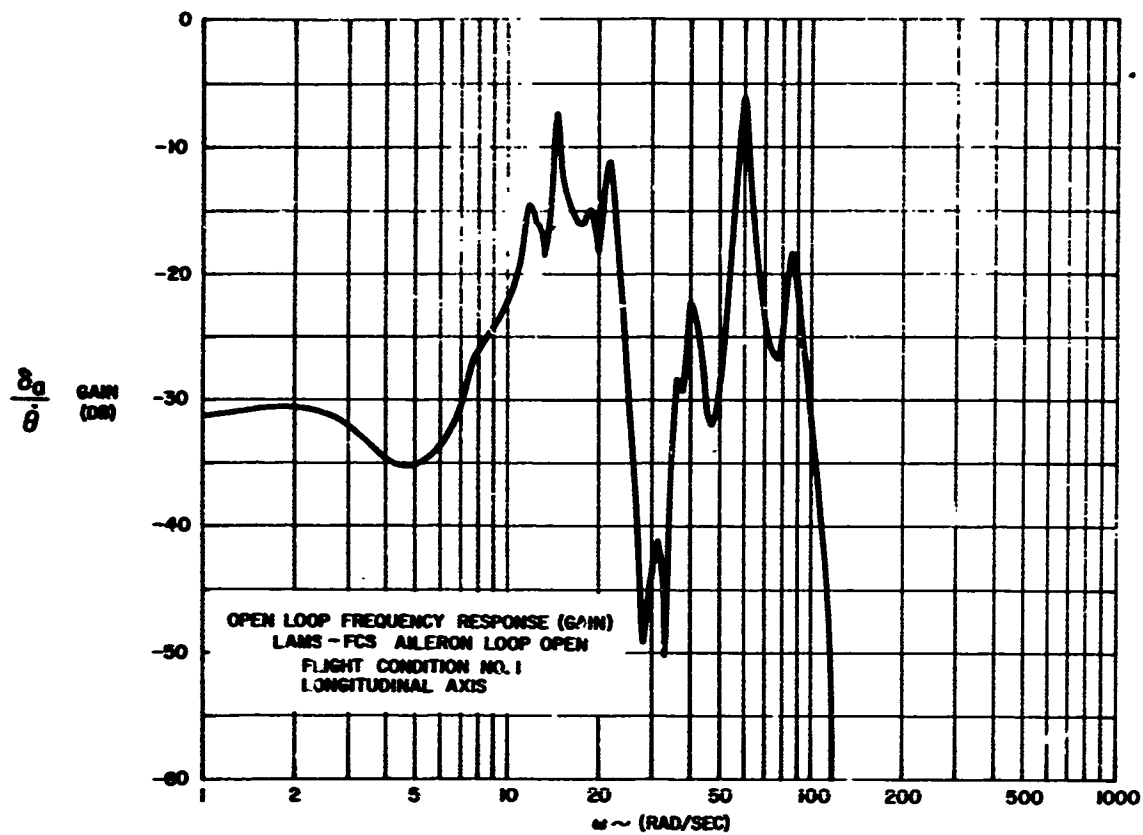


FIGURE 36

TABLE XIII
LAMS-FCS
SPOILER LOOP MARGINS - LONGITUDINAL AXIS
FLIGHT CONDITION 1

CRITICAL FREQUENCY (RAD/SEC)	GAIN MARGIN AT NOMINAL PHASE (DB)	PHASE MARGIN* AT NOMINAL GAIN (DEG)	GAIN MARGIN AT WORST PHASE (DB)
3.5		151	
6.3			Unstable 4.1
7.3		71	
11.6			9.8
14.1			5.2
17.6			2.3
21.6			5.3
30.2	13.8		
35.7			20.0
39.8			21.1
47.7	34.6		
59.7	19.4		
60.1			19.4
81.2			31.3
91.6			31.2
109.1			34.7
129.5			37.1

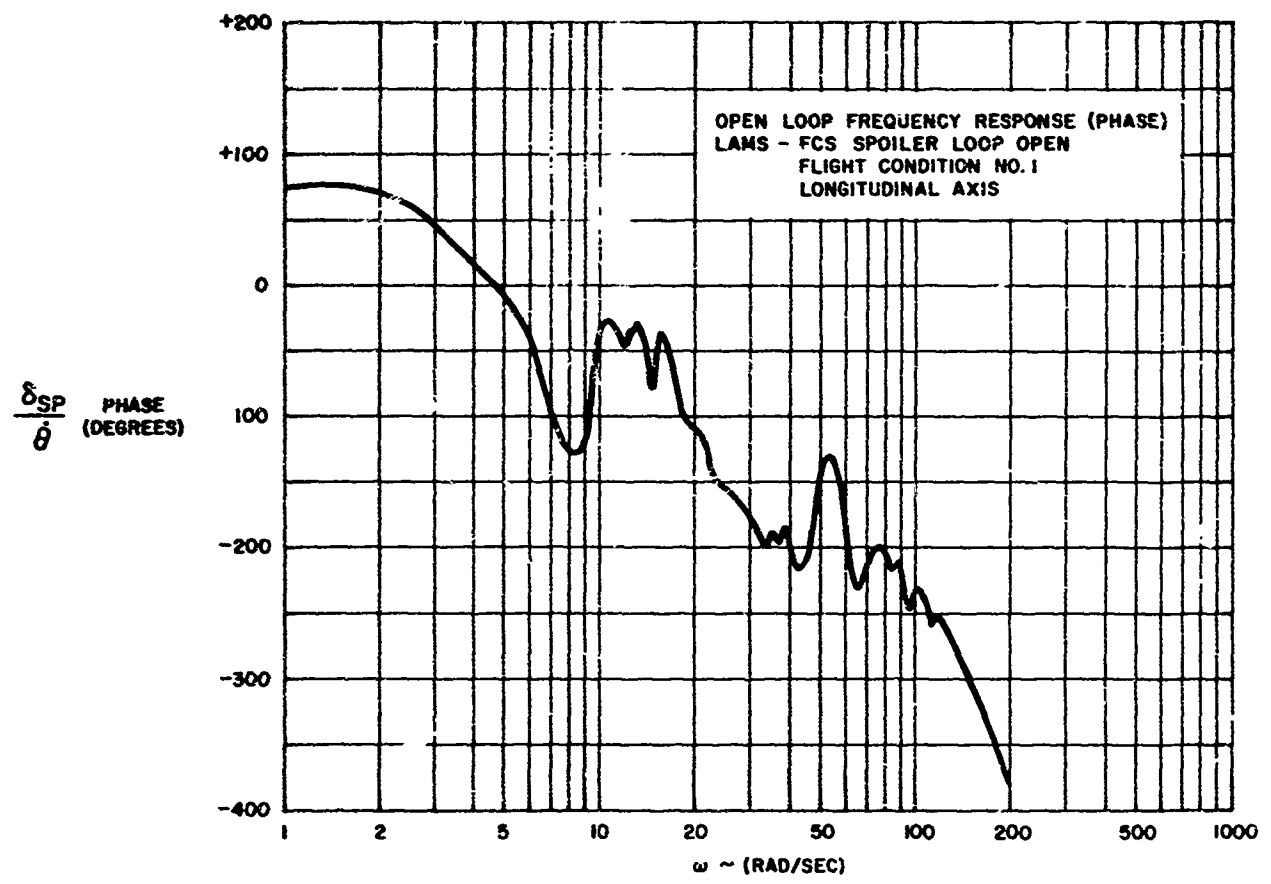
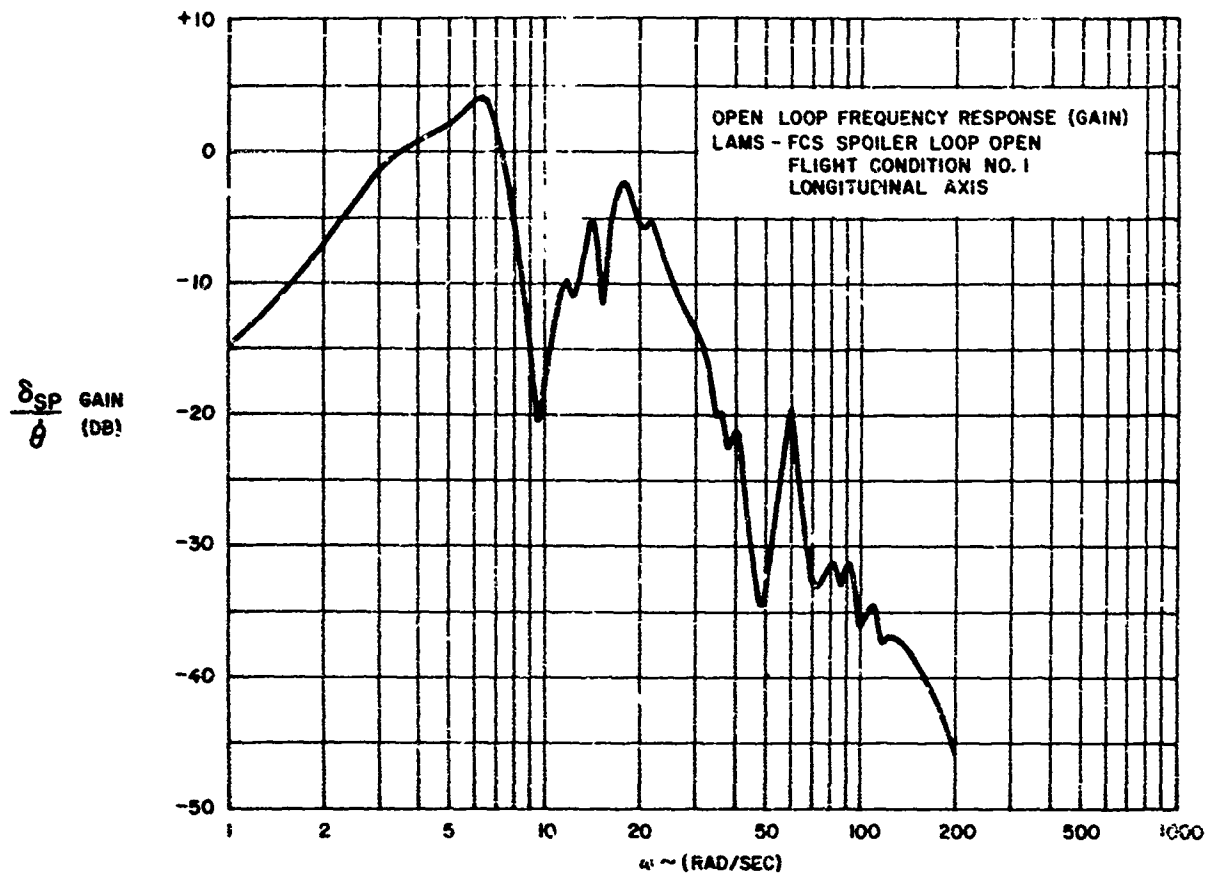


FIGURE 37

TABLE XIV
LAMS-FCS LONGITUDINAL EIGENVALUES

FLIGHT CONDITION 1

FREE AIRPLANE DATA				AUGMENTED AIRPLANE DATA		
Mode	Root Locations	ζ	$\frac{\omega_n}{f_n}$	Root Locations	ζ	$\frac{\omega_n}{f_n}$
SP	$-1.08 \pm j 2.28$.428	2.52 .401	$-1.57 \pm j 2.29$.565	2.78 .442
1	$-.98 \pm j 6.65$.146	6.71 1.07	$-.84 \pm j 7.65$.109	7.70 1.23
2	$-.67 \pm j 12.00$.056	12.00 1.91	$-.62 \pm j 12.08$.051	12.08 1.92
3	$-.44 \pm j 12.68$.035	12.68 2.02	$-.44 \pm j 12.70$.035	12.70 2.02
4	$-.60 \pm j 14.65$.041	14.65 2.34	$-.48 \pm j 14.72$.033	14.72 2.35
5	$-1.28 \pm j 14.88$.086	14.88 2.37	$-1.24 \pm j 15.03$.082	15.03 2.40
6	$-1.59 \pm j 16.71$.095	16.71 2.66	$-3.18 \pm j 19.18$.164	19.42 3.10
7	$-.74 \pm j 19.64$.038	19.64 3.13	$-.71 \pm j 19.41$.037	19.41 3.09
8	$-1.82 \pm j 21.49$.085	21.49 3.42	$-1.36 \pm j 21.73$.063	21.73 3.46
9	$2.42 \pm j 33.56$.072	33.56 5.35	$-2.43 \pm j 33.37$.074	33.37 5.32
10	$-1.62 \pm j 36.36$.045	36.36 5.79	$-1.58 \pm j 36.36$.043	36.36 5.79
11	$-1.14 \pm j 37.62$.030	37.62 5.98	$-1.14 \pm j 37.63$.030	37.63 5.93
12	$-2.21 \pm j 39.83$.055	39.83 6.03	$-2.23 \pm j 39.90$.056	39.90 6.05
13	$-7.98 \pm j 45.72$.172	46.40 7.38	$-7.76 \pm j 45.64$.168	46.39 7.36
14	$-1.80 \pm j 57.05$.032	57.05 9.08	$-1.79 \pm j 57.09$.031	57.09 9.09
15	$-2.05 \pm j 59.35$.035	59.35 9.44	$-1.49 \pm j 60.21$.025	60.21 9.53
16	$-4.90 \pm j 61.59$.080	61.59 9.81	$-5.05 \pm j 61.34$.082	61.34 9.84
17	$-4.00 \pm j 64.71$.062	64.71 10.30	$-4.18 \pm j 64.22$.065	64.22 10.21
18	$-4.38 \pm j 83.56$.052	83.56 13.30	$-4.05 \pm j 83.65$.048	83.65 13.32
19	$-5.42 \pm j 88.16$.061	88.16 14.02	$-6.18 \pm j 88.10$.070	88.10 14.01
20	$-8.72 \pm j 94.16$.093	94.16 15.00	$-7.96 \pm j 94.37$.084	94.37 14.91
21	$-4.57 \pm j 94.86$.048	94.86 15.10	$-4.77 \pm j 94.70$.050	94.70 15.08
22	$-4.13 \pm j 113.38$.036	113.38 18.05	$-3.95 \pm j 113.35$.035	113.35 18.05

TABLE XV
LAMS-FCS LONGITUDINAL EIGENVALUES

FLIGHT CONDITION 2

FREE AIRPLANE DATA				AUGMENTED AIRPLANE DATA		
Mode	Root Locations	ζ	$\frac{\omega_n}{f_n}$	Root Locations	ζ	$\frac{\omega_n}{f_n}$
SP	- .76 ± j 1.65	.415	1.83 .291	-1.46 ± j 1.79	.637	2.32 .369
1	- .82 ± j 6.00	.135	6.05 .962	- .68 ± j 7.03	.097	7.03 1.12
2	- .66 ± j11.61	.057	11.61 1.85	- .61 ± j11.72	.052	11.72 1.87
3	- .41 ± j12.64	.032	12.64 2.01	- .40 ± j12.65	.032	12.65 2.01
4	- .89 ± j14.00	.064	14.00 2.23	- .85 ± j14.44	.059	14.44 2.30
5	- .56 ± j14.73	.038	14.73 2.35	- .56 ± j14.69	.038	14.69 2.34
6	-1.08 ± j16.44	.066	16.44 2.62	-2.35 ± j17.14	.136	17.30 2.75
7	- .69 ± j19.61	.035	19.61 3.12	- .60 ± j19.52	.031	19.52 3.11
8	-1.30 ± j21.35	.058	21.35 3.40	- .79 ± j21.49	.039	21.49 3.42
9	-1.91 ± j33.16	.058	33.16 5.28	-1.92 ± j33.10	.058	33.10 5.27
10	-1.41 ± j36.27	.039	36.27 5.77	-1.44 ± j36.32	.040	36.32 5.78
11	-1.13 ± j37.62	.030	37.62 5.98	-1.13 ± j37.63	.030	37.63 5.98
12	-1.80 ± j39.87	.045	39.87 6.35	-1.95 ± j39.91	.049	39.91 6.35
13	-5.48 ± j44.85	.121	45.20 7.20	-5.52 ± j44.75	.122	45.10 7.18
14	-1.77 ± j57.05	.031	57.05 9.07	-1.80 ± j57.05	.032	57.05 9.07
15	-1.95 ± j59.65	.033	59.65 9.50	-1.70 ± j60.62	.028	60.62 9.65
16	-3.46 ± j62.01	.056	62.01 9.86	-3.76 ± j62.06	.061	62.06 9.87
17	-3.44 ± j65.73	.052	65.73 10.45	-3.45 ± j65.25	.053	65.25 10.33
18	-3.57 ± j83.82	.043	83.82 13.34	-3.36 ± j84.05	.040	84.05 13.37
19	-4.52 ± j89.11	.051	89.11 14.18	-5.15 ± j88.64	.053	88.64 14.10
20	-4.88 ± j94.03	.052	94.03 14.97	-4.50 ± j93.82	.048	92.32 14.92
21	-5.88 ± j96.36	.062	96.36 15.32	-5.79 ± j96.64	.060	96.64 15.33
22	-3.89 ± j113.49	.034	113.49 18.08	-3.70 ± j113.48	.033	113.48 18.03

TABLE XVI
LAMS-FCS LONGITUDINAL EIGENVALUES
FLIGHT CONDITION 3

FREE AIRPLANE DATA				AUGMENTED AIRPLANE DATA		
Mode	Root Locations	ζ	$\frac{\omega_n}{f_n}$	Root Locations	ζ	$\frac{\omega_n}{f_n}$
SP	- .74 \pm j 2.06	.338	2.19 .348	-1.47 \pm j 2.11	.571	2.58 .411
1	- .70 \pm j 6.62	.105	6.65 1.06	- .67 \pm j 7.86	.085	7.86 1.25
2	- .57 \pm j11.92	.048	11.92 1.90	- .53 \pm j12.04	.044	12.04 1.92
3	- .40 \pm j12.66	.032	12.66 2.01	- .40 \pm j12.68	.032	12.68 2.02
4	- .79 \pm j14.48	.055	14.48 2.30	- .88 \pm j15.00	.059	15.00 2.38
5	- .61 \pm j15.26	.040	15.26 2.43	- .52 \pm j15.14	.034	15.14 2.41
6	-1.13 \pm j17.47	.065	17.47 2.78	-2.91 \pm j19.49	.147	19.72 3.14
7	- .71 \pm j19.69	.036	19.69 3.13	- .65 \pm j19.54	.033	19.54 3.11
8	-1.37 \pm j24.30	.056	24.30 3.87	- .86 \pm j24.17	.036	24.17 3.84
9	-1.96 \pm j35.64	.055	35.64 5.67	-1.94 \pm j35.43	.055	35.43 5.64
10	-1.31 \pm j37.48	.035	37.48 5.96	-1.29 \pm j37.46	.034	37.46 5.96
11	-1.16 \pm j37.70	.031	37.70 6.00	-1.16 \pm j37.71	.031	37.71 6.00
12	-2.00 \pm j42.57	.047	42.57 6.78	-2.03 \pm j42.66	.048	42.66 6.80
13	-4.65 \pm j47.55	.098	47.55 7.57	-4.58 \pm j47.46	.097	47.46 7.55
14	-1.79 \pm j58.08	.031	58.08 9.24	-1.81 \pm j58.09	.031	58.09 9.24
15	-3.84 \pm j63.29	.061	63.29 10.08	-3.50 \pm j63.69	.055	63.69 10.14
16	-2.66 \pm j64.60	.041	64.60 10.30	-2.62 \pm j65.37	.040	65.37 10.40
17	-2.64 \pm j68.62	.039	68.62 10.92	-2.59 \pm j67.96	.038	67.96 10.80
18	-4.29 \pm j86.90	.049	86.90 13.82	-4.19 \pm j87.00	.048	87.00 13.83
19	-3.96 \pm j91.13	.043	91.13 14.50	-4.36 \pm j90.97	.048	90.97 14.49
20	-6.07 \pm j96.78	.063	96.78 15.40	-5.90 \pm j96.74	.061	96.74 15.40
21	-4.10 \pm j105.80	.039	105.80 16.82	-4.31 \pm j105.66	.041	105.66 16.80
22	-3.77 \pm j117.46	.032	117.46 18.70	-3.68 \pm j117.47	.031	117.47 18.70

TABLE XVII
LAMS-FCS
RUDDER LOOP MARGINS - LATERAL-DIRECTIONAL AXIS
FLIGHT CONDITION 1

CRITICAL FREQUENCY (RAD/SEC)	GAIN MARGIN AT NOMINAL PHASE (DB)	PHASE MARGIN AT NOMINAL GAIN (DEG)	GAIN MARGIN AT WORST PHASE (DE)
1.7		93	
9.1			22.0
12.1			20.6
13.1			21.3
14.8	19.9		
17.2			17.1
26.2			32.3
27.9	33.9		
39.7	28.5		
40.9			27.1
58.6			25.3
81.0			17.9
81.6	18.0		

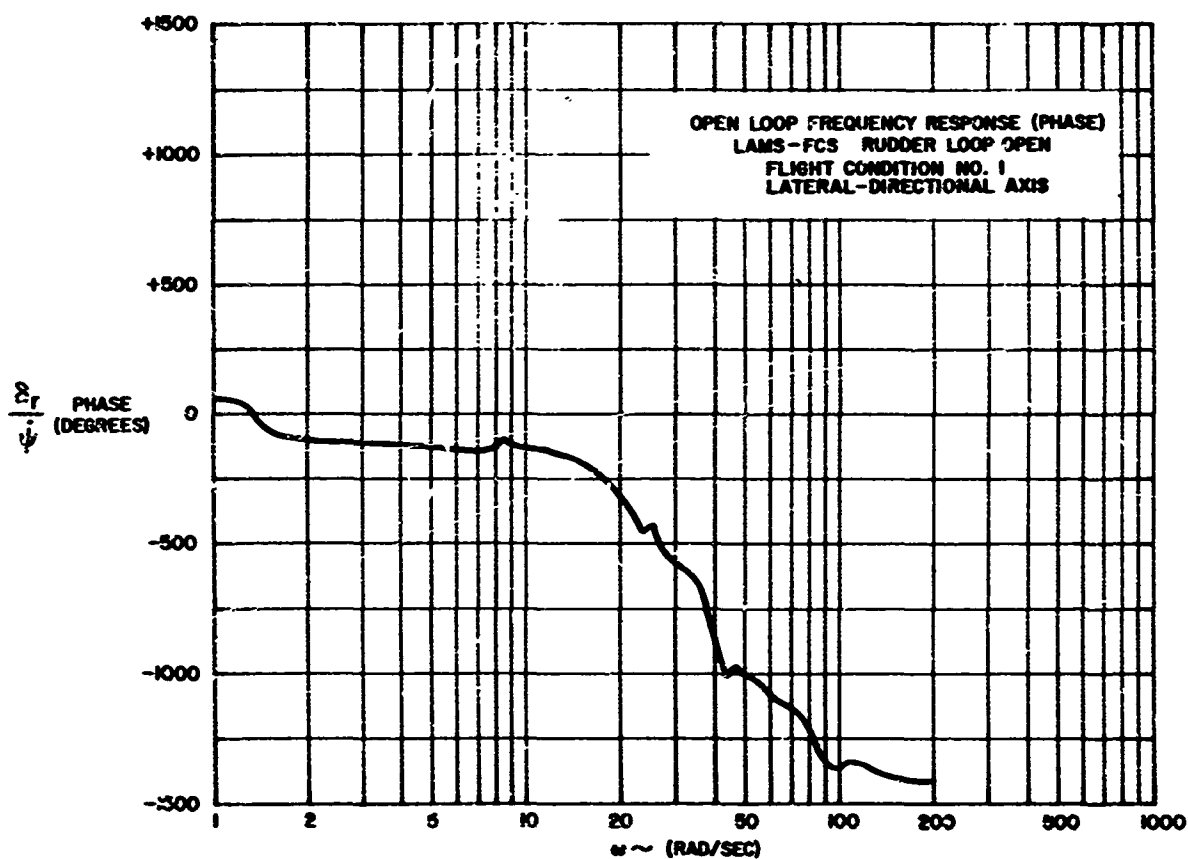
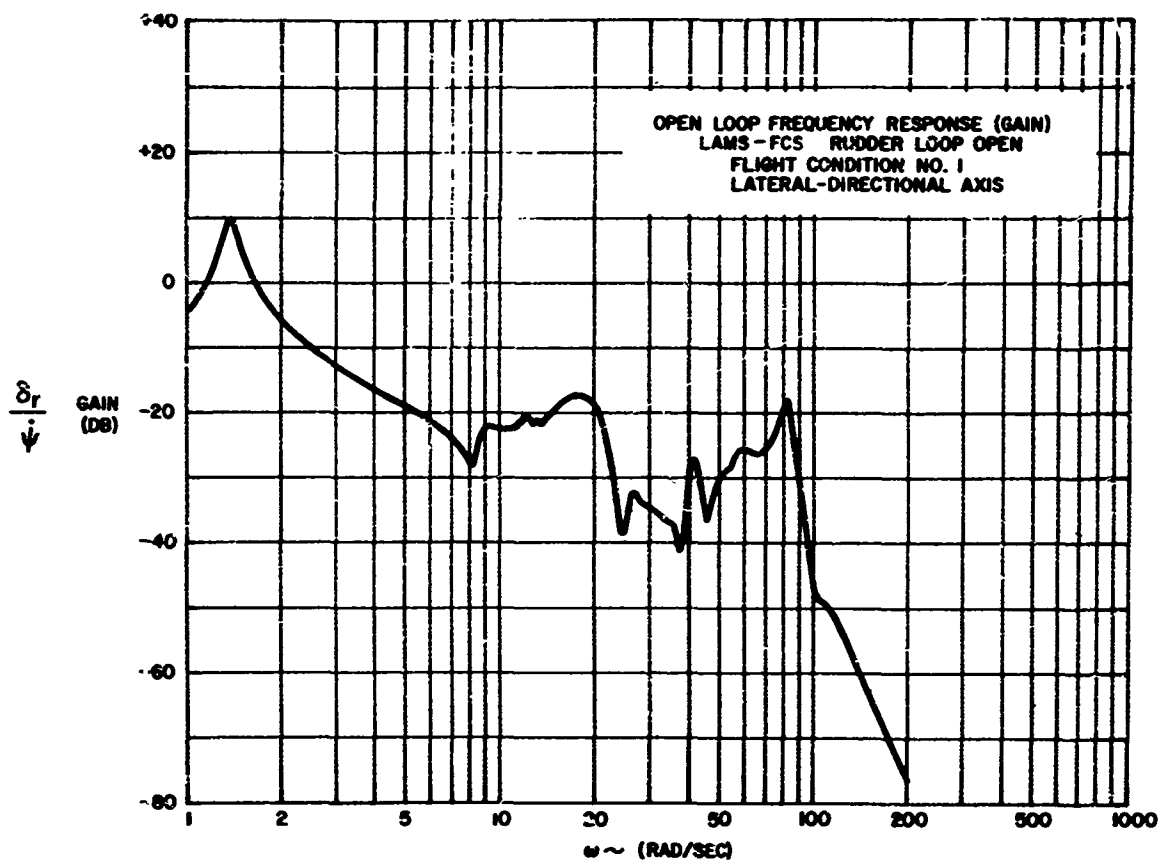


FIGURE 38

TABLE XVIII
LAMS-FCS
AILERON LOOP MARGINS - LATERAL-DIRECTIONAL AXIS

FLIGHT CONDITION 1

CRITICAL FREQUENCY (RAD/SEC)	GAIN MARGIN AT NOMINAL PHASE (DB)	PHASE MARGIN* AT NOMINAL GAIN (DEG)	GAIN MARGIN AT WORST PHASE (DB)
6.3			21.8
8.5			25.0
12.0			8.2
16.0	17.7		
20.5			11.1
25.4			9.3
32.6	18.2		
38.9	45.5		
41.1	18.8		
41.9			18.3
56.1			14.9
72.8			17.7

*System is Gain Stabilized

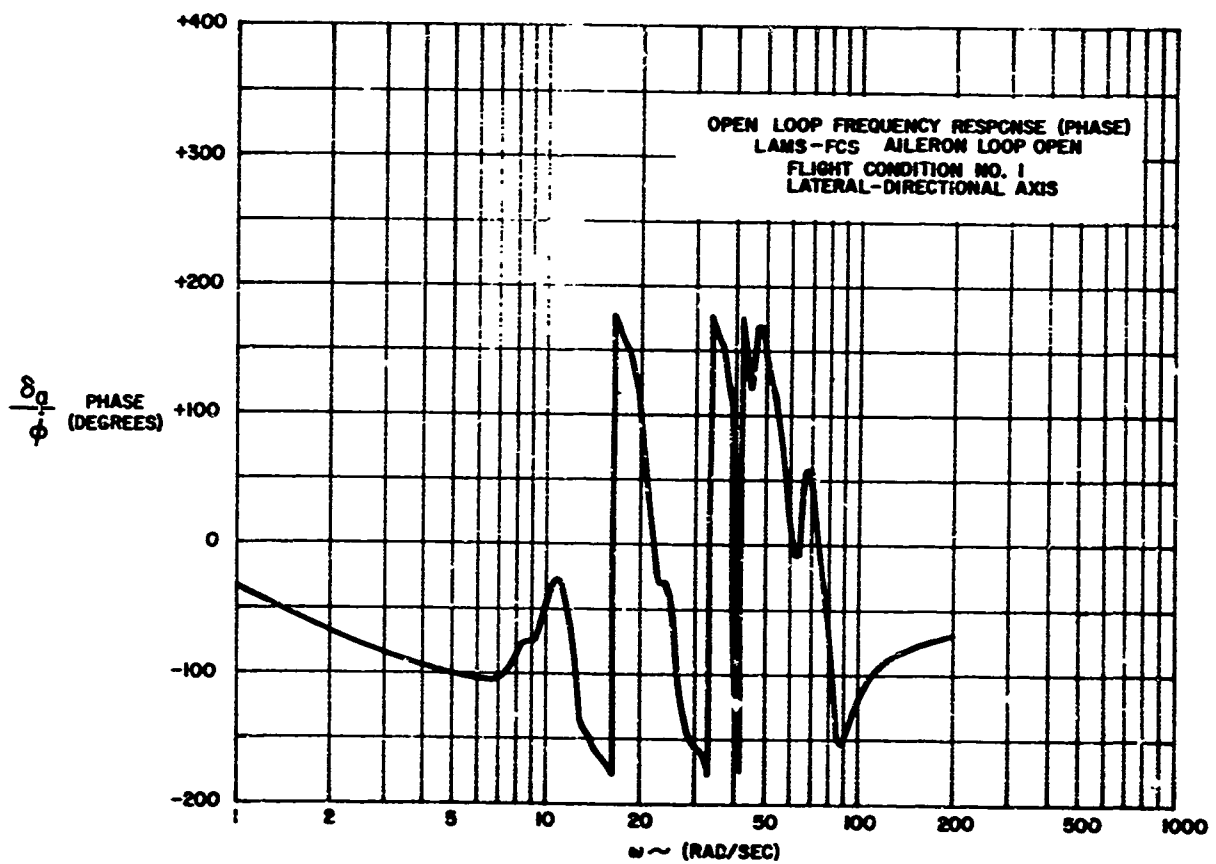
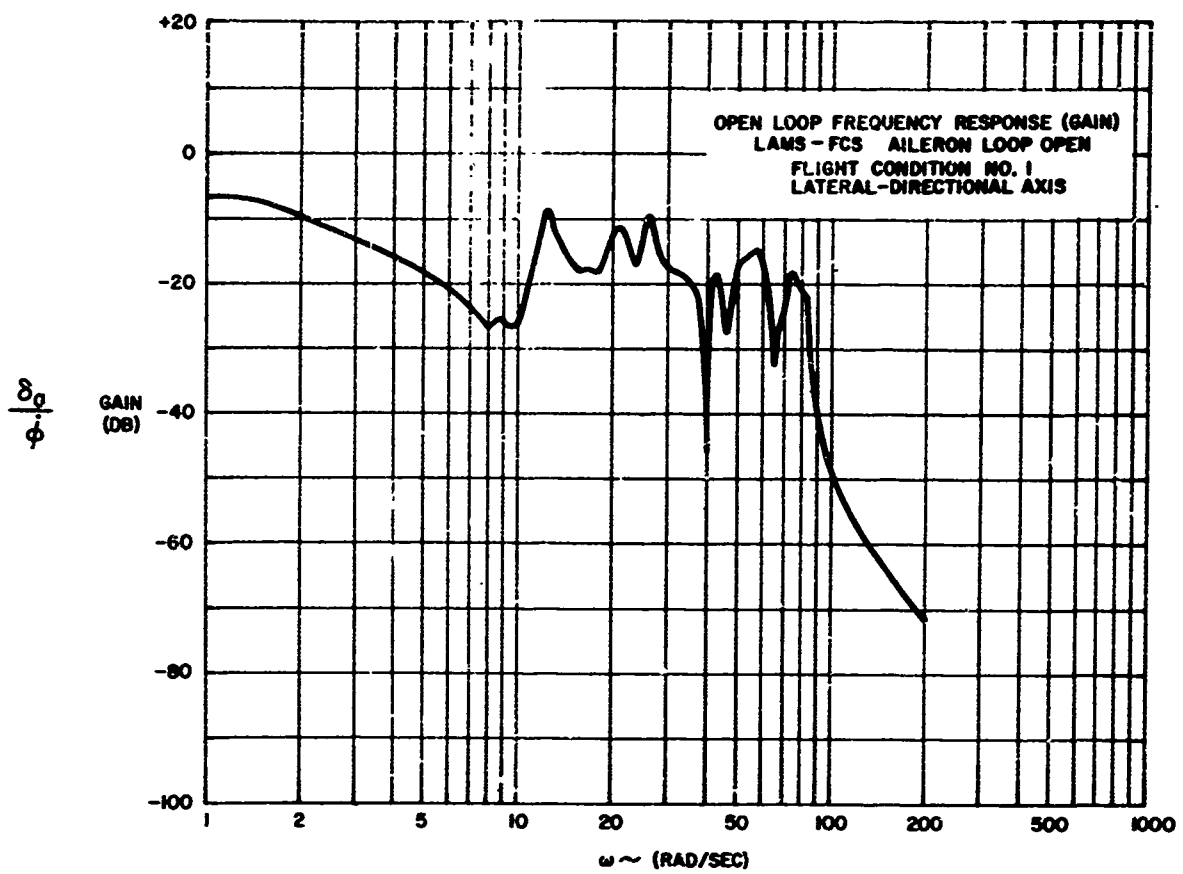


FIGURE 39

TABLE XIX
LAMS-FCS LATERAL-DIRECTIONAL EIGENVALUES
FLIGHT CONDITION 1

FREE AIRPLANE DATA				AUGMENTED AIRPLANE DATA		
Mode	Root Locations	ζ	$\frac{\omega_n}{f_n}$	Root Locations	ζ	$\frac{\omega_n}{f_n}$
DR	$-.072 \pm j 1.37$.053	1.37 .218	$-.38 \pm j 1.40$.262	1.45 .231
1	$-.63 \pm j 8.33$.076	8.33 1.33	$-.69 \pm j 8.34$.083	8.34 1.33
2	$-.71 \pm j 11.88$.060	11.88 1.89	$-.84 \pm j 12.27$.069	12.27 1.95
3	$-.41 \pm j 12.84$.032	12.84 2.04	$-.44 \pm j 12.80$.034	12.80 2.04
4	$-1.73 \pm j 12.85$.133	13.00 2.07	$-1.64 \pm j 12.64$.129	12.75 2.03
5	$-.85 \pm j 16.41$.052	16.41 2.61	$-.84 \pm j 16.43$.051	16.43 2.62
6	$-2.10 \pm j 16.76$.124	16.90 2.69	$-1.88 \pm j 16.43$.114	16.55 2.64
7	$-1.63 \pm j 19.74$.083	19.74 3.14	$-1.35 \pm j 19.44$.070	19.44 3.10
8	$-1.41 \pm j 21.05$.070	21.05 3.35	$-1.69 \pm j 21.37$.079	21.37 3.40
9	$-1.05 \pm j 25.33$.041	25.33 4.02	$-1.22 \pm j 25.66$.048	25.66 4.08
10	$-2.78 \pm j 31.26$.089	31.26 4.98	$-2.79 \pm j 31.36$.086	31.36 4.99
11	$-1.14 \pm j 36.76$.031	36.76 5.85	$-1.14 \pm j 36.77$.031	36.77 5.85
12	$-1.19 \pm j 37.30$.032	37.30 5.93	$-1.20 \pm j 37.29$.032	37.29 5.93
13	$-6.45 \pm j 38.26$.168	38.40 6.11	$-6.51 \pm j 38.13$.169	38.60 6.14
14	$-1.57 \pm j 39.32$.040	39.32 6.25	$-1.64 \pm j 39.36$.042	39.36 6.26
15	$-1.35 \pm j 43.21$.043	43.21 6.87	$-1.32 \pm j 43.01$.042	43.01 6.84
16	$-3.33 \pm j 49.07$.068	49.07 7.80	$-2.97 \pm j 49.36$.060	49.36 7.85
17	$-4.05 \pm j 57.77$.070	57.77 9.20	$-4.49 \pm j 56.84$.079	56.84 9.04
18	$-4.77 \pm j 64.12$.074	64.12 10.20	$-4.56 \pm j 64.34$.071	64.34 10.22
19	$-4.40 \pm j 67.82$.065	67.82 10.80	$-4.49 \pm j 67.71$.066	67.71 10.78
20	$-3.05 \pm j 72.25$.042	72.25 11.50	$-3.44 \pm j 71.77$.043	71.77 11.42
21	$-3.30 \pm j 81.04$.041	81.04 12.90	$-2.59 \pm j 81.04$.032	81.04 12.30

TABLE XX
LAMS-FCS LATERAL-DIRECTIONAL EIGENVALUES

FLIGHT CONDITION 2

FREE AIRPLANE DATA				AUGMENTED AIRPLANE DATA		
Mode	Root Locations	ζ	ω_n f_n	Root Locations	ζ	ω_n f_n
DR	$-.044 \pm j 1.08$.041	1.08 .172	$-.48 \pm j 1.06$.413	1.16 .185
1	$-.54 \pm j 7.82$.069	7.82 1.24	$-.56 \pm j 7.80$.072	7.80 1.24
2	$-1.20 \pm j 10.79$.111	10.85 1.73	$-1.19 \pm j 10.18$.110	10.83 1.73
3	$-.62 \pm j 12.29$.050	12.29 1.96	$-.62 \pm j 12.33$.050	12.33 1.97
4	$-.41 \pm j 12.85$.032	12.85 2.04	$-.43 \pm j 12.86$.033	12.86 2.04
5	$-1.42 \pm j 15.98$.089	15.98 2.54	$-1.33 \pm j 15.77$.084	15.77 2.51
6	$-.73 \pm j 16.64$.044	16.64 2.65	$-.67 \pm j 16.63$.040	16.63 2.65
7	$-1.22 \pm j 19.56$.062	19.56 3.12	$-1.11 \pm j 19.47$.057	19.47 3.10
8	$-1.06 \pm j 21.19$.050	21.19 3.38	$-1.17 \pm j 21.30$.055	21.30 3.39
9	$-.94 \pm j 25.46$.037	25.46 4.05	$-1.02 \pm j 25.61$.040	25.61 4.07
10	$-2.04 \pm j 30.85$.066	30.85 4.91	$-2.07 \pm j 30.86$.067	30.86 4.91
11	$-4.66 \pm j 36.41$.127	36.70 5.84	$-4.69 \pm j 36.26$.128	36.60 5.83
12	$-1.13 \pm j 36.77$.031	36.77 5.85	$-1.14 \pm j 36.78$.031	36.78 5.85
13	$-1.16 \pm j 37.30$.031	37.30 5.94	$-1.16 \pm j 37.29$.031	37.29 5.94
14	$-1.45 \pm j 39.25$.037	39.25 6.24	$-1.43 \pm j 39.23$.036	39.23 6.24
15	$-1.66 \pm j 43.15$.038	43.15 6.87	$-1.62 \pm j 43.17$.037	43.17 6.87
16	$-2.57 \pm j 49.07$.052	49.07 7.81	$-2.51 \pm j 49.25$.051	49.25 7.84
17	$-3.18 \pm j 57.44$.055	57.74 9.14	$-3.26 \pm j 57.28$.057	57.28 9.12
18	$-3.70 \pm j 65.31$.057	65.31 10.40	$-3.65 \pm j 65.31$.056	65.39 10.40
19	$-3.57 \pm j 67.95$.052	67.95 10.81	$-3.59 \pm j 67.88$.053	67.88 10.81
20	$-2.72 \pm j 72.30$.038	72.30 11.50	$-2.80 \pm j 71.99$.039	71.94 11.47
21	$-3.00 \pm j 81.21$.037	81.21 12.92	$-2.69 \pm j 81.30$.033	81.30 12.93

TABLE XXI
LAMS-FCS LATERAL-DIRECTIONAL EIGENVALUES

FLIGHT CONDITION 3

FREE AIRPLANE DATA				AUGMENTED AIRPLANE DATA		
Mode	Root Locations	ζ	ω_n f_n	Root Locations	ζ	ω_n f_n
DR	$-.048 \pm j 1.24$.039	1.24 .197	$-.41 \pm j 1.26$.309	1.33 .212
1	$-.47 \pm j 8.18$.057	8.18 1.30	$-.51 \pm j 8.19$.062	8.19 1.30
2	$-.85 \pm j 11.55$.074	11.55 1.84	$-.99 \pm j 11.60$.085	11.60 1.85
3	$-.75 \pm j 12.53$.060	12.53 2.00	$-.54 \pm j 12.52$.045	12.52 2.00
4	$-.45 \pm j 12.91$.035	12.91 2.06	$-.53 \pm j 12.95$.041	12.95 2.06
5	$-.76 \pm j 16.48$.046	16.48 2.62	$-.78 \pm j 16.42$.047	16.42 2.62
6	$-1.56 \pm j 17.86$.037	17.86 2.84	$-1.38 \pm j 17.77$.078	17.77 2.83
7	$-1.25 \pm j 19.86$.063	19.86 3.16	$-1.28 \pm j 19.78$.065	19.78 3.15
8	$-.90 \pm j 22.91$.039	22.91 3.64	$-.84 \pm j 22.94$.037	22.94 3.65
9	$-.98 \pm j 27.09$.036	27.09 4.32	$-1.11 \pm j 27.47$.040	27.47 4.37
10	$-2.04 \pm j 31.90$.064	31.90 5.07	$-2.05 \pm j 31.96$.064	31.96 5.09
11	$-1.13 \pm j 36.87$.031	36.87 5.87	$-1.14 \pm j 36.86$.031	36.86 5.87
12	$-1.16 \pm j 37.38$.031	37.38 5.95	$-1.16 \pm j 37.35$.031	37.35 5.95
13	$-4.02 \pm j 38.77$.103	39.10 6.22	$-4.03 \pm j 38.77$.105	39.10 6.22
14	$-1.35 \pm j 41.42$.033	41.42 6.59	$-1.43 \pm j 41.32$.036	41.32 6.57
15	$-2.03 \pm j 45.70$.044	45.70 7.27	$-1.85 \pm j 45.38$.041	45.38 7.23
16	$-2.74 \pm j 51.78$.053	51.78 8.24	$-2.60 \pm j 52.17$.050	52.17 8.30
17	$-3.64 \pm j 65.23$.056	65.23 10.38	$-3.30 \pm j 65.09$.058	65.09 10.36
18	$-3.93 \pm j 67.14$.058	67.14 10.69	$-3.72 \pm j 67.33$.055	67.33 10.72
19	$-2.34 \pm j 72.29$.039	72.29 11.50	$-3.02 \pm j 71.81$.042	71.81 11.42
20	$-2.98 \pm j 80.95$.037	80.95 12.90	$-3.00 \pm j 81.21$.037	81.21 12.92
21	$-3.66 \pm j 85.13$.043	85.13 13.55	$-3.46 \pm j 85.51$.040	85.51 13.60

4.2.2 Flutter Analyses Results

The objective of the flutter analyses was to insure that the aircraft with hydraulically powered controls, Baseline SAS, and LAMS-FCS have an adequate flutter boundary for the intended LAMS test vehicle useage.

4.2.2.1 Basic Aircraft and Baseline SAS

The results of these analyses show a wing-body mode at approximately 3.2 Hz in the antisymmetric axis to be the most critical with respect to flutter. However, this mode clears the aircraft design envelope with the equivalent aircraft structural damping included. Based on the results of these analyses, the basic aircraft with hydraulically powered controls and Baseline SAS does have an adequate flutter boundary for all altitudes, gross weights and airspeeds up to and including the maximum airspeed for straight and level flight (400 KEAS and Mach .90).

4.2.2.2 LAMS-FCS

As discussed in Section 3.7.1.2, two aircraft gross weights (350 and 270 KIPS) were analyzed for flight condition one, and two gross weights (270 and 241 KIPS) were analyzed for flight condition three. The results of these analyses are as follows:

- Flight Condition 1 analyses indicate that the aircraft with the LAMS-FCS included has an adequate flutter boundary up to and including the airplane design speed (400 KEAS) at 10,000 feet or below for aircraft gross weights from 350 to 270 KIPS.
- Flight Condition 3 analyses indicate that the aircraft with the LAMS-FCS included has an adequate flutter boundary up to and including the maximum straight and level Mach .90 at 32,700 feet for gross weights between 270 to 241 KIPS.

The parametric studies accomplished during this program (with respect to the longitudinal, lateral, and directional control system stiffness, aileron and rudder actuator dynamics, and the non-linear aileron hinge moment) showed no significant effect to the flutter boundaries noted above. The analyses conducted for the 270 KIP configuration with the revised LAMS spoiler configuration using only panels 1, 2, 13, and 14 indicated no significant change in flutter boundary. Therefore, the LAMS-FCS is considered to be flutter cleared for the configurations noted above.

4.3 Predicted LAMS Handling Qualities

4.3.1 Aircraft Response Predictions

The predicted Dutch roll handling qualities for the Baseline SAS and the LAMS flight control system are shown on the criterion plot, Figure 9. These values are those obtained from a 24 degree-of-freedom model. The predicted dynamic characteristics of both systems are within the design requirement and represent a significant improvement over the basic aircraft.

Short period characteristics are indicated on the criterion plot, Figure 8. The Baseline SAS is essentially equivalent to the basic aircraft. The LAMS-FCS marginally degrades the short period handling qualities. Although at Flight Condition 3 the LAMS-FCS is not within the desired operating region, it is still within the acceptable area. In all instances, the short period damping ratio exceeds the minimum specified value of 0.40.

Predicted values for the roll time constant are listed in the table below:

ROLL TIME CONSTANT - SEC.			
FLIGHT CONDITION	BASIC AIRPLANE	BASELINE SAS	LAMS FLIGHT CONTROL SYSTEM
1	1.05	1.07	1.16
2	1.05	1.05	1.70
3	1.36	1.33	1.50

Predicted spiral mode time to half amplitude for FC-1 and FC-3 were 252 seconds and 506 seconds respectively. Time to double amplitude for FC-2 was 258.5 seconds.

4.3.2 Simulator Predicted Performance

With three test subjects per configuration, the flight simulator was used to investigate effects on Baseline SAS and LAMS-FCS performance for turbulence intensity ranging from light turbulence (rms = 1 ft/sec) to heavy turbulence (rms = 10 ft/sec). A range of gains were included to see if the SAS gains would effect the handling qualities appreciably. The data obtained from the study is presented in graphical form, Figures 40 through 45 and in Appendix C. The ordinate of these graphs is the Cooper rating categorized into three general regions of operation.

- 1-3.5 satisfactory operation
 - 3.5-6.5 unsatisfactory operation
 - 6.5-8 unacceptable operation
- } acceptable operation

The abscissa depicts the SAS gain in terms of the nominal gain. At the 100 percent gain level the longitudinal, lateral, and directional SAS's are all operating at their nominal gain setting. There is some scatter in the data which can be attributed to a learning curve effect. For example, during the earlier runs of each flight condition, the pilot may not have become completely accustomed to the simulator or the systems being simulated. A different run schedule was utilized for each pilot to minimize this effect.

It should be pointed out that the Dutch roll damping values which are correlated to gain levels in paragraphs 4.3.2.1 and 4.3.2.2 are those obtained from a quasi-elastic analysis and may differ slightly from those of the 24 degree-of-freedom model which is the basis for Figure 9 .

4.3.2.1 Baseline SAS

Referring to the data plots for the FC-1 Baseline SAS in Figures 40 through 42 and FC-2 and 3, Appendix C, it is noticed that there are very minor changes in pilot rating with a change in directional Baseline SAS gain for all three flight conditions. This results because the lowest gain points still give Dutch roll damping, $\zeta\omega$, in excess of the recommended value of $\zeta\omega = .35$. Note that there is an appreciable change in the rating due to the increase in turbulence intensity, but the ratings are still in the acceptable region of the Cooper scale.

A variation of gain for the longitudinal Baseline SAS does not cause any major change in pilot rating. This too was anticipated since the B-52 has always had satisfactory characteristics in the longitudinal axis. The basic aircraft characteristics are such that the frequency lift sensitivity and damping ratio fall within the satisfactory region on the longitudinal criterion plot. Note again the decrease in handling qualities due to the increase in turbulence.

Changes in lateral Baseline SAS gains did not improve nor degrade the aircraft handling qualities. This insensitivity to change results from two facts: the basic aircraft roll time constant is not much greater than one; and, as other investigations have shown, decreasing the roll time constant to values less than one does not improve the handling qualities.

4.3.2.2 LAMS-FCS

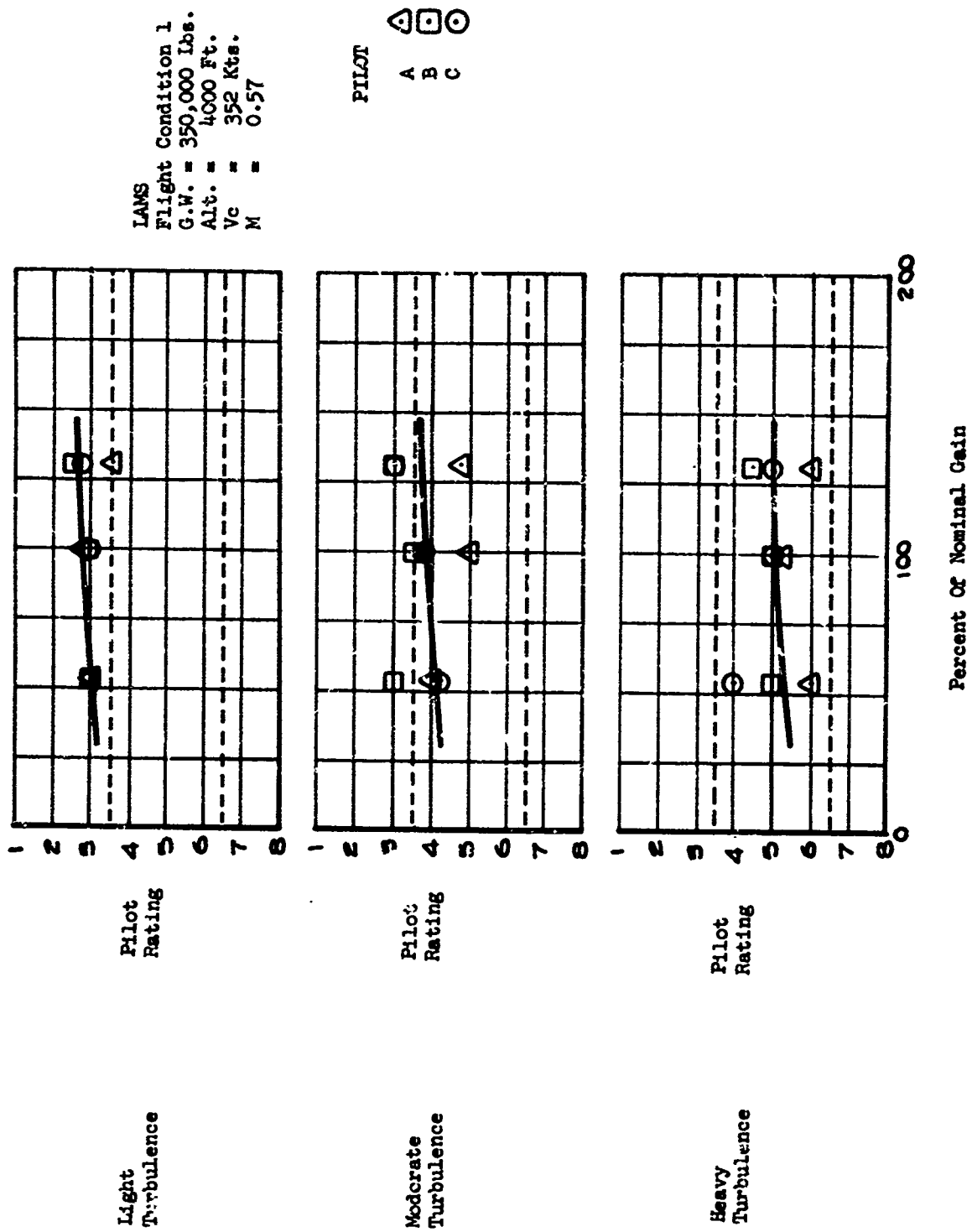
Plotted data for FC-1 in Figures 43 through 45 and for FC-2 and 3 in Appendix C, represents the handling qualities evaluation of gain variations for the LAMS-FCS. For Flight Condition 1, the directional axis ratings are better at the nominal gain setting than for the unaugmented aircraft (i.e., gains equal to zero). The Dutch roll damping values for the low gain, nominal gain and high gain points are $\zeta\omega = .265$, $.325$, and $.467$ respectively. Note that only the low gain point is appreciably less than the recommended values of $\zeta\omega = .35$.

The data for Flight Condition 2 shows essentially no change in pilot rating for the gain variation selected. However, for this case the values of $\zeta\omega$ for the low, nominal, and high gain points are $.33$, $.23$, and $.49$ respectively.

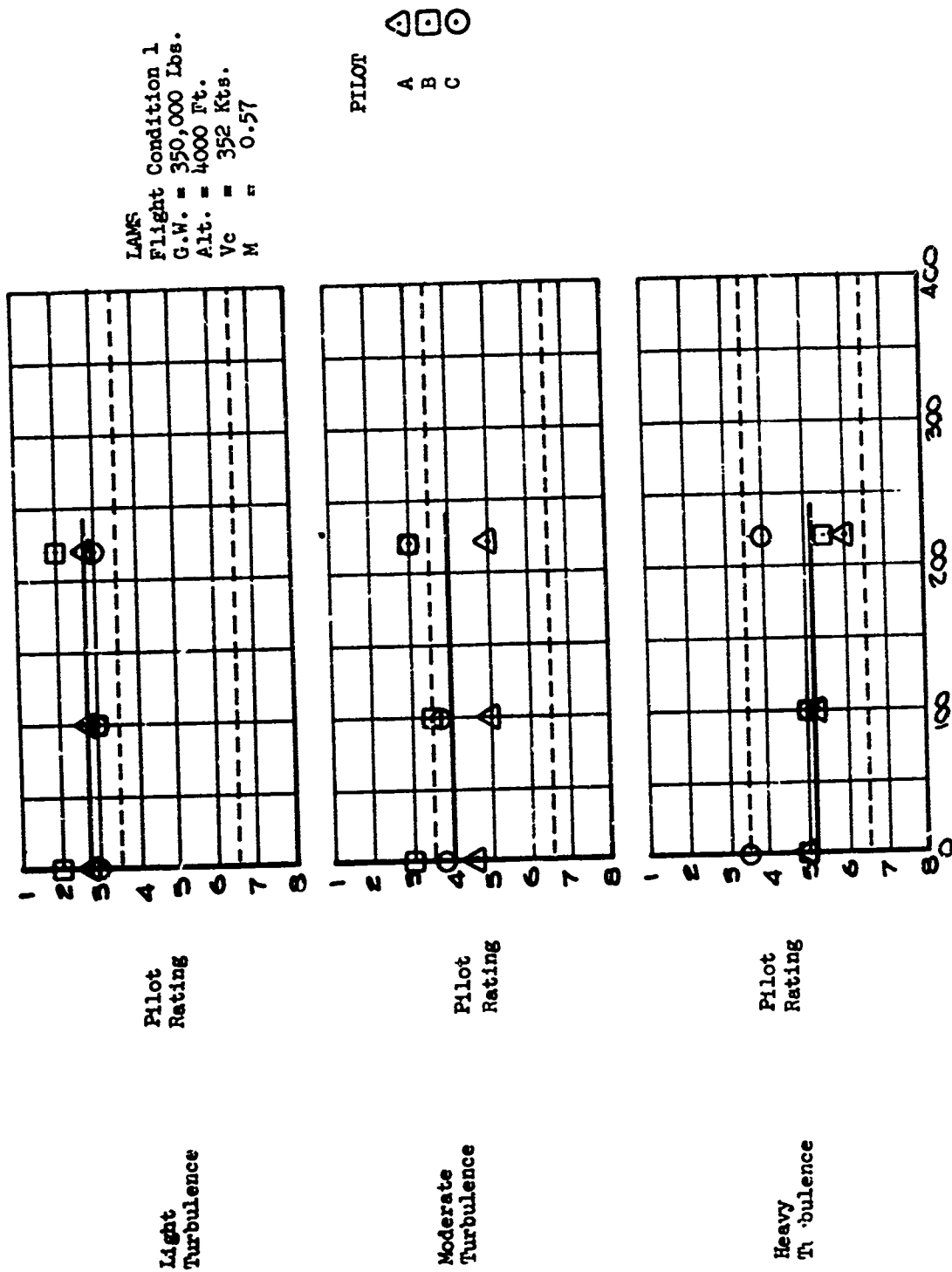
The ratings for Flight Condition 3 show some variation with gain, but not appreciable. Again, this can be compared to the damping values of $.265$, $.427$, and $.547$ for low, nominal, and high gain levels.

Again note the effect of turbulence intensity. An increase in intensity, from light to heavy turbulence, causes a decrease in pilot rating of approximately two. The effects of the LAMS longitudinal FCS gains on pilot rating are essentially the same as the effects of the longitudinal Baseline SAS, i.e., the ratings are essentially unaffected by pitch SAS gain.

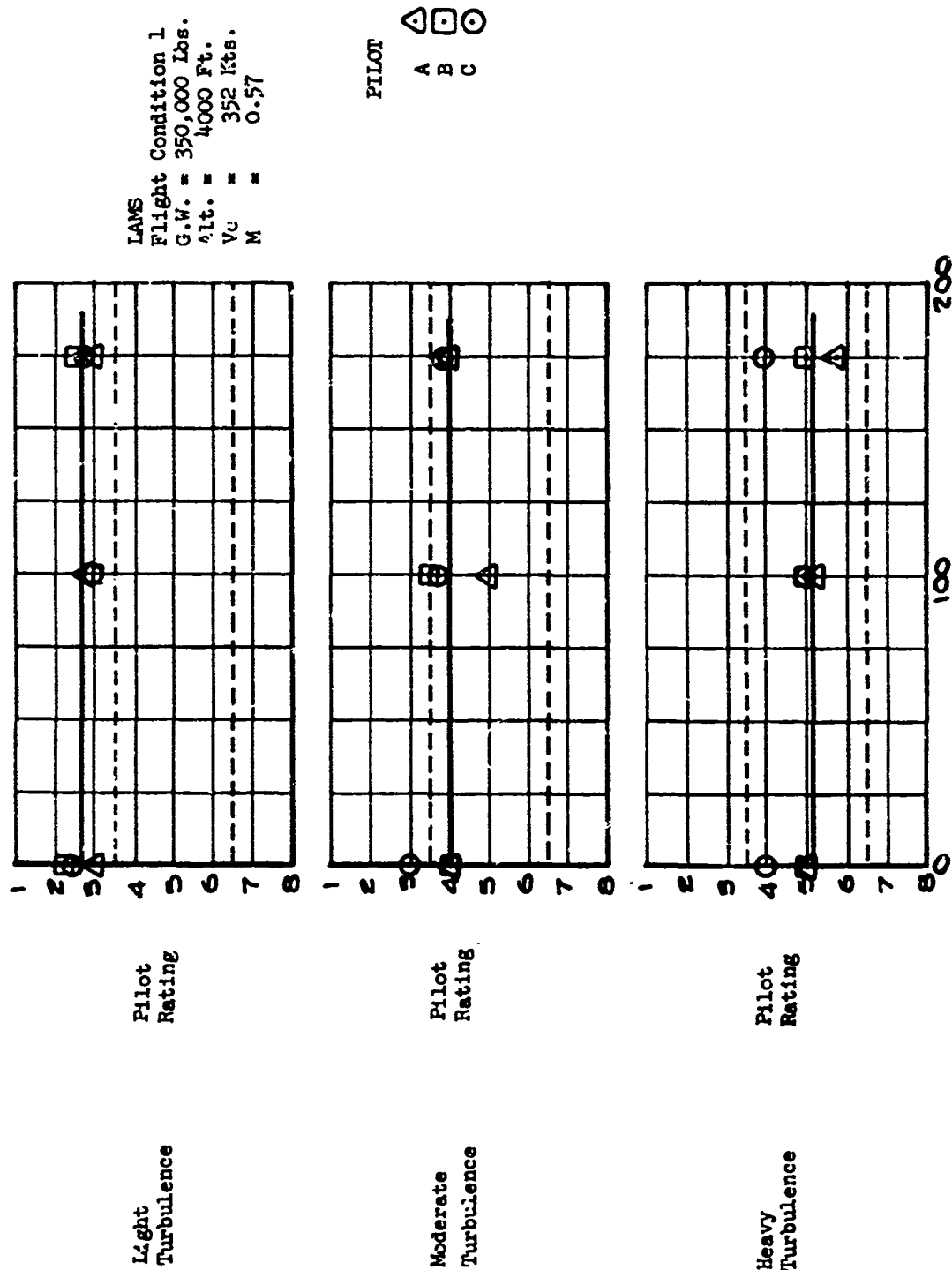
Rather than evaluate only variations in gain, three configurations of LAMS Lateral FCS were investigated. They were: no roll augmentation; a roll SAS with a feed forward and feedback network which gives the same roll response (due to a step wheel) as the basic aircraft; and a third configuration (similar to the second except for a different forward gain) which gives an improved roll response for small wheel inputs and improved roll damping. As shown by the data presented in Figure 45 and Appendix C, there is essentially no change in the pilot opinion due to any of these changes.



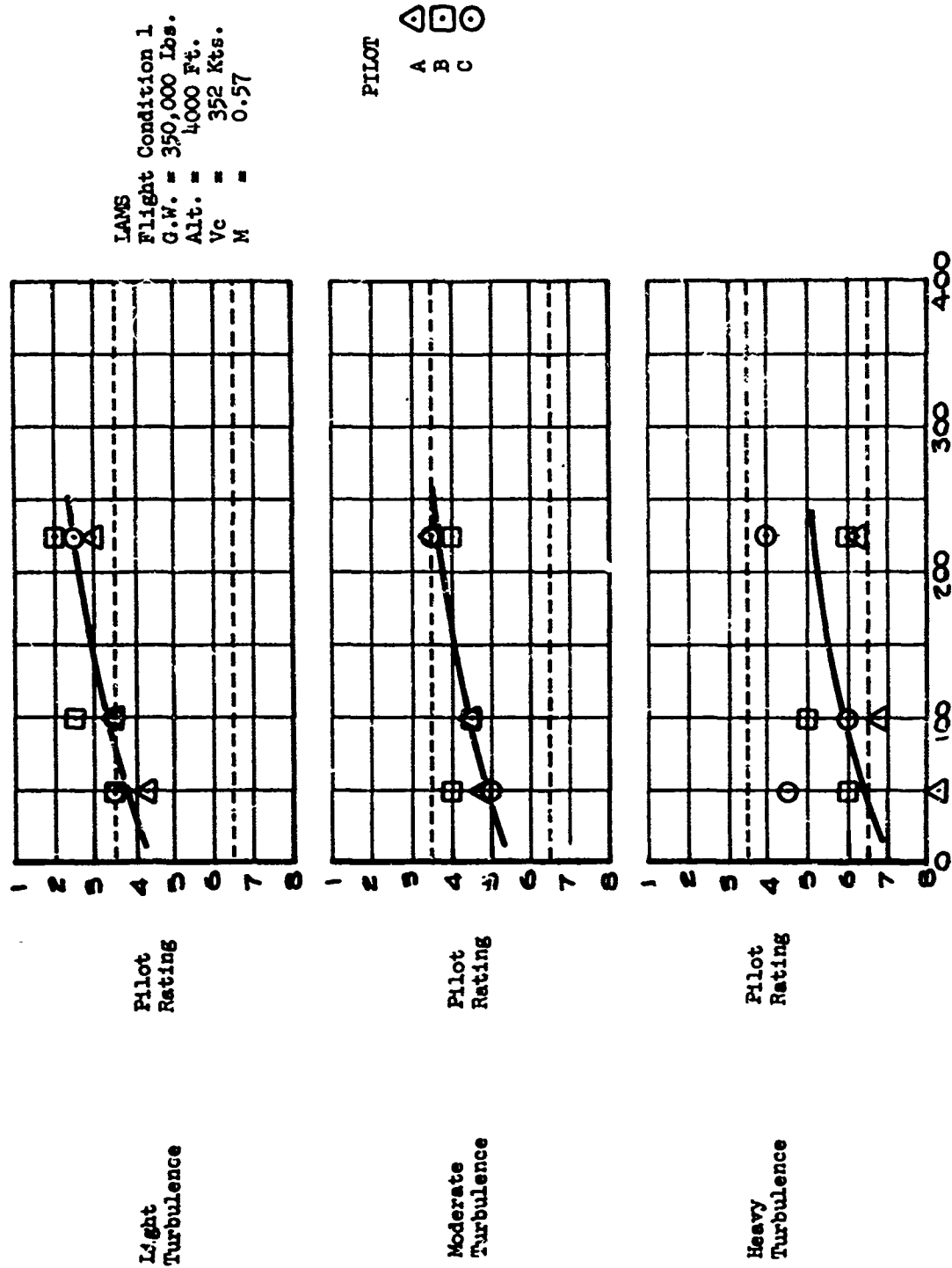
BASELINE SAS - DIRECTIONAL AXIS GAIN VARIATIONS
FIGURE 40



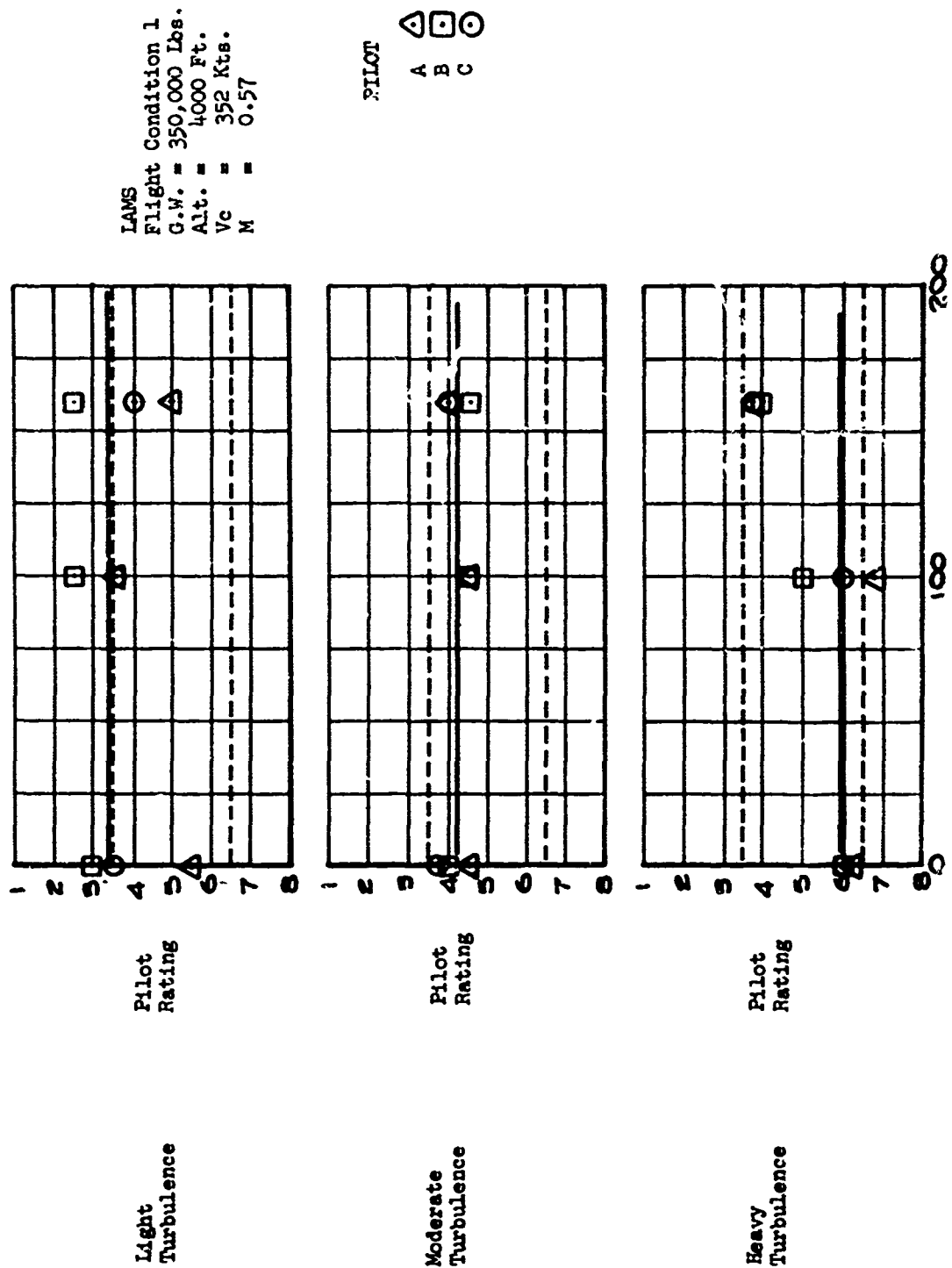
Percent Of Nominal Gain
BASELINE SAS - LONGITUDINAL AXIS GAIN VARIATIONS
FIGURE 41



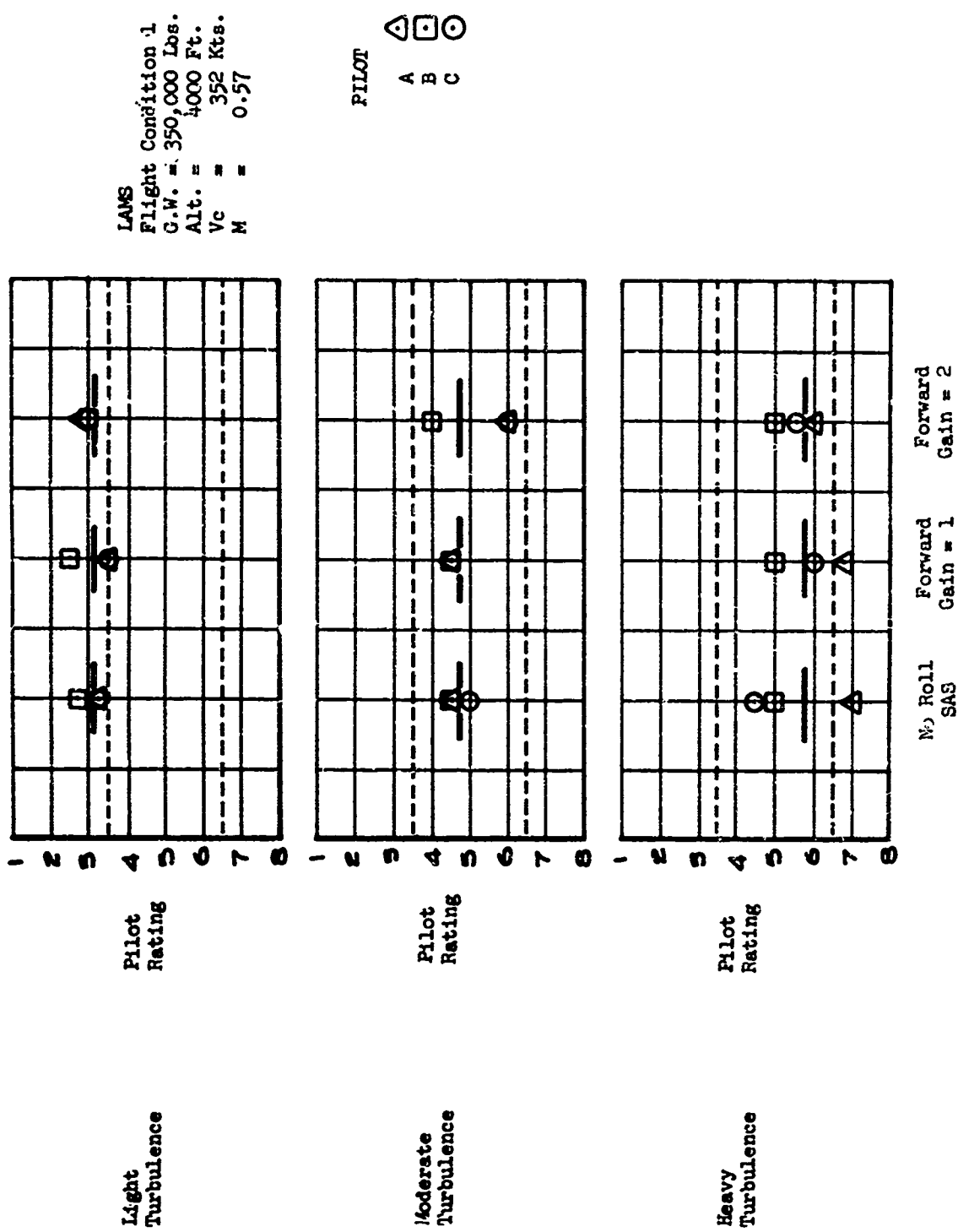
Percent Of Nominal Gain
 BASELINE SAS - LATERAL AXIS GAIN VARIATIONS
 FIGURE 42



LAMS FCS - DIRECTIONAL AXIS GAIN VARIATIONS
FIGURE 12



LAMS FCS - LONGITUDINAL AXIS GAIN VARIATIONS
FIGURE 44



LAMs FCS - LATERAL AXIS GAIN VARIATIONS
 FIGURE 45

4.4 Structural Performance Predictions

The LAMS-FCS modified the B-52 loading in turbulence to achieve reductions in fatigue damage rates, stresses, and accelerations. The LAMS Flight Control System reduced fatigue damage rates at the key wing stress points by more than $1/3$ with respect to the Baseline SAS. Also, of importance is the fact that the structural loads were reduced throughout the airframe and not just at the performance index stations. The ride quality at the pilot station was improved slightly, with the remainder of the fuselage showing varying amounts of improvement over its length.

A theoretical evaluation of the structural performance in turbulence of the B-52 with LAMS Flight Control System included computations of RMS shears, bending moments, torsional moments, and accelerations throughout the aircraft. Subsequent performance was defined in terms of fatigue damage accumulation rates and peak stresses at selected stations and acceleration power spectral densities at the crew compartment. The LAMS Flight Control System is compared with the Baseline SAS and the B-52 without SAS.

The performance predictions were based on sixty-four degrees-of-freedom mathematical models (32 symmetric and 32 antisymmetric) plus control surface actuator and SAS dynamics. Three components of random turbulence were included; lateral gusts, symmetric vertical gusts, and antisymmetric vertical (rolling) gusts. A time lag was used for the gust inputs to each aerodynamic panel to describe the gradual penetration of the aircraft into the gusts. Approximated Kussner and Wagner lift growth functions were used.

The rms structural moment, "A", due to a unit rms gust is plotted as a function of airframe station in Figures 46 through 50. These figures show that the LAMS-FCS is generally able to reduce the structural response with respect to the Baseline SAS. The responses which show the greatest benefit due to the LAMS-FCS are the wing vertical bending moment (20 per cent reductions), and the fuselage vertical bending moment forward of Body Station 1050 (40 per cent reductions). Aft of this point on the fuselage the LAMS-FCS causes increases in vertical bending moment.

Wing chordwise (fore and aft) bending moment and fuselage side bending moment show 30 per cent reductions with respect to the NO SAS configuration but show very little reduction with respect to the Baseline SAS. Wing torsional moment shows an increased response with the LAMS-FCS on.

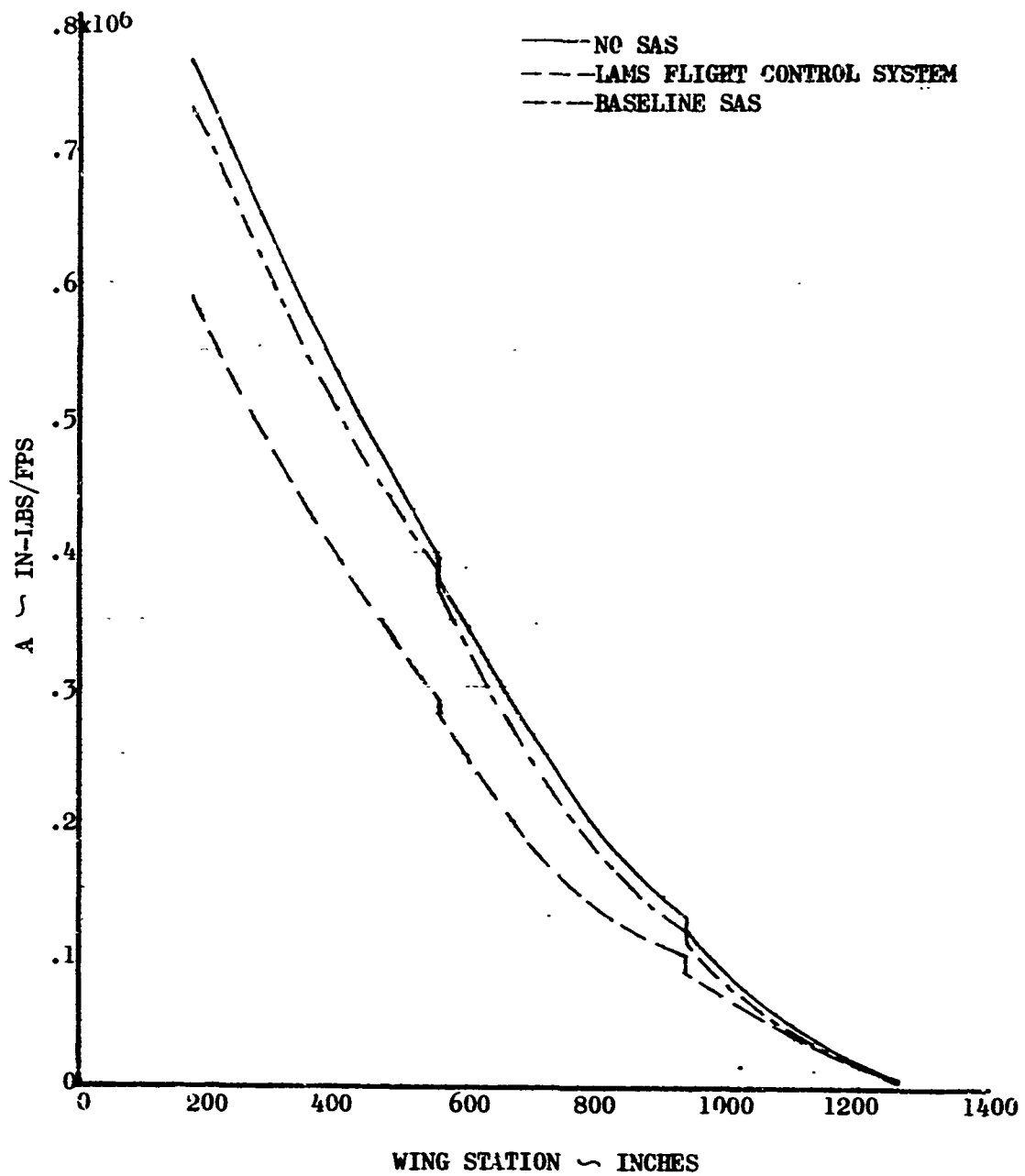
Airframe acceleration responses are presented in Figures 11, 12 and 51. The LAMS-FCS slightly reduces the accelerations in the forward fuselage with respect to the Baseline SAS and the NO SAS configurations. The accelerations on the wing are reduced up to 10 per cent with respect to the Baseline SAS outboard of W.B.L. 475 by the LAMS-FCS. Inboard of this station the acceleration level with the LAMS-FCS on is greater than the Baseline SAS but is reduced with respect to the NO SAS configuration.

A power spectral density of the Body Station 172 (pilot's station) vertical acceleration is presented in Figure 52. The response levels are slightly reduced by the LAMS-FCS.

The results of the stress exceedance study are presented in Tables XXII through XXIV and in Figures 53 through 55. The tables show that the expected number of ultimate stress exceedances per hour and per year based on the mission presented in the Introduction are reduced by the LAMS Flight Control System with respect to Baseline SAS except for some tail loads where the Baseline SAS is superior. The bargraphs, Figures 53 through 55 show peak incremental stresses (for an exceedance level of .001 per hour). Expected wing peak stresses are reduced 16-33 per cent with respect to Baseline SAS and 23-36 per cent with respect to NO SAS. Expected fuselage peak stresses are reduced 3-22 per cent with respect to Baseline SAS and 28-40 per cent with respect to NO SAS. Horizontal tail peak stresses are 10 per cent greater than Baseline SAS, but 10 per cent less than NO SAS. Expected peak stress at Fin Station 135 are reduced 35-40 per cent by both Baseline SAS and LAMS Flight Control System from the NO SAS condition.

The fatigue damage rates per year are presented in Tables I, XXV, and XXVI and in Figure 10. The LAMS-FCS is shown to reduce the fatigue damage rate 35 per cent at the wing stations with respect to the Baseline SAS and 40 per cent with respect to NO SAS. Fuselage, stabilizer, and fin show fatigue damage rate decreases of from 50 per cent to 85 per cent with both the LAMS-FCS and Baseline SAS, compared with NO SAS. There is little difference at these stations between Baseline SAS and the LAMS-FCS.

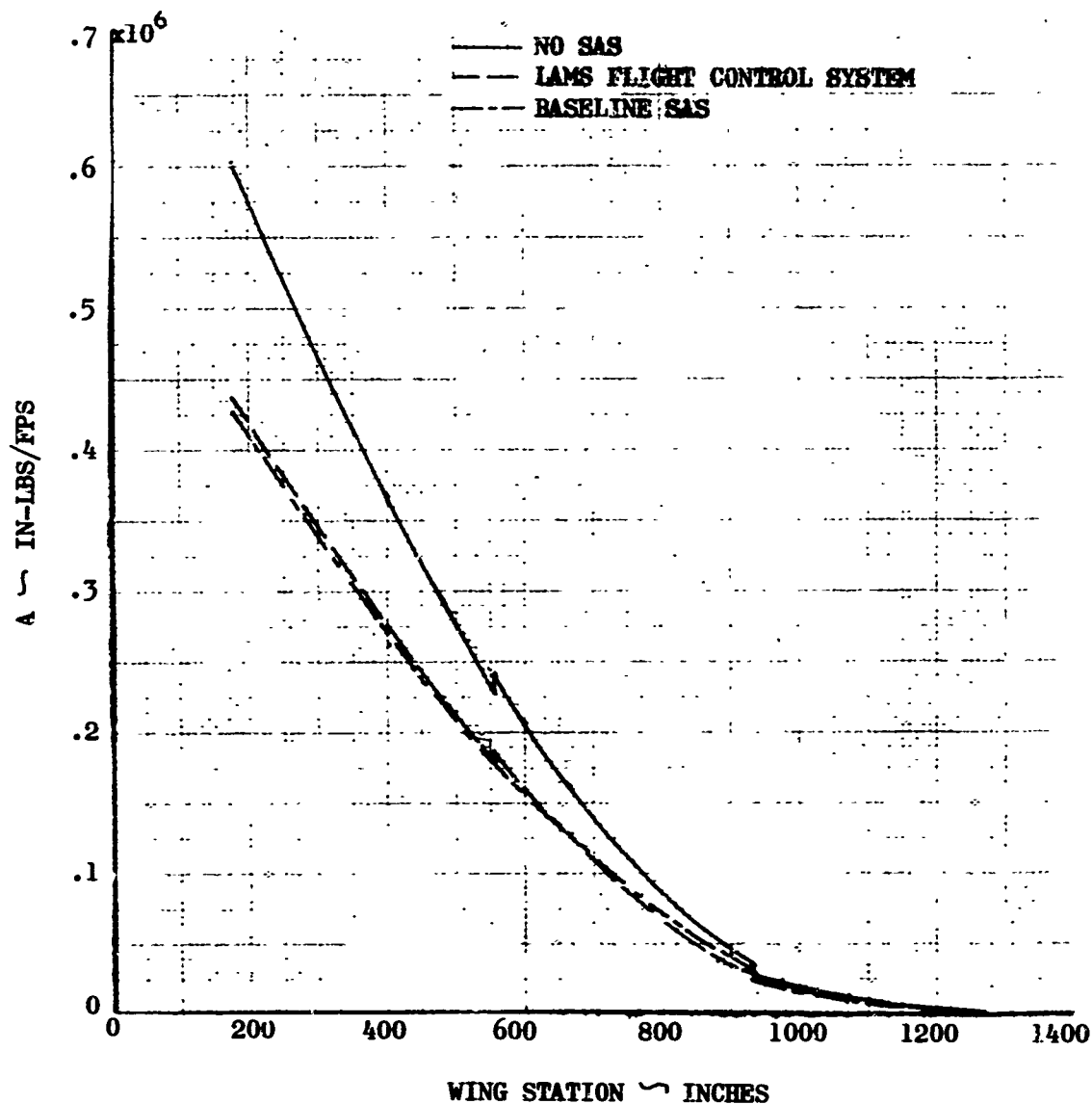
RMS WING VERTICAL BENDING MOMENT PER UNIT GUST
LAMS FLIGHT CONDITION 1 (350000 LBS, 350 KTS EAS, 4000 FT)



RMS WING VERTICAL BENDING MOMENT

FIGURE 46

RMS WING CHORDWISE BENDING MOMENT PER UNIT GUST
 LAMS FLIGHT CONDITION 1 (350000 LBS, 350 KTS EAS, 4000 FT)



RMS WING CHORDWISE BENDING MOMENT

FIGURE 47

RMS WING TORSIONAL MOMENT PER UNIT GUST
LAMS FLIGHT CONDITION 1 (350000 LBS, 350 KTS EAS, 4000 FT)

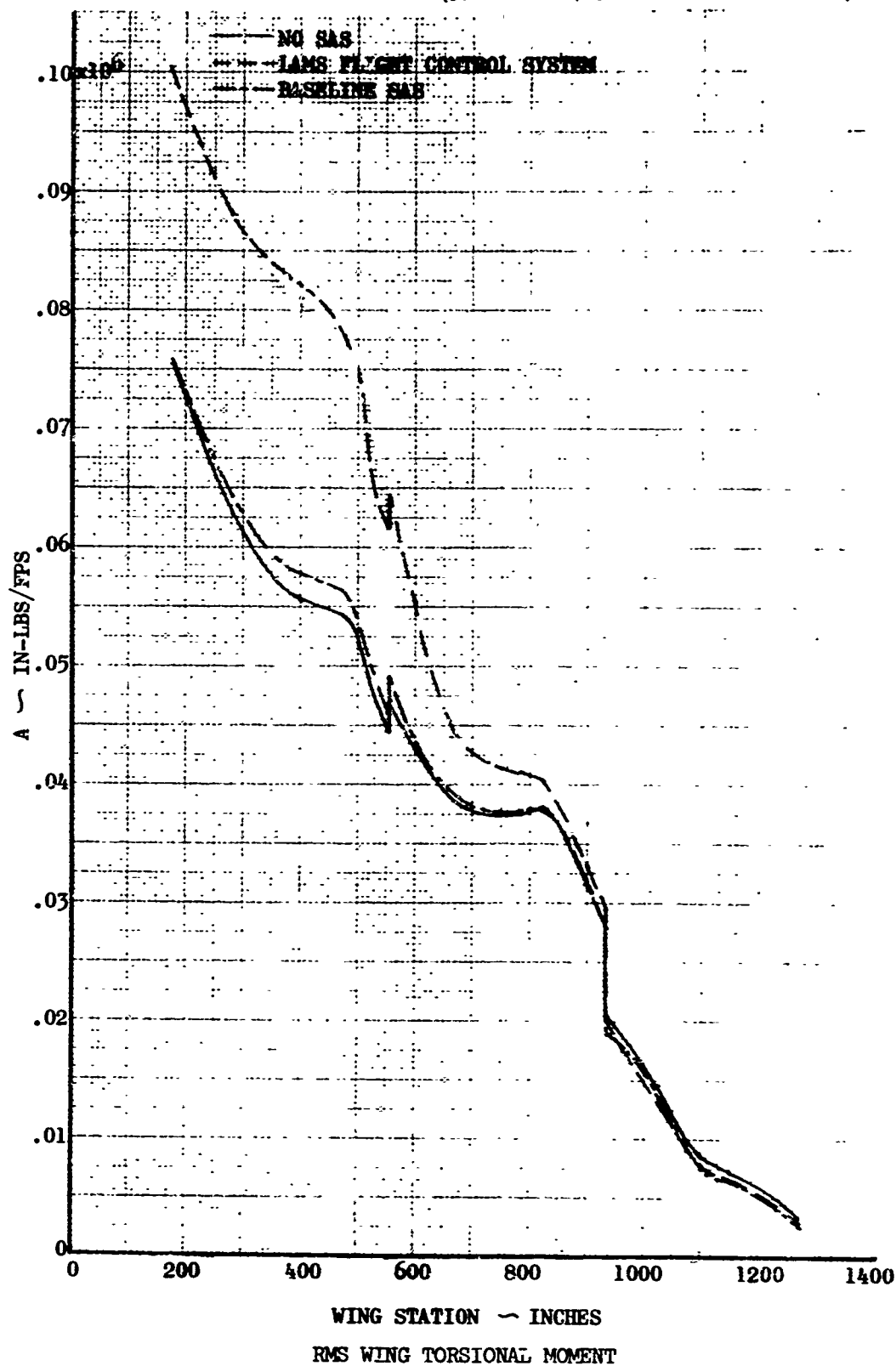
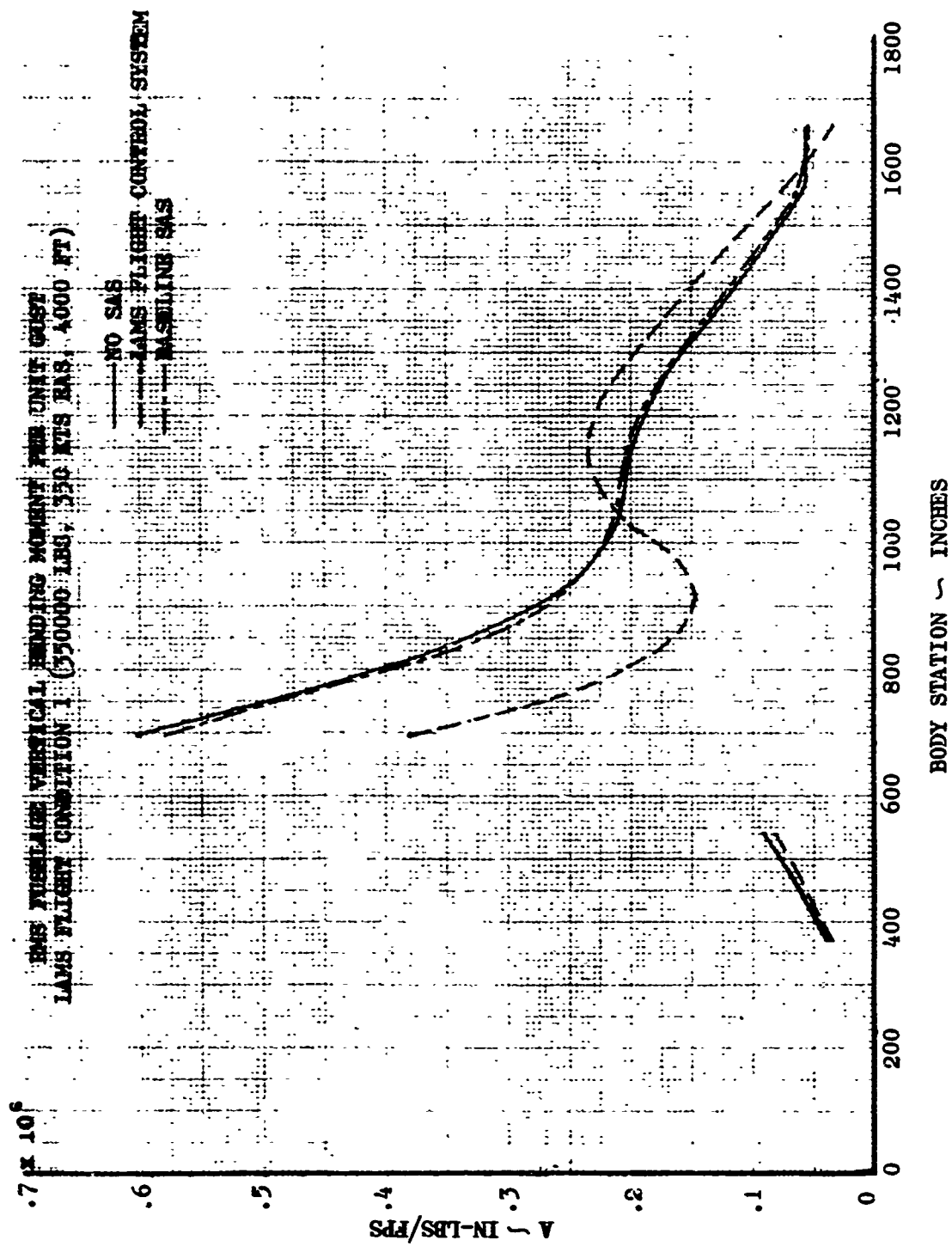
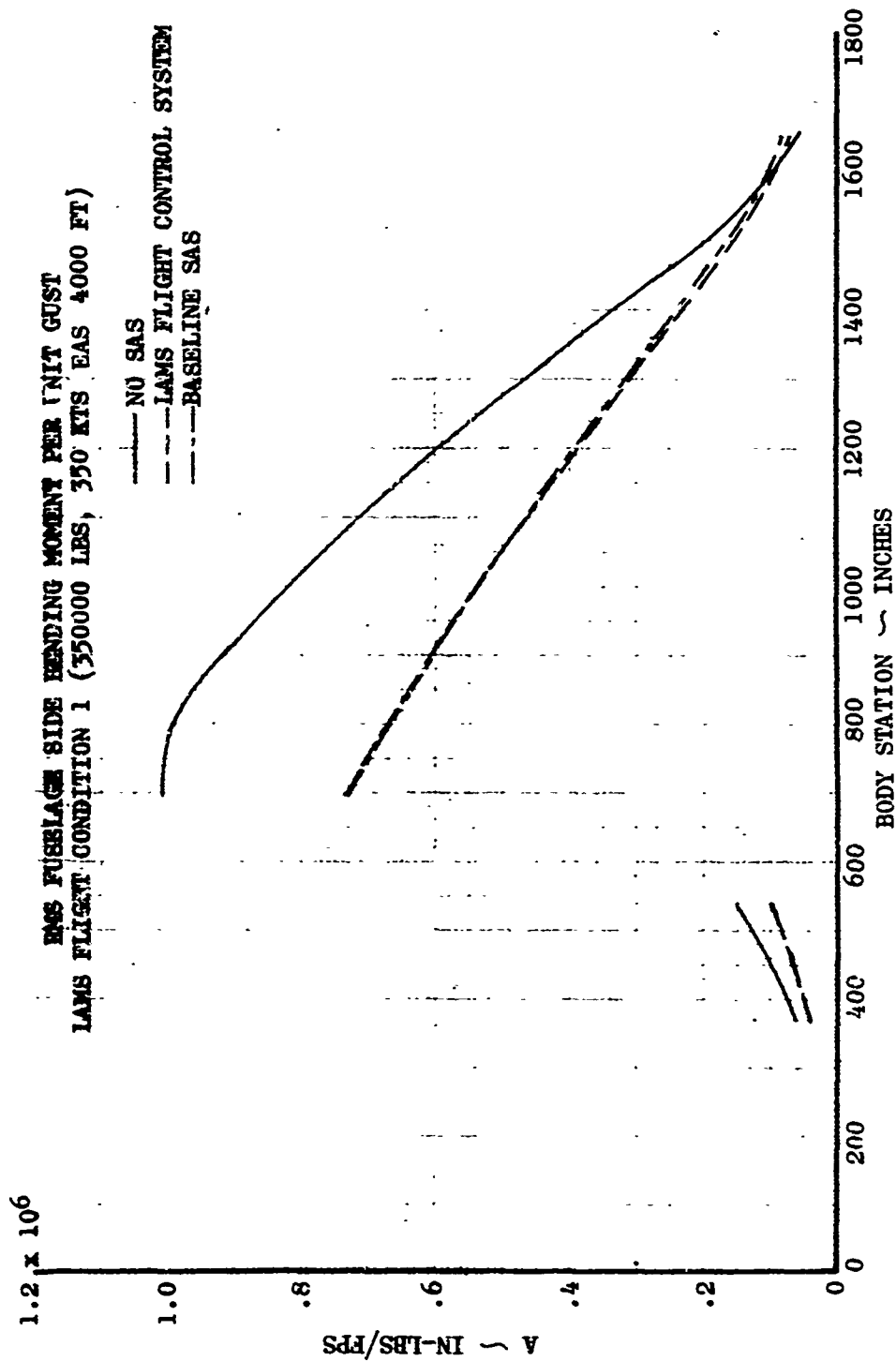


FIGURE 48



RMS FUSELAGE VERTICAL BENDING MOMENT

FIGURE 49



RMS FUSELAGE SIDE BENDING MOMENT

FIGURE 50

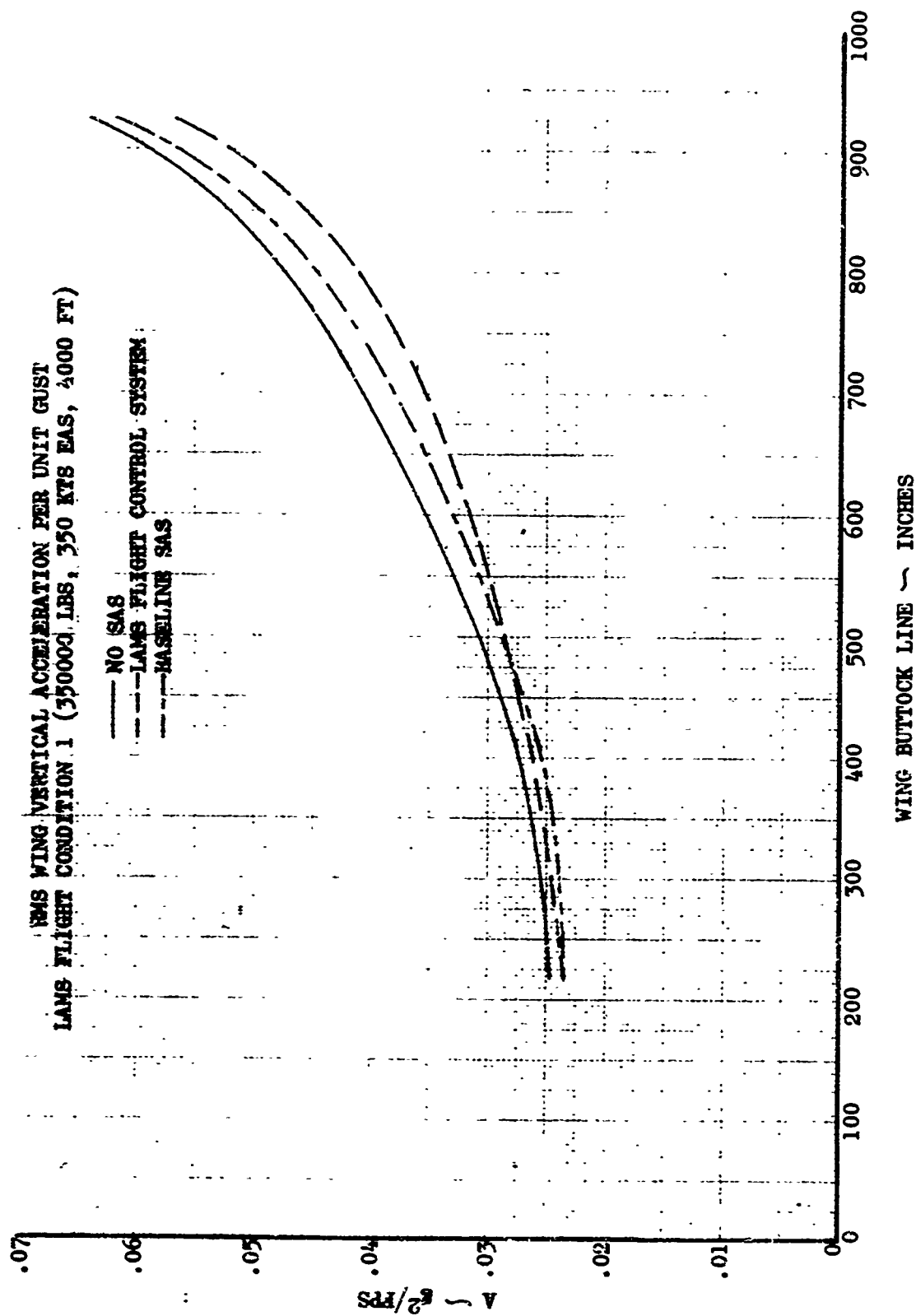
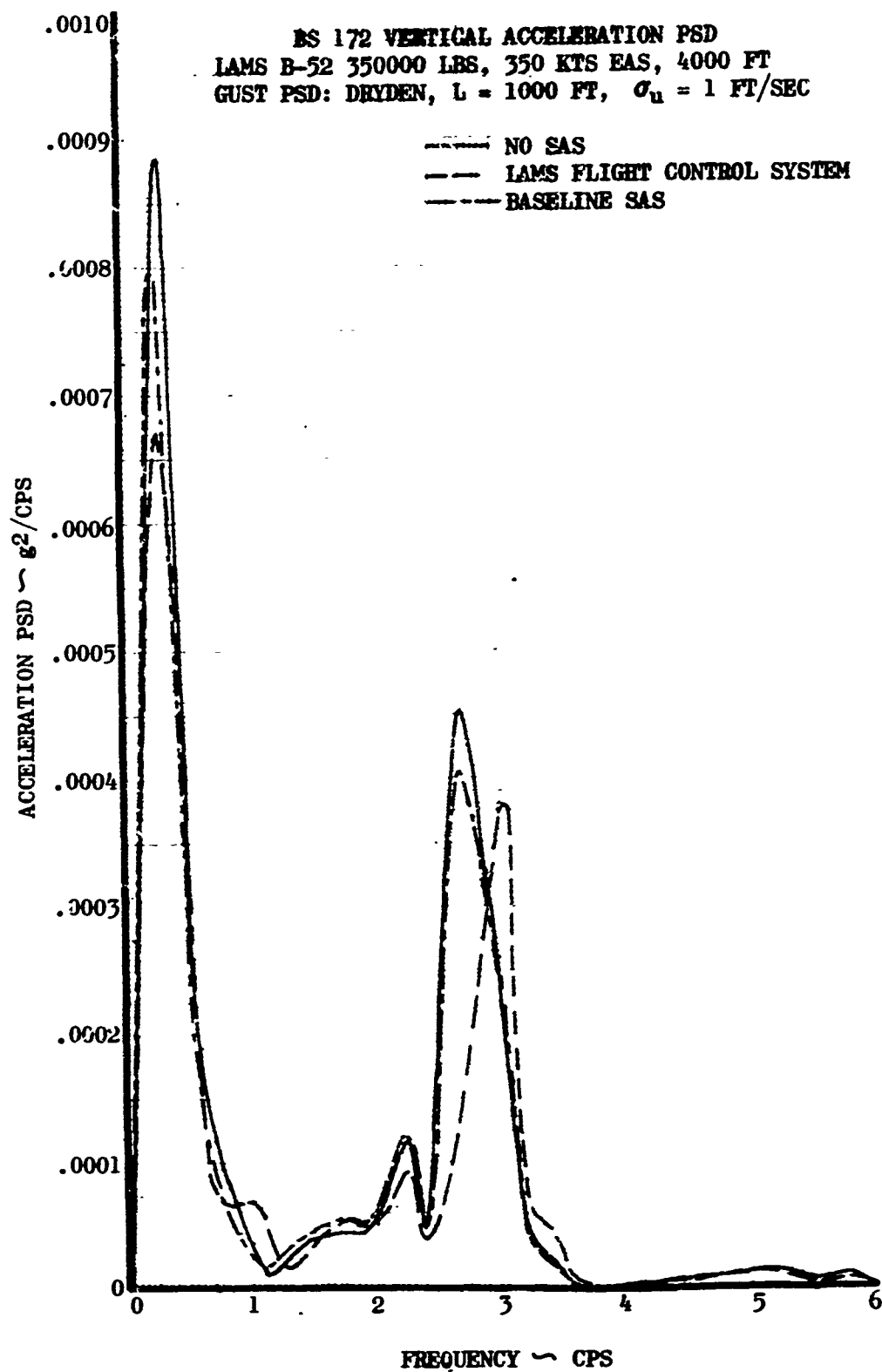


FIGURE 51



BS 172 VERTICAL ACCELERATION PSD

FIGURE 52

TABLE XXII
LAMS ULTIMATE STRESS EXCEEDANCES DUE TO TURBULENCE

NO SAS (CONTROLS LOCKED)
2 SPOILERS UP 15°
COMBINED VERTICAL, LATERAL, & ROLLING GUSTS
CONTOUR LOW LEVEL & CRUISE ENVIRONMENT'S
ARE FROM ECP 1128 (B-52 DATA)

STRESS LOCATION	ULTIMATE STRESS EXCEEDANCES PER HOUR			EXCEEDANCES PER YEAR*
	COND. 1	COND. 2	COND. 3	
W.S. 282 S-7	3.7×10^{-12}	1.8×10^{-15}	1.4×10^{-23}	9.3×10^{-11}
W.S. 516 S-5	2.2×10^{-12}	4.4×10^{-15}	3.3×10^{-21}	5.5×10^{-11}
W.S. 899 S-3	4.5×10^{-14}	4.2×10^{-16}	1.0×10^{-18}	1.1×10^{-12}
B.S. 805 U.L.	1.6×10^{-18}	8.1×10^{-28}	3.3×10^{-25}	4.0×10^{-17}
B.S. 1028 U.L.	3.3×10^{-18}	1.2×10^{-28}	2.6×10^{-24}	8.3×10^{-17}
S.B.L. 32 SPAR	1.6×10^{-24}	2.8×10^{-39}	5.7×10^{-37}	4.0×10^{-23}
F.S. 135 SPAR	1.5×10^{-9}	2.1×10^{-14}	1.9×10^{-14}	3.8×10^{-8}

COND. 1 = CONTOUR LOW-LEVEL, 350,000 LBS., 350 KEAS, 4000 FT. ALT.

COND. 2 = CONTOUR LOW-LEVEL, 350,000 LBS., 240 KEAS, 4000 FT. ALT.

COND. 3 = CRUISE, 270,000 LBS., MACH .77, 32,700 FT. ALT.

*ANNUAL USAGE = 25 HOURS @ COND. 1
 +39 HOURS @ COND. 2
 +511 HOURS @ COND. 3

**For comparisons only. Fin side loads cannot exceed 85%
of design loads at flight conditions 2 or 3 due to $C_{L_{max}}$.

TABLE XXIII
LAMS ULTIMATE STRESS EXCEEDANCES DUE TO TURBULENCE

BASELINE SAS (ROLL, PITCH, AND YAW)
2 SPOILERS UP 15°
COMBINED VERTICAL, LATERAL, & ROLLING GUSTS
CONTOUR LOW LEVEL & CRUISE ENVIRONMENTS
ARE FROM ECP 1128 (B-52 DATA)

STRESS LOCATION	ULTIMATE STRESS EXCEEDANCES PER HOUR			EXCEEDANCES PER YEAR*
	COND. 1	COND. 2	COND. 3	
W.S. 282 S-7	7.2×10^{-13}	2.0×10^{-16}	2.1×10^{-25}	1.8×10^{-11}
W.S. 516 S-5	5.1×10^{-13}	6.7×10^{-16}	2.9×10^{-22}	1.3×10^{-11}
W.S. 899 S-3	1.0×10^{-15}	7.3×10^{-18}	1.9×10^{-20}	2.5×10^{-14}
B.S. 805 U.L.	7.8×10^{-26}	2.8×10^{-38}	5.7×10^{-35}	2.0×10^{-24}
B.S. 1028 U.L.	1.0×10^{-25}	8.8×10^{-42}	1.2×10^{-32}	2.5×10^{-24}
S.B.L. 32 SPAR	9.5×10^{-32}	1.1×10^{-55}	3.2×10^{-52}	2.4×10^{-30}
F.S. 135 SPAR	1.6×10^{-17}	3.9×10^{-27}	7.4×10^{-27}	4.0×10^{-16}

COND. 1 = CONTOUR LOW-LEVEL, 350,000 LBS., 350 KEAS, 4000 FT. ALT.

COND. 2 = CONTOUR LOW-LEVEL, 350,000 LBS., 240 KEAS, 4000 FT. ALT.

COND. 3 = CRUISE, 270,000 LBS., MACH .77, 32,700 FT. ALT.

*ANNUAL USAGE = 25 HOURS @ COND. 1
 +39 HOURS @ COND. 2
 +511 HOURS @ COND. 3

**For comparison only. Fin side loads cannot exceed 85%
of design loads at flight conditions 2 or 3 due to $C_{l_{max}}$.

TABLE XXIV
LAMS ULTIMATE STRESS EXCEEDANCES DUE TO TURBULENCE
LAMS FLIGHT CONTROL SYSTEM (ROLL, PITCH, AND YAW)
2 SPOILERS UP 15°
COMBINED VERTICAL, LATERAL, & ROLLING GUSTS
CONTOUR LOW LEVEL & CRUISE ENVIRONMENTS
ARE FROM ECP 1128 (B-52 DATA).

STRESS LOCATION	ULTIMATE STRESS EXCEEDANCES PER HOUR			EXCEEDANCES PER YEAR*
	COND. 1	COND. 2	COND. 3	
W.S. 282 S-7	1.311×10^{-16}	3.578×10^{-22}	1.944×10^{-39}	3.3×10^{-15}
W.S. 516 S-5	8.229×10^{-18}	3.097×10^{-22}	3.637×10^{-34}	2.1×10^{-16}
W.S. 899 S-3	1.015×10^{-19}	1.090×10^{-23}	3.715×10^{-25}	2.5×10^{-18}
B.S. 805 U.L.	8.902×10^{-30}	8.931×10^{-49}	6.145×10^{-43}	2.2×10^{-28}
B.S. 1028 U.L.	2.245×10^{-26}	2.494×10^{-47}	1.498×10^{-41}	5.6×10^{-25}
S.B.L. 32 SPAR	2.404×10^{-28}	1.207×10^{-48}	2.078×10^{-48}	6.0×10^{-27}
F.S. 135 SPAR	2.5×10^{-17}	4.2×10^{-31}	2.4×10^{-29}	6.3×10^{-16}

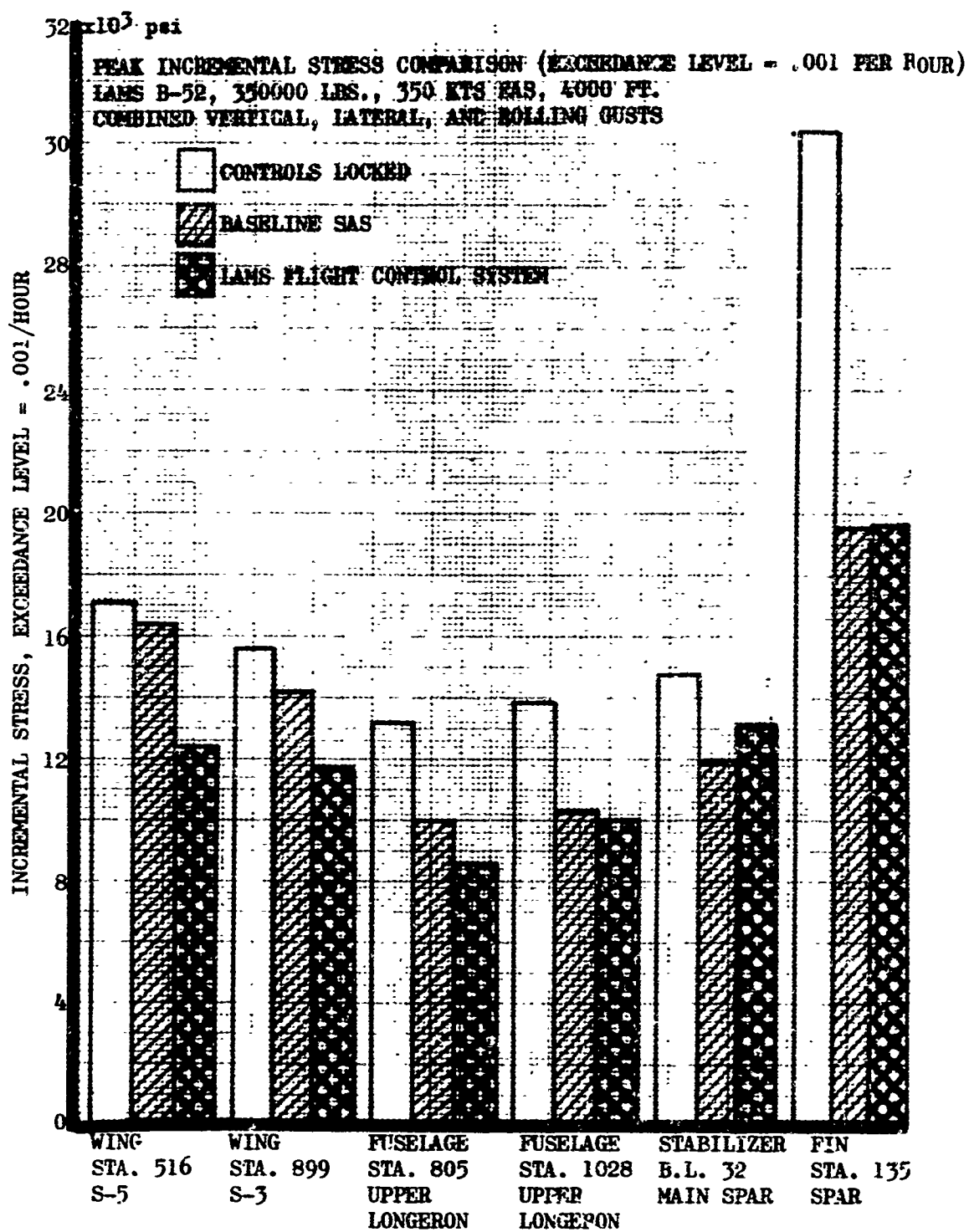
COND. 1 = CONTOUR LOW-LEVEL, 350,000 LBS., 350 KEAS, 4000 FT. ALT.

COND. 2 = CONTOUR LOW-LEVEL, 350,000 LBS., 240 KEAS, 4000 FT. ALT.

COND. 3 = CRUISE, 270,000 LBS., MACH .77, 32,700 FT. ALT.

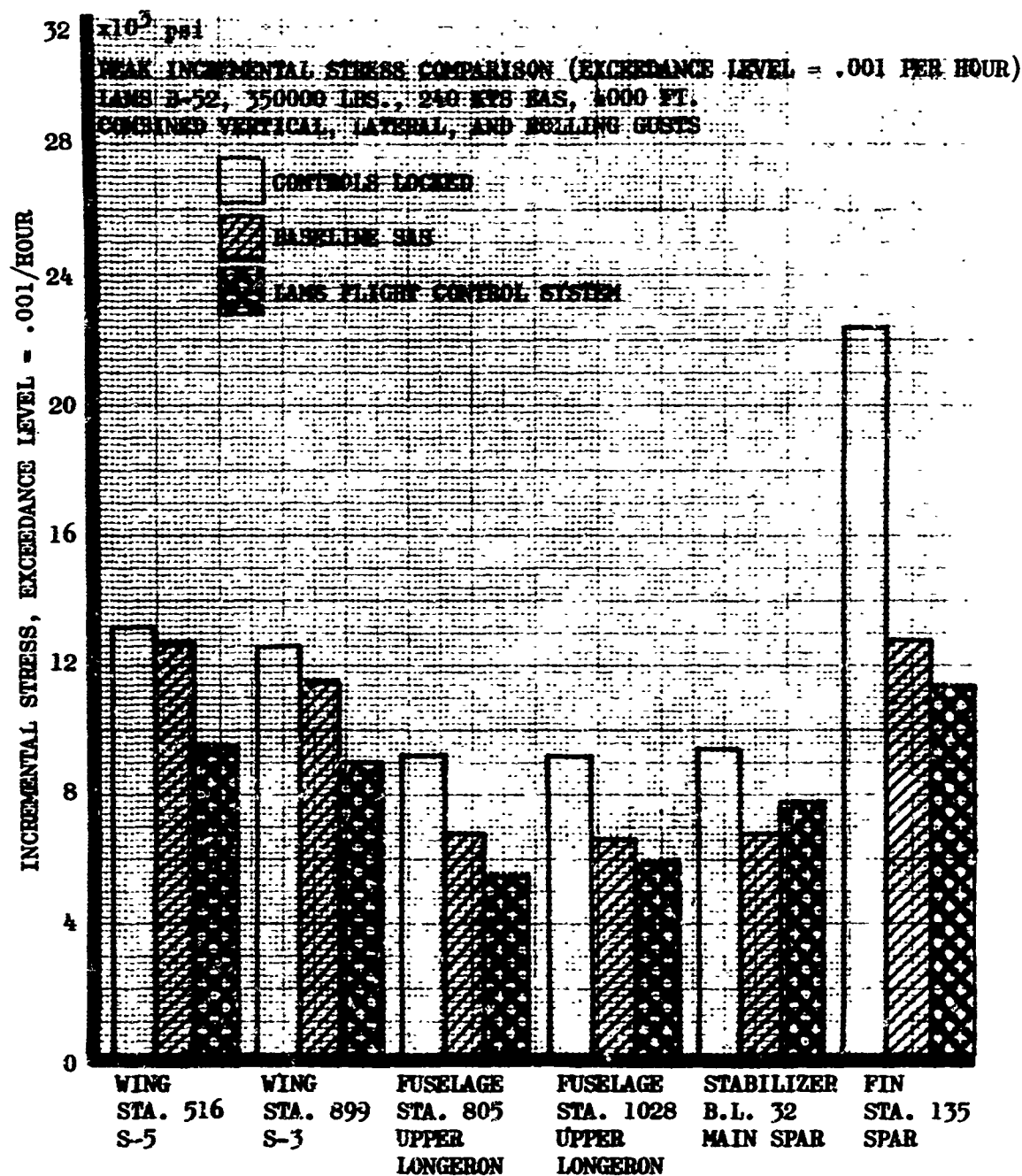
*ANNUAL USAGE = 25 HOURS @ COND. 1
 +39 HOURS @ COND. 2
 +511 HOURS @ COND. 3

**For comparison only. Fin side loads cannot exceed 85% of design loads at flight conditions 2 or 3 due to $C_{l_{max}}$.



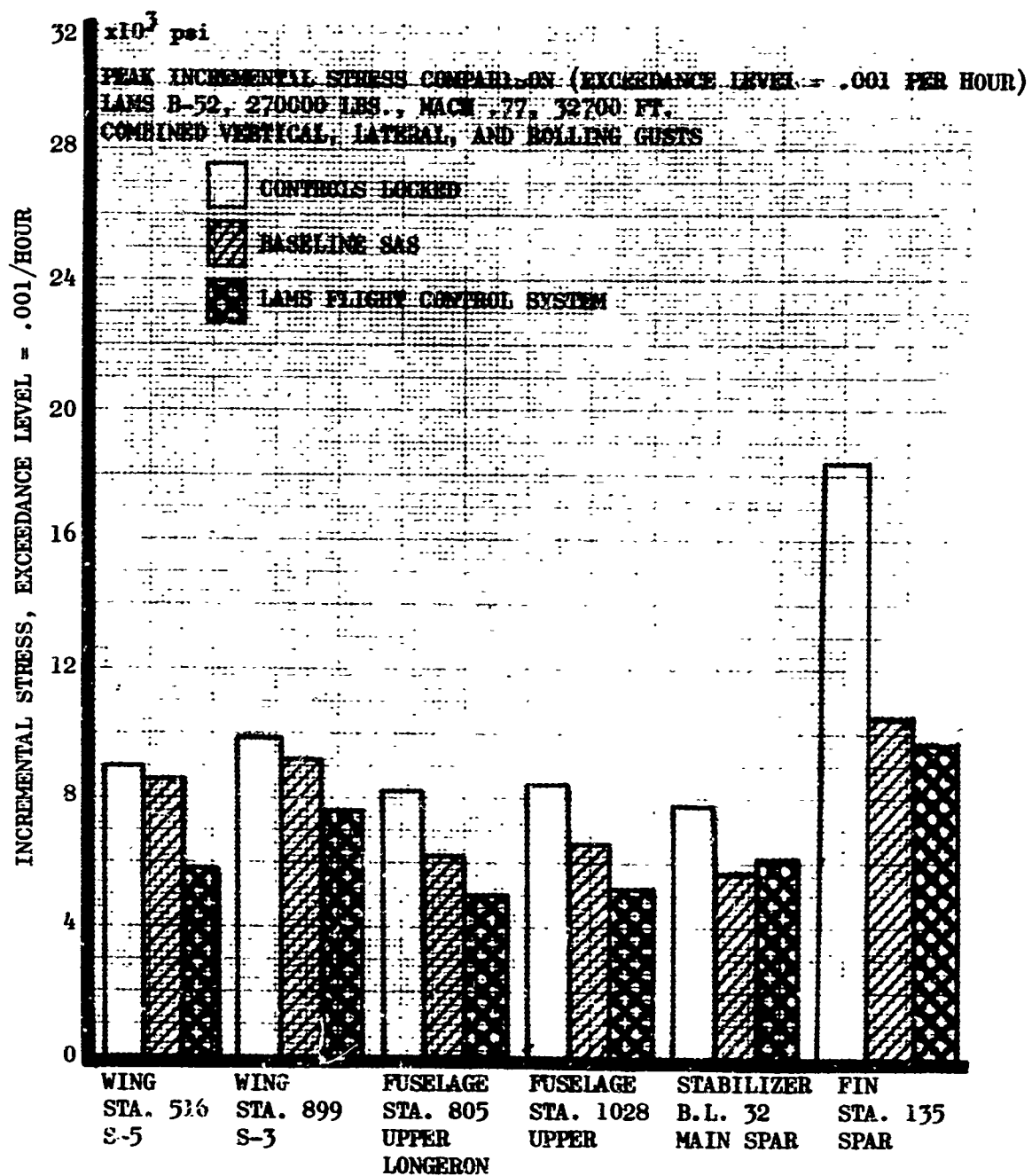
PEAK INCREMENTAL STRESS COMPARISON

FIGURE 53



PEAK INCREMENTAL STRESS COMPARISON

FIGURE 54



PEAK INCREMENTAL STRESS COMPARISON

FIGURE 55

TABLE XXV
LAMS FATIGUE DAMAGE RATES DUE TO TURBULENCE

NO SAS (CONTROLS LOCKED)
2 SPOILERS UP 15°
COMBINED VERTICAL, LATERAL, & ROLLING GUSTS
CONTOUR LOW LEVEL & CRUISE ENVIRONMENTS
ARE FROM ECP 1128 (B-52 DATA)

STRESS LOCATION	DAMAGE PER HOUR			DAMAGE PER YEAR*
	COND. 1	COND. 2	COND. 3	
W.S. 282 S-7	2.97×10^{-3}	1.64×10^{-3}	$.013 \times 10^{-3}$.145
W.S. 516 S-5	2.89×10^{-3}	1.74×10^{-3}	$.020 \times 10^{-3}$.150
W.S. 899 S-3	2.24×10^{-3}	1.36×10^{-3}	$.029 \times 10^{-3}$.124
B.S. 805 U.L.	$.768 \times 10^{-3}$	$.135 \times 10^{-3}$	$.0048 \times 10^{-3}$.0269
B.S. 1028 U.L.	$.939 \times 10^{-3}$	$.126 \times 10^{-3}$	$.0080 \times 10^{-3}$.0325
S.B.L. 32 SPAR	$.052 \times 10^{-3}$	$.0022 \times 10^{-3}$	$.0002 \times 10^{-3}$.0015
F.S. 135 SPAR	$.997 \times 10^{-3}$	$.188 \times 10^{-3}$	$.0061 \times 10^{-3}$.0354

COND. 1 = CONTOUR LOW-LEVEL, 350,000 LBS., 350 KEAS, 4000 FT. ALT.

COND. 2 = CONTOUR LOW-LEVEL, 350,000 LBS., 240 KEAS, 4000 FT. ALT.

COND. 3 = CRUISE, 270,000 LBS., MACH. .77, 32,700 FT. ALT.

*ANNUAL USAGE = 25 HOURS ● COND. 1
+39 HOURS ● COND. 2
+511 HOURS ● COND. 3

TABLE XXVI
LAMS FATIGUE DAMAGE RATES DUE TO TURBULENCE

BASELINE SAS (ROLL, PITCH, AND YAW)
2 SPOILERS UP 15°
COMBINED VERTICAL, LATERAL, & ROLLING GUSTS
CONTOUR LOW LEVEL & CRUISE ENVIRONMENTS
ARE FROM ECP 1128 (B-52 DATA)

STRESS LOCATION	DAMAGE PER HOUR			DAMAGE PER YEAR*
	COND. 1	COND. 2	COND. 3	
W.S. 282 S-7	2.76×10^{-3}	1.40×10^{-3}	$.011 \times 10^{-3}$.133
W.S. 516 S-5	2.71×10^{-3}	1.60×10^{-3}	$.019 \times 10^{-3}$.140
W.S. 899 S-3	1.90×10^{-3}	1.16×10^{-3}	$.026 \times 10^{-3}$.196
B.S. 805 U.L.	$.294 \times 10^{-3}$	$.040 \times 10^{-3}$	$.0015 \times 10^{-3}$.0097
B.S. 1028 U.L.	$.345 \times 10^{-3}$	$.028 \times 10^{-3}$	$.0029 \times 10^{-3}$.0112
S.B.L. 32 SPAR	$.016 \times 10^{-3}$	$.0002 \times 10^{-3}$	$.00003 \times 10^{-3}$.0004
F.S. 135 SPAR	$.181 \times 10^{-3}$	$.018 \times 10^{-3}$	$.0007 \times 10^{-3}$.0056

COND. 1 = CONTOUR LOW-LEVEL, 350,000 LBS., 350 KEAS, 4000 FT. ALT.

COND. 2 = CONTOUR LOW-LEVEL, 350,000 LBS., 240 KEAS, 4000 FT. ALT.

COND. 3 = CRUISE, 270,000 LBS., MACH. .77, 32,700 FT. ALT.

*ANNUAL USAGE = 25 HOURS @ COND. 1
 +39 HOURS @ COND. 2
 +511 HOURS @ COND. 3

4.5 Performance Sensitivity Results

4.5.1 LAMS Longitudinal FCS

The results of the longitudinal performance definition study indicated the LAMS-FCS would operate satisfactorily for the levels, frequencies, and kinds of input signals used during SAS operation. The responses to discrete pulse inputs of various frequencies and random gust inputs all tend to follow the same trends. Actuator hysteresis depending on the RMS gust level, has a noticeable but not serious effect. Control column input responses with LAMS engaged were well matched to those of the free aircraft.

Results of the longitudinal axis sensitivity analysis indicate that modal coefficient variations are in some cases, destabilizing. Variations in mode frequency and in flight control system time constants have no significant destabilizing effects. This is also the case with actuator hysteresis. These results are summarized in Tables XXVII, XXVIII, and XXIX for Flight Conditions 1, 2, and 3 respectively as indicated by the Symbols 1, 2, and 3.

The parameter variation column lists the percentage variations of evaluated aircraft parameters. A unity coefficient associated with a parameter would designate a nominal value; a 1.25 coefficient is a 25 per cent increase from nominal, and a .75 coefficient is a 25 per cent decrease from nominal.

The longitudinal LAMS failure analysis, presented in Table XXX, included hardover and open failures of each rate gyro and control surface actuator. All hardover failures except for the aileron actuator were considered serious in that large normal accelerations occur and stresses approach those required for structural failure. An open failure of one of the rate gyros is also serious in that it results in the flight control system being statically unstable. Various other open failures lead to increases in RMS levels of stresses and pilot's acceleration but not unmanageable situations.

4.5.2 LAMS Lateral-Directional FCS Results

The lateral-directional performance definition results indicated that the LAMS system would operate satisfactorily for the levels, frequencies, and kinds of input signals used during SAS operation.

Results of the sensitivity analysis of the LAMS Lateral-Directional FCS indicate that variations in gyro pickups and mode frequencies are not destabilizing. The analysis results are summarized in Tables XXXI, XXXII, and XXXIII for the three flight conditions checked. Deviations of 10 per cent or more from nominal are obtained at wing station 899 and body station 1028. Pilot's acceleration is sensitive to variations in mode 9 frequency. It is interesting to note that a 25 per cent reduction in frequency materially reduces pilot's acceleration at Flight Conditions 2 and 3. The effect is not seen at Flight Condition 1 where pilot acceleration RMS values increase from nominal for either an increase or decrease in mode 9 frequency.

TABLE XXVII

**Effect of Parameter Variations on LAMS
Performance, Longitudinal Axis, Flight
Condition 1**

Parameter Variation	Pilot's Acceleration RMS Variations					Stress at Wing Station 516 RMS Variations					Stress at Wing Station 800 RMS Variations					Stress at Body Station 1000 RMS Variations				
	Percent Reduction		Percent Increase			Percent Reduction		Percent Increase			Percent Reduction		Percent Increase			Percent Reduction		Percent Increase		
	Over 20	10 to 20	5 to 10	Less than 5	Notes	Over 20	10 to 20	5 to 10	Less than 5	Notes	Over 20	10 to 20	5 to 10	Less than 5	Notes	Over 20	10 to 20	5 to 10	Less than 5	Notes
	Over 20	10 to 20	5 to 10	Less than 5	Notes	Over 20	10 to 20	5 to 10	Less than 5	Notes	Over 20	10 to 20	5 to 10	Less than 5	Notes	Over 20	10 to 20	5 to 10	Less than 5	Notes
Gyro pickup																				
Gyro δ_y FF 1	1.250				B					B					B					B
0.750 ₁			1						1					1					1	
1.250 ₁			1						1					1					1	
0.750 ₁			1						1					1					1	
1.250 ₂			1						1					1					1	
0.750 ₂			1						1					1					1	
Gyro δ_x WB 11	1.250				B					B					B					B
0.750			1						1					1					1	
1.250 ₁			1					1						1					1	
0.750 ₁			1					1						1					1	
1.250 ₂			1					1						1					1	
0.750 ₂			1					1						1					1	
Gyro δ_y AF 10	1.250				B					B					B					B
0.750			1						1					1					1	
1.250 ₁			1						1					1					1	
0.750 ₁			1						1					1					1	
1.250 ₂			1						1					1					1	
0.750 ₂			1						1					1					1	
Mode frequency																				
1.250 ₁			1			1								1						
0.750 ₁			1						1					1					1	
1.250 ₂		1						1			1			1				1		
0.750 ₂				1				1					1					1		
1.250 ₃			1					1					1					1		
0.750 ₃			1					1					1					1		
Time constants:																				
Integrator: +10%			1						1					1					1	
Lag: -10%			1					1						1				1		
Lead-lag network: ±15%			1					1						1				1		
Actuator hysteresis:																				
$W_E = 2$ ft/sec rms			1						1					1					1	
4 ft/sec rms			1						1					1					1	
6 ft/sec rms			1						1					1					1	
10 ft/sec rms			1						1					1					1	
15 ft/sec rms			1						1					1					1	
Open failures:																				
Elevator actuator			1						1					1					1	
Aileron actuator			1						1					1					1	
Spoiler actuator			1						1					1					1	
Forward rate gyro			1						1					1					1	
AR rate gyro					B					B					B					B
Wing rate gyro			1						1					1					1	

NOTES: (B) Statistically unstable.

TABLE XXVIII

**Effect of Parameter Variations on LAMS
Performance, Longitudinal Axis, Flight
Condition 2**

Parameter Variation	Pitch's Acceleration RMS Variations						Stress at Wing Station 416 RMS Variations						Stress at Wing Station 399 RMS Variations						Stress at Body Station 102a RMS Variations					
	Percent Reduction			Percent Increase			Percent Reduction			Percent Increase			Percent Reduction			Percent Increase			Percent Reduction			Percent Increase		
	Over 30	30 to 20	10 to 10	5 to 10	Less than 5	Notes	Over 30	30 to 20	10 to 10	5 to 10	Less than 5	Notes	Over 30	30 to 20	10 to 10	5 to 10	Less than 5	Notes	Over 30	30 to 20	10 to 10	5 to 10	Less than 5	Notes
Gyro pickup:																								
Gyro δ_y FF 2	1.25 ₀	0.75 ₀				B						B						B						B
	1.25 ₁			2						2							2					2		
	1.25 ₂			2						2							2					2		
	0.75 ₁			2						2							2					2		
	1.25 ₃			2						2							2					2		
	1.75 ₀			2						2							2					2		
Gyro δ_x WS 11	1.25 ₀					B						B						B						B
	0.75 ₀			2						2							2					2		
	1.25 ₁			2						2							2					2		
	0.75 ₁			2						2							2					2		
	1.75 ₀			2						2							2					2		
	0.75 ₀			2						2							2					2		
Gyro δ_y AF 10	1.25 ₀			2		B				2		B					2		B			2		B
	0.75 ₀			2						2							2					2		
	1.25 ₁			2						2							2					2		
	0.75 ₁			2						2							2					2		
	1.25 ₂			2						2							2					2		
	0.75 ₂			2						2							2					2		
Mode frequency:	1.25 ₁			2			2									2					2			
	0.75 ₁			2						2						2					2			
	1.25 ₀	2								2						2					2			
	0.75 ₀			2			2									2					2			
	1.25 ₀			2						2						2					2			
	0.75 ₀	2								2						2					2			
Time-constants:																								
Integrator: +15%				2						2						2					2			
Lag: -15%				2			2									2					2			
Lead-lag network: ±15%				2						2						2					2			
Actuator hysteresis:																								
$\dot{w}_x = 2$ ft/sec rms				2							2					2					2			
4 ft/sec rms				2							2					2					2			
6 ft/sec rms				2							2					2					2			
10 ft/sec rms				2							2					2					2			
15 ft/sec rms				2							2					2					2			
Open failures:																								
Elevator actuator				2							2					2					2			
Aileron actuator				2							2					2					2			
Spoller actuator				2							2					2					2			
Forward rate gyro				2							2					2					2			
Air rate gyro						B						B						B						B
Wing rate gyro				2							2					2					2			

NOTES:
(B) Statistically unacceptable.

Effect of Parameter Variations on LAMS Performance, Longitudinal Axis, Flight Condition 3

NOTES:
(B) Slightly unstable.
(C) Data may be in error.

TABLE XXX

Effects of Hardover Actuator and Gyro Failures, Longitudinal Axis

Parameter	Normal Acceleration at Pilot's Location			Normal Acceleration at Aircraft c.g.			Stress at Wing Station 518			Stress at Wing Station 889			Stress at Body Station 1028		
	Peak Value (g's)	Time to Peak (sec)	Steady State (g's)	Peak Value (g's)	Time to Peak (sec)	Steady State (g's)	Peak Value (psi)	Time to Peak (sec)	Steady State (psi)	Peak Value (psi)	Time to Peak (sec)	Steady State (psi)	Peak Value (psi)	Time to Peak (sec)	Steady State (psi)
Flight condition 1:															
Elevator actuator	5.0	2.0	3.5	4.0	1.7	3.1	34,000	1.8	20,000	40,000	1.5	25,000	15,000	0.2	2,000
Aileron actuator	0.2	2.0	0.2	0.2	1.0	0.2	1,000	0.2	1,000	4,000	1.2	3,000	4,000	0.2	3,000
Spoiler actuator	0.6	1.5	0.6	0.9	0.9	0.7	10,000	0.4	500	5,000	0.2	5,000 ⁽²⁾	8,000	0.5	8,000
Forward rate gyro	2.1	2.0	2.1	3.1	0.9	3.1	11,000	0.6, 0.6 ⁽⁴⁾	22,000 ⁽²⁾	9,000	0.8, 0.6 ⁽⁴⁾	26,000 ⁽²⁾	4,000	0.1	1,000 ⁽²⁾
Aft rate gyro	3.4	2.0	2.4	3.2	2.0	3.2	34,000	2.0	24,000	28,000	2.0	26,000	6,500	0.1	1,000
Wing rate gyro (one)	2.2	2.5	2.2	2.0	2.5	2.0	30,000	2.0	30,000	26,000	2.0	26,000	9,500	1.5	8,500
Flight condition 2:															
Elevator actuator	1.6	2.6	1.4	1.6	2.2	1.3	20,000	2.2	17,000	21,500	2.2	16,000	2,500	0.2	1,400
Aileron actuator	0.11	0.2	0.08	0.08	0.9	0.08 ⁽²⁾	1,000	0.4	300	1,200	1.5	1,200	900	0.6	800
Spoiler actuator	0.21	1.6	0.23	0.31	1.0	0.22	7,800	0.4	1,800	2,800	0.2	1,000 ⁽²⁾	1,800	0.6	1,200
Forward rate gyro	0.7	0.2, 0.4 ⁽⁴⁾	1.4 ⁽²⁾	1.3	3.7	1.3	8,000	0.9, 2.8 ⁽⁴⁾	15,000 ⁽²⁾	6,800	0.7, 4.0 ⁽⁴⁾	16,000 ⁽²⁾	9,500	0.2, 4.9	6,500 ⁽²⁾
Aft rate gyro	1.5	1.8	1.5	1.5	2.0	1.5	16,000	1.6	16,000	17,000	2.0	17,000	2,300	0.2	1,200
Wing rate gyro (one)	1.1	2.2	1.1	1.1	2.4	1.1	20,000	2.5	20,000	18,000	2.6	18,000	2,800	2.5	2,500
Flight condition 3:															
Elevator actuator	3.4	1.8	2.5	3.6	1.6	2.6	26,000	1.2	19,000	31,000	1.6	24,000	7,500	0.2	6,500
Aileron actuator	0.15	0.3	0.25	0.15	1.0	0.15	1,000 ⁽²⁾	0.3	1,000 ⁽²⁾	2,500	1.5	2,000	2,000	0.2	2,000
Spoiler actuator	0.82	1.4	0.53	0.78	1.0	0.47	9,000	0.4	2,000	4,000	0.2	2,000 ⁽²⁾	6,100	0.2	4,000
Forward rate gyro	2.6	4.6	2.6	2.5	4.4	2.5	10,000 ⁽²⁾	0.4, 4.4 ⁽⁴⁾	14,000 ⁽²⁾	8,000	0.6, 4.5	19,000 ⁽²⁾	6,000	0.3	4,500
Aft rate gyro	2.6	2.0	2.6	2.6	1.8	2.6	17,000	1.6	16,000	22,000	2.0	21,000	5,500	0.8	8,000
Wing rate gyro (one)	1.7	2.6	1.7	1.7	2.5	1.7	19,000	2.6	19,000	20,000	2.5	20,000	9,500	2.3	9,500

(1) For steadily increasing functions, value 8-10 seconds after failure is used.

(2) Peak and steady-state values have opposite signs

(3) Time to 90 percent of asymptotic functions.

(4) First figure is time to initial peak, second figure is time to 90 percent of final value (used where initial peak is of significant but smaller amplitude than final).

TABLE XXXI

Effect of Parameter Variations on LAMS Performance, Lateral Axis, Flight Condition 1

Parameter Variation	Pilot's Acceleration RMS Variations						Stress at Wing Station 516 RMS Variations						Stress at Wing Station 909 RMS Variations						Stress at Body Station 1038 RMS Variations						Stress at Fin Station 135 RMS Variations							
	Percent Reduction			Percent Increase			Percent Reduction			Percent Increase			Percent Reduction			Percent Increase			Percent Reduction			Percent Increase			Percent Reduction			Percent Increase				
	Over 30	10 to 30	5 to 10	Less than 5	5 to 10	10 to 30	Over 30	10 to 30	5 to 10	Less than 5	5 to 10	10 to 30	Over 30	10 to 30	5 to 10	Less than 5	5 to 10	10 to 30	Over 30	10 to 30	5 to 10	Less than 5	5 to 10	10 to 30	Over 30	10 to 30	5 to 10	Less than 5				
Mode Slopes:																																
Gyro $\psi_{AP} 2$, 135° ψ																																
Gyro $\psi_{AP} 2$, 75° ψ																																
Gyro $\delta_{AP} 2$, 135° δ																																
Gyro $\delta_{AP} 2$, 75° δ																																
Gyro $\psi_{AP} 8$, 135° ψ																																
Gyro $\psi_{AP} 8$, 75° ψ																																
Gyro $\psi_{AP} 10$, 135° ψ																																
Gyro $\psi_{AP} 10$, 75° ψ																																
Gyro $\psi_{FF} 8$, 135° ψ																																
Gyro $\psi_{FF} 8$, 75° ψ																																
Gyro $\psi_{FF} 1$, 135° ψ																																
Gyro $\psi_{FF} 1$, 75° ψ																																
Gyro $\psi_{FF} 6$, 135° ψ																																
Gyro $\psi_{FF} 6$, 75° ψ																																
Gyro $\psi_{FF} 8$, 135° ψ																																
Gyro $\psi_{FF} 8$, 75° ψ																																
Mode frequencies:																																
135° ω , Mode 1																																
75° ω , Mode 1																																
135° ω , Mode 9																																
75° ω , Mode 9																																
Open Failures (A)																																
Gyro $\psi_{AP} 2$																																
Gyro $\psi_{FF} 8$																																
Gyro $\psi_{AP} 8$																																
Gyro $\psi_{AP} 10$																																
Gyro $\delta_{AP} 2$																																
Gyro $\delta_{AP} 8$																																
Gyro $\delta_{AP} 10$																																
Gyro $\delta_{AP} 2$																																
Gyro $\delta_{AP} 8$																																
Gyro $\delta_{AP} 10$																																
Actuator: δ_r																																
θ_a																																

TABLE XXXII

Effect of Parameter Variations on LAMS Performance,
Lateral Axis, Flight Condition 2

Parameter Variation	Pitch Acceleration RMS Variations						Wing Station 516 RMS Variations						Wing Station 608 RMS Variations						Body Station 1038 RMS Variations						Tail Station 135 RMS Variations						
	Percent Reduction			Percent Increase			Percent Reduction			Percent Increase			Percent Reduction			Percent Increase			Percent Reduction			Percent Increase			Percent Reduction			Percent Increase			
	Over 30	20 to 30	10 to 20	5 to 10	Less than 5	Over 30	20 to 30	10 to 20	5 to 10	Less than 5	Over 30	20 to 30	10 to 20	5 to 10	Less than 5	Over 30	20 to 30	10 to 20	5 to 10	Less than 5	Over 30	20 to 30	10 to 20	5 to 10	Less than 5	Over 30	20 to 30	10 to 20	5 to 10	Less than 5	
Mode alone:																															
Gyro ψ_{AP} 3, 135 ψ					3					2																					
75 ψ					2					2																					
Gyro δ_{AP} 3, 135 δ					2					2																					
75 δ					2					2																					
Gyro ψ_{AP} 6, 135 ψ					2					2																					
75 ψ					2					2																					
Gyro ψ_{AP} 10, 135 ψ					2					2																					
75 ψ					2					2																					
Gyro ψ_{AP} 3, 135 ψ					2					2																					
75 ψ					2					2																					
Mode frequencies:																															
135 ω , Mode 1					2					2																					
75 ω , Mode 1					2					2																					
135 ω , Mode 9					2					2																					
75 ω , Mode 9					2					2																					
Open failures:																															
Gyro ψ_{AP} 2					2					2																					
ψ_{AP} 6					2					2																					
ψ_{AP} 9					2					2																					
ψ_{AP} 10					2					2																					
δ_{AP} 3					2					2																					
δ_{AP} 14					2					2																					
Actuator: δ_R					2					2																					
δ_a					2					2																					

TABLE XXXIII
Effect of Parameter Variations on LAMS Performance,
Lateral Axis, Flight Condition 3

Parameter Variation	Pilot's Acceleration RMS Variations						Stress at Wing Station 516 RMS Variations						Stress at Wing Station 899 RMS Variations						Stress at Body Station 1028 RMS Variations						Stress at Fin Station 135 RMS Variations					
	Percent Reduction			Percent Increase			Percent Reduction			Percent Increase			Percent Reduction			Percent Increase			Percent Reduction			Percent Increase			Percent Reduction			Percent Increase		
	Over 30	20 to 30	10 to 30	3 to 10	Less than 3	Notes	Over 30	20 to 30	10 to 30	3 to 10	Less than 3	Notes	Over 30	20 to 30	10 to 30	3 to 10	Less than 3	Notes	Over 30	20 to 30	10 to 30	3 to 10	Less than 3	Notes	Over 30	20 to 30	10 to 30	3 to 10	Less than 3	Notes
Mode slopes:																														
Gyro $\psi_{AF} 2$ 1296 μ				3																										
Gyro $\psi_{AF} 3$ 766 μ				3																										
Gyro $\psi_{AF} 5$ 1256 μ				3																										
Gyro $\psi_{AF} 6$ 756 μ				3																										
Gyro $\psi_{AF} 8$ 1257 μ				3																										
Gyro $\psi_{AF} 9$ 755 μ				3																										
Gyro $\psi_{AF} 5$ 1255 μ				3																										
Gyro $\psi_{AF} 5$ 756 μ				3																										
Mode frequencies:																														
125 μ , mode 1				3																										
75 μ , mode 1				3																										
125 μ , mode 2				3																										
75 μ , mode 0				3																										
Open failures:																														
Gyro $\psi_{AF} 2$				3																										
$\psi_{AF} 5$				3																										
$\psi_{AF} 6$				3																										
$\psi_{AF} 10$				3																										
$\psi_{AF} 3$				3																										
$\psi_{AF} 14$				3																										
Actuator h_r				3																										
δ_a				3																										

Note A: Excrescence counter variations are plotted in Figures 42, 44, and 45.

Open failure results included in the RMS variations summarized in Tables XXXI, XXXII, and XXXIII indicate that yaw rate gyro failures can degrade LAMS performance to that of the free aircraft or worse.

Hardover failures do not appear to be serious in the Lateral-Directional axis. Hardover failure transient responses indicate that responses are essentially stable commands equivalent to full authority pilot commands. Response damping is not degraded below that of the free aircraft.

4.6 LAMS FCS Longitudinal Design Modification Results

LAMS-FCS spoiler loop design modification effects are illustrated by comparing modified eigenvalues with those presented in Section 4.2. Longitudinal axis eigenvalues, mode damping values, and mode frequencies are presented in Tables XXXIV and XXXV for Flight Conditions 1 and 3. These Tables show the effect of including aircraft equivalent structural damping and lift growth on the spoilers in addition to including the revised system gains as shown in Figure 6. The revised spoiler loop system gains resulted in a 25 degree phase lead at the structural mode 1 frequency and a 20 degree phase lead at the structural mode 6 frequency as referenced to the original system gains.

TABLE XXXIV
REVISED IAMS LONGITUDINAL FCS EIGENVALUES
FLIGHT CONDITION 1

Mode	Root Locations	ζ	ω_n f_n
SP	$-1.47 \pm j 2.63$.488	3.02 .48
1	$-.92 \pm j 7.46$.122	7.52 1.20
2	$-.59 \pm j 12.13$.049	12.14 1.93
3	$-.24 \pm j 12.70$.019	12.70 2.02
4	$-.23 \pm j 14.73$.016	14.73 2.34
5	$-1.07 \pm j 15.06$.071	15.09 2.40
6	$-2.70 \pm j 18.70$.143	18.90 3.01
7	$-.45 \pm j 19.44$.023	19.45 3.09
8	$-1.19 \pm j 21.71$.055	21.74 3.46
9	$-1.96 \pm j 33.44$.059	33.50 5.33
10	$-1.06 \pm j 36.39$.029	36.41 5.79
11	$-.57 \pm j 37.64$.015	37.64 5.99
12	$-1.67 \pm j 39.93$.042	39.96 6.36
13	$-7.16 \pm j 45.73$.155	46.30 7.37
14	$-.94 \pm j 57.11$.016	57.12 9.09
15	$-.66 \pm j 60.23$.011	60.23 9.59
16	$-4.17 \pm j 61.82$.068	61.96 9.86
17	$-3.17 \pm j 64.32$.049	64.40 10.25
18	$-2.79 \pm j 83.73$.033	83.78 13.33
19	$-4.83 \pm j 88.10$.055	88.23 14.04
20	$-6.85 \pm j 94.55$.073	94.80 15.09
21	$-3.31 \pm j 94.77$.035	94.83 15.09
22	$-2.26 \pm j 113.40$.020	113.42 18.05

TABLE XXXV
REVISED LAMS LONGITUDINAL FCS EIGENVALUES
FLIGHT CONDITION 3

Mode	Root Locations	ζ	ω_n f_n
SP	$-1.38 \pm j 2.35$.51	2.73 .435
1	$-.76 \pm j 7.76$.098	7.76 1.23
2	$-.50 \pm j 12.09$.041	12.09 1.93
3	$-.21 \pm j 12.69$.017	12.69 2.02
4	$-.63 \pm j 15.02$.042	15.02 2.39
5	$-.21 \pm j 15.19$.019	15.19 2.42
6	$-2.33 \pm j 19.09$.121	19.28 3.07
7	$-.40 \pm j 19.56$.020	19.56 3.11
8	$-.65 \pm j 24.32$.027	24.32 3.87
9	$-1.43 \pm j 35.47$.040	35.47 5.65
10	$-.73 \pm j 37.48$.019	37.48 5.97
11	$-.59 \pm j 37.72$.016	37.72 6.00
12	$-1.42 \pm j 42.67$.033	42.67 6.80
13	$-3.92 \pm j 47.52$.083	47.52 7.56
14	$-.94 \pm j 58.11$.016	58.11 9.24
15	$-2.63 \pm j 63.71$.041	63.71 10.13
16	$-1.69 \pm j 65.33$.026	65.33 10.40
17	$-1.51 \pm j 68.07$.022	68.07 10.83
18	$-2.90 \pm j 87.07$.033	87.07 13.85
19	$-2.97 \pm j 90.96$.033	90.96 14.50
20	$-4.51 \pm j 96.89$.046	96.89 15.40
21	$-2.70 \pm j 105.73$.026	105.73 16.80
22	$-1.92 \pm j 117.50$.016	117.50 18.70

5.0 **HARDWARE DESIGN**

5.1 **Introduction**

This section discusses hardware which has been designed to implement the IAMS program. The section encompasses the hydraulic actuators, the hydraulic power system, the control system electrical/electronics, special hardware, such as analog computers, oscillograph, and function generators, and the fly-by-wire system, and the Honeywell IAMS-FCS computer.

5.2 **Boeing Hardware Design**

5.2.1 **Aileron Actuator**

The original aileron was controlled by two tabs; a control tab which was operated by a cable system to the control wheel and a trim and balance tab driven by an electric motor.

When converting to the hydraulically powered aileron system, the aileron gust dampers, and the aileron trim tab actuators were removed. The trim tab was fixed to the aileron, and the mechanical linkage from the control quadrant to the control tab was replaced with a push rod to the aileron actuator. The control tab linkage was attached to fixed structure to provide boost tab operation (5:1) when the aileron actuator displaced the aileron.

The aileron actuator is a hydraulic servo actuator which positions the aileron in response to mechanical control inputs transmitted from the control wheel, electrical signals from a stability augmentation system, electrical trim input from trim switches, or simultaneous combinations of all inputs. Aileron position feedback is obtained from a mechanical linkage attached to the actuator piston rod.

The aileron actuator was designed to be in accordance with the requirements summarized in Table XXXVI and Figures 56 and 58.

The functional diagram of the aileron actuator is shown in Figure 57.

The aileron actuator has full electrical authority ± 17 degrees and the specification required the capability of full manual override of any electrical command with no reduction in mechanical authority. The requirement was not implemented in the aileron actuator due to an error in design by the actuator supplier. This error was not corrected, because the additional cost and time required to incorporate a revision to the actuator was not warranted; this same design requirement was applicable to the spoiler control valve, and the spoiler authority was more than adequate to override the effect of hardover aileron rolling moment.

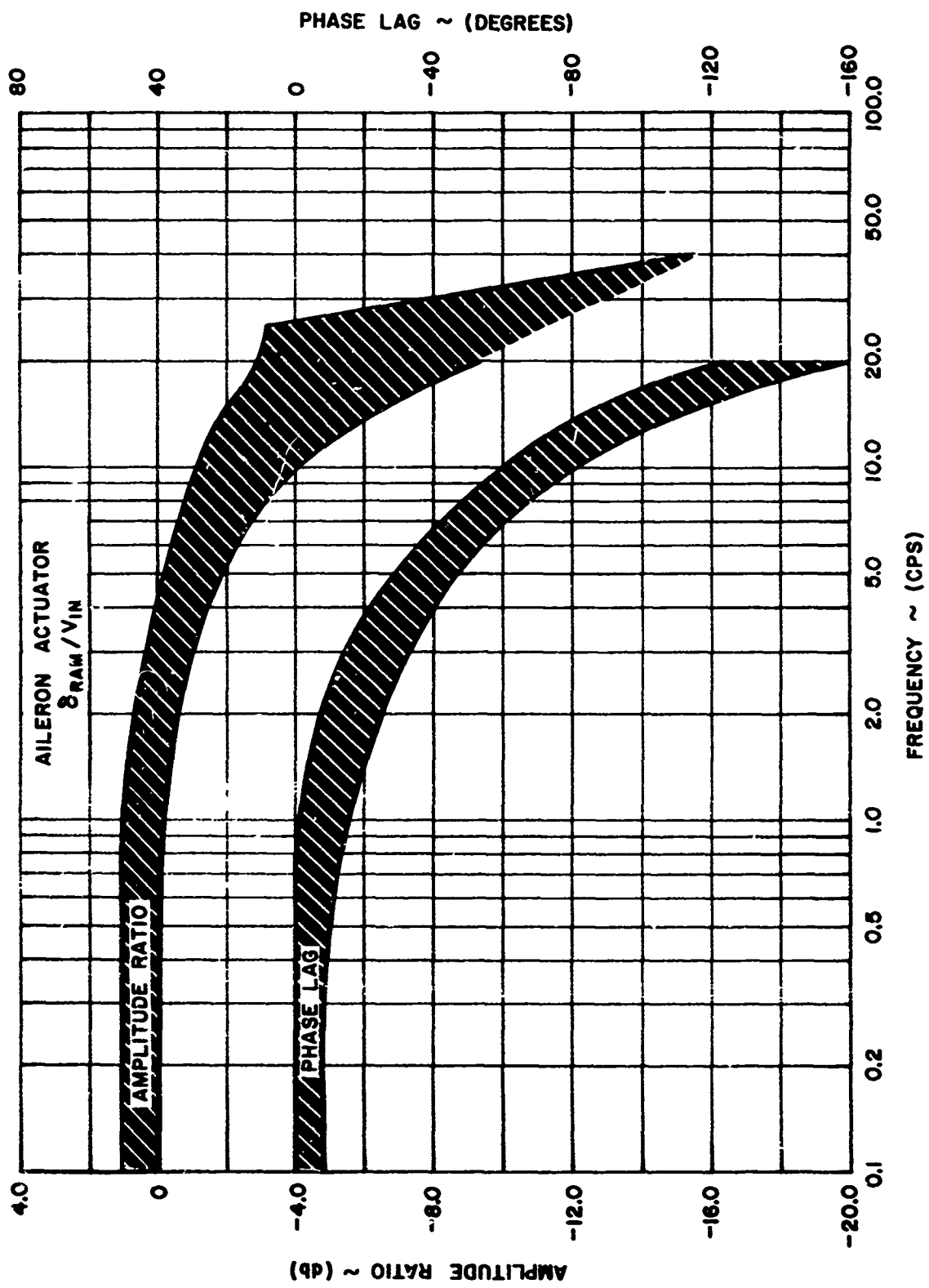
Additional features of the aileron actuator were the integrated force feedback piston required for stability compensation, and the delay valve which limited actuator centering rate to 60 degrees per second upon electrical shutdown.

TABLE XXXVI
SPOILER ACTUATION SYSTEM SPECIFICATIONS

Operating Pressure	3000 psi
Ambient Temperature Range	-65° to +180° F
Fluid Temperature Range	-40° to +225° F
Altitude	Sea Level to 60,000 Ft.
Surface Displacement	60°
No Load Rate 2 Panel Configuration	220 deg/sec
No Load Rate 3 Panel Configuration	140 deg/sec
Open Loop Gain 2 Panel Configuration	40 deg/sec/deg
Open Loop Gain 3 Panel Configuration	27 deg/sec/deg
Effective Piston Area Up	1.92 in ²
Effective Piston Area Down	.92 in ²
Force Capability Per Panel Up	5700 lbs
Stroke	6.25 in.
Crank Arm	5.62 in.

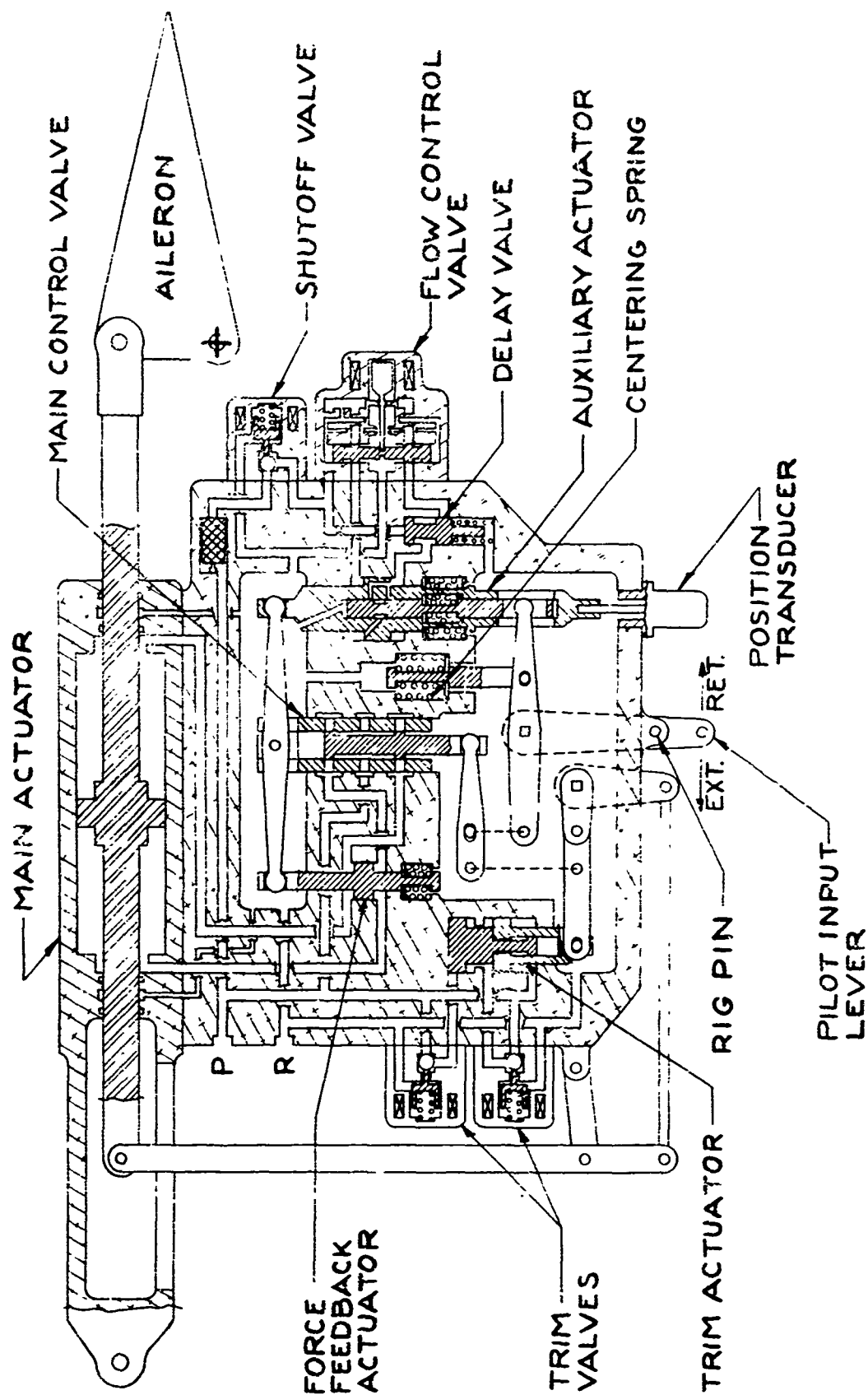
AILERON ACTUATOR SYSTEM SPECIFICATIONS

Operating Pressure	3000 psi
Ambient Temperature Range	-65° to +180° F
Fluid Temperature Range	-40° to +225° F
Altitude	Sea Level to 60,000 Ft.
Surface Displacement	±17°
No Load Rate	120 deg/sec
Weight	74 lbs
Open Loop Gain	45 deg/sec/deg
Effective Piston Area	2.03 in ²
Force Capability	6090 lbs
Stroke	6.14 in.
Crank Arm	10.5 in.



THEORETICAL CLOSED LOOP FREQUENCY RESPONSE

FIGURE 56



AILERON ACTUATOR FUNCTIONAL DIAGRAM

FIGURE 57

5.2.2 Spoiler Actuation System (Integrated Spoiler Servo Valve)

The spoiler servo valve is an integrated unit designed to supply metered hydraulic flow to the spoiler segment actuators in response to electrical fly-by-wire, and/or stability augmentation commands, electrical air-brake, mechanical pilot input, and mechanical position feedback commands from the existing follow-up linkage system.

The spoilers were divided into groups of four outboard segments and three inboard segments. Due to design and fabrication problems, the spoiler servo valve proved unsatisfactory for SAS inputs. Therefore, the system was modified to utilize only the two outboard spoiler segments for LAMS-FCS control, see Section 5.2.3. The remaining five segments were grouped three inboard and two outboard. With this new configuration, the spoiler actuation system is required to accomplish all of the functions listed above with the exception of LAMS-FCS and meet the specifications listed in Table XXXVI.

A functional diagram of the spoiler servo valve is shown in Figure 59 and the initial specified auxiliary actuator open loop frequency response is presented in Figure 58.

5.2.3 LAMS-FCS Spoiler Actuation

Command signal implementation for the longitudinal LAMS-FCS is provided with special servo-actuators which control the two outboard spoiler panels on each wing. These LAMS-FCS spoiler actuators were configured by modifying the existing actuator on Spoiler Panels 1, 2, 13, and 14. Each actuator was fitted with a special manifold which adapted a Model 31 Moog electro-hydraulic flow control valve to the unit. A position transducer was fitted to the actuator piston rod to provide a complete servo-actuator and are connected to the hydraulic power system in the outboard wing.

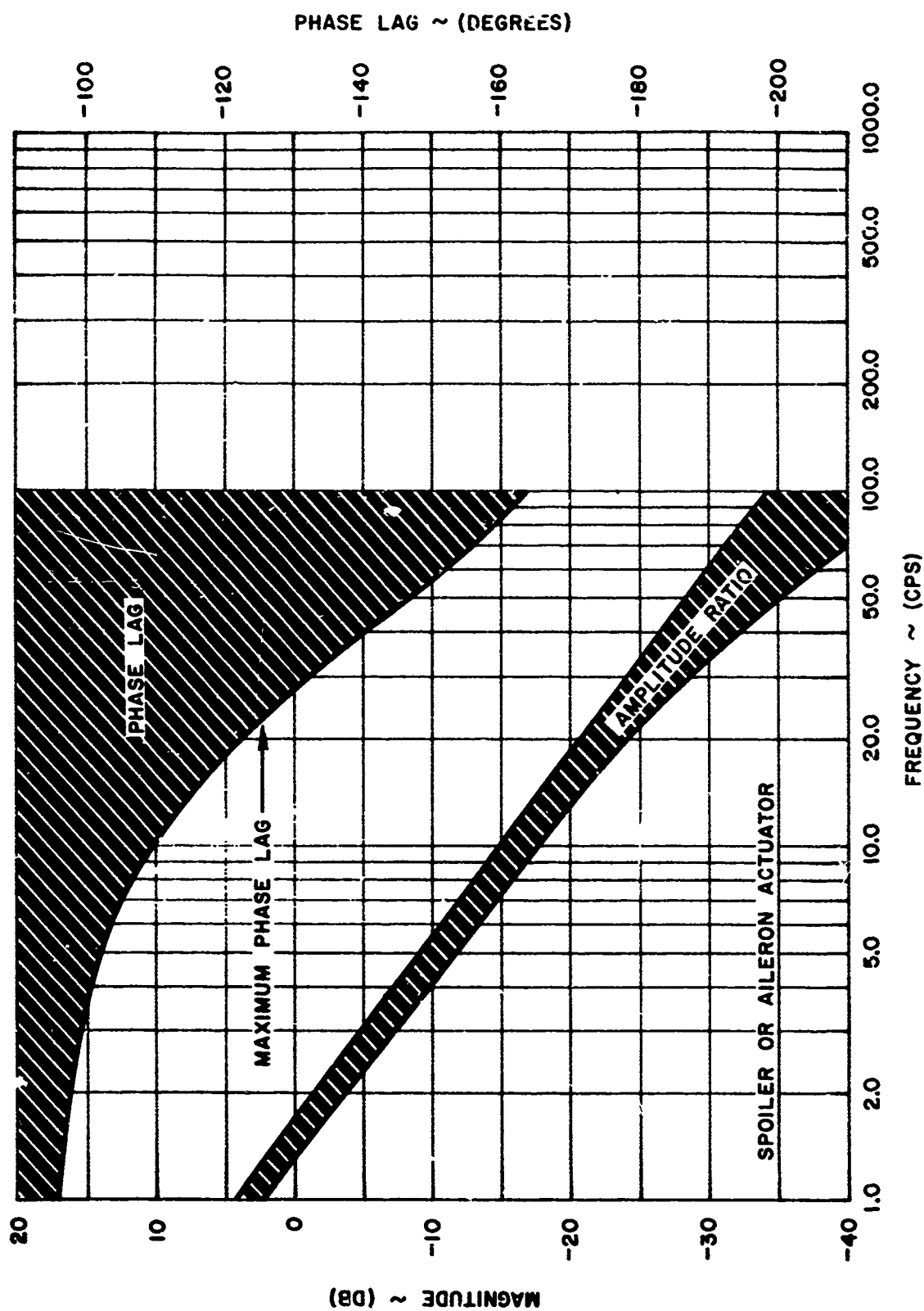
The spoiler actuators respond to plus and minus command inputs and provide spoiler surface deflection of plus 45 degrees and minus 15 degrees from a plus 15 degree deflection bias point.

The SAS spoiler actuators are designed to meet criteria listed in Table XXXVIII and Figure 60.

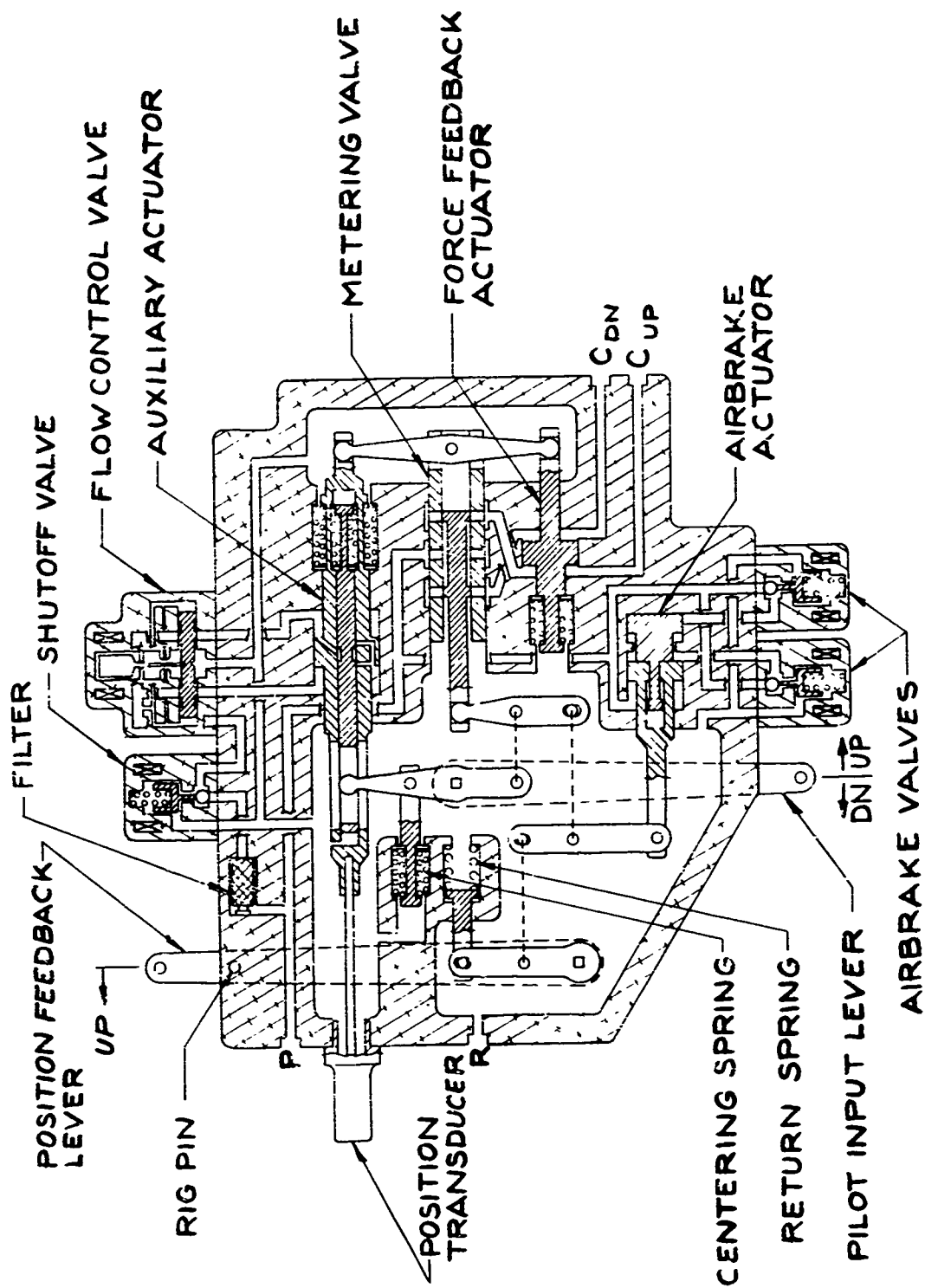
5.2.4 Rudder and Elevator Actuators

The hydraulic actuators used for driving the rudder and elevator are of a dual tandem configuration and designed in accordance with MIL-C-5503, MIL-H-8775 and MIL-E-7080. The elevator and rudder power control actuators differ only in envelope dimensions, force output and stroke.

Each actuator employs differential pressure limiters for limiting the maximum force output, a dual tandem piston and cylinder, two electrical shutoff valves, two auxiliary actuators, two position transducers, one dual main control valve, two main actuator bypass valves, four filters, two electrical connectors and an internal summing linkage system.



THEORETICAL AUXILIARY ACTUATOR OPEN LOOP FREQUENCY RESPONSE
FIGURE 58



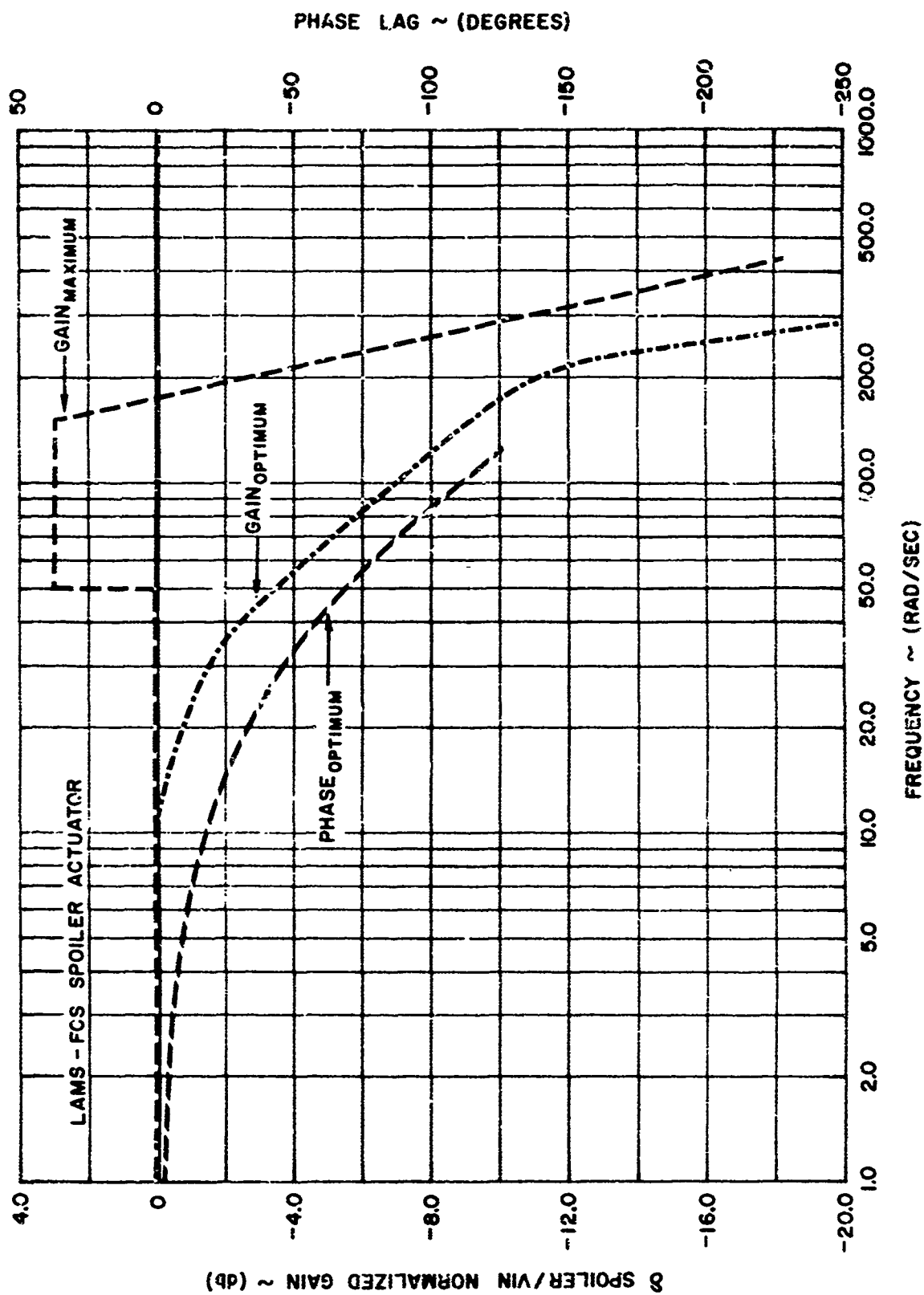
SPOILER VALVE FUNCTIONAL DIAGRAM

FIGURE 59

TABLE XXXVII

LAMS-FCS SPOILER ACTUATION SYSTEM SPECIFICATIONS

Operating Pressure	3000 psi
Ambient Temperature Range	-65° to +180°F
Fluid Temperature Range	-40° to +225°F
Altitude	Sea Level to 60,000 Ft.
Gain Margin	10 db
Phase Margin	70°
Open Loop Gain	43 Sec ⁻¹
Stroke	6.25 in.
Effective Piston Area Up	1.92 in.
Effective Piston Area Down	.92 in.
Force Capability-Per Panel Up	5,700 lbs.
Crank Arm	5.62 in.



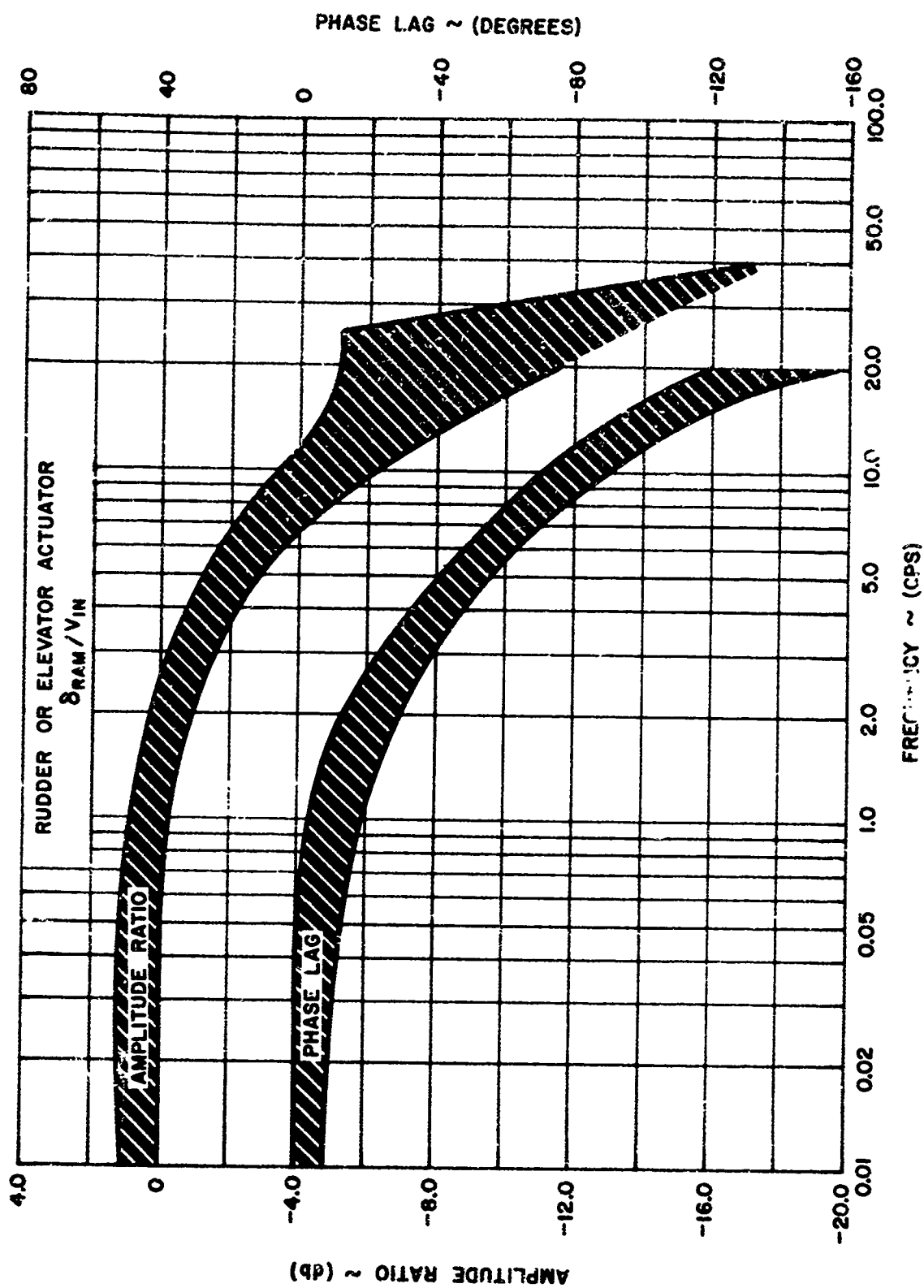
THEORETICAL CLOSED LOOP FREQUENCY RESPONSE
FIGURE 60

TABLE XXXVIII
 RUDDER ACTUATOR SPECIFICATIONS

Operating Pressure	3000 psi
Ambient Temperature Range	-65° to +180° F
Fluid Temperature Range	-40° to +225° F
Altitude	Sea Level to 60,000 Ft.
Surface Displacement	±19°
No Load Rate	80 deg/sec
Weight	44 lbs
Open Loop Gain	45 deg/sec/deg
Effective Piston Area	2.44 in ²
Force Capability	7320 lbs
Stroke	±1.30 in.
Crank Arm	4.00 in.

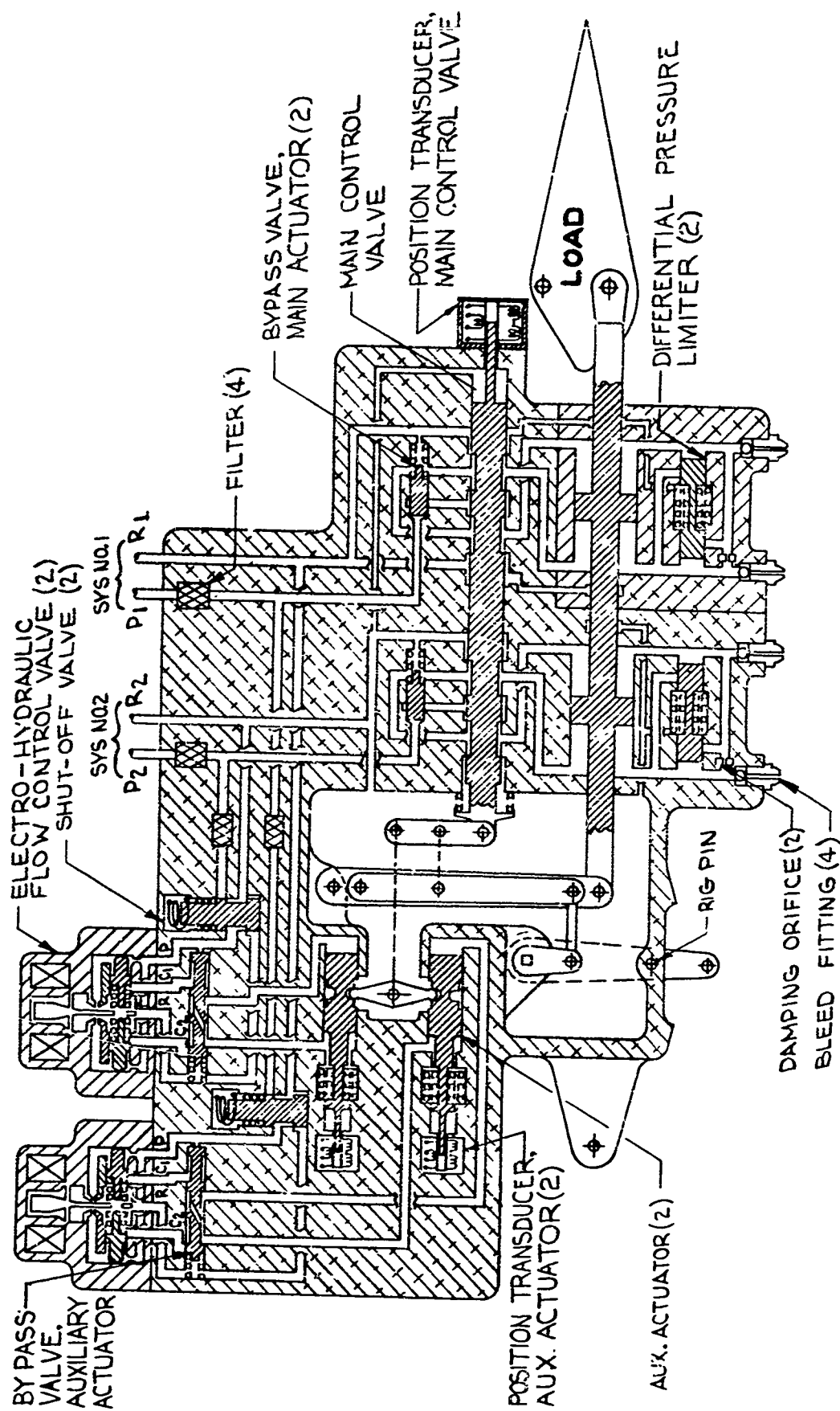
ELEVATOR ACTUATOR SPECIFICATIONS

Operating Pressure	3000 psi
Ambient Temperature Range	-65° to +180° F
Fluid Temperature Range	-40° to +225° F
Altitude	Sea Level to 60,000 Ft.
Surface Displacement	±19°
No Load Rate	80 deg/sec
Weight	57 lbs
Open Loop Gain	45 deg/sec/deg
Effective Piston Area	3.51 in ²
Force Capability	10,530 lbs
Stroke	±1.47 in.
Crank Arm	4.5 in.



THEORETICAL CLOSED LOOP FREQUENCY RESPONSE

FIGURE 61



UDDER OR ELEVATOR ACTUATOR FUNCTIONAL DIAGRAM

FIGURE 62

In addition, the elevator actuators contain two rate limiting bypass valves for the purpose of limiting control surface rates induced by electrical shutdown of the SAS portion of the actuator.

The following components are interchangeable on all actuators:

Electro-hydraulic Flow Control Valves

Shutoff Valves

Position Transducers

Main Actuator Bypass Valves

Filters

The differential pressure limiters are non-interchangeable.

The criteria for the design of the rudder and elevator actuators are listed in Table XXXVIII and Figure 61.

A functional diagram of the actuator is shown in Figure 62.

5.2.5 Hydraulic Power System Design

The hydraulic power system design consisted of augmenting the power capability of the existing systems and the installation of two additional systems in the aft body of the airplane for powering the rudder and elevators.

5.2.5.1 Roll Axis Hydraulic Power System

Hydraulic power for actuating the ailerons and the spoilers is provided by six separate hydraulic systems. The primary source of power for each system is provided by an engine driven hydraulic pump. A pump is mounted on each engine of the airplane except on engines #2 and #8. Each of the hydraulic systems is supplemented with an electric motor driven pump and an accumulator to augment flow. The four left outboard spoiler panels are powered by the number one engine system, the three left inboard spoilers are powered by the number three engine system and the left aileron is powered by the number four engine system. A similar arrangement exists in the right hand wing. In addition to driving the spoilers, the outboard systems provide actuation power for the tip protection landing gear. The systems powered by engines #4 and #5 power the ailerons and also provide power for stabilizer trim actuation, landing gear actuation, and other utility functions. A block diagram of the basic LAMS test vehicle hydraulic systems is shown in Figure 63. Figure 64 shows the hydraulic systems as modified for the LAMS program. The hydraulic systems are the 3000 psi type and use MIL-R-5606 fluid. The flow capacity of each engine driven pump is 12 gpm. The flow of the auxiliary (electric motor) pump in each aileron system is 6 gpm and the auxiliary pump in each spoiler system is 3.8 gpm. A 100 cubic inch accumulator was installed in each of the systems powered by engines #1 and #7. Each of the other four systems was provided with a 50 cubic inch accumulator.

The accumulators were located as close to the aileron or spoiler actuators as practical to increase effectiveness.

5.2.5.2 Rudder-Elevator Hydraulic Power System

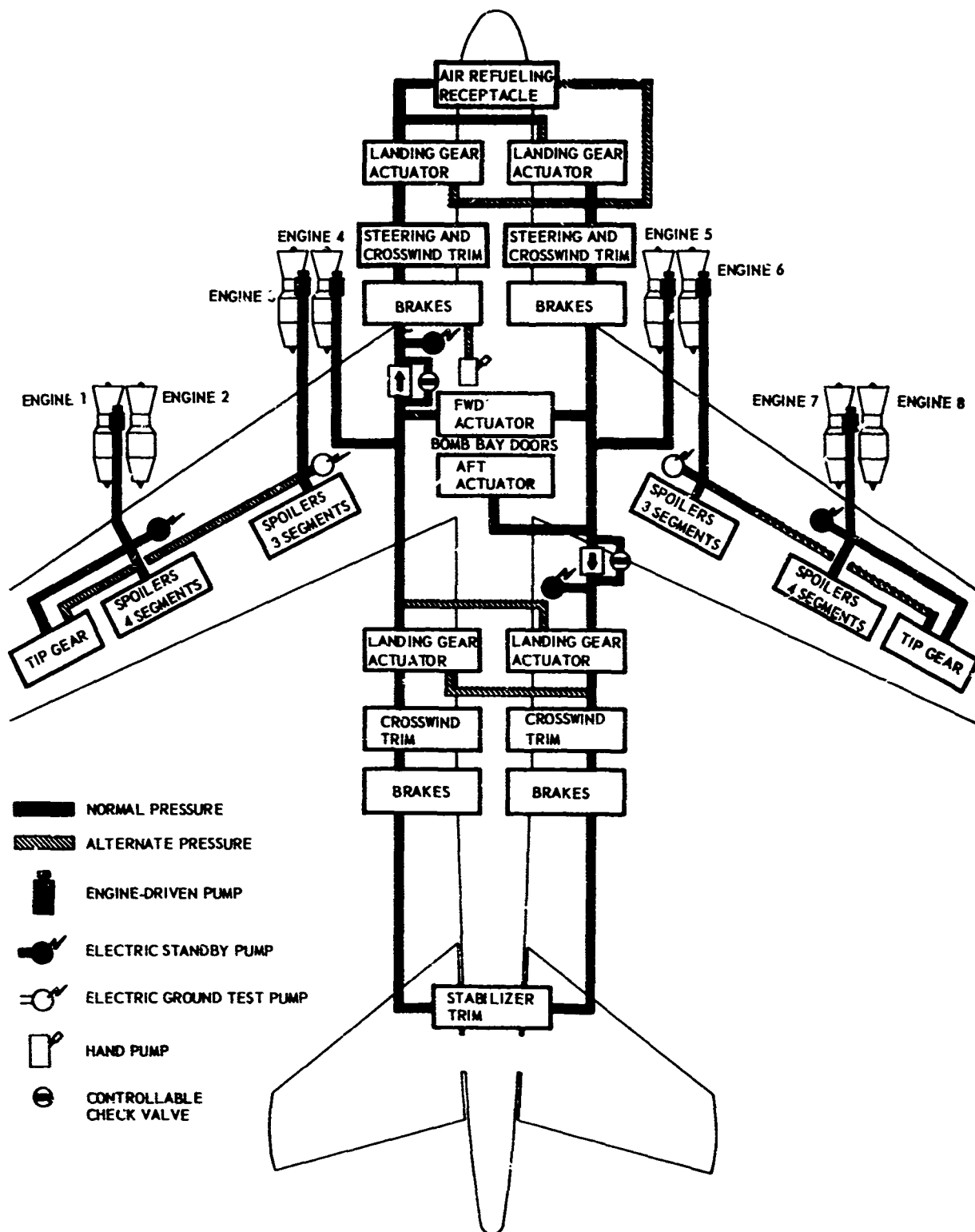
A trade study was accomplished to determine the most feasible power supply configuration for the rudder and elevators which would provide adequate reliability and could be installed on either the B-52G or H without modification. Considerations in the trade study were as follows:

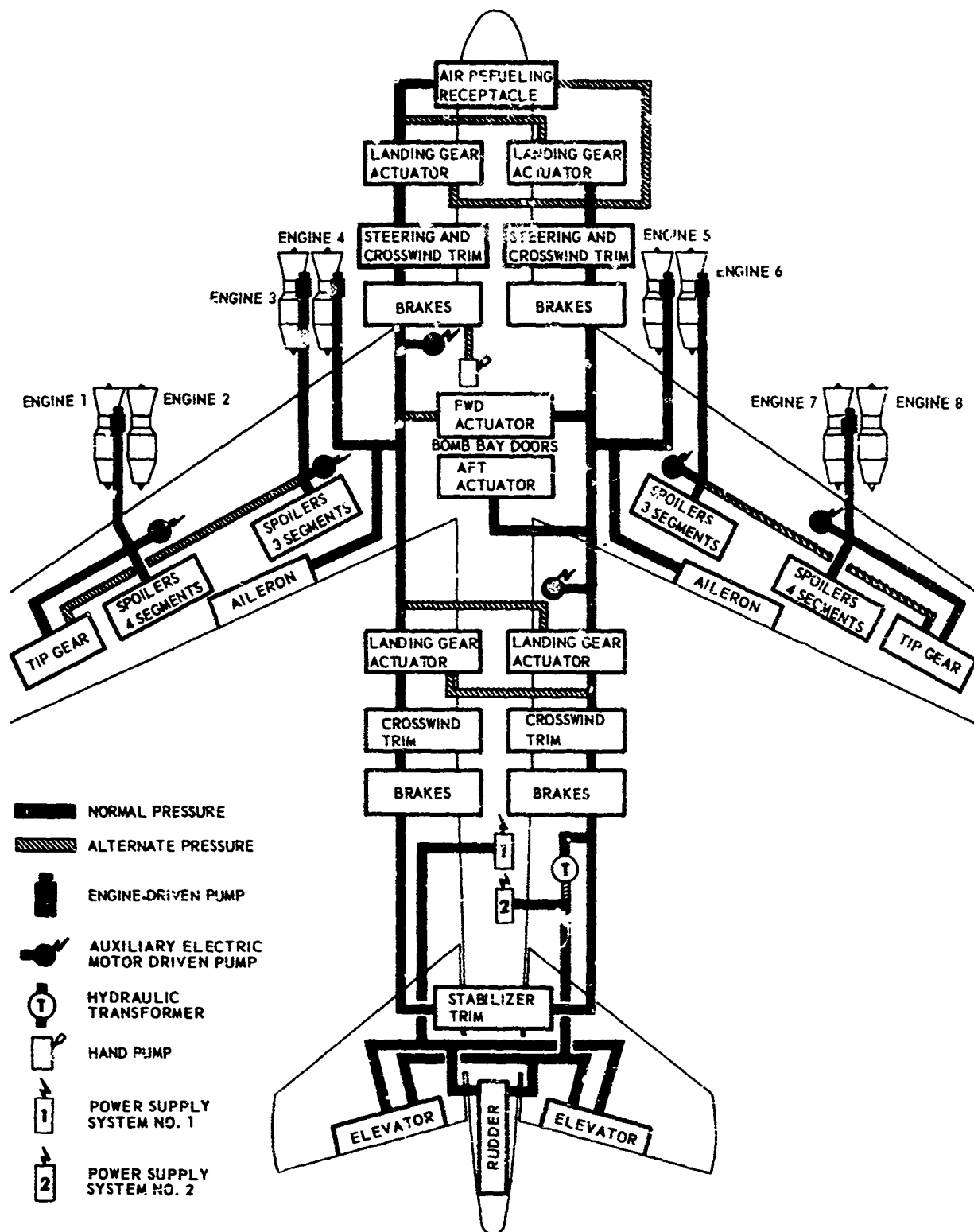
- Reliability
- Weight
- Cost
- Complexity of Installation
- Maintainability

The primary source of hydraulic power for the rudder-elevator system is provided by two electric motor driven pumps. Two separate systems are provided and each system has a self-pressurizing reservoir. A standby source of hydraulic power is provided by a hydraulic motor driven pump (transformer) that is powered by the Number 5 engine drive system. The rudder-elevator systems are shown in location in Figure 64. A more detailed block diagram of the systems is presented in Figure 65.

The electric motor driven pump assembly consists of a variable delivery axial piston hydraulic pump and a 3 phase 118/205 volt, Class A, induction motor. The assembly is rated at 2700 psi at 6 gpm (full flow) and 3000 psi at zero flow.

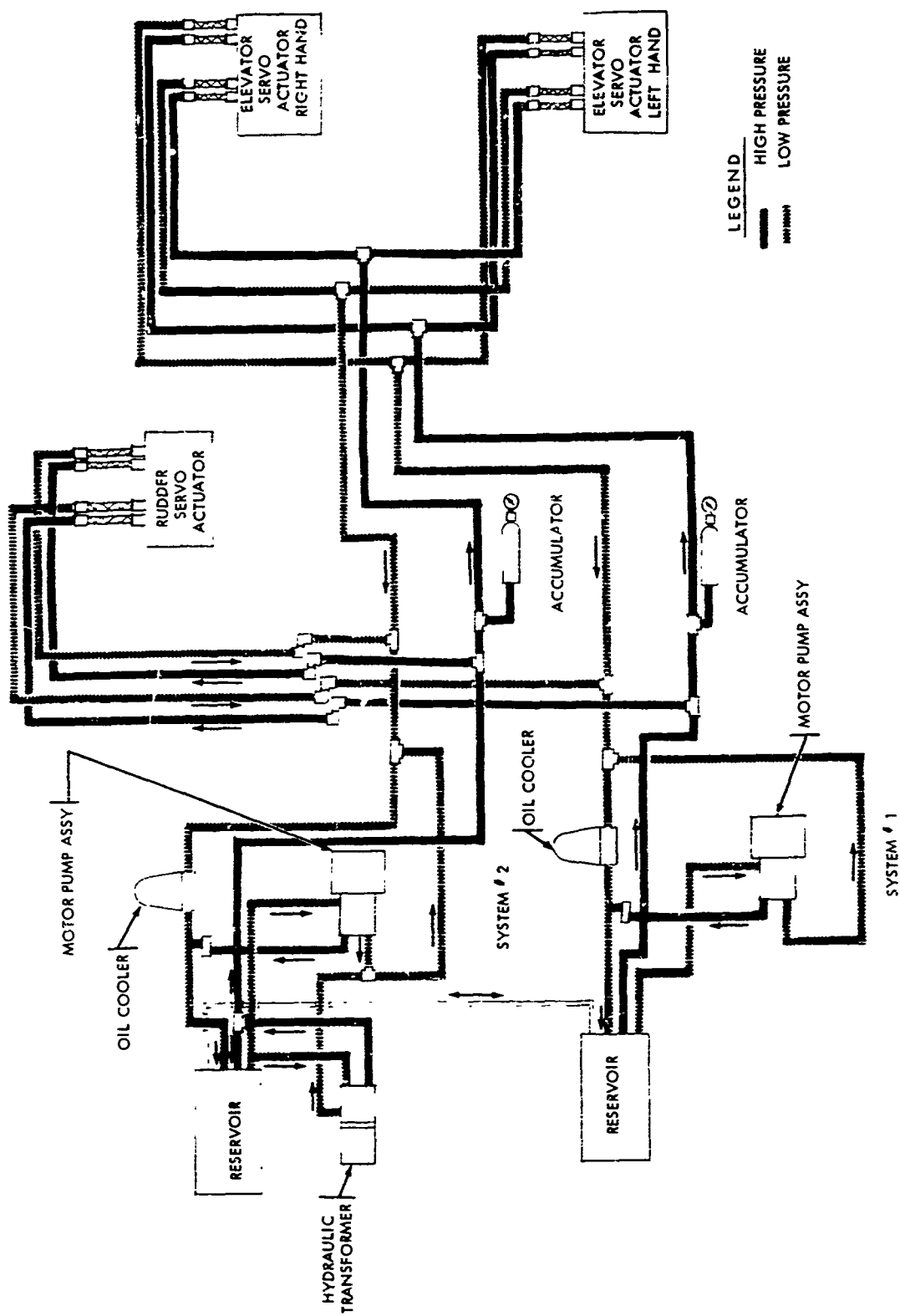
The hydraulic transformer is incorporated in System No. 2 to provide emergency power in the event of failure of the primary systems. The hydraulic motor utilizes power from the aircraft LH body hydraulic system to drive the pump. The unit is designed to deliver flow when the input differential pressure across the motor and flow regulator is 2950 psi and the rudder-elevator hydraulic system differential pressure across the pump drops to $2600 + \frac{50}{-130}$ psi. The transformer will continue to deliver flow until the rudder-elevator hydraulic system differential pressure reaches 2800 psi, and will then stall. Rated flow of the hydraulic motor driven pump is two gpm at 2200 psi pump side differential.





BASIC LAMS TEST VEHICLE HYDRAULIC CONFIGURATION AFTER LAMS MODIFICATION

FIGURE 64



RUDDER-ELEVATOR HYDRAULIC SYSTEM

FIGURE 65

5.2.6 Electronic Sensors

Position, rate and acceleration sensors are used in the control system, some being implicit in the control loop while others are used for safety monitor and/or Flight Test data acquisition purposes. A list of the system sensors is tabulated in Table XXXIX and located in the aircraft in Figure 66.

5.2.6.1 Position Sensors

Two types of position sensors are found in the control system: D.C. and A.C. The D.C. sensors are conductive plastic potentiometers and may be either rotary or linear. Potentiometers are used for pilot's control position and surface positions.

Potentiometers are supplied with ± 15 volts excitation from the interface electronics power supplies. In order to provide optimum scale factors, rotary potentiometers are designed with extra taps so that excitation may be applied at a point near the maximum slider rotation. Buffer amplifiers are provided in the interface electronics to isolate the potentiometers from other disturbing circuit elements and to provide gain change capabilities where required.

The A.C. type of position sensor is the LVDT (Linear Variable Differential Transformer) sensing the auxiliary actuator position in the control actuator. This sensor is a necessary element in the auxiliary actuator control loop. Since the output is 400 cycle A.C., a ring demodulator and buffer amplifier are used to convert the signal to the required D.C.

5.2.6.2 Rate Sensors

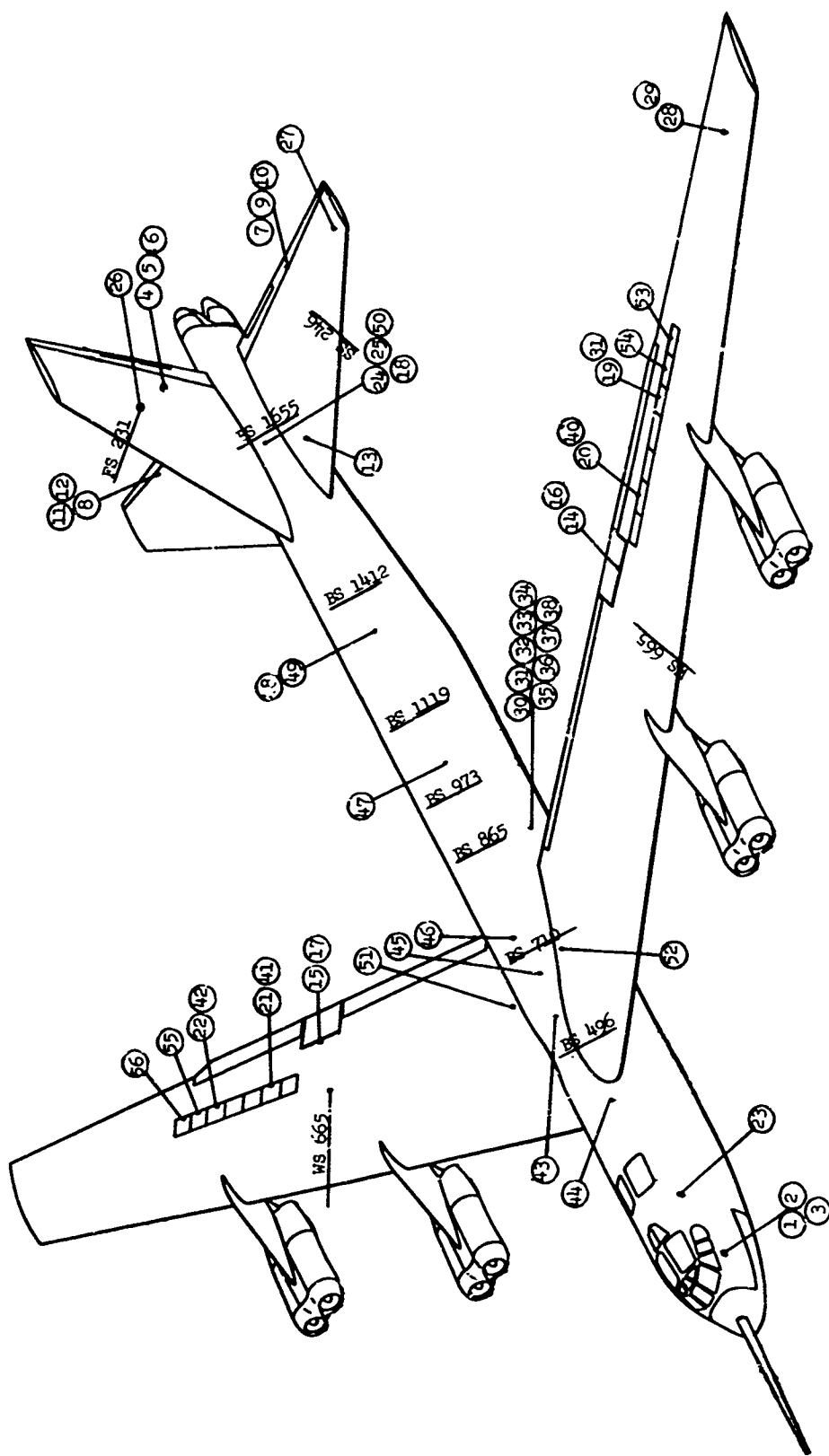
The rate sensors utilized in the control system are miniature rate gyros in two ranges: 0-20 degrees/sec and 0-40 degrees/sec. The undamped natural frequency is above 20 cps. The output is A.C. and a demodulator and buffer amplifier are required to provide D.C. signals. The scale factor is changed to an appropriate value in the buffer amplifier. An isolated self test coil is provided and will allow the gyro to be torqued with an external signal to simulate an actual rate input. A pulse train output is provided to allow confirmation of correct motor operation.

5.2.6.3 Acceleration Sensors

The acceleration sensors used are linear accelerometers of the force balance type and contain an internal control amplifier and feedback loop. As supplied, the output is a current source with a scale factor of 0.20 ma/g. Thus, a buffer amplifier is required and the voltage scale factor is determined by the feedback resistor used. The frequency response is extremely high, with the undamped natural frequency greater than 750 cps. This necessitates the use of low pass filters in the buffer amplifier. An isolated torquing coil is provided to allow an external input to simulate acceleration inputs. Frequency response to torquing inputs matches that for acceleration inputs. The accelerometer is supplied by ± 15 volts from the interface electronics power supplies.

TABLE XXXIX
ELECTRONIC SENSORS

ITEM NO.	VARIABLE	ITEM NO.	VARIABLE
1	Control wheel position, pilot	40	Spoiler #6 auxiliary actuator position
2	Control column position, pilot	41	Spoiler #9 auxiliary actuator position
3	Rudder pedal position	42	Spoiler #12 auxiliary actuator position
4	Rudder position	43	Rate of Pitch, BS566BWL179
5	Rudder auxiliary actuator position 1	44	Rate of Yaw, BS426BWL179
6	Rudder auxiliary actuator position 2	45	Rate of Yaw, BS695BWL238
7	Left elevator position	46	Rate of Roll, BS805BWL238
8	Right elevator position	47	Rate of Yaw, BS1028BSL238
9	Left elevator auxiliary act. position 1	48	Rate of Yaw, BS1377BWL 187.7
10	left elevator auxiliary act. position 2	49	Rate of Pitch, BS1377BWL 187.7
11	Right elevator auxiliary act. position 1	50	Rate of Roll, BS1655BWL205
12	Right elevator auxiliary act. position 2	51	Rate of Pitch RT, WS11BWL720
13	Horizontal stabilizer position	52	Rate of Pitch, LT, WS 11 BWL 720
14	Left aileron position	53	Spoiler #1 position
15	Right aileron position	54	Spoiler #2 position
16	Left aileron auxiliary actuator position	55	Spoiler #13 position
17	Right aileron auxiliary actuator position	56	Spoiler #14 position
18	Pitch parallel servo position		
19	Spoiler #3 position		
20	Spoiler #6 position		
21	Spoiler #9 position		
22	Spoiler #12 position		
23	Vertical acceleration, nose		
24	Normal acceleration, tail		
25	Lateral acceleration, tail		
26	Lateral acceleration fin elastic axis		
27	Vertical acceleration, L stab.		
28	Long acceleration, L wing		
29	Vert acceleration, L wing		
30	Normal acceleration, c.g.		
31	Roll acceleration at c.g.		
32	Pitch acceleration at c.g.		
33	Yaw rate, CG		
34	Pitch rate, CG		
35	Roll rate, CG		
36	Roll at CG		
37	Pitch at CG		
38	Yaw at CG		
39	Spoiler #3 auxiliary actuator position		



SENSOR LOCATIONS

FIGURE 66

5.2.7 Interface Electronics

Interface electronics system provides the nucleus of the electrical/electronics system installation. All control signals pass through some portion of this system. These include, for example, pilot's control inputs to the computer, computer output to the actuators, feedback sensors to the computers, and Flight Test data acquisition. In addition, safety monitor, inflight data monitoring, and system engagement control functions are included in the interface electronics.

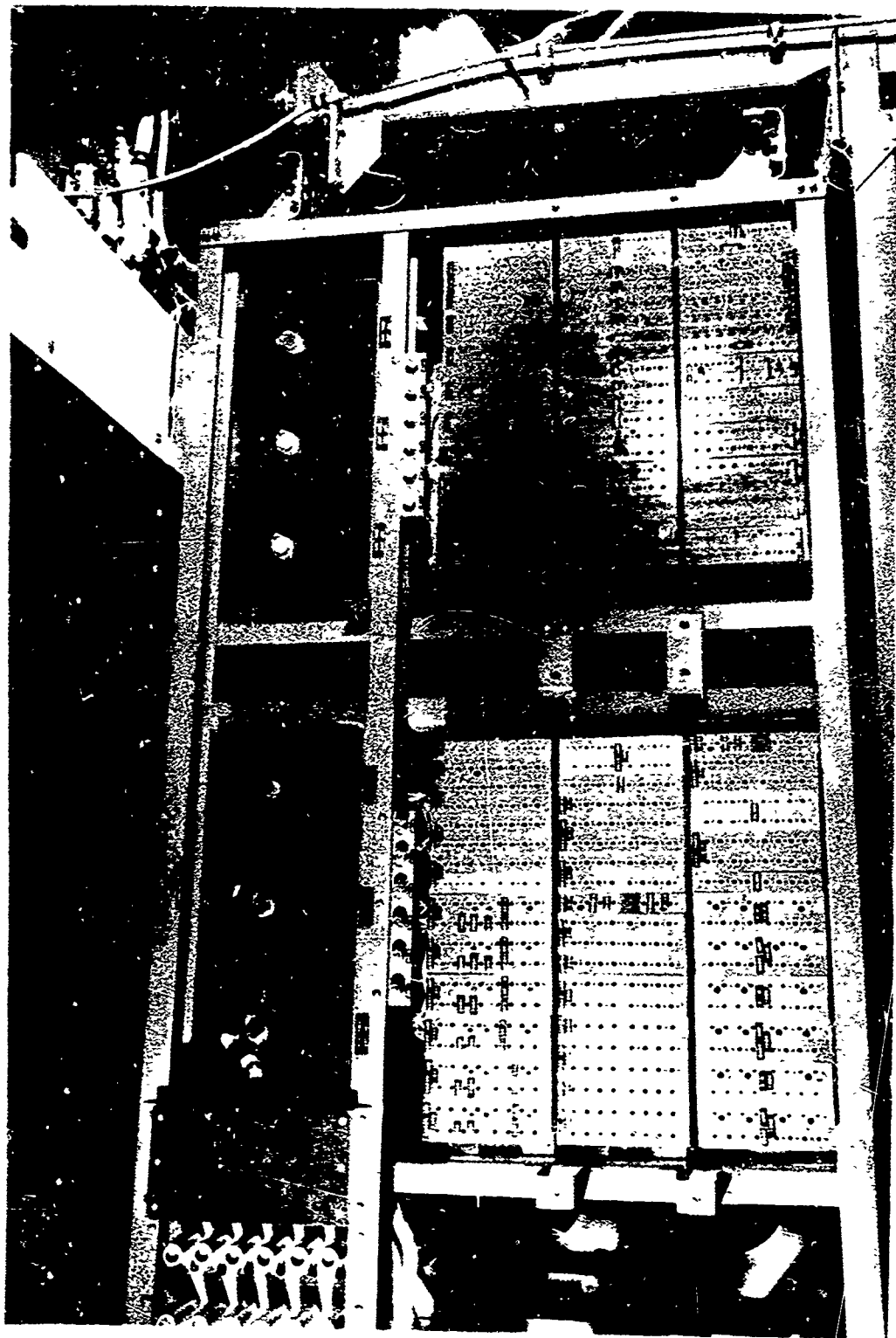
Interface amplifiers are used to isolate the sensor outputs from the computers. They are also used to isolate sensor and computer outputs from the read-out devices. This eliminates sensor loading effects and permits filtering or other necessary signal conditioning ahead of the input to the computer or read-out device. The interface amplifiers are solid state D.C. operational amplifiers with ± 10 volt output. These amplifiers are located on the lower flight deck and in the pressurized tail gunner's compartment. This choice of location allows short wire runs from sensors to the isolating amplifiers while still maintaining amplifiers in a desirable environment. Signal to noise ratio problems are also reduced by providing low impedance signal paths. The physical structure of the electronics installation are shown in Figures 67 and 68. An interpatch panel receives all flight control loop input and output signals. This panel consists of a removable patch board containing 408 jack connections and a mating base panel. Since all signals feed through the interpatch base panel into the removable board and back out the base panel, any desired routing of signals may be wired on the removable board. The removable patch board will normally be prewired on the ground prior to flight, but is accessible for qualified personnel to make inflight changes.

The system block diagram is presented in Figure 69.

5.2.7.1 Servo Actuator Electronic Equipment

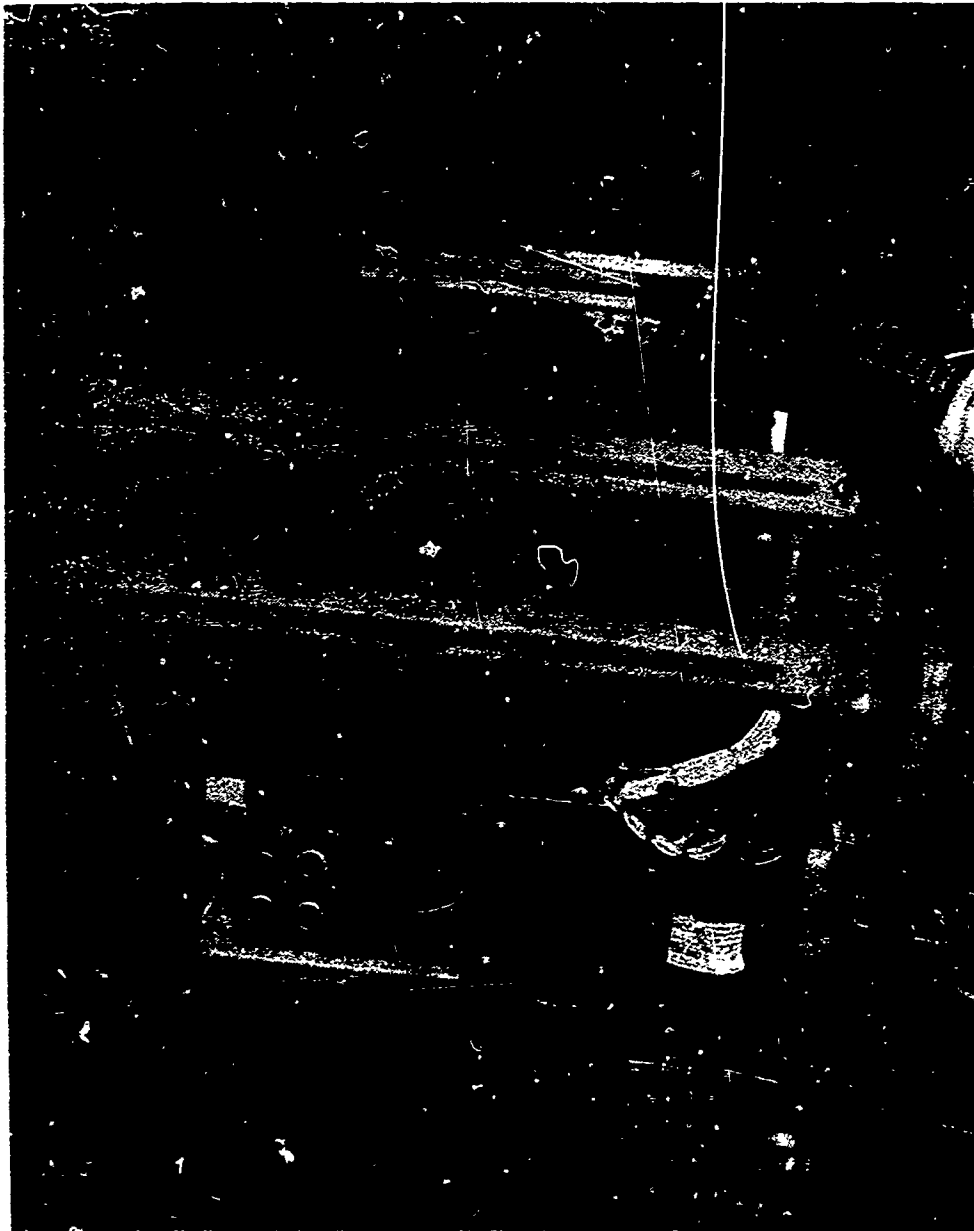
There are 16 series servo actuators and one parallel servo actuator in the flight control system. The parallel servo is a lower bandpass actuator consisting of an electric motor servo and drive amplifier. This servo is obtained from existing A/A42G-11 AFCS hardware and used to implement the pitch axis fly-by-wire commands from the evaluation pilot. The series servo actuators, located in the integrated hydraulic packages, employ D.C. electrohydraulic valve coils with a typical resistance of 1000 ohms per coil. Normally, two coils are used and the maximum required control input current is 8 ma. differential or 4 ma. per coil. This current is supplied by a solid state, ± 10 volts operational D.C. amplifier. Differences in the 16 series servo actuator electronics are discussed in the following paragraphs.

The rudder actuator has two independent electrical series servo actuators, each commanding up to 10 degrees of rudder travel and, operating together, commanding up to 20 degrees of travel. Each channel has a variable reluctance position transducer within the rudder actuator package to provide position feedback to the servo amplifier. The output of the transducer is a modulated 400 cps signal. This output signal is demodulated at the amplifier to provide a D.C. position signal. Each rudder series servo loop thus requires a servo amplifier, a demodulator, associated components and a power



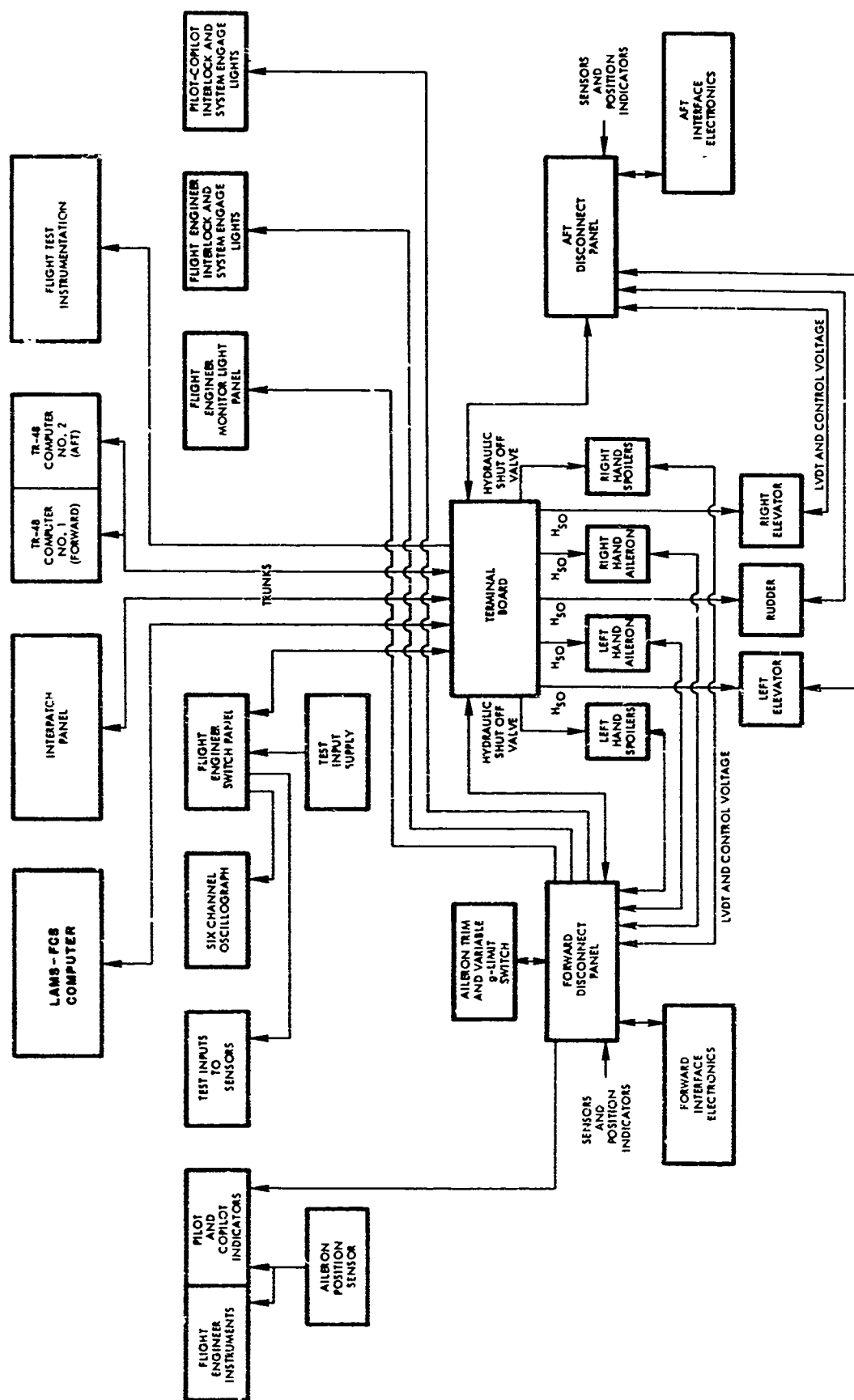
FORWARD INTERFACE ELECTRONICS RACK

FIGURE 67



AFT INTERFACE ELECTRONICS RACK

FIGURE 68



LAMS SYSTEM BLOCK DIAGRAM

FIGURE 69

source. The two channels of the rudder servo system operate from separate power supplies. The demodulators operate from 26V, 400 cps power supplied by a standard instrument transformer operating from a voltage regulating transformer.

The two aileron actuators and the four integrated spoiler valve actuation packages contain a single series servo actuator channel and similar servo electronic equipment is supplied for them.

The servo electronic equipment used for operation of the rudder, elevator, aileron actuators and the integrated spoiler actuation package is discussed below.

The servo amplifier is the output point of the electrical control system. It's function is to apply the control signals to the electro-hydraulic control valve and to close the loop around the auxiliary actuator so that auxiliary actuator position is an accurate and linear function of the electrical inputs. The valve coil is part of a flow control valve which, in turn, supplies flow to the piston of the auxiliary actuator, making the position of the auxiliary actuator a function of the integral of the current through the coil. The position of the auxiliary actuator is measured by a Linear Variable Differential Transformer (LVDT) whose output is a 400 cps signal with an amplitude proportion to the position. Thus the servo amplifier system must supply current to the valve coil and receive the demod output to close the loop.

In general, bandwidth of about a decade above the highest structural frequency is desired to sufficiently separate auxiliary actuator response from control system response. Considering the open loop characteristics of the servo amplifier/auxiliary actuator/LVDT/demod system to be essentially a pure integration (higher order effects ignored) leads to a unity gain crossover at 150 radians/sec.

As a result of testing various servo valves, the transfer function of the servo valve is taken to be

$$Q/I_o = \frac{K_{SV}}{\frac{s^2}{630^2} + \frac{2(.71s)}{630} + 1} \text{ in}^3/\text{sec/ma}$$

ignoring the coil. The coils taken in parallel are considered to be 500 ohms resistive in series with 3.5 henries inductance.

The auxiliary actuator is nearly a pure integrator and its transfer function is considered to be

$$\frac{A}{Q} = \frac{K_A}{S} \text{ in/in}^3/\text{sec}$$

The response of the LVDT is taken to be $\frac{V_{LVDT}}{A} = K \text{ VRMS/in}$

The demodulator is a full wave diode ring design and with the included filtering has a response of

$$\frac{V_{DEMOD}}{V_{LVDT}} = \frac{1}{\frac{s^2}{500^2} + \frac{2(.7)s}{500} + 1} \quad \text{VDC/VRMS}$$

There is a residual ripple of about 1 percent at 800 cps at the filter output.

Utilizing computer studies, it was determined that for a static loop gain of 1500 (implying an amplifier gain of 158 ma/volt) required a compensation function described by

$$\frac{\frac{s}{12.5} + 1}{(s+1) \left[\frac{s}{5000} + 1 \right]^2}$$

When the compensation described above is applied and the amplifier gain is 158 ma/volt, a considerable 800 cps ripple is found at the amplifier output. This could cause damage or eventual failure of the servo valve. A notch filter with the characteristic

$$\frac{\frac{s^2}{5000^2} + 1}{\frac{s}{5000} + 1}$$

was added to provide addition rejection of the 800 cps ripple.

Applying all the above factors and assuming that the servo amplifier is a perfect current source achieves an open loop transfer function of

$$G(s)H(s) = \frac{1500 \left[\frac{s}{12.5} + 1 \right] \left[\frac{s^2}{5000^2} + 1 \right]}{(s+1) \left[\frac{s}{5000} + 1 \right]^3 \left[\frac{s^2}{500^2} + \frac{2(.7)s}{500} + 1 \right] \left[\frac{s^2}{630^2} + \frac{2(.7)s}{630} + 1 \right]}$$

with the feedback being

$$H(s) = \frac{\frac{s^2}{5000^2} + 1}{\left[\frac{s^2}{500^2} + \frac{2(.7)s}{500} + 1 \right] \left[\frac{s}{5000} + 1 \right]^2}$$

Figure 70 shows this function plotted. The theoretical closed loop response is shown in Figure 71. The curves for most sluggish and most ringing response are based on parameter changes beyond those normally expected. Maximum theoretical peaking is about 1 db. The phase margin is 60 degrees, the gain margin is 9 db and the crossover frequency is 125 rad/sec.

Considering the direct coupled nature of the control system, SAS or FBW engagement could cause a considerable airframe transient or step input to the control surface. The effects of these inputs can be reduced by turning the gain of the servo amplifier from zero to the nominal value slowly after the solenoid valve has been turned on. One method of accomplishing this involves a light sensitive silicon resistor and a light source. It contains the resistor and the light source in a light tight housing. The resistance of the resistor is very high (megohms) in the dark and is reduced in proportion to the light flux falling on it.

By operating the lamp from an appropriate time varying voltage source, the servo amp gain can be varied linearly. The ramp is adjusted to vary the gain from 0 to 158 ma/volt in approximately 2 seconds. Two "Resistors" are connected in parallel on each servo amp to improve reliability.

5.2.7.2 Control and Monitor System

The control loop and monitor system located at the test engineer's station, Figure 72, includes controls for ground checkout, inflight checkout, safety monitor, safety interlock, servo engagement, and inflight data monitoring.

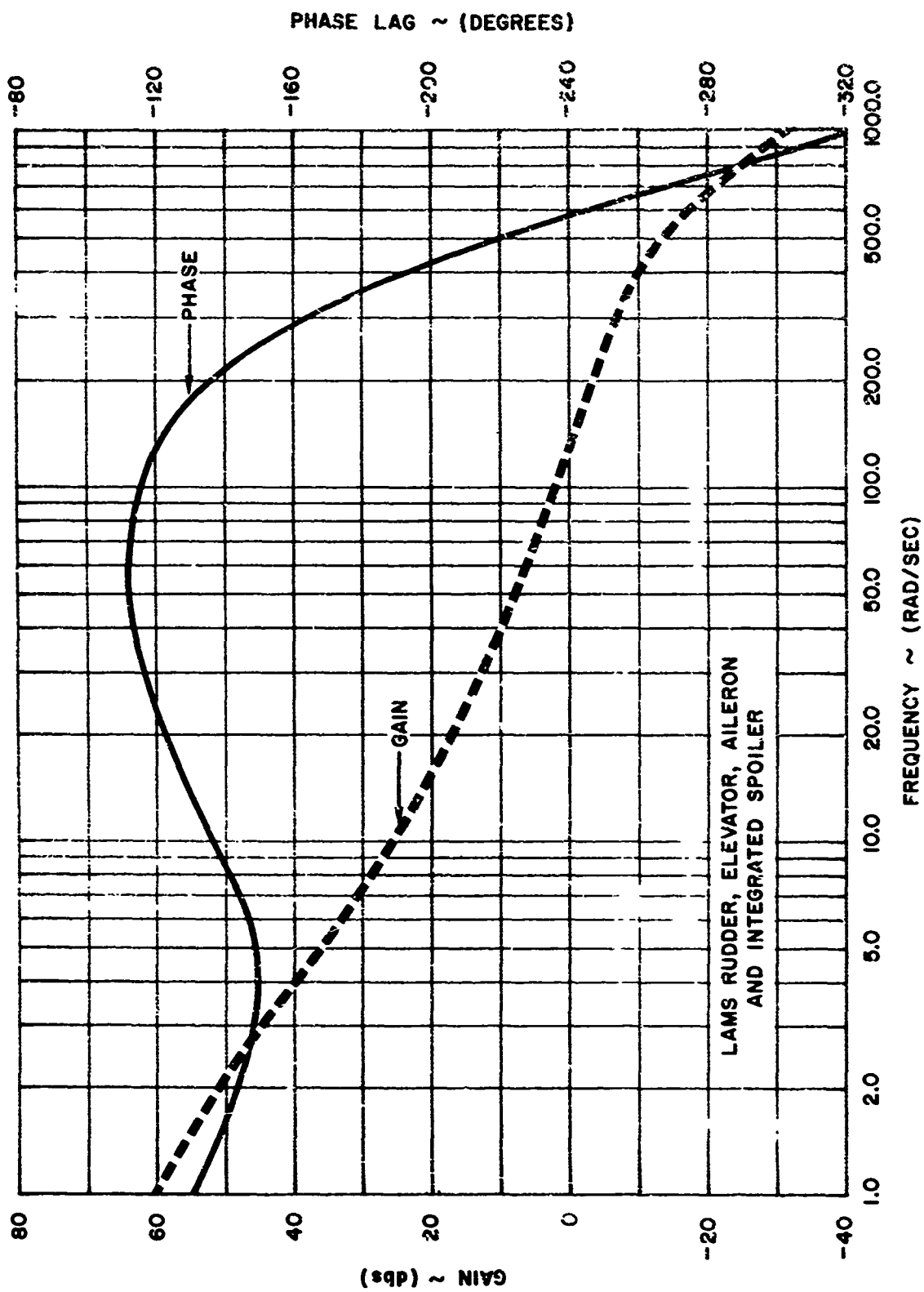
The safety monitor system provides visual indication of unsafe conditions before system engagement and/or control loop disengagement during operation if preset tolerances are exceeded. Items monitored include: power supply voltages, servo amplifier outputs, control surface positions, vertical acceleration and structural accelerations.

Power supply voltages are monitored for changes from their correct values. Deviation of ± 2 volts will disengage the control system and illuminate an indicator. Vertical and structural accelerations are monitored for deviations from preset limits. Excessive acceleration sensor signals cause disengagement of the control system and illuminate warning lamps. Acceleration sensor locations and acceleration limits now being used are listed in Table XL.

The pilot's aileron trim panel contains switching for selection of the vertical acceleration limits. The incremental g levels available are .5, .75, 1.0, and 1.25 for the pull up limits and .25, .5, and .75 for the push over limits. The aileron trim panel is shown in Figure 73.

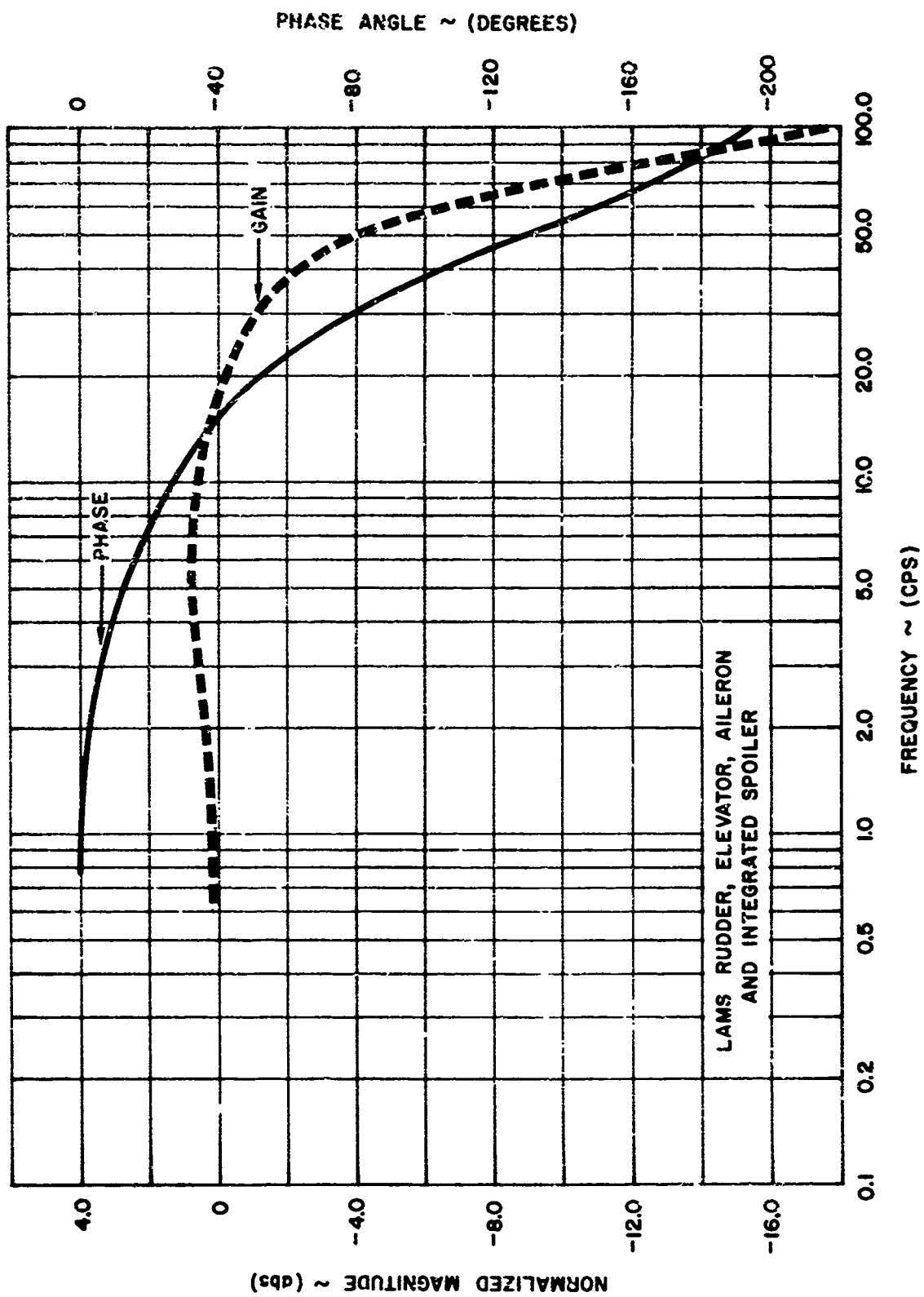
Servo amplifier output voltages are compared with preset values and cause control system disengagement and illumination of a warning light when the output signals exceed the preset values.

The aileron and spoiler control surface positions are presented on instruments in the test engineers station.



AUXILIARY ACTUATOR OPEN LOOP FREQUENCY RESPONSE

FIGURE 70



AUXILIARY ACTUATOR CLOSED LOOP FREQUENCY RESPONSE

FIGURE 71

Position sensors used for control surface position indication are rotary conductive plastic potentiometers attached to the control surface hinge point near the actuator hinge point. The aileron position indicators at the test engineer's station are a pair of vertical scale instruments calibrated ± 17 degrees. They receive their signal inputs from rotary potentiometers at the aileron hinge. Conditioning is provided in the interface electronics to allow adjustment of zero position, scale factor, and reduce noise inputs to the indicators. Spoiler position indication is provided by four vertical scale indicators. Calibration is 0 to 60 degrees. Signals are provided from potentiometers at the spoiler hinge points and the signal conditioning provided is identical to that for the aileron position indicators. The indicator lamps are connected in a latching circuit and permit manual testing and resetting of all indicator lamps by the test engineer. The system warning lamp panel and control surface instruments are shown in Figure 72.

Inflight data monitoring is accomplished by use of the direct writing oscillograph, the TR-48 analog computer digital voltmeter, a two channel oscilloscope, and indicators installed in the pilot's and test engineer's stations.

The oscillograph is a modified version of the standard laboratory instrument using paper that develops under ultraviolet light supplied by a xenon lamp. Six channels of the oscillograph are used and paper speeds of 0.25, 1, 4, 16, and 64 inches/second are available. The oscillograph is located below the forward computer.

The oscillograph switching panel is used in conjunction with the "quick look" oscillograph to provide the test engineer with the capability to monitor any set of data points in the system. Additional switching allows any of those data points to be connected to the forward computer digital voltmeter for critical level monitoring. The oscillograph switching panel is shown in Figure 72.

Items monitored include: power supplies, servo amplifier outputs, rate and acceleration sensor outputs, control surface positions, and auxiliary actuator positions, and various intermediate test points in the flight control system signal paths.

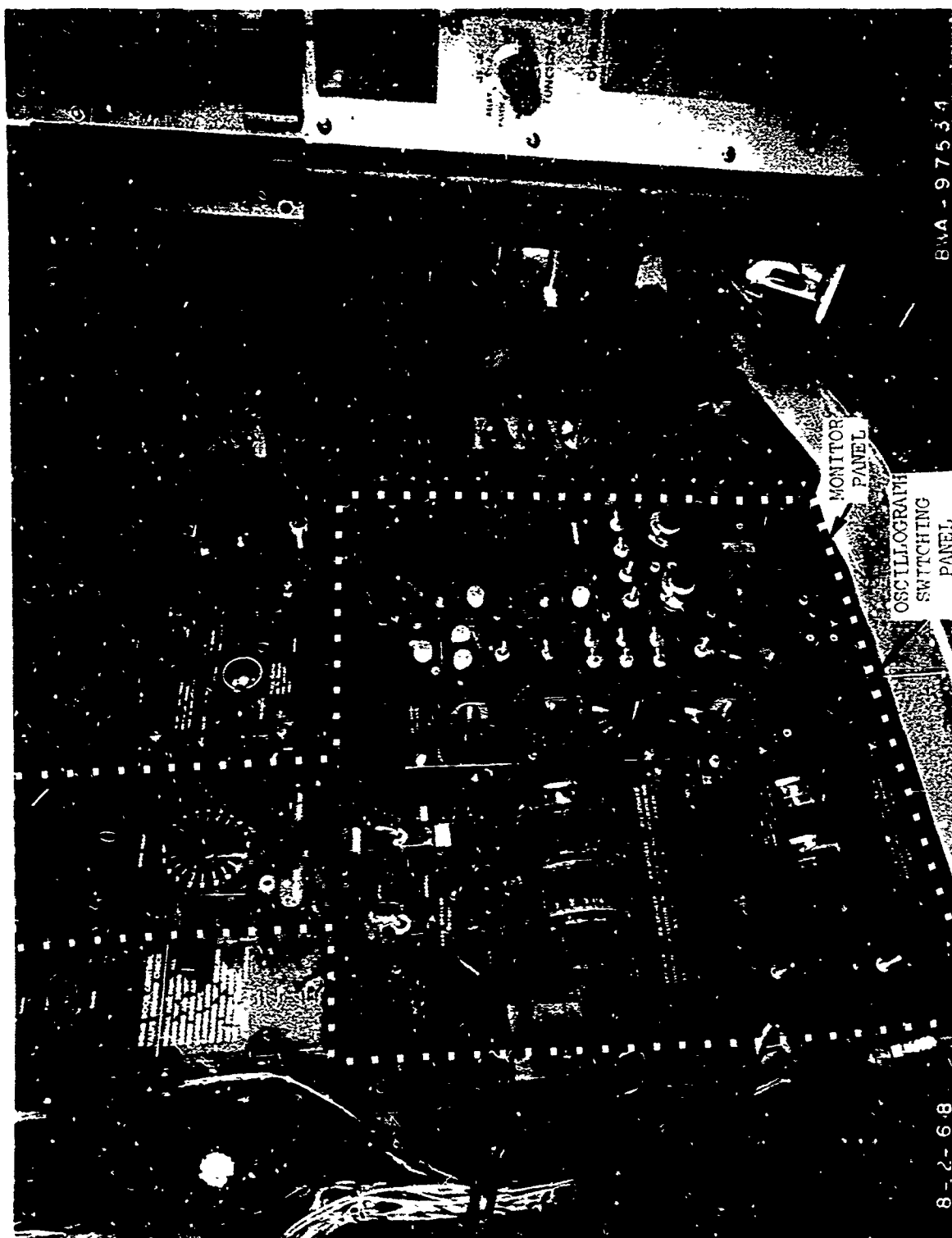
The test engineer has the capability to disable any oscillograph channel if recording of that channel is not desired or required.

Also included on the oscillograph switching panel are a master power switch, an engage inhibit switch, and lamps to indicate system status, i.e., ready, engaged, disengaged. The function of the master power switch is self-explanatory. The engage inhibit switch inhibits the operation of the pilot's engage switches at the discretion of the test engineer. It cannot, however, disengage the control system once it has been engaged.

The dual channel oscilloscope may be used for monitoring of any of the data points available on the oscillograph. In addition, it is used to check proper operation of the rate sensors motor speed. Selection of these signals is obtained from switches on the system warning lamp panel and the rate gyro motor test panel.

TABLE XL
MONITOR SYSTEM ACCELEROMETERS

DESCRIPTION	INCREMENTAL ACCELERATION LIMIT
Left Wing Station 1359, Rear Spar, Vertical	±3.0 g
Left Wing Station 1359, Chordwise	±1.2 g
Body Station 172, Vertical	±1.0 g
Body Station 1655, Vertical	±2.0 g
Body Station 1655, Lower Longeron, Lateral	±2.5 g
Fin Station 354, Auxiliary Spar Lateral	±3.0 g
Left Hand Stabilizer Station 425 Vertical	±3.0 g



TEST ENGINEER'S STATION

FIGURE 72

Seven special indicators are installed on the pilot's panel. These are rudder pedal force, rudder position, sideslip indication, normal acceleration, elevator position, column force, and aileron position. All indicators except the aileron position indicator are meter movements and are supplied signals from electrical instrumentation points. The aileron position indicator is a dual synchro unit having two scales, one for each aileron. Synchro transmitters at the aileron hinge points provide drive signals for the indicator.

The test engineer is provided instruments for monitoring aileron position, spoiler position, and 49 section interface electronics rack temperature.

In order to monitor environmental conditions surrounding the 49 section interface electronics rack, a thermistor and associated bridge circuitry has been installed in a 49 section module. A meter calibrated in degrees Fahrenheit and connected to the thermistor circuitry is installed at the test engineer's station to indicate the temperature at the thermistor location. In addition, two thermal switches are installed in the 49 section and when a preset temperature limit is exceeded indicators are illuminated in the test engineer's station.

5.2.7.3 Engage Control

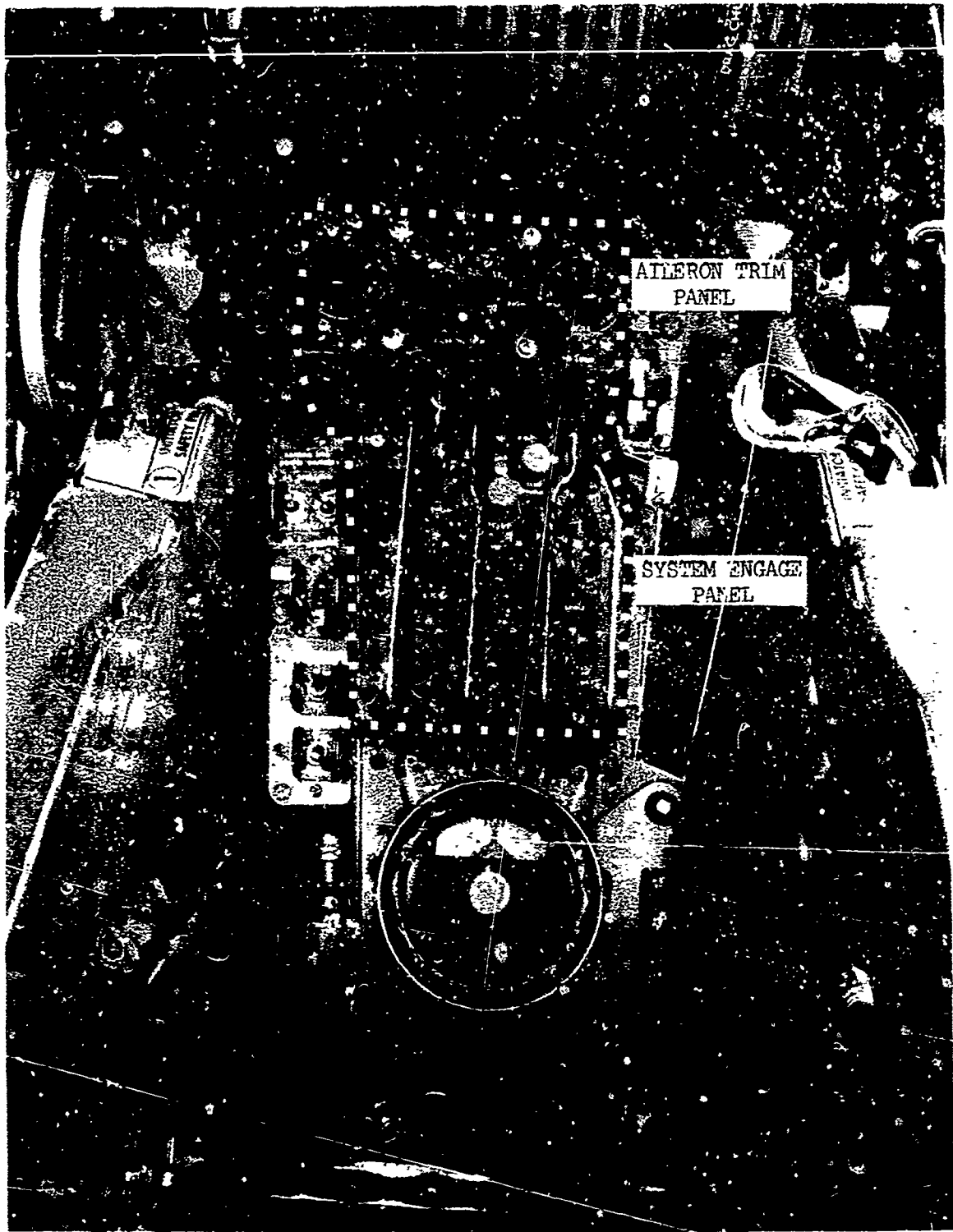
Engagement of the control loop modes to the actuator control valves is controlled by a switch panel located between the evaluation pilot and the monitor pilot on the aisle stand as shown in Figure 73.

The control modes provided are pitch FBW, pitch SAS, roll FBW, roll SAS, Yaw FBW, and Yaw SAS, may be selected independently of each other with the exception that roll FBW cannot be selected unless pitch FBW has already been selected. The engage switch is used to engage the control system after the appropriate modes have been selected.

In order to reduce the possibility of large engage transients, an interlock system inhibits the engagement of a new mode after the control system has been engaged. A test switch, located on a separate panel, allows the servo amplifiers to be turned on without turning on the actuator solenoids. This function can be used either for ground testing or for inflight testing.

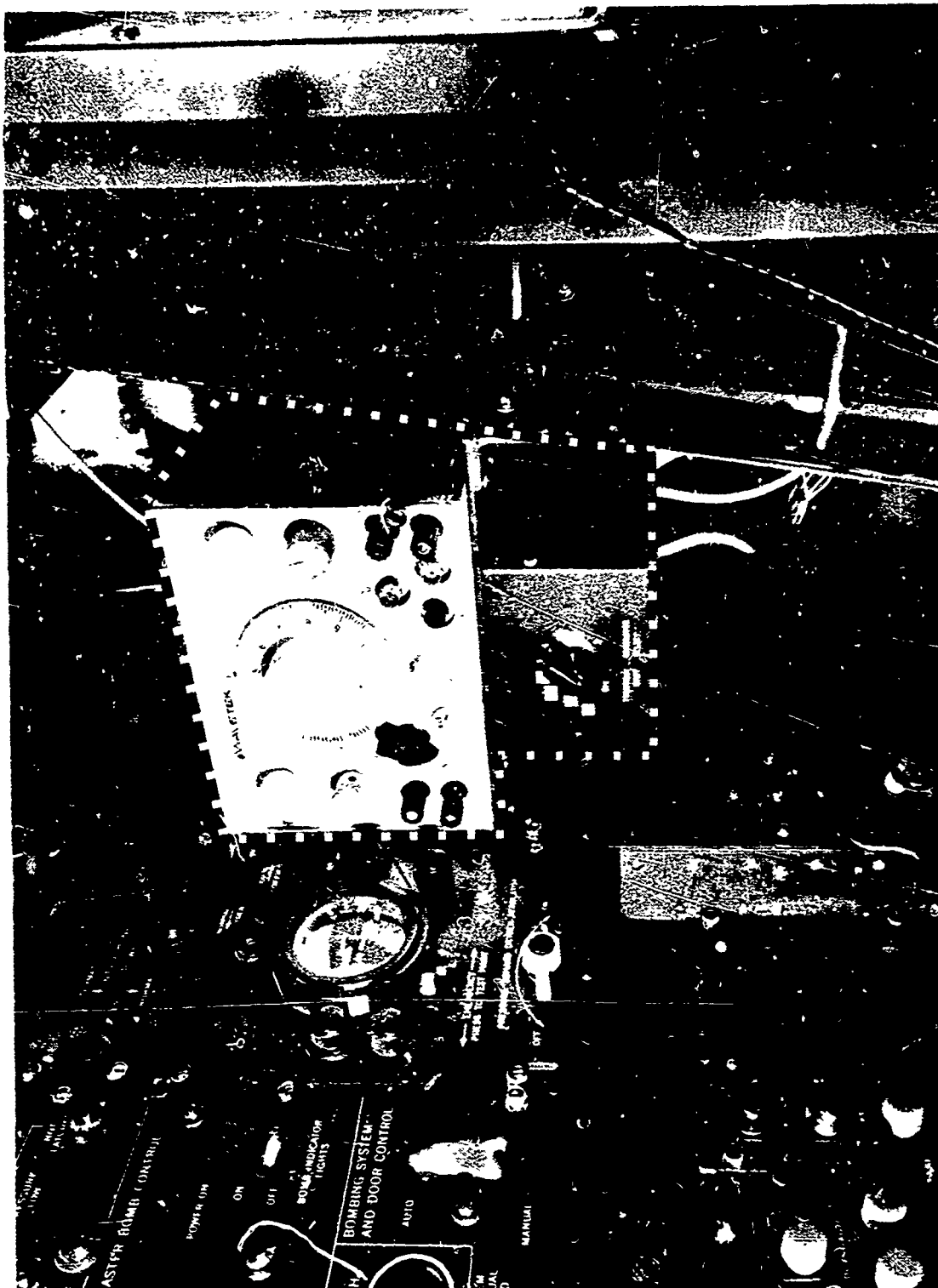
In order to provide the capability to preselect the modes which will be allowed during a particular flight condition, the ground end of each mode select switch is connected to the interpatch panel. A jumper from the appropriate point to ground must then be provided at the interpatch panel before the mode can be engaged. These modes will be determined before flight and jumpers installed accordingly. In the case of the pitch FBW mode, the solenoid is automatically connected to ground if the roll FBW solenoid has been grounded.

There are eleven 28 volt D.C. output lines from the engage control panel terminating on the interpatch panel. The 28 VDC level is present when the given mode switch is on and either the engage switch or the test switch is on. This output is used to enable the optical relays in the servo



COCKPIT AISLE STAND

FIGURE 73



TRANSIENT FUNCTION GENERATOR

FIGURE 74

amplifiers. Four more outputs provide 28 VDC at the interpatch panel a mode has been selected and when the engage switch is on. This voltage is not provided when the test switch is on. The engage switch cannot be turned on when the test switch is on. Likewise, the test switch cannot be turned on when the engage switch is on.

Before the control system can be engaged, several peripheral conditions must be met. The first of these is that 28 VDC and system ground must exist. If the failure monitor, the vertical acceleration monitor or the structural mode monitor is tripped, a portion of the 28 volt power is removed and the control system cannot be engaged or will be disengaged if the condition occurs after engagement but is interlocked such that it cannot cause system disengagement. The autopilot release switches in the control wheels and the force link switch on the monitor pilot's control column are connected to cause disengagement when they are operated. In addition to this the solenoid valves and the servo amplifiers will be shut off if the interpatch panel is removed.

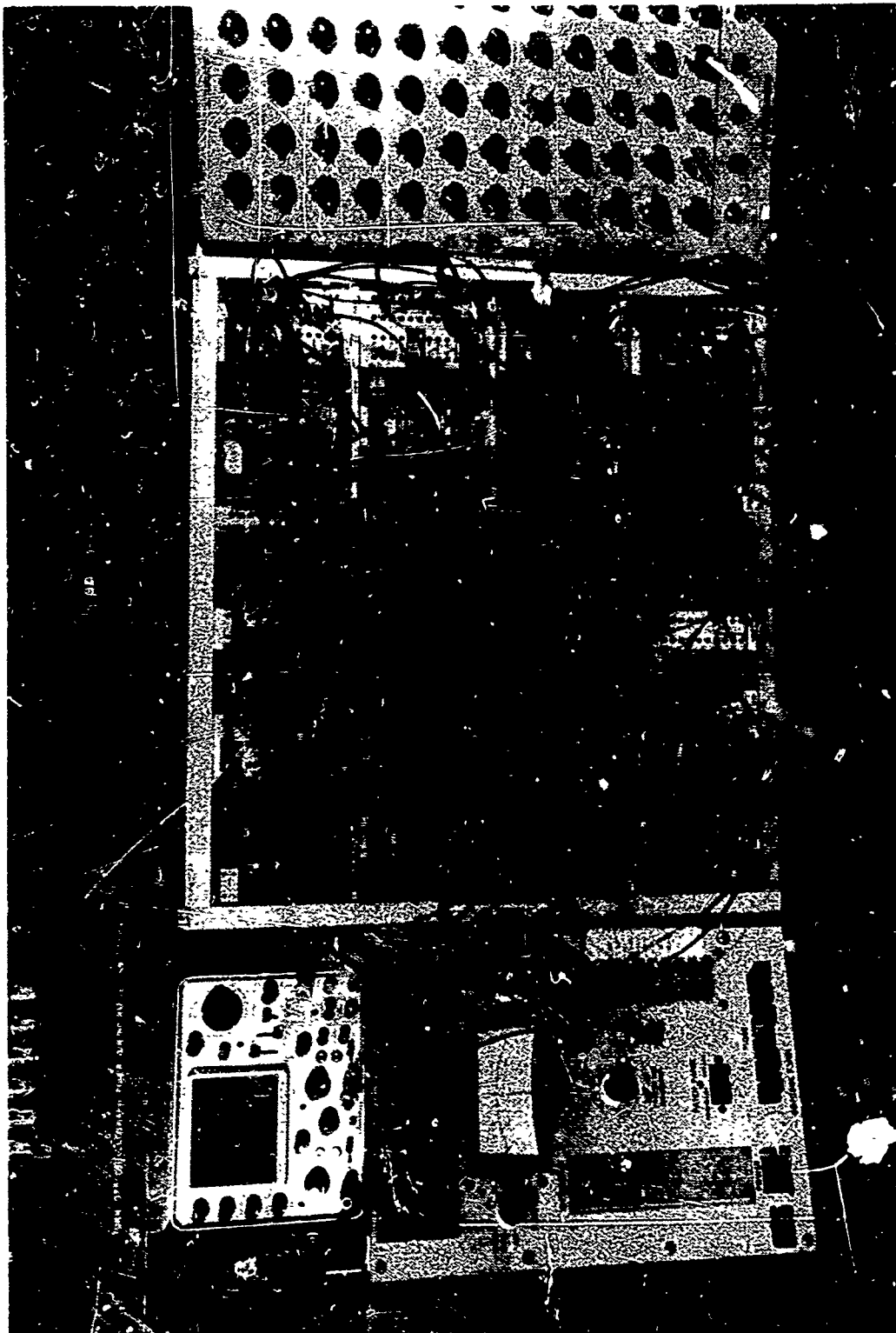
Lamps are located on the engage control panel to indicate that the system is engaged or ready to be engaged. The ready lamp functions when all of the failure monitor conditions have been satisfied and the inhibit, test, and engage switches are in the off position. Disengage lamps are located on the instrument panel in front of the evaluation pilot and the monitor pilot so that recognition that some failure has disengaged the control system will occur immediately. The three status indicator lamps are duplicated at the test engineer's station.

In addition to the engage and test panels, the aileron trim panel is located in the pilot's aisle stand. The aileron trim panel actually provides two functions: Control of aileron trim and control of vertical acceleration disconnect levels. Aileron trim is implemented in steps of 1, 2, and 3 degrees. A switch provides a 28 VDC signal to solenoid valves contained within the aileron actuators, which in turn provide the required trim.

A compact, transistorized function generator is installed in the test engineer's station for ground and inflight testing and is shown in Figure 74. The function generator is capable of providing sine, ramp, triangular, and square wave outputs over a range of 0.005 cps to one megacycle and is modified to allow selection of 1/2, 1, 2, 3, or 4 cycles of excitation or free run operation. The test engineer selects the required number of cycles of excitation to be applied to the control surface. The function generator output signals are conditioned by the analog computers and summed with control signals in the valve drive amplifiers.

5.2.8 Analog Computers

The analog computers in the electrical/electronics system are two model TR-48 general purpose units modified for the airborne environment and are presented in Figure 75. The computers are mounted in a space frame with high frequency vibration isolator supports and are equipped to provide the variable linear, nonlinear and time based functions as required. The computers condition the electrical signals from various feedback and control sensors and the fly-by-wire transducers to produce signals for actuation of the electrohydraulic servo control valves in the control surface actuators



TR-48 ANALOG COMPUTER FORWARD INSTALLATION

FIGURE 75

and also provide safety functions through signal monitoring and furnish limited inflight control system evaluation data.

The computer, as programmed, can be tested inflight prior to each control system engagement and computer patch panels may be changed to fulfill different flight control system requirements.

5.2.8.1 Computer Power Source

The analog computers, normally a laboratory instrument, operate on 60 cps AC power while the aircraft power is 400 cps. The cost and difficulty made modification of the computer for 400 cps power impractical. Therefore, a pair of frequency converters are installed to change the 115 volt, 400 cps power to 115 volt, 60 cps. The frequency converters also supply power to the "quick look" oscillograph. The converters are connected such that unit 2 operates the two computers while the unit 1 operates the oscillograph. In the event of failure of the unit 2, the computers are automatically switched to the unit 1 and the oscillograph is disconnected.

5.2.9 Fly-By-Wire

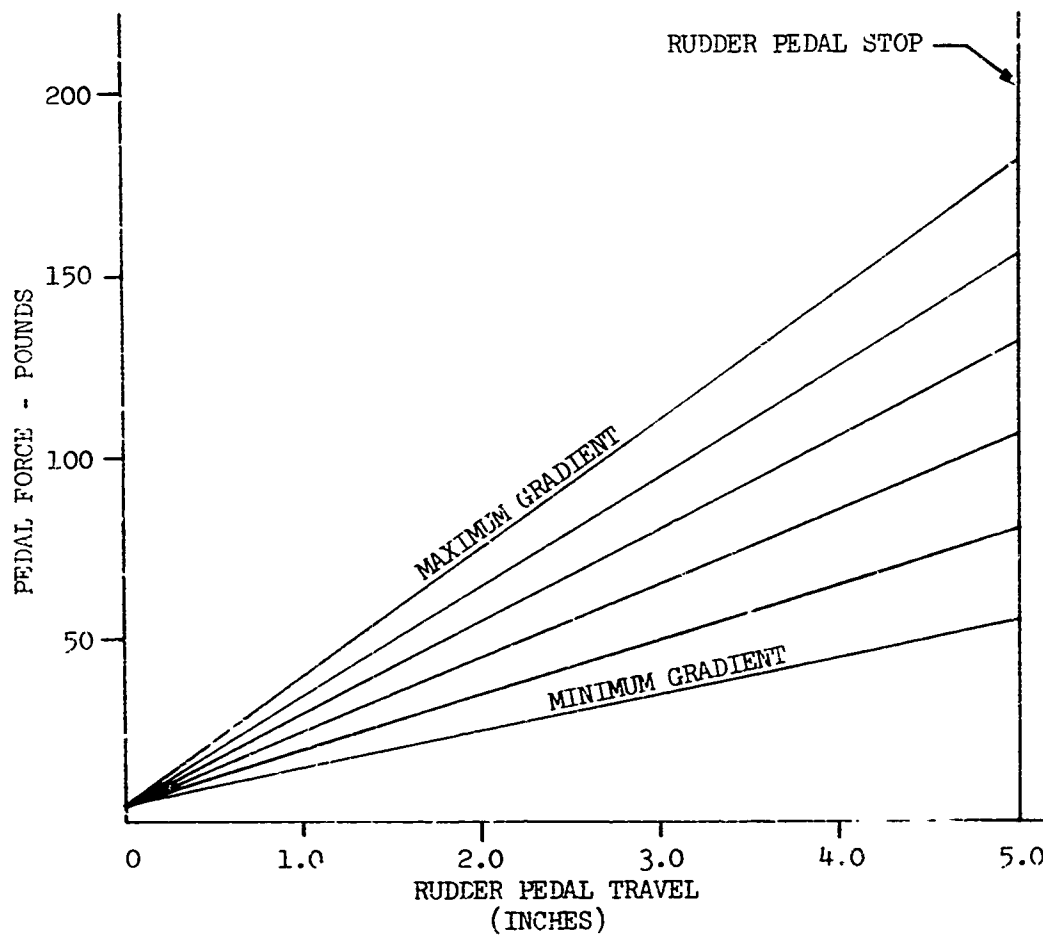
In the normal configuration of a B-52 E, flight controls are cable connected directly to tabs on the surfaces. With the installation of hydraulic actuator packages for surface control, new methods of providing the connection from the pilot to the control surface are feasible. In order to provide stability augmentation capability, provisions are made in the actuators for electrical control of surface position. As a bonus, these electrical input capabilities allow, with appropriate connections, pilot control of surface through electrical or "fly-by-wire" means.

For the LANS B-52 E test vehicle, the pilot's column, wheel, and rudder pedals are disconnected from the normal control cables and connected to springs for centering and force gradient control as presented in Figures 76 through 78. Position potentiometer indicate electrically the position of the controls. The pitch axis force feel system consists of a two-way spring cartridge and an eddy current damper. The spring cartridge, via spring selection, can provide three different force gradients. All gradients radiate from a five pound column breakout force to a full travel column force of 120 pounds (high gradient), 80 pound (intermediate gradient) or 45 pound (low gradient). The damper insures that the maximum column displacement rate is never greater than the maximum elevator servo rate (80 degrees/sec), reflected back to the column. The damper has an adjustment feature that insures its compatibility with whichever spring cartridge configuration is selected.

The yaw axis force feel system incorporates a set of leaf springs and multi-attach point actuation levers. This combination can produce six different force gradients and has the capability of providing a pedal breakout force anywhere between 5 to 25 pounds. Full travel pedal force can be obtained between the range of 55 pounds (low gradient plus five pound breakout) to 200 pounds (high gradient plus 25 pound breakout).

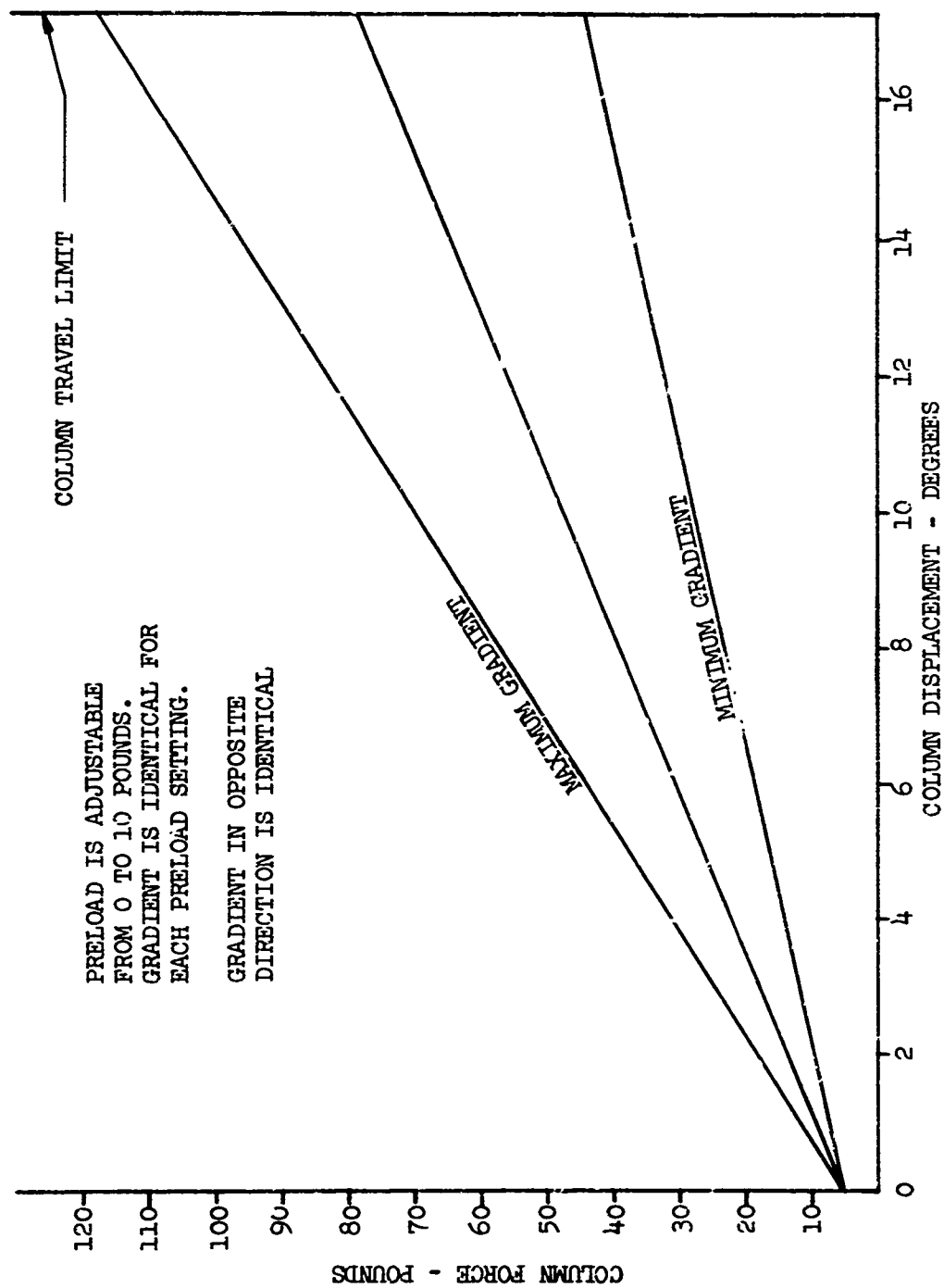
PRELOAD ADJUSTABLE FROM
0 TO 20 POUNDS. GRADIENTS
ARE IDENTICAL FOR ALL
PRELOAD ADJUSTMENTS

GRADIENT IN OPPOSITE
DIRECTION IS IDENTICAL



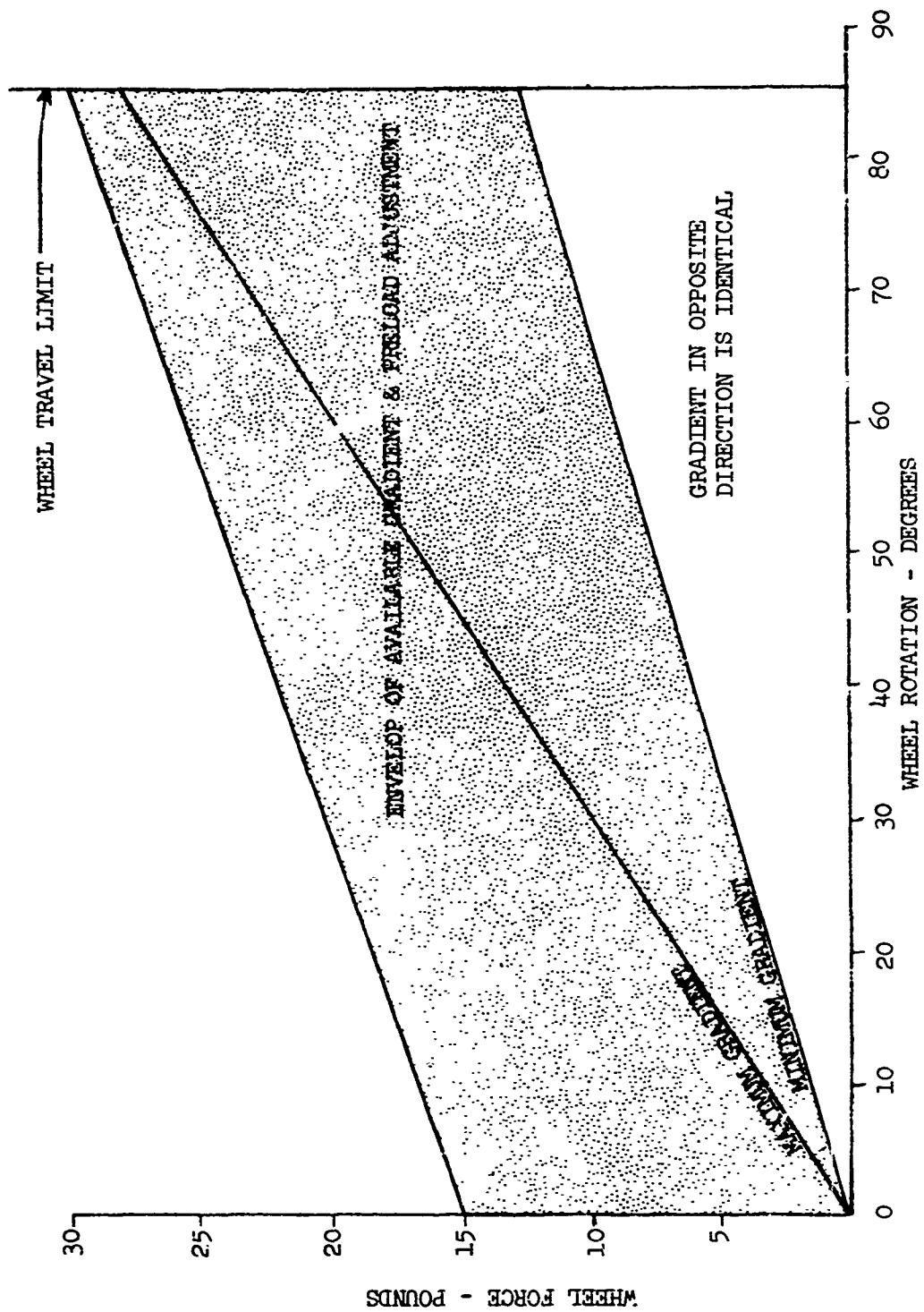
RUDDER PEDAL TRAVEL VS RUDDER PEDAL FORCE, EVALUATION PILOT

FIGURE 76



COLUMN FORCE VS COLUMN DISPLACEMENT, EVALUATION PILOT

FIGURE 77



WHEEL FORCE VS WHEEL ROTATION, EVALUATION PILOT

FIGURE 78

The roll axis force feel is provided by a torsion bar spring. Four different force gradients can be derived from this spring by selection of various anchor points. Wheel breakout forces anywhere between three and fifteen pounds can be obtained by adjustments at these anchor points. Full travel wheel forces can be adjusted between 3 and 30 pounds by selection of proper gradient and breakout force.

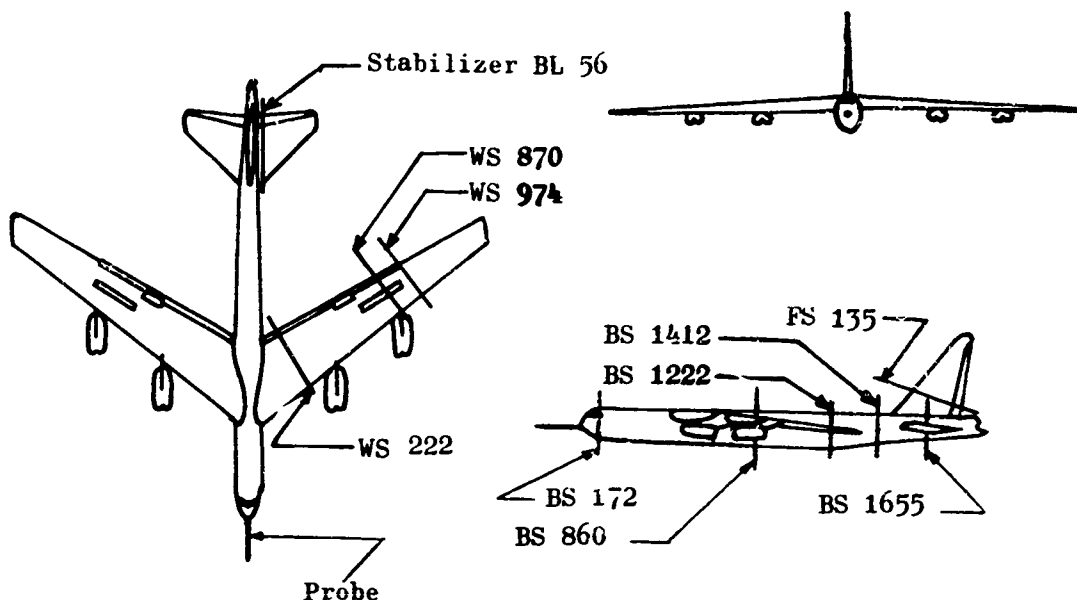
In its most simple form, fly-by-wire could be accomplished by direct connection from the control position potentiometers to the surface actuator electrical inputs. Through appropriate valve drive amplifiers. However, the normal path is through the analog computer where frequency shaping and/or gain scheduling can be applied to allow control design flexibility.

5.2.10 Load Instrumentation

The LAMS B-52 carried instrumentation to record structural responses and gust data continuously during flight through turbulence. Spectral analysis of the data provided a basis for comparison of the aircraft with No SAS, Baseline SAS, and LAMS Flight Control System. The signals from strain gages, accelerometers, potentiometers, the gust probe instrumentation and a clock were recordable by pilot command; all data reduction was done by ground equipment.

Recorded load instrumentation provided the following data and are shown in Figure 79.

- Gust components--longitudinal, lateral, and vertical velocities at the probe.
- Accelerations--vertical and lateral at Body Stations 172, 860, and 1655.
- Control surface positions--left and right aileron, left and right elevator, left and right outboard spoilers, rudder.
- Control surface actuator forces--left and right aileron, left and right elevator, rudder.
- Wing bending moments--vertical and chordwise moments at Wing Stations 222, 820, and 974, both left and right.
- Fuselage bending moments--vertical and side moments at Body Stations 1222 and 1412.
- Horizontal tail bending moments--vertical moments at Buttock Line 56, left and right.
- Vertical tail bending moment--side moment at Fin Station 135.



AIRCRAFT LOAD INSTRUMENTATION LOCATIONS

FIGURE 79

5.3 Honeywell Hardware Design

5.3.1 LAMS FCS Computer

The LAMS FCS computer is composed of two devices, the LAMS computer and the Flight Condition Gain Switch.

The LAMS computer as pictured in Figure 80, is housed in an aluminum frame structure with six external connectors; one providing input-output signal access, one for power input, one for interconnecting the computer and the Flight Condition Gain Switch, and three for supplying test points to be used in conjunction with the suitcase tester.

Input power required for operation of the LAMS computer is a single phase, 400 Hz, 115 VAC RMS signal capable of supplying 30 watts maximum. The LAMS computer can operate within specifications over a temperature range from 0 degrees F to 120 degrees F and can survive in a non-operating temperature range from -30 degrees F to 150 degrees F.

Within the LAMS computer are fourteen control signal gain adjust potentiometers and analog electronics mounted on ten plug-in printed circuit boards. The analog electronics are composed of solid state, integrated circuit operational amplifiers and associated circuitry which is used to provide analog blending (summation of signals in specific ratios), gain scheduling, and signal conditioning necessary for proper operation of the LAMS system.

Input signals to the LAMS computer are from two sources; the ten rate sensors and the FBW column, wheel and rudder pedal transducers. These signals are scaled in the interface electronics before being provided as input signals to the LAMS computer. Once the LAMS computer has completed blending, shaping and gain scheduling these input signals, the resulting output analog signals are used as command signals to the servo amplifiers which can drive rudder, elevator, symmetric spoiler and combinations of symmetric or antisymmetric aileron actuators.

The gain and phase from signal input to signal output are nominal ± 5.0 percent for D.C. gain, nominal ± 10 percent for A.C. gain, and nominal ± 7 degrees per phase.

The Flight Condition Gain Switch is a three-position, single-pole rotary switch which allows selection of three discrete sets of LAMS control system gains in the LAMS computer that correspond to three specific flight conditions.

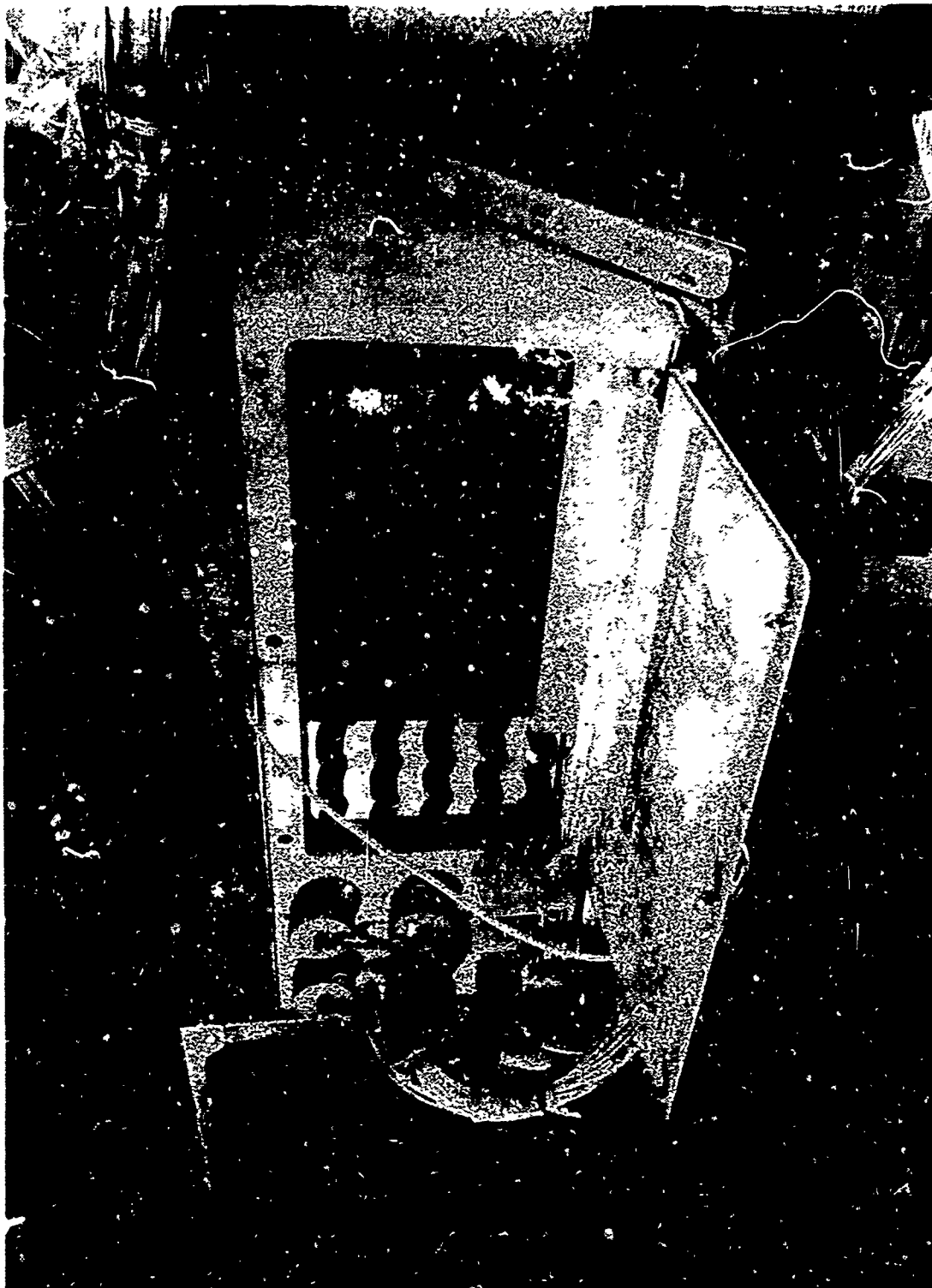
Nondestructive functional and environmental tests were performed on the LAMS computer space parts, and gain switch to assure flight worthiness of the equipment.

5.3.2 LAMS FCS Suitcase Tester

The LAMS suitcase tester presented in Figure 81, is a portable unit used to test the LAMS system in the laboratory or while installed in the aircraft. The tester is used to functional test the complete LAMS system or the individual printed circuit boards contained in the LAMS computer.

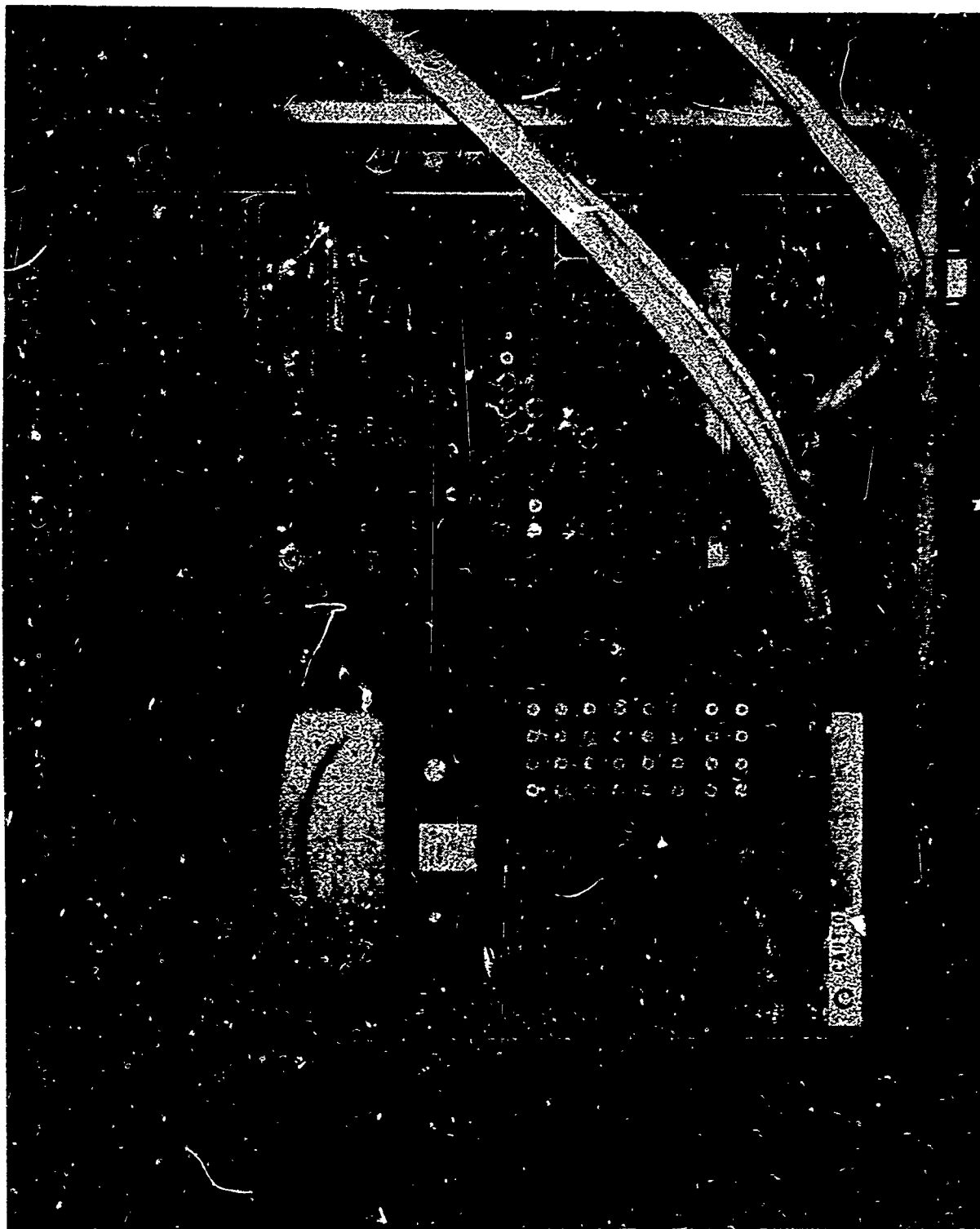
There are eight connectors on the front panel of the tester; six for interconnection with the LAMS computer, one for the printed circuit board module checkout, and one for providing 115 VAC 400 Hz single-phase power and chassis ground to the tester. Cable assemblies, associated with these connectors are provided with the tester.

A built in DC power supply and potentiometer allow test signals of 0 to ± 10 V DC to be applied to the LAMS computer or one of the printed circuit modules. The resulting output signals and intermediate points are made available at test jacks on the front panel of the tester and can be read out on a DC vacuum tube volt meter which is also mounted on the front panel. Shorting switches are used to bypass the hi-pass filters and wash-outs during D.C. gain checks.



LAMS-FCS COMPUTER

FIGURE 80



LAMS-FCS SUITCASE TESTER

FIGURE 81

6.0 CONCLUSIONS

The conclusions are presented in two parts. The first referring to the total LAMS program effort as documented in four volumes. The second part is concluding the study and design presented in the foregoing material.

6.1 Conclusions, LAMS Program

Contemporary analysis and synthesis techniques were successfully applied in the Loads Alleviation and Mode Stabilization (LAMS) program to a B-52 test vehicle. Using these techniques, an operable flight control system (FCS) was defined and produced in hardware. The LAMS FCS successfully controlled selected structural modes and alleviated gust loads due to turbulence in flight demonstration.

Similar techniques were applied to a low altitude and high speed flight condition for the C-5A airplane. Significant reductions in fatigue damage rates and fuselage accelerations were predicted by the analysis.

6.2 Conclusions, LAMS B-52 System Analysis, Synthesis, and Design

6.2.1 Criteria

The criteria established for flight controller definition provided adequate design and performance assessment and included elements common to analysis and flight demonstration.

6.2.2 Math Models

The math models used for structural load design proved adequate for design and synthesis of the gust alleviation and structural mode control system developed for the LAMS B-52, subject to the following conditions:

To assess the system stability a number of modes higher in frequency than those controlled were included in the model.

The most complete model available was required to determine stability and system performance. However, smaller models (using selected structural modes) for design investigation and system synthesis proved useful.

Separation of the models of the longitudinal axis from the lateral-directional axes provided adequate design data for the LAMS FCS.

6.2.3 Techniques

Adequate techniques including simulation, math modeling, synthesis methods, etc. were available to design the LAMS FCS.

Initial LAMS B-52 studies indicated that airframe responses resulting from gust alleviation control precluded design of a control system with load alleviation as its unique function.

A close working relationship and good communication between four major technologies; Aerodynamics, Structures, Controls, and Mechanisms, was essential to accomplish design of the LAMS system.

Several powerful analysis programs were helpful in LAMS; however, the experience and insight of the designers was the predominant factor in form and adequacy of the system synthesized.

6.2.4 Hardware

A B-52 test vehicle modification was designed and implemented on NB-52E; AF56-632. Subsequent control analysis indicated that the test vehicle would be an adequate test bed for demonstration of the LAMS FCS.

Present state-of-the-art in electronic hardware is adequate for implementation of LAMS type systems.

Adequate hydraulic actuation hardware was obtained for the LAMS test vehicle. Design difficulty was incurred in achieving the required dynamic response and as a result of high mechanical gain requirements.

6.2.5 Performance

The LAMS FCS, one of a family of controllers which could be defined, does meet the design and performance criteria established.

7.0

REFERENCES

1. Eggleston, John M. and Diederick, NACA Report 1321, 'Theoretical Calculation of the Power Spectra of the Rolling and Yawing Moments of a Wing in Random Turbulence,' 1957.
2. Boeing Document D3-6753, "Technical Development Program for a Flight Control System."
3. Skelton, G., "Wind Effects on Aerospace Vehicles," Honeywell Inc. Technical Document R-RD 6371, March 1965.
4. Skelton, G., et al., "Design of a Load Relief Control System," Honeywell Inc. Technical Document 2013-FR1.
5. Athons, M. and Levine, W.S., "On the Numerical Solution of the Matrix Riccati Differential Equation Using a Runge-Kutta Scheme," Report ESL-R-276, Massachusetts Institute of Technology, Project DSR 76105.

APPENDIX A - OPTIMAL CONTROL THEORY

The optimal control law derivation and structural performance measure derivation are presented in this appendix.

Quadratic theories, as applied in LAMS, solved the following problem: Let $r(t)$ be a vector of responses whose magnitudes are to be constrained; let Q be a symmetric, positive indefinite matrix; and let J^* be the scalar performance index

$$J^* = E\{r(t)' Q r(t)\} = \sum_{i,j} Q^{ij} E\{r^i(t) r^j(t)\}$$

where E is the expectation operator (over the sample space of disturbing inputs), the prime (') superscript indicates a vector transpose, and the i and j superscripts indicate vector and matrix components. The quadratic control problem is to find the linear feedback controller which minimizes J^* .

The goal of the LAMS B-52 study is to reduce fatigue damage rate and pilot acceleration through automatic control.

1. Analytical Measure of Ride Qualities and Structural Integrity

Two accepted analytical measures of the structural integrity of an airframe member--an estimate of the likelihood of exceeding its static ultimate strength and an estimate of its fatigue lifetime. Both assume that the inputs disturbing the vehicle are Gaussian and that the stress responses produced are linear functionals of those inputs.

The fatigue estimate is based on the Miner linear-cumulative-damage hypothesis (Reference 3). The expected lifetime, $E\{T_f\}$, of the member can be written analytically in the form

$$E\{T_f\} = \frac{1}{f(\sigma_s, \sigma_s^*)}$$

where σ_s , σ_s^* are standard deviations of stress and stress rate produced by gusts of one foot per second standard deviation (Reference 3). The term, f , is monotone increasing in σ_s , σ_s^* for reasonable standard deviations, but is a much stronger function of σ_s than σ_s^* ; i.e.,

$$\frac{\partial f}{\partial \sigma_s} \gg \frac{\partial f}{\partial \sigma_s^*}$$

Use of the fatigue estimate, $E\{T_f\}$, requires an assumption that no stresses larger than the static ultimate strength occur. To account for this possibility, it is assumed that disturbances of high intensity occur in random "bursts", so that the time before too large a stress occurs can be considered to be Poisson distributed; i.e.,

Prob (stress always less than the ultimate strength in an interval of T seconds)

$$= e^{-\lambda T}$$

where λ is the expected number of occasions of exceeding the ultimate strength in a one-second interval. The "burst" assumption is intuitively reasonable as the gust field consists of occasional turbulent patches in long stretches of non-turbulent air.

Using the Rice level-crossing formula (Reference 4), the expected number of seconds, $E\{T_e\}$, before too large a stress occurs is

$$E\{T_e\} = \frac{1}{\lambda}$$

where λ is a function of the RMS stress and stress rates, and

$$\lambda = \lambda(\sigma_s, \sigma_s^{\cdot})$$

As with the fatigue formula f , λ is monotone in σ_s , σ_s^{\cdot} for reasonable stresses, and is dominated by σ_s (Reference 3); i.e.,

$$\frac{\partial \lambda}{\partial \sigma_s} > > \frac{\partial \lambda}{\partial \sigma_s^{\cdot}}$$

A structural member can then fail either from fatigue or by experiencing too large a stress before its fatigue lifetime has run out. Assuming the event with the shorter expected time is the more likely, the obvious performance measure for a single structural member is the minimum of the pair

$$\text{MIN} [E\{T_f\}, E\{T_e\}]$$

or, what is the same, the maximum of the pair

$$\text{MAX} [f(\sigma_s, \sigma_s^{\cdot}), (\sigma_s, \sigma_s^{\cdot})]$$

This applies only to a single airframe member. Since the shortest expected lifetime over all members defines the vehicle lifetime, the structural integrity measure for the entire vehicle is

$$\text{MAX} \quad \left\{ \text{MAX} \left[f(\sigma_s, \sigma_s^*), \lambda(\sigma_s, \sigma_s^*) \right] \right\}$$

(all airframe members)

The goal of control then is to reduce this measure. This produces the formulation:

$$\text{MIN} \quad \left\{ \text{MAX} \left(\text{all airframe members} \right) \left(\text{MAX} \left[f(\sigma_s, \sigma_s^*), \lambda(\sigma_s, \sigma_s^*) \right] \right) \right\}$$

controller

Mean-square linear accelerations were used in the study as ride quality measures because, while they are not quite as meaningful as criteria which take human response to motion spectra into account, they are by far the most convenient criteria analytically. In the pitch and lateral axes this produced the ride quality measures

Pitch $E\{\ddot{z}_p^2\}$ = Mean-square vertical acceleration experienced by pilot

Lateral $E\{\ddot{y}_p^2\}$ = Mean-square lateral acceleration experienced by pilot

Handling quality criteria are usually expressed in terms of ideal stick responses, or equivalently, as ideal pole locations. A mathematical property of optimal controllers permitted ignoring handling qualities early in the design. The property is that the quadratic-optimum controller and a linear feedforward controller (from the disturbance input), and the feedback controller is independent of the statistics of the disturbing input. This independence, proved below, implied that one could first design a feedback controller for structural integrity and ride qualities in gusts, and later design an input filter (from stick commands) for good handling qualities. Handling qualities therefore were not considered in the optimization formulation.

The above mathematical property conforms both with control design practice and with textbook control theories. One normally designs the feedback loop first for bandwidth, smoothness of frequency response, pole locations, etc., and then adds input rates, lagged inputs, etc., to produce desired command-responses.

It remained to combine ride qualities and structural integrity measures in a single, overall performance measure. Again, there was no theory for doing this as the measures, one employing expected lifetimes and the other mean-square responses, are very different. Only one property of the combined measure could definitely be specified. Since $f(\sigma_s, \sigma_s^*)$, $\gamma(\sigma_s, \sigma_s^*)$, $E\{\ddot{z}_p^2\}$, and $E\{\ddot{y}_p^2\}$ are all monotone increasing in the response covariances, decreasing any response covariance while holding the

others constant will always improve performance. That is, let $r(t)$ be the vector of stresses, stress rates, and accelerations to be controlled, $r_i(t)$ to be one of the components of $r(t)$, and

$$J \left(E\{r_1(t)^2\}, E\{r_2(t)^2\}, \dots E\{r_n(t)^2\} \right)$$

be the combined index. Then J must have the property

$$\frac{\partial J}{\partial E\{r_i(t)^2\}} > 0 \text{ for all } i.$$

2. Derivation of Performance Measure

Since the relationship between the fatigue estimate and the RMS stress and stress rates is complex, it is not desirable to use fatigue damage as a performance measure. Consequently an equivalent performance measure is needed.

Let r_i be the i th controlled response of a finite-order linear system; let $J \left(E\{r_1^2\}, \dots E\{r_n^2\} \right)$ be any function of mean-square responses satisfying

$$\frac{\partial J}{\partial E\{r_i^2\}} > 0 \text{ for } i = 1, \dots, n.$$

Then, if there exists a linear controller minimizing J , that controller minimizes as well the quadratic J^* defined by

$$J^* = \sum_{i=1}^n Q_i E\{r_i^2\}$$

where Q_i are the partial derivatives

$$Q_i = \frac{\partial J}{\partial E\{r_i^2\}}$$

evaluated with the $E\{r_i^2\}$ produced by the controller minimizing J (Reference 4).

This states that if a performance index is monotone increasing in the response variances in the neighborhood of the optimum, then the controller minimizing the index minimizes the quadratic J^* as well. The combined structural integrity-ride qualities criterion possesses this property.

In addition, the only responses which should be included in J^* are those appearing in J , namely stresses, stress rates \dot{y}_p , and \ddot{y}_p . Flexure mode amplitudes, mode rates, etc., should not be included. Choosing the quadratic weights would be answered by the last equation above if the combined performance measure J were specified. Since no basis for constructing a meaningful combined measure J was available, it was necessary to attack the choice of weights iteratively. The following procedure was used:

- a. Estimate quadratic weights. Then compute the quadratic optimum controller, the response variances produced by the controller, and the functions $f(\sigma_s, \dot{\sigma}_s)$, $\gamma(\sigma_s, \dot{\sigma}_s)$, $E\{\ddot{z}_p^2\}$, and $E\{\ddot{y}_p^2\}$ produced by those variances.
- b. If either of the mean-square accelerations is too large (to satisfy intuitive notions of what they should be), increase the weight, Q_1 , on that acceleration and repeat step 1.
- c. Calculate the partial derivatives $\frac{\partial f}{\partial \sigma_s}$, $\frac{\partial f}{\partial \dot{\sigma}_s}$, $\frac{\partial \lambda}{\partial \sigma_s}$, and $\frac{\partial \lambda}{\partial \dot{\sigma}_s}$. Increase the weights, Q_1 , on those stress and stress rate responses with the largest partial derivatives, and repeat step 1.
- d. Terminate this process when a controller is produced that acceptably improves structural integrity and ride qualities.

The quadratic weights chosen to start the iteration were the reciprocals of the mean-square responses of the uncontrolled airplane:

$$Q_1 = \frac{1}{E\{r_1(t)^2\}}$$

This proved to be an excellent choice.

3. Derivation of Optimal Control Law

The controller minimizing the quadratic cost function J^* can be found by a conventional Lagrange multiplier manipulation, as follows.

- a. Formulation - Let $x_1(t)$ be the state vector of the vehicle, $u(t)$ be the vector of inputs to the elevator, rudder, and other actuators, $v(t)$ be the vector of gust inputs, and $r(t)$ be the vector of responses whose magnitudes are to be constrained. The vehicle perturbation equations can then be written in the vector differential equation form

$$\dot{x}_1(t) = F_{11} x_1(t) + F_{12} v(t) + G_{11} u(t)$$

$$r(t) = H_1 x_1(t) + H_2 v(t) + D u(t)$$

Let gust vector, $v(t)$, be generated by a finite-order linear filter driven by white noise, $\eta(t)$. Let $x_2(t)$ be the state vector for this filter, so that

$$\dot{x}_2(t) = F_{22} x_2(t) + G_{12} \eta(t)$$

$$v(t) = H_3 x_2(t)$$

where

$$E\{\eta(t) \eta(\tau)'\} = N \delta(t-\tau)$$

where $\delta(t)$ is the Dirac delta function and the prime (') superscript indicates a vector or matrix transpose.

Define the combined state vector

$$x(t) = \begin{bmatrix} x_1(t) \\ x_2(t) \end{bmatrix}$$

satisfying

$$\dot{x}(t) = Fx(t) + G_1 u(t) + G_2 \eta(t)$$

$$r(t) = Bx(t) + Du(t)$$

where

$$F = \begin{bmatrix} F_{11} & F_{12} & H_3 \\ 0 & & F_{22} \end{bmatrix}$$

$$G_1 = \begin{bmatrix} G_{11} \\ 0 \end{bmatrix}$$

$$G_2 = \begin{bmatrix} 0 \\ G_{12} \end{bmatrix}$$

$$H = \begin{bmatrix} H_1 & H_2 \end{bmatrix}$$

The simplest (and best performing) controller for a linear system is a linear combination of states:

$$u(t) = K x(t)$$

Assuming this form, the control problem is to find the gains, K , which minimize

$$J^* = E\{r(t)' Q(t) r(t)\}$$

where Q is the diagonal matrix

$$Q = \begin{bmatrix} Q_1 & & 0 \\ & \ddots & \\ 0 & & Q_n \end{bmatrix}$$

- b. Covariance Equations - It is convenient to recast the above problem in terms of covariance equations. Defining these, let X and R denote the state and response covariance matrices

$$X(t) = E\{x(t) x(t)'\}$$

$$R(t) = E\{r(t) r(t)'\}$$

The term, $E\{r_1(t)^2\}$, then the i^{th} diagonal term in $R(t)$.

With the above controller,

$$\dot{x}(t) = (F + G_1 K) x(t) + G_2 \eta(t)$$

$$r(t) = (H + DK) x(t)$$

so that

$$\begin{aligned} R(t) &= E \{ r(t) r(t)' \} \\ &= (H + DK) E \{ x(t) x(t)' \} (H + DK)' \\ &= (H + DK) X(t) (H + DK)' \end{aligned}$$

Solving for $X(t)$, the solution for $x(t)$ is

$$x(t) = e^{(F + G_1 K)t} x(0) + \int_0^t e^{(F + G_1 K)(t-\tau)} G_2 \eta(\tau) d\tau$$

Then,

$$\begin{aligned} x(t) x(t)' &= e^{(F+G_1 K)t} x(0) x(0)' e^{(F+G_1 K)'} t \\ &\quad + e^{(F+G_1 K)t} x(0) \int_0^t \left[e^{(F+G_1 K)(t-\tau)} G_2 \eta(\tau) \right]' d\tau \\ &\quad + \int_0^t e^{[F+G_1 K](t-\tau)} G_2 \eta(\tau) d\tau x(0)' e^{(F+G_1 K)t'} \\ &\quad + \int_0^t \int_0^t \left[e^{(F+G_1 K)(t-\tau)} G_2 \eta(\tau) \eta(y)' G_2' \right. \\ &\quad \left. e^{(F+G_1 K)(t-y)'} \right] d\tau dy \end{aligned}$$

and

$$E\{x(t) x(t)'\} = X(t)$$

$$\begin{aligned} &= e^{(F+G_1 K)t} X(0) e^{(F+G_1 K)'t} \\ &+ e^{(F+G_1 K)t} \int_0^t E\{x(0)\eta(\tau)'\} G_2 e^{(F+G_1 K)(t-\tau)'} d\tau \\ &+ \int_0^t e^{(F+G_1 K)(t-\tau)} G_2 E\{\eta(\tau)x(0)'\} d\tau e^{(F+G_1 K)(t-\tau)'} \\ &+ \int_0^t \int_0^t e^{(F+G_1 K)(t-\tau)} G_2 E\{\eta(\tau)\eta(y)'\} G_2' e^{(F+G_1 K)(t-y)'} d\tau dy \end{aligned}$$

with η white noise,

$$E\{x(0)\eta(\tau)'\} = 0 \text{ for } \tau \geq 0$$

and

$$E\{\eta(\tau)\eta(y)'\} = N\delta(\tau-y)$$

so that

$$\begin{aligned} X(t) &= e^{(F+G_1 K)t} X(0) e^{(F+G_1 K)'t} \\ &+ \int_0^t \int_0^t e^{(F+G_1 K)(t-\tau)} G_2 N\delta(\tau-y) G_2' e^{(F+G_1 K)(t-y)'} d\tau dy \\ &= e^{(F+G_1 K)t} \left[X_0 + \int_0^t e^{-(F+G_1 K)\tau} G_2 N G_2' e^{-(F+G_1 K)\tau'} d\tau \right] e^{(F+G_1 K)t} \end{aligned}$$

Differentiating with respect to t , $X(t)$ satisfies the covariance differential equation

$$\dot{X}(t) = (F+G_1 K)X(t) + X(t)(F+G_1 K)' + G_2 N G_2'$$

In the stationary case, $X(t)$ and $R(t)$ are constants, so

$$\dot{X}(t) = X$$

$$\dot{X} = 0 = (F+G_1 K) X + X (F+G_1 K)' + G_2 N G_2'$$

$$R(H+DK) X (H+DK)'$$

The trace, TR , of a square matrix is defined as the sum of its diagonal components:

$$TR[W] = \sum_i w^{ii}$$

The trace operator has the permutation property

$$TR [ABC] = TR [CAB] = TR [BCA]$$

The J^* term can be written

$$\begin{aligned} J^* &= \sum_i Q_i E \{r_i(t)\}^2 \\ &= E \{r(t)' Q(t) r(t)\} \\ &= \sum_{i,j} Q_{ij} E \{r_j(t) r_i(t)\} \\ &= TR[QR] \\ &= TR[Q(H+DK) X(H+DK)'] \\ &= TR[(H+DK)' Q(H+DK)X] \end{aligned}$$

The control problem, then, is to find the gains, K , which minimize

$$J^* = TR[Q(H+DK)X(H+DK)']$$

subject to the constraint equation

$$\dot{X} = 0 = (F+G_1 K)X + X(F+G_1 K)' + G_2 N G_2'$$

- c. Lagrange Multipliers = The most convenient way to handle the X constraint equation is through the use of Lagrange multipliers. Let S be a matrix of such multipliers, one for each term in \dot{X} . With

$$\sum_{i,j} S^{ij} \dot{X}^{ij} = \text{TR}[\dot{SX}]$$

one can then regard K , X , S as independent variables and minimize the sum

$$J^* = \text{TR}[(H+DK)'Q(H+DK)X] + \text{TR}\left[\left[(F+G_1K)X+X(F+G_1K)+G_2N G_2'\right]\right]$$

The J^* term is then minimized at the values of K , X , S where

$$\frac{\partial J^*}{\partial S} = 0 = (F+G_1K)X+X(F+G_1K)+G_2N G_2'$$

$$\frac{\partial J^*}{\partial X} = 0 = (F+G_1K)'S+S(F+G_1K)+(H+DK)'Q(H+DK)$$

$$\frac{\partial J^*}{\partial K} = 0 = 2D'Q(H+DK)X+2G_1'SX$$

Solving the last equation for K produces

$$K = -(D'QD)^{-1}(D'QH+G_1'S)$$

These three algebraic equations must then be solved for K , X , S .

- d. Properties of the Optimal Solution - It is noted that the gains, K , and Lagrange multipliers, S , are the solutions of

$$K = -(D'QD)^{-1}(D'QH+G_1'S)$$

$$0 = (F+G_1K)'S+S(F+G_1K)+(H+DK)'Q(H+DK)$$

so that the gains and Lagrange multipliers are independent of the state covariance, X , of the noise input, N , and of the noise input matrix, G_2 . Substituting the last equation into J^* produces

$$\begin{aligned} J^* &= \text{TR}[SG_2N G_2'] \\ &= \text{TR}[G_2SG_2'N] \end{aligned}$$

so that the terms of G_2SG_2' are the partial derivatives of the performance index, J^* , with respect to the noise covariance, N .

Further, breaking K and S into components of dimension x_1 and x_2 (the dimensions of the vehicle state and wind-filter state respectively),

$$K = \begin{bmatrix} K_1 & K_2 \end{bmatrix},$$

$$S = \begin{bmatrix} S_{11} & S_{12} \\ S_{21} & S_{22} \end{bmatrix}$$

There results

$$K_1 = - (D'QD)^{-1}(D'QH_1 + G_{11}'S_{11})$$

$$K_2 = - (D'QD)^{-1}(D'QH_2 + G_{11}'S_{12})$$

and

$$0 = (F_{11} + G_{11}K_1)'S_{11} + S_{11}(F_{11} + G_{11}K_1) + (H_1 + DK_1)'Q(H_1 + DK_1)$$

$$0 = F_{22}'S_{22} + S_{22}F_{22} + (H_2 + DK_2)'Q(H_2 + DK_2)$$

$$0 = (F_{11} + G_{11}K_1)'S_{12} + S_{11}(F_{12}H_3 + G_{11}K_2) + S_{12}F_{22} + (H_1 + DK_1)'Q(H_2 + DK_2)$$

where the F , G , H definitions originally specified for vehicle and wind filter have been used. Examination of these equations reveals that feedback gains (K_1 , from the vehicle states) are independent of F_{12} , H_3 , F_{22} , so that they are completely independent of the wind filters. That is, they are completely independent of all characteristics of the disturbance inputs, and will be the same no matter what the inputs are. The feedforward gains (K_2 , from the wind-filter states) are, however, dependent both on the form of wind filter and the vehicle dynamics (they are still independent of the amplitude of the winds, determined by N).

This result will hold if pilot inputs are added to the above problem. Therefore, one can, in general, ignore the disturbance inputs in constructing feedback controller, K_1 , and afterwards account for these inputs by properly choosing feedforward gains, K_2 . This justified not including handling qualities in the optimization, as stick commands are mathematically equivalent to disturbing inputs.

e. Digital Solutions - It remains to solve the two equations

$$K = -(D'QD)^{-1}(D'QH+G_1'S)$$

$$0 = (F+G_1K)'X+S(F+G_1K)+(H+DK)'Q(H+DK)$$

for K, and to find X and R, given K, from

$$0 = (F+G_1K)X+X(F+G_1K)'+G_2'NG_2'$$

$$R = (H+DK)X(H+DK)'$$

Three different computer programs were written to solve these equations. The first two solved the differential equation

$$\dot{S}(t) = F+G_1K(t)'S(t)+S(t)(F+G_1K(t)) + [H+DK(t)]'Q H+DK(t)$$

$$K(t) = (D'QD)^{-1}[D'QH+G_1'S(t)]$$

until they converged, and then solved

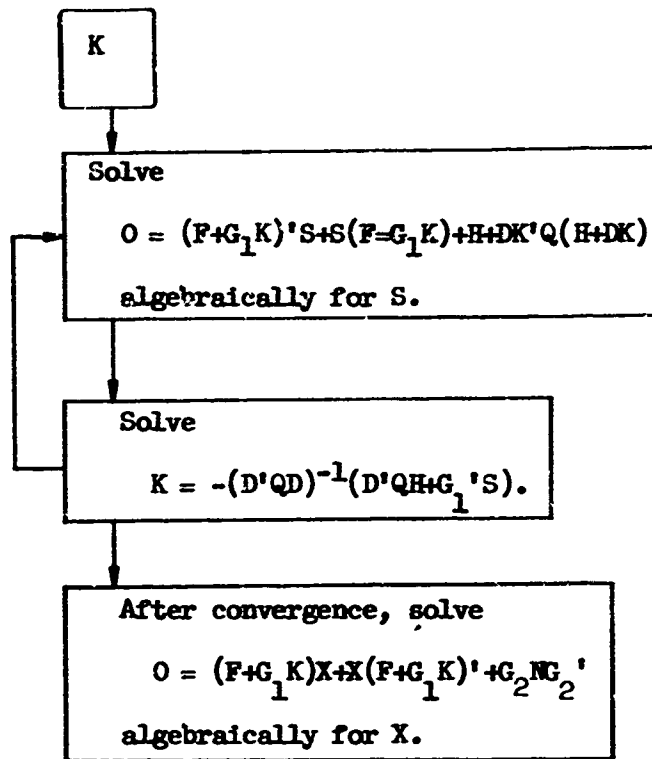
$$\dot{X}(t) = (F+G_1K)X(t)+X(t)(F+G_1K)+G_2'NG_2'$$

until it converged, using the converged gains, K. The first program solved a discrete time (sampled data) version of the above equations obtained by reformulating the above problem in terms of difference equations. It was a relatively slow program, but it was exact (within roundoff errors) and well suited for debugging errors in modeling (in F, G₁, H, D). The solution time is approximately proportional to the cube of the dimension of x.

The second program directly solved the above differential equations with a Runge-Kutta extrapolation routine (Reference 5). It is almost exactly three times faster than the first program, but the extrapolations are inexact and diverge if too large an extrapolation interval is chosen.

The third program solved the algebraic equations by successive substitution. The procedure is:

Choose a value for



If a good first selection of K is made, this routine converges very rapidly. It is memory-limited, however, and a 32,000-bit machine cannot handle much above a tenth-order system. The convergence time is approximately proportional to the sixth power of the system order, so this program is useful only for low-order systems. Also, this routine requires determinant evaluations, and it is thus quite sensitive to roundoff errors.

Almost all IAMS calculations were done with the first program above. It was an expansion of a program written for an earlier study; it was the first program written of the three; and its authors were sure it was completely debugged.

4. Optimal Control Law

Table XLIV presents the flight condition 1 optimal control law defined from optimal control theory. The RMS stresses, stress rates, and pilot station accelerations for the defined optimal controller are given in Table XLV.

Numerous simplifications of the initial optimal control laws resulted in the IAMS Longitudinal FCS described in Section 3.6.1. As the control laws were modified, the predicted structural performance was also altered, see Section 4.4.

TABLE XLI
OPTIMAL CONTROL LAW FOR FLIGHT CONDITION 1 LONGITUDINAL AXIS

State Variables	Control Gains		
	u_e	u_a	u_{δ_s}
p_1	-71.89	1810.0	-101.0
p_2	225.5	1257.0	-126.0
p_3	8.386	55.57	-2.098
α_g	-87.75	184.0	6.652
δ_e	74.65	123.6	-3.931
δ_a	-0.3976	3.117	-0.2881
δ_{sp}	5.663	-14.74	-4.557
u_{δ_e}	-171.3	-27.06	1.530
u_{δ_a}	7.514	-83.50	4.316
α	27.76	1230.0	-63.58
x_α	-41.09	1720.0	-91.68
y_α	-64.97	1508.0	-91.88
$\dot{\theta}$	-18.54	56.63	-0.4068
x_θ	-25.77	29.70	-0.3526
y_θ	-4.122	35.02	-1.549
ψ_1	-6.496	34.62	-4.043
\dot{q}_1	-2.481	5.420	-0.8133
x_{q_1}	-1.172	-13.01	-0.6726
y_{q_1}	-0.6505	3.652	-0.2619
q_2	-16.57	598.1	-37.90
\dot{q}_2	4.277	13.84	-2.552

TABLE XLI
(Continued)

OPTIMAL CONTROL LAW FOR FLIGHT CONDITION 1 LONGITUDINAL AXIS

State Variables	Control Gains		
	u_e	u_a	u_{δ_e}
\dot{x}_{q_2}	5.448	-164.2	7.516
y_{q_2}	1.405	-11.62	0.8063
q_6	-182.7	1603.0	-88.02
\dot{q}_6	14.40	20.31	-3.477
x_{q_6}	16.72	23.69	-2.056
y_{c_6}	-0.3529	5.323	-0.3626

TABLE XLII

OPTIMAL CONTROLLER PERFORMANCE LONGITUDINAL AXIS

Aircraft Station	Flight Condition I	
	Free Aircraft	Controlled Aircraft
RMS stress		
WS 516	229.4	65.91
WS 899	137.4	53.11
BS 805	121.4	94.8
BS 1028	105.1	66.56
SBL 32	150.2	322.2
FS 135	-----	-----
RMS stress rate		
WS 516	1110.0	516.0
WS 899	706.0	406.0
BS 805	524.0	560.0
BS 1028	476.0	1085.0
SBL 32	1029.0	1930.0
FS 135	-----	-----
Pilot's Acceleration	0.0129 g	0.0053 g

APPENDIX B = STABILITY DATA

The predicted stability data for IAMS flight conditions 2 and 3 are presented in this appendix. Bode plots show gain and phase for the entire system frequency spectrum and tables indicate minimum gain or phase margins at discrete frequencies.

TABLE XLIII
LONGITUDINAL AXIS - ELEVATOR LOOP MARGINS
FLIGHT CONDITION 2

CRITICAL FREQUENCY (RAD/SEC)	GAIN MARGIN AT NOMINAL PHASE (DB)	PHASE MARGIN AT NOMINAL GAIN (DEG)	GAIN MARGIN AT WORST PHASE (DB)
2.3		90	
6.6			6.9
11.5			15.5
14.7			17.3
19.1			18.7
19.3	19.0		
19.9	23.6		
21.2	17.4		
21.4			17.2
37.8			28.3
43.3			27.6
60.8			22.3
84.8			21.7
112.2			28.2
113.8	29.0		

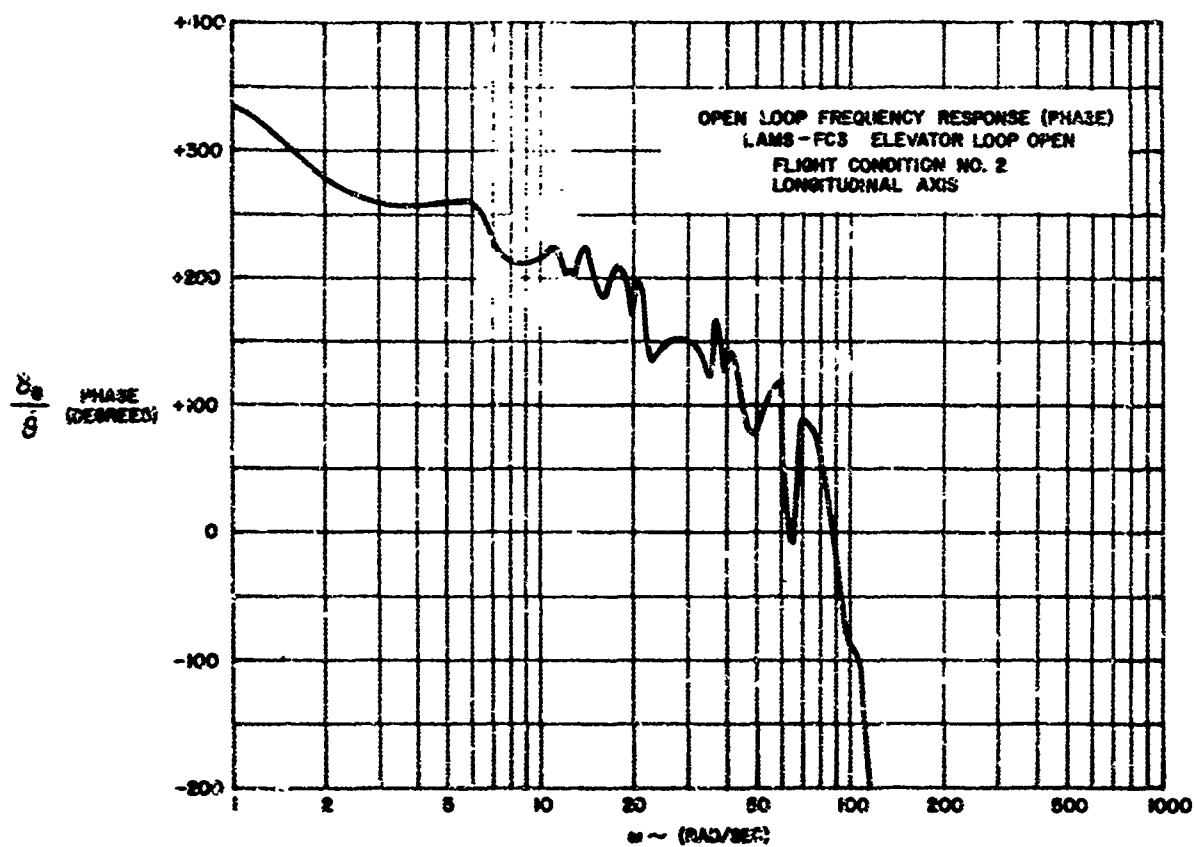
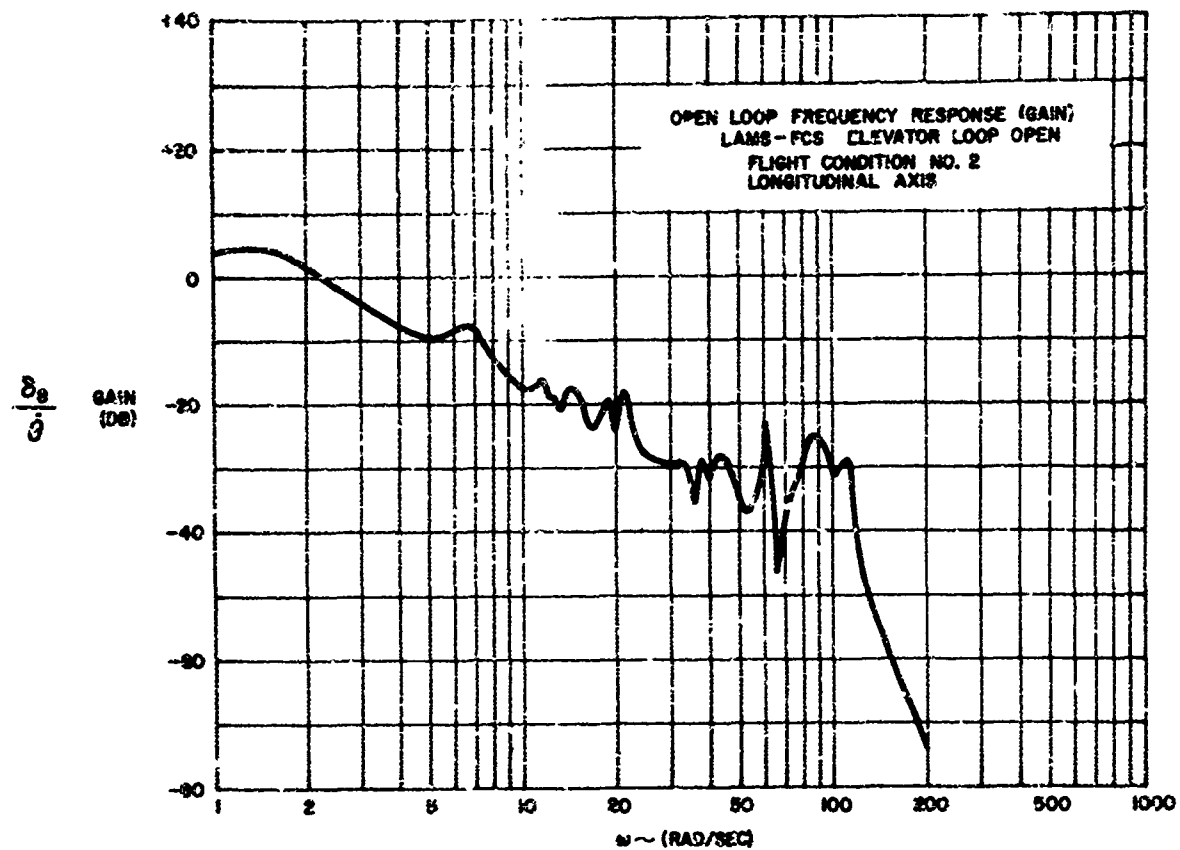


FIGURE 82

TABLE XLIV
LONGITUDINAL AXIS - AILERON LOOP MARGINS
FLIGHT CONDITION 2

CRITICAL FREQUENCY (RAD/SEC)	GAIN MARGIN AT NOMINAL PHASE (DB)	PHASE MARGIN* AT NOMINAL GAIN (DEG)	GAIN MARGIN AT WORST PHASE (DB)
11.6			17.0
14.5			7.3
18.5			10.0
21.1			10.9
21.8	12.8		
32.0			38.1
36.2			28.6
40.3			21.3
59.8			6.7
63.6	12.8		
86.8			17.7
122.3			52.5

* System is Gain Stabilized

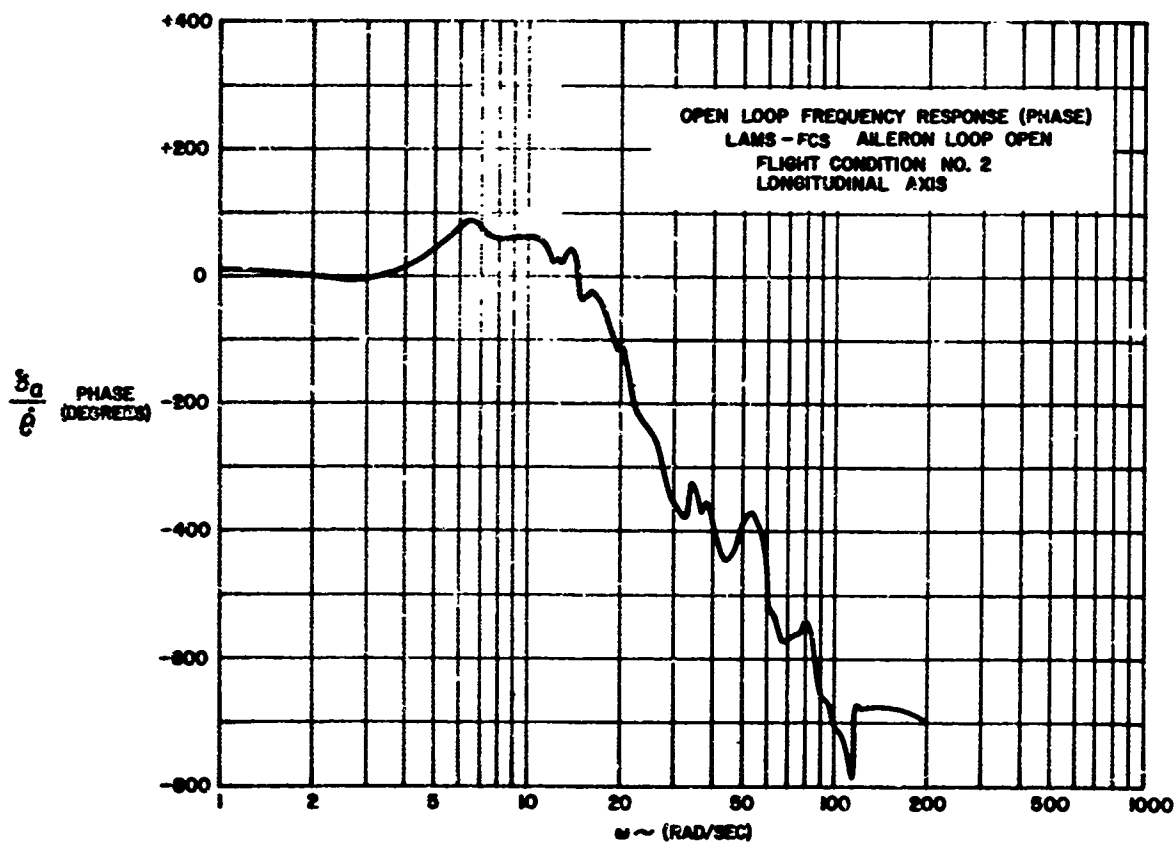
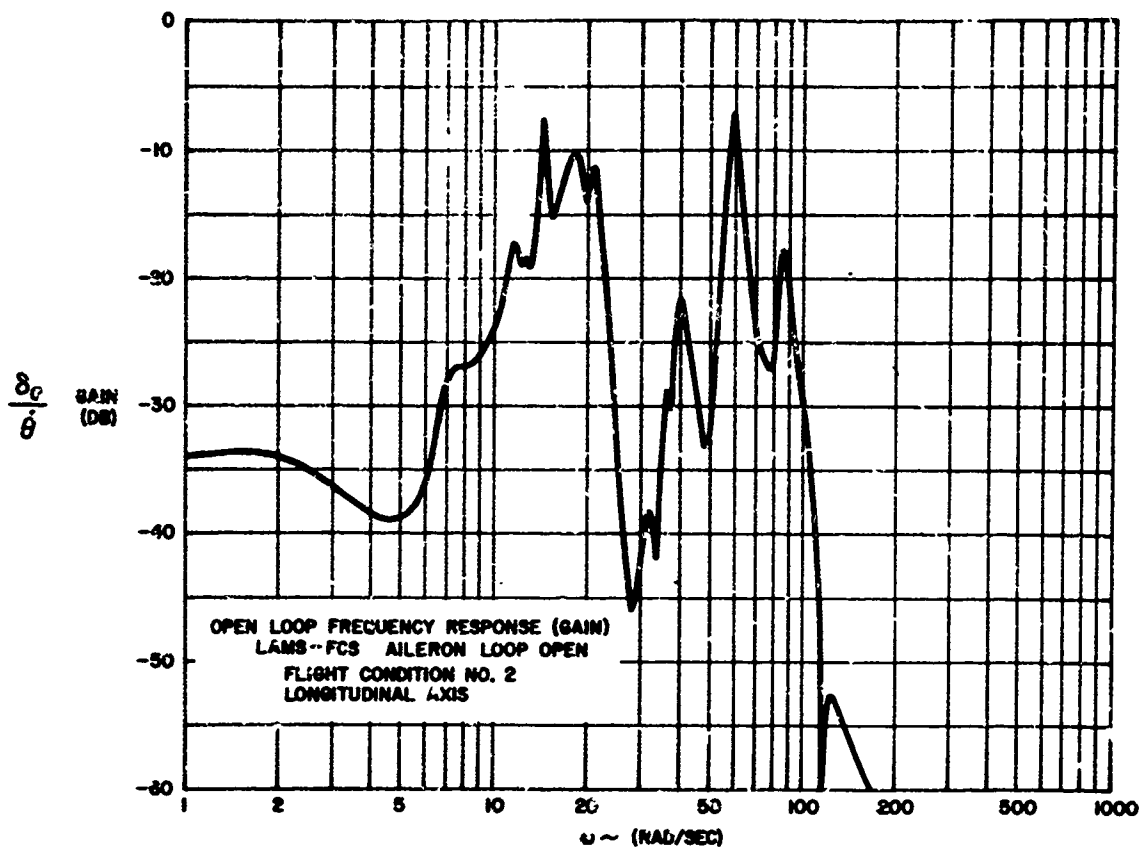


FIGURE 83

TABLE XLV
LONGITUDINAL AXIS - SPOILER LOOP MARGINS
FLIGHT CONDITION 2

CRITICAL FREQUENCY (RAD/SEC)	GAIN MARGIN AT NOMINAL PHASE (DB)	PHASE MARGIN AT NOMINAL GAIN (DEG)	GAIN MARGIN AT WORST PHASE (DB)
4.7		168	
6.0			Unstable 4.1
6.8		123	
11.4			13.0
13.8			7.1
17.1			7.4
21.4			9.9
28.5	18.5		
35.6			26.1
37.8			28.0
48.8	42.2		
60.6	23.9		
60.7			23.9
82.1			36.5
92.3			38.9
108.6			40.0
123.0			42.4

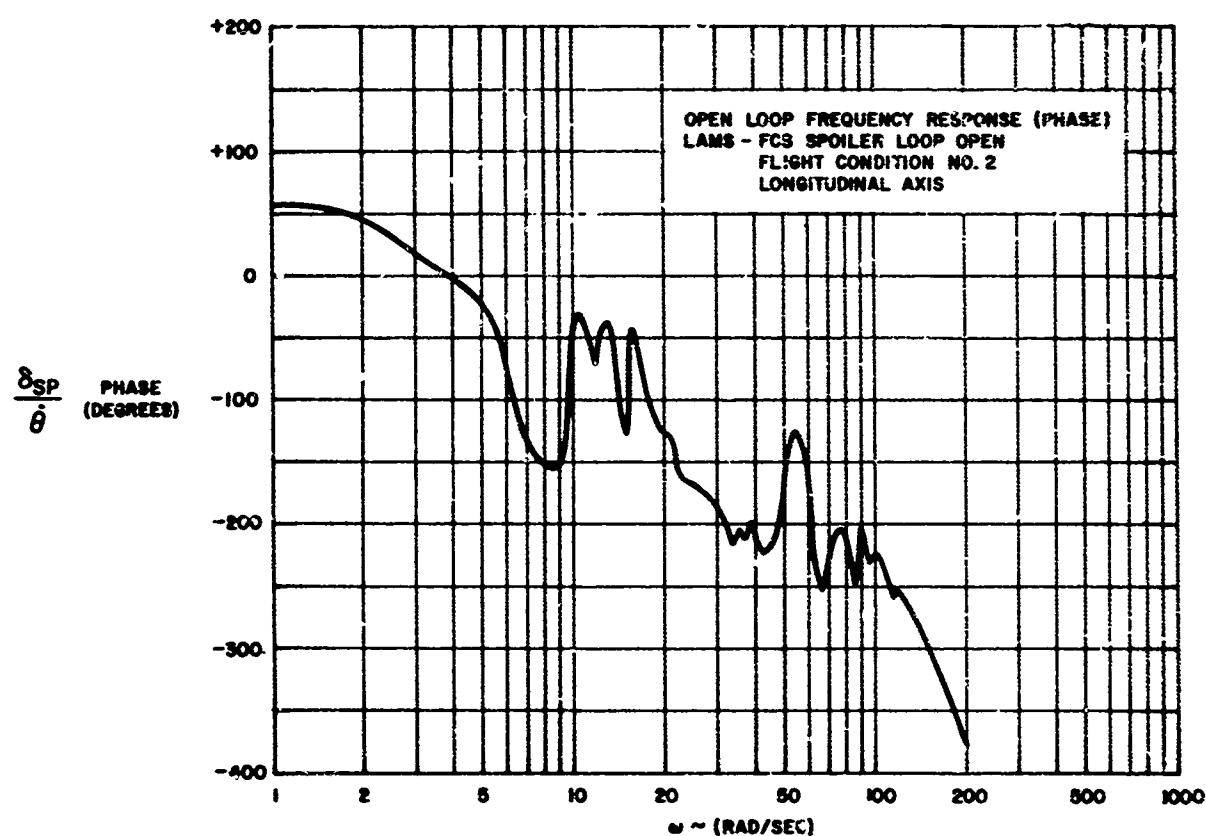
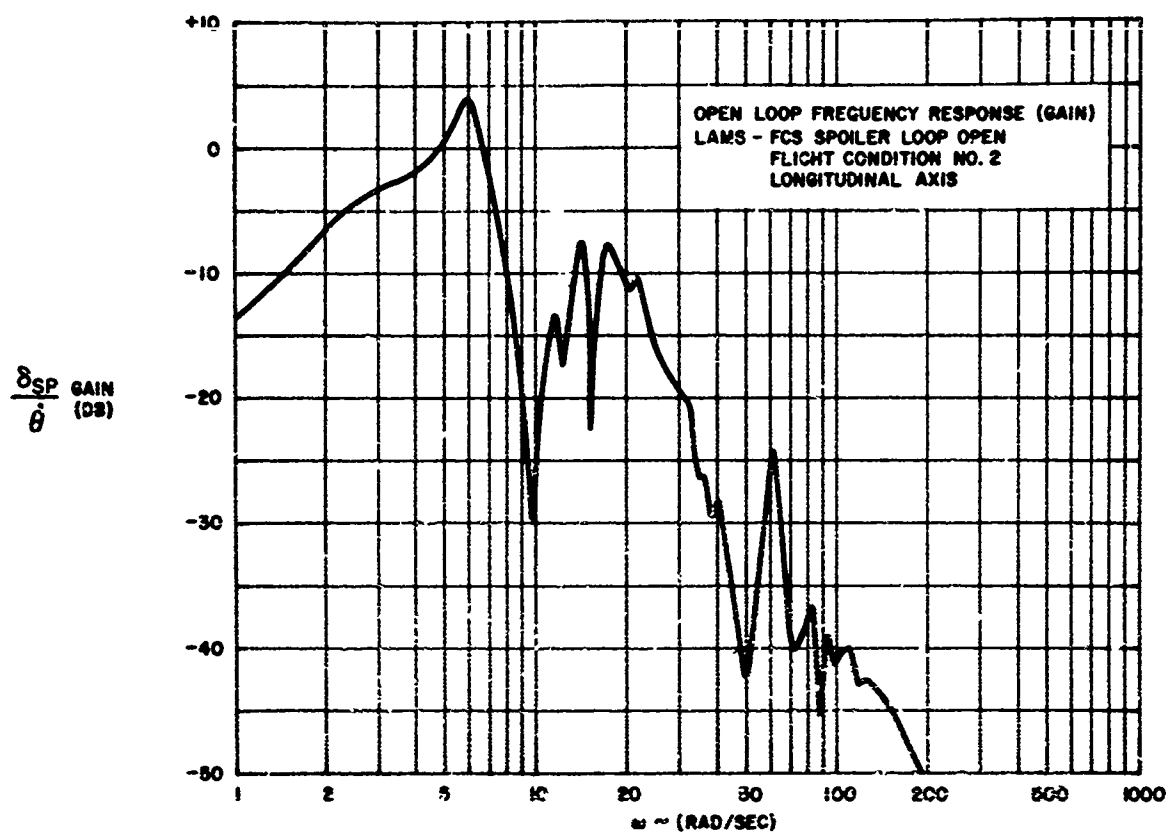


FIGURE 84
211

TABLE XLVI
LONGITUDINAL AXIS - ELEVATOR LOOP MARGINS

FLIGHT CONDITION 3

CRITICAL FREQUENCY (RAD/SEC)	GAIN MARGIN AT NOMINAL PHASE (DB)	PHASE MARGIN AT NOMINAL GAIN (DEG)	GAIN MARGIN AT WORST PHASE (DB)
2.5		92	
7.4			6.2
11.9			14.6
14.7			15.7
16.0	19.5		
19.3			20.3
20.5	33.2		
23.4	20.3		
24.1			19.0
35.2			24.7
47.4			33.7
65.1			27.9
92.0			29.4
107.9			36.6
125.0	45.0		

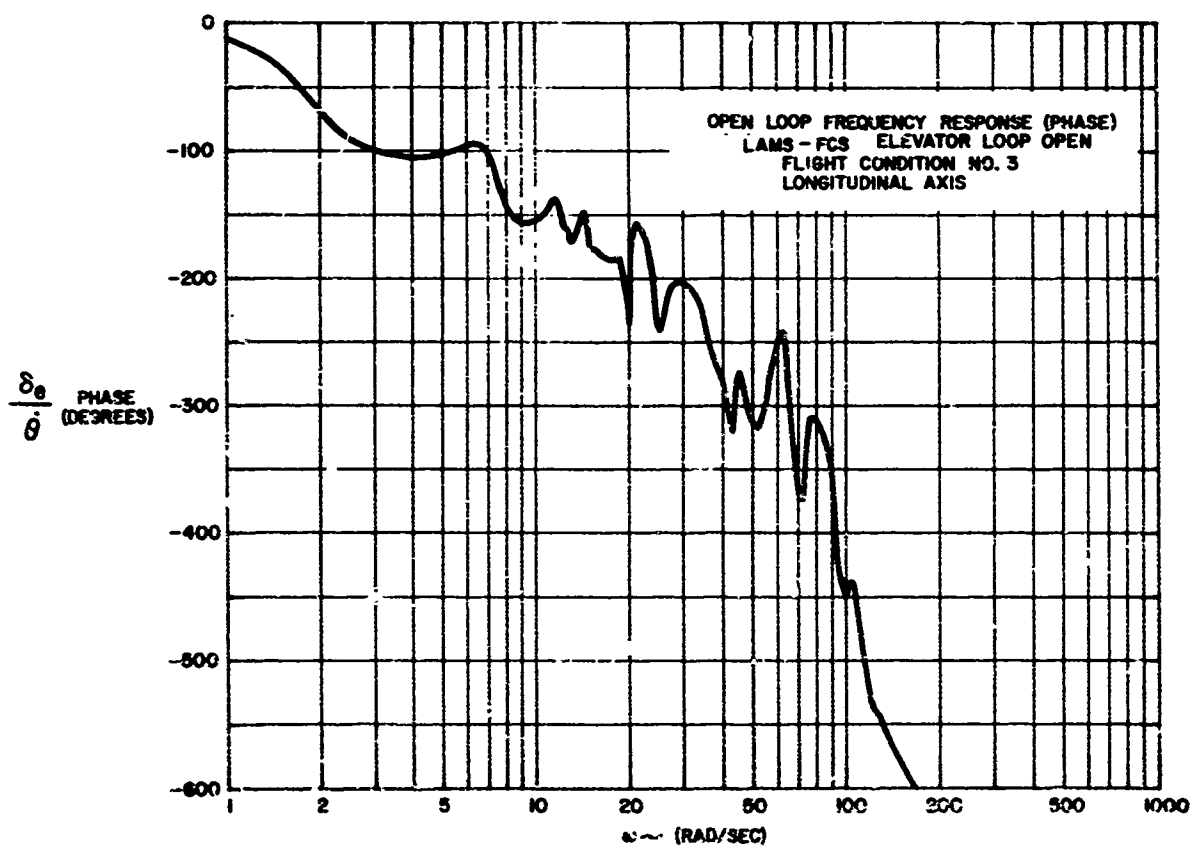
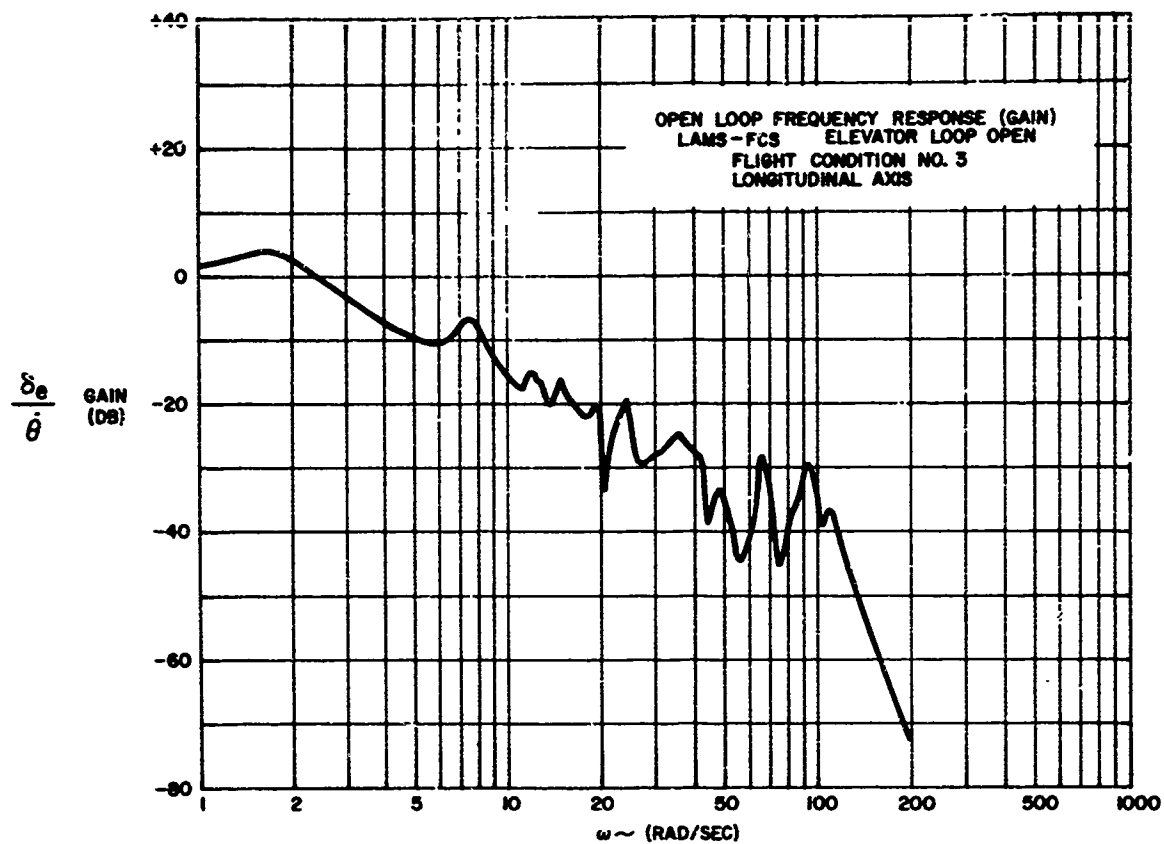


FIGURE 85
213

TABLE XLVII

LONGITUDINAL AXIS - AILERON LOOP MARGINS

FLIGHT CONDITION 3

CRITICAL FREQUENCY (RAD/SEC)	GAIN MARGIN AT NOMINAL PHASE (DB)	PHASE MARGIN* AT NOMINAL GAIN (DEG)	GAIN MARGIN AT WORST PHASE (DB)
11.8			17.7
14.8			7.2
19.0			18.1
23.9			11.7
24.6	14.1		
29.4	39.6		
34.5			39.6
34.7	39.6		
42.7			24.9
65.3			9.1
67.1	10.3		
89.6			23.6
105.8			27.1

* System is Gain Stabilized

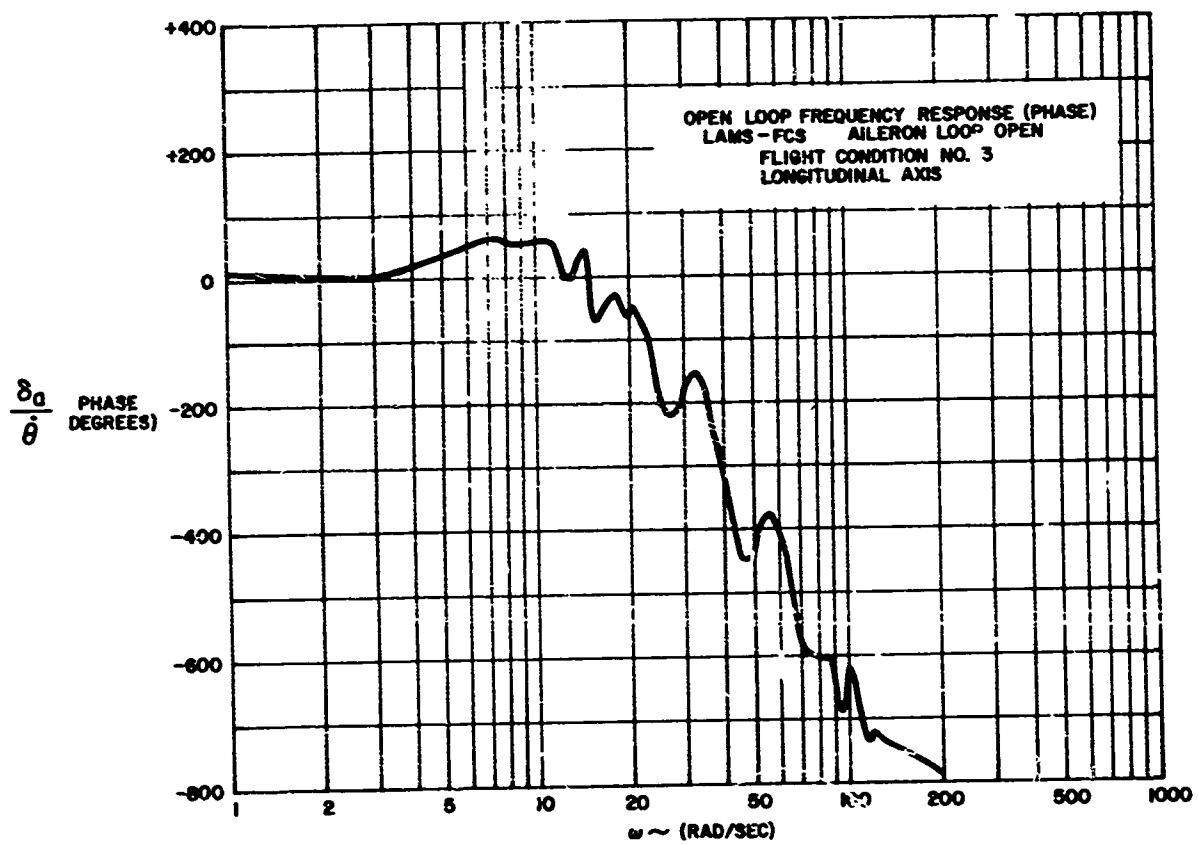
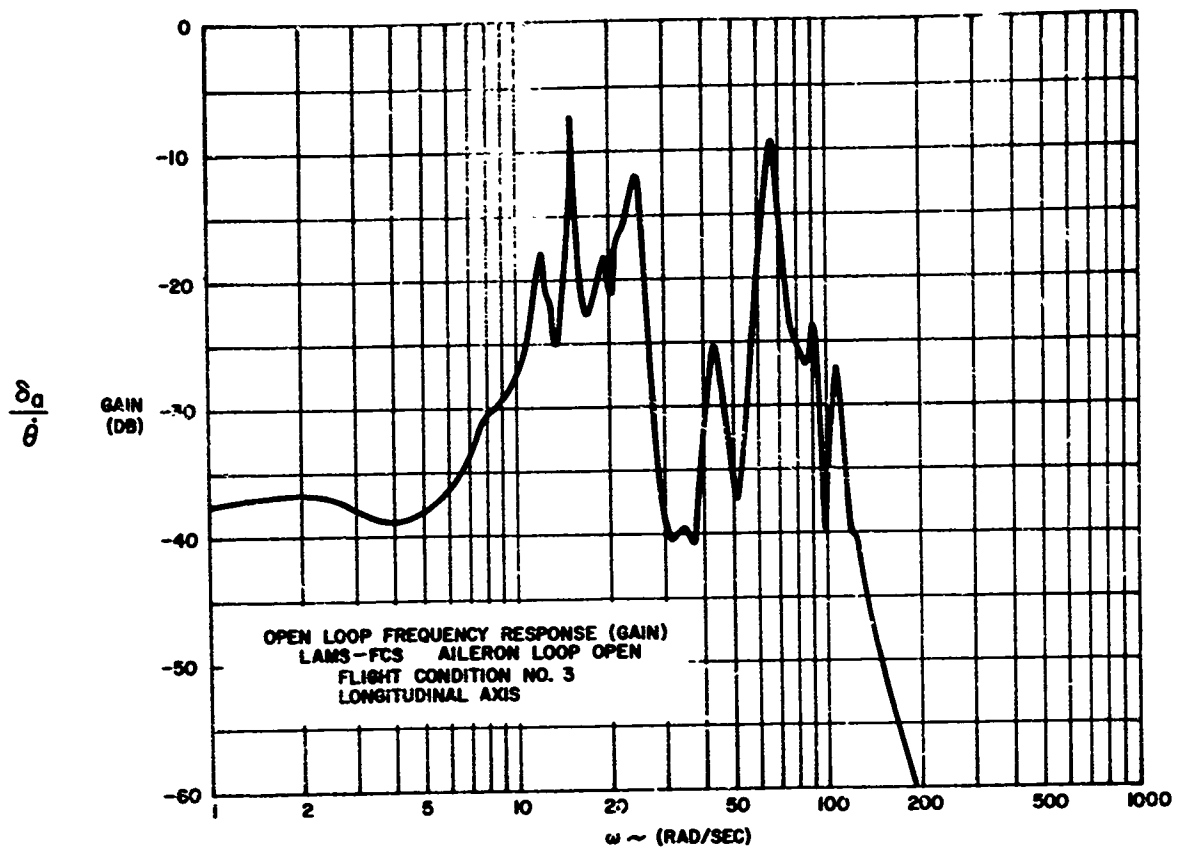


FIGURE 86

TABLE XLVIII
LATERAL-DIRECTIONAL AXIS - RUDDER LOOP MARGINS

FLIGHT CONDITION 2

CRITICAL FREQUENCY (RAD/SEC)	GAIN MARGIN AT NOMINAL PHASE (DB)	PHASE MARGIN AT NOMINAL GAIN (DEG)	GAIN MARGIN AT WORST PHASE (DB)
1.5		86	
11.9			19.9
14.7	18		
16.8			16.2
26.3			32.1
27.3	32.5		
30.4			31.8
35.6			30.7
39.7	32.4		
41.6			30.2
58.4			24.0
81.7	17.6		

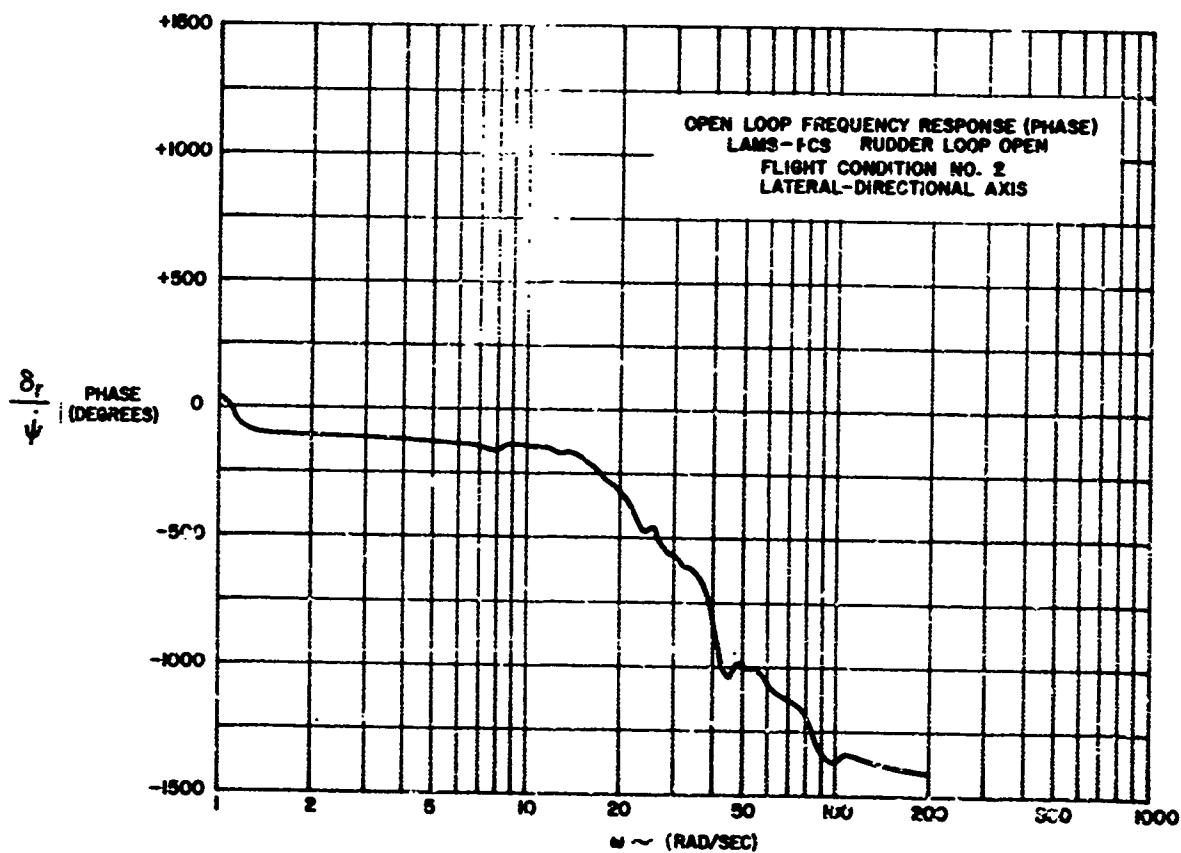
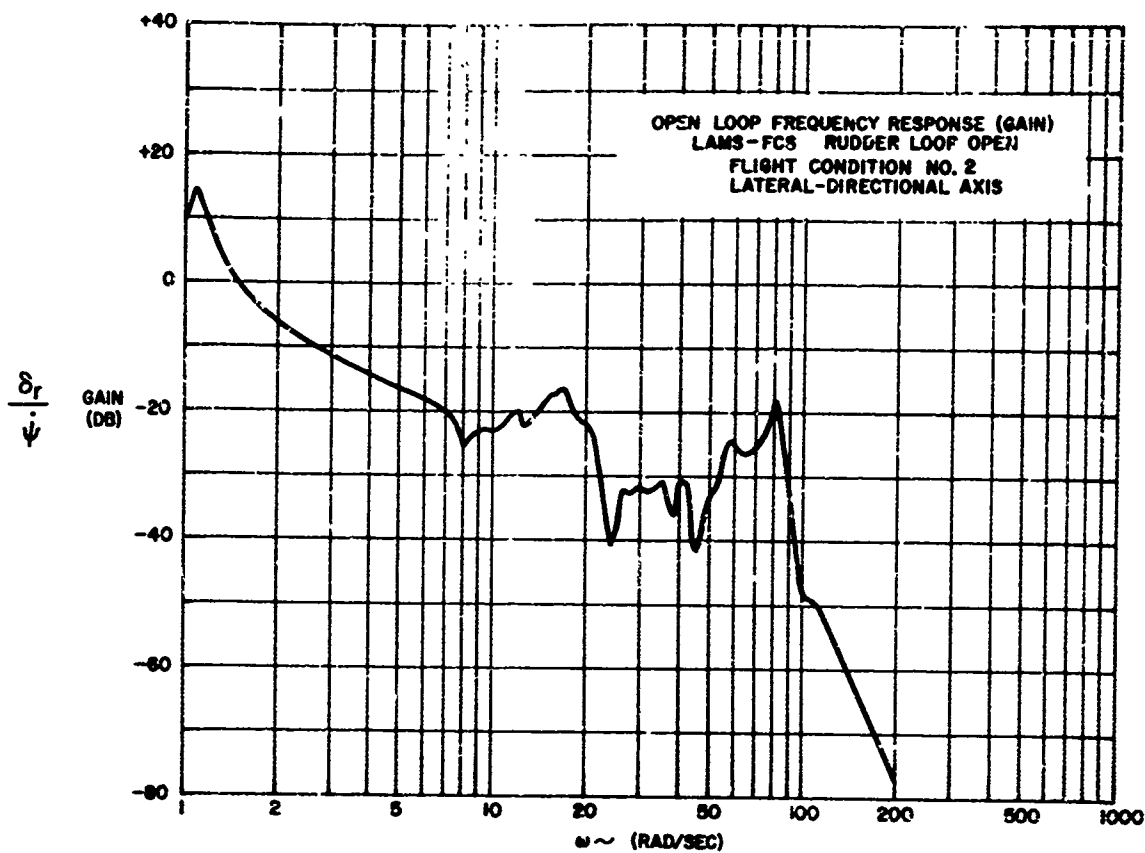


FIGURE 87

TABLE XLIX

LATERAL-DIRECTIONAL AXIS - AILERON LOOP MARGINS

FLIGHT CONDITION 2

CRITICAL FREQUENCY (RAD/SEC)	GAIN MARGIN AT NOMINAL PHASE (DB)	PHASE MARGIN* AT NOMINAL GAIN (DEG)	GAIN MARGIN AT WORST PHASE (DB)
8.0			26.5
12.3			20.3
13.1			21.7
15.5	24.5		
20.5			17.3
25.6			14.5
34.0	25.8		
42.8	23.8		
45.8	29.1		
48.4	23.0		
56.7			18.9
72.8			20.8

* System is Gain Stabilized

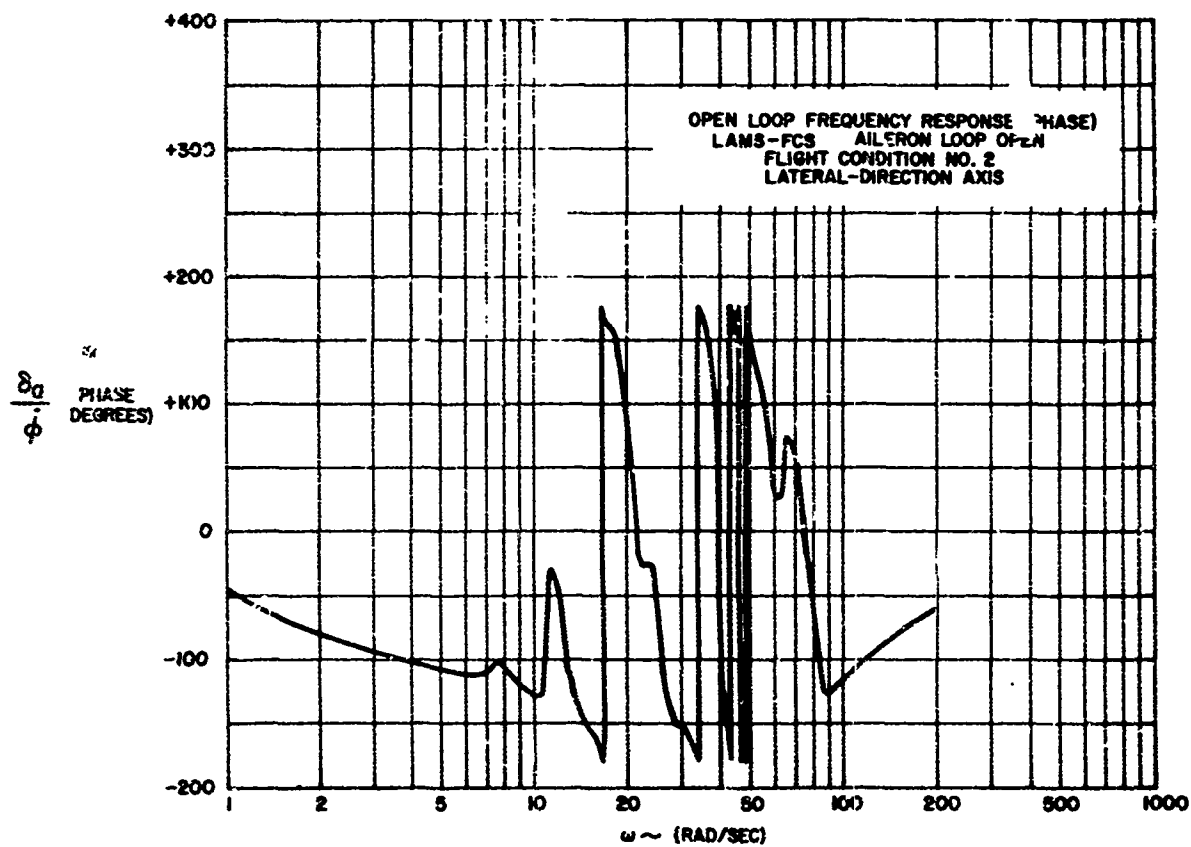
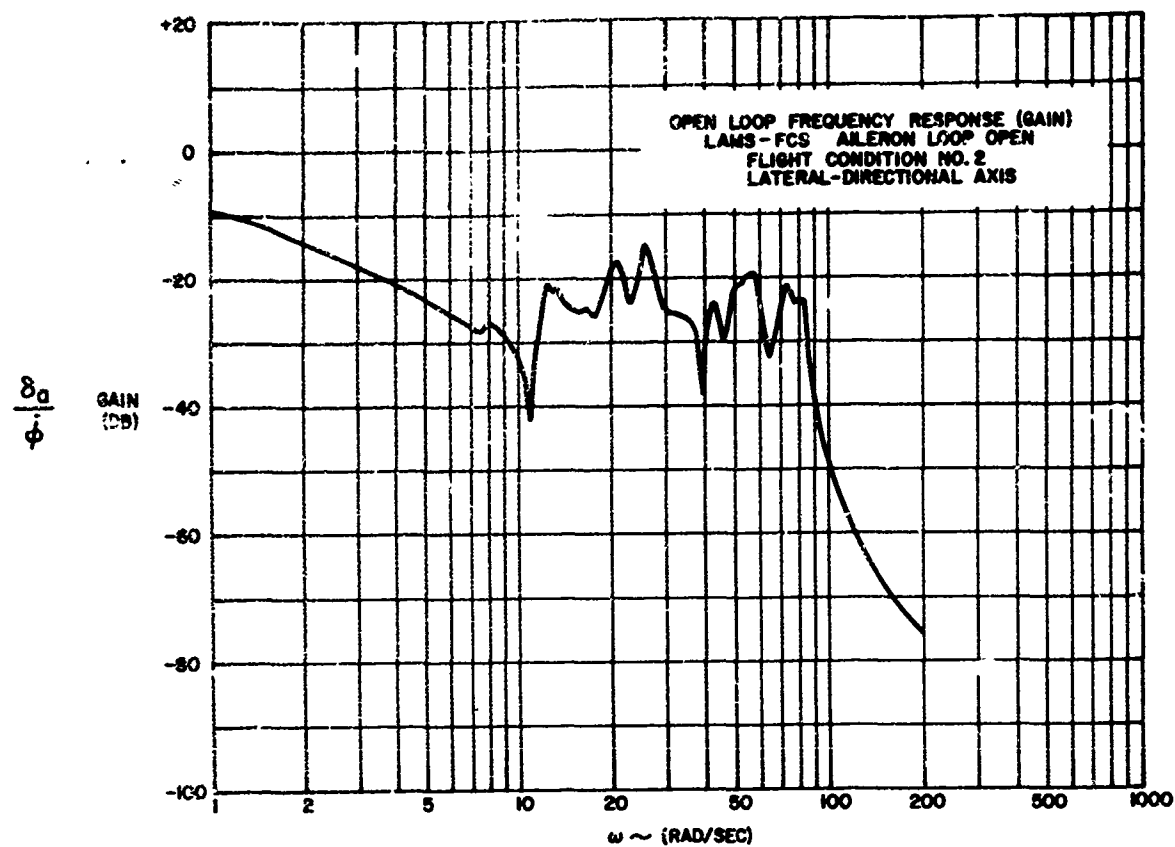


FIGURE 68

TABLE L
LATERAL-DIRECTIONAL AXIS - RUDDER LOOP MARGINS

FLIGHT CONDITION 3

CRITICAL FREQUENCY (RAD/SEC)	GAIN MARGIN AT NOMINAL PHASE (DB)	PHASE MARGIN AT NOMINAL GAIN (DEG)	GAIN MARGIN AT WORST PHASE (DB)
1.6		86	
8.8			21.7
12.8			18.7
15.6	20.8		
16.0			20.5
17.7			19.9
22.4			26.8
27.9			25.0
28.8	26.1		
35.1			32.0
40.1	50.0		
41.1	38.0		
42.0			34.7
53.5			31.0
66.5			24.4
81.3			21.6
107.6			46.6

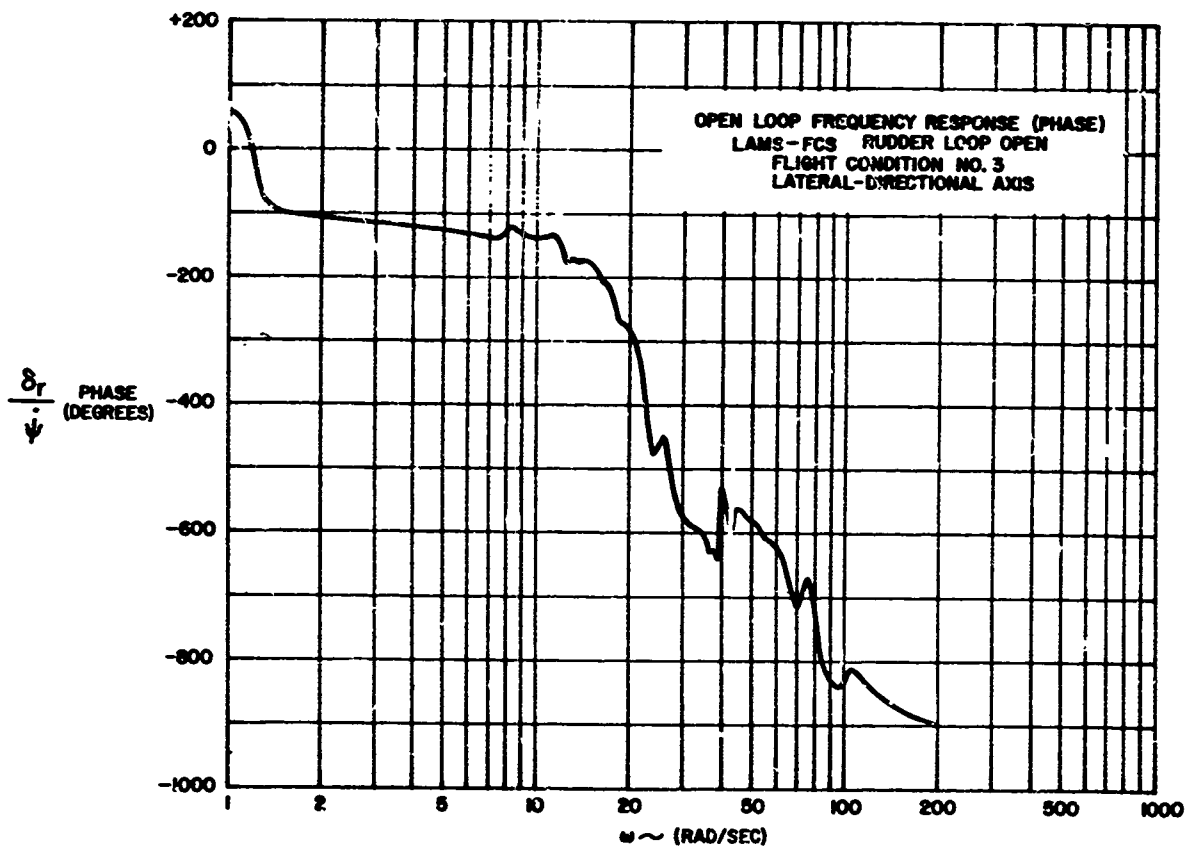
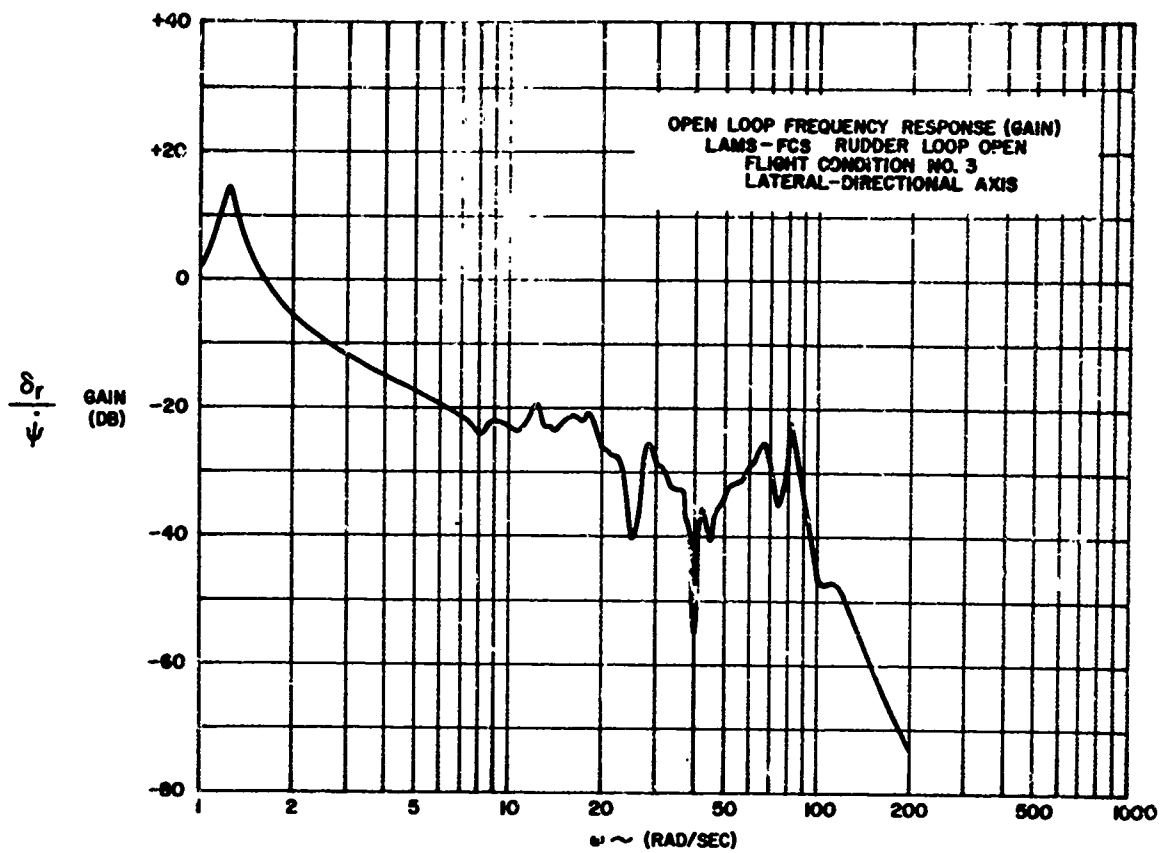


FIGURE 89

TABLE LI
LATERAL-DIRECTIONAL AXIS - AILERON LOOP MARGINS
FLIGHT CONDITION 3

CRITICAL FREQUENCY (RAD/SEC)	GAIN MARGIN AT NOMINAL PHASE (DB)	PHASE MARGIN* AT NOMINAL GAIN (DEG)	GAIN MARGIN AT WORST PHASE (DB)
8.3			24.0
12.1			13.0
13.4			20.1
15.5	23.9		
16.9	30.7		
17.5	25.0		
19.6			21.0
27.2			7.5
33.1	19.2		
40.0			24.2
43.3	24.0		
45.6			20.9
51.8			20.9
53.4			22.0
72.0			20.1

* System is Gain Stabilized

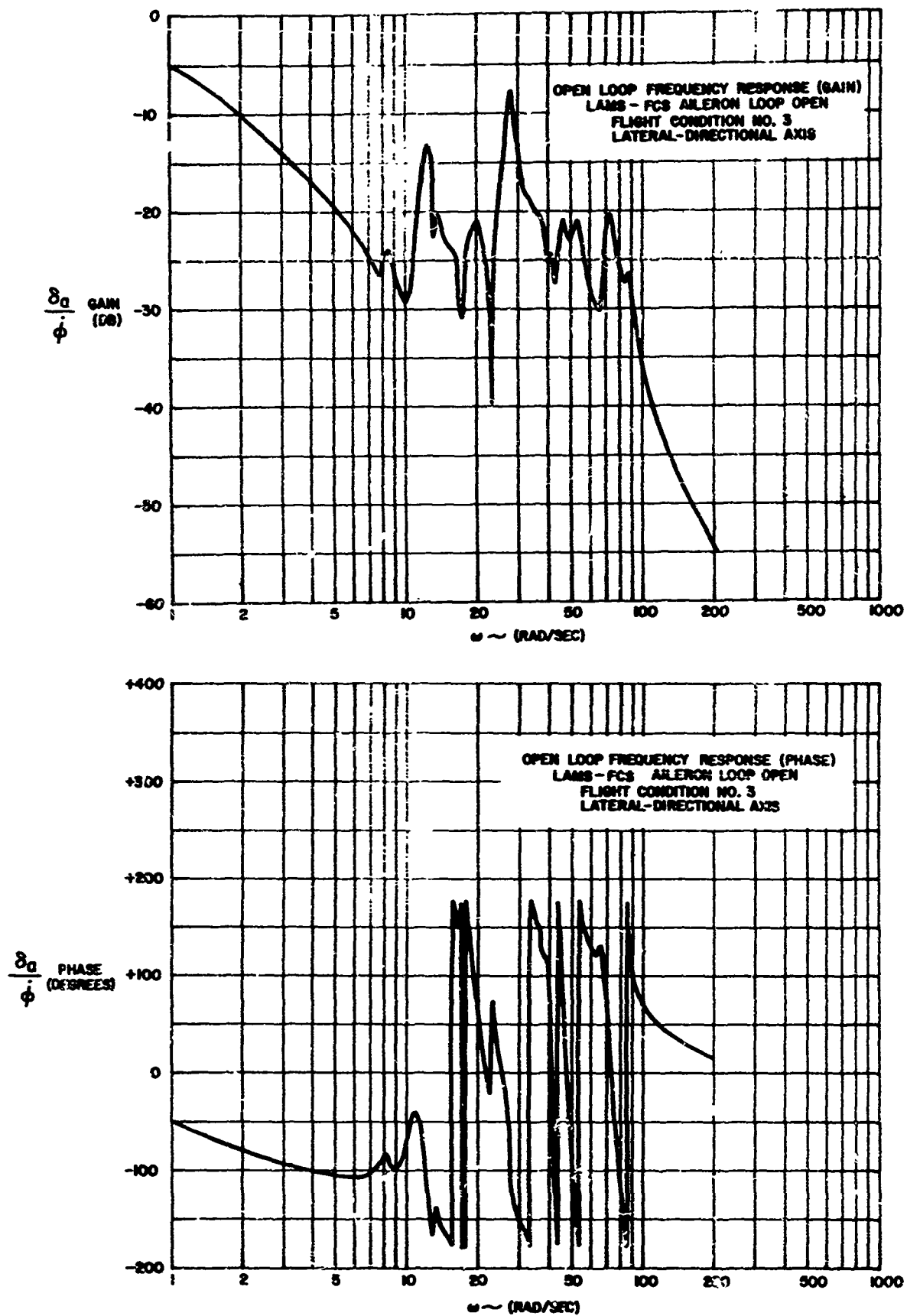
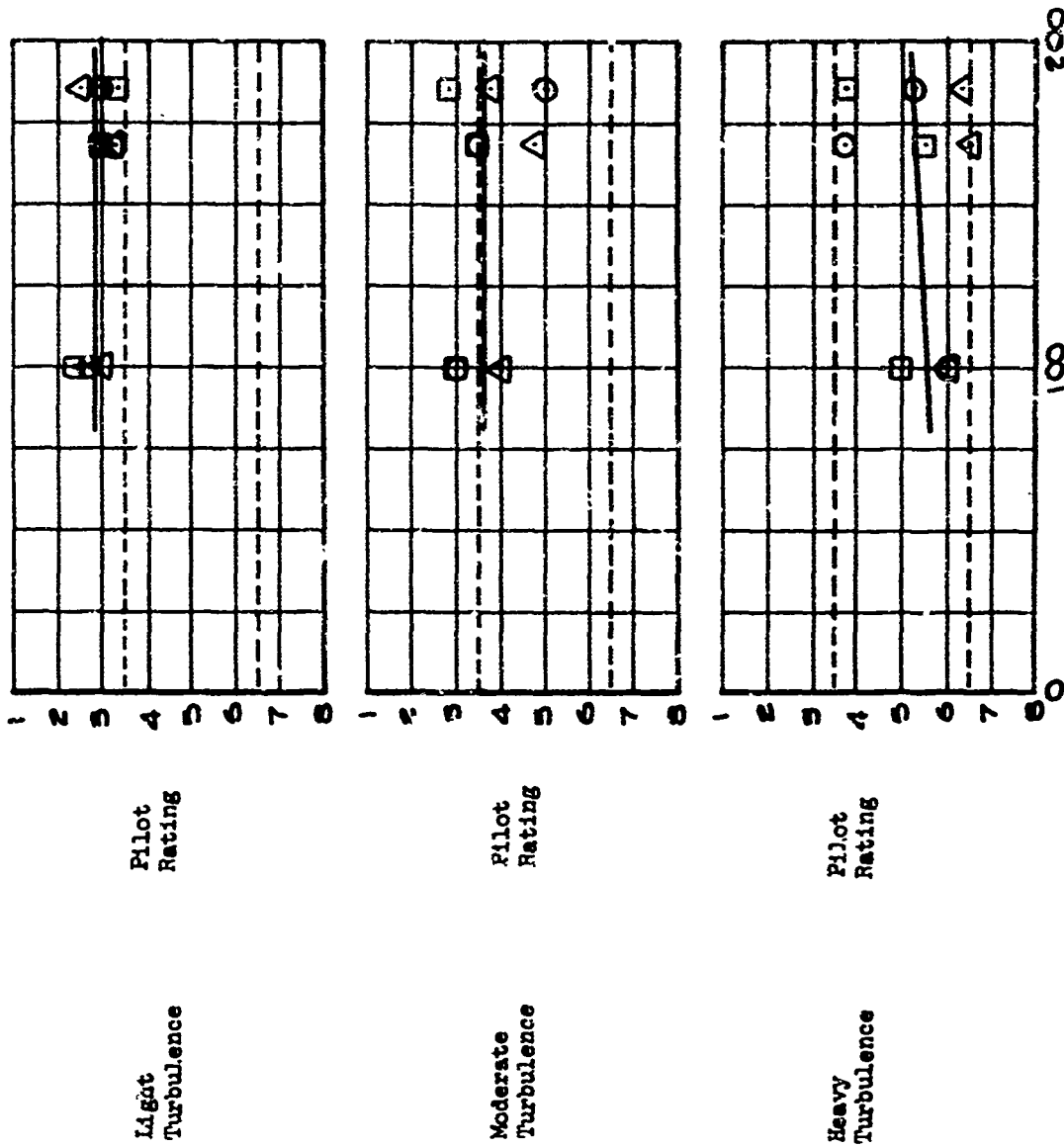


FIGURE 90

APPENDIX C - HANDLING QUALITIES DATA

Pilot ratings obtained from simulator studies for LAMS flight conditions 2 and 3 are presented in this appendix.

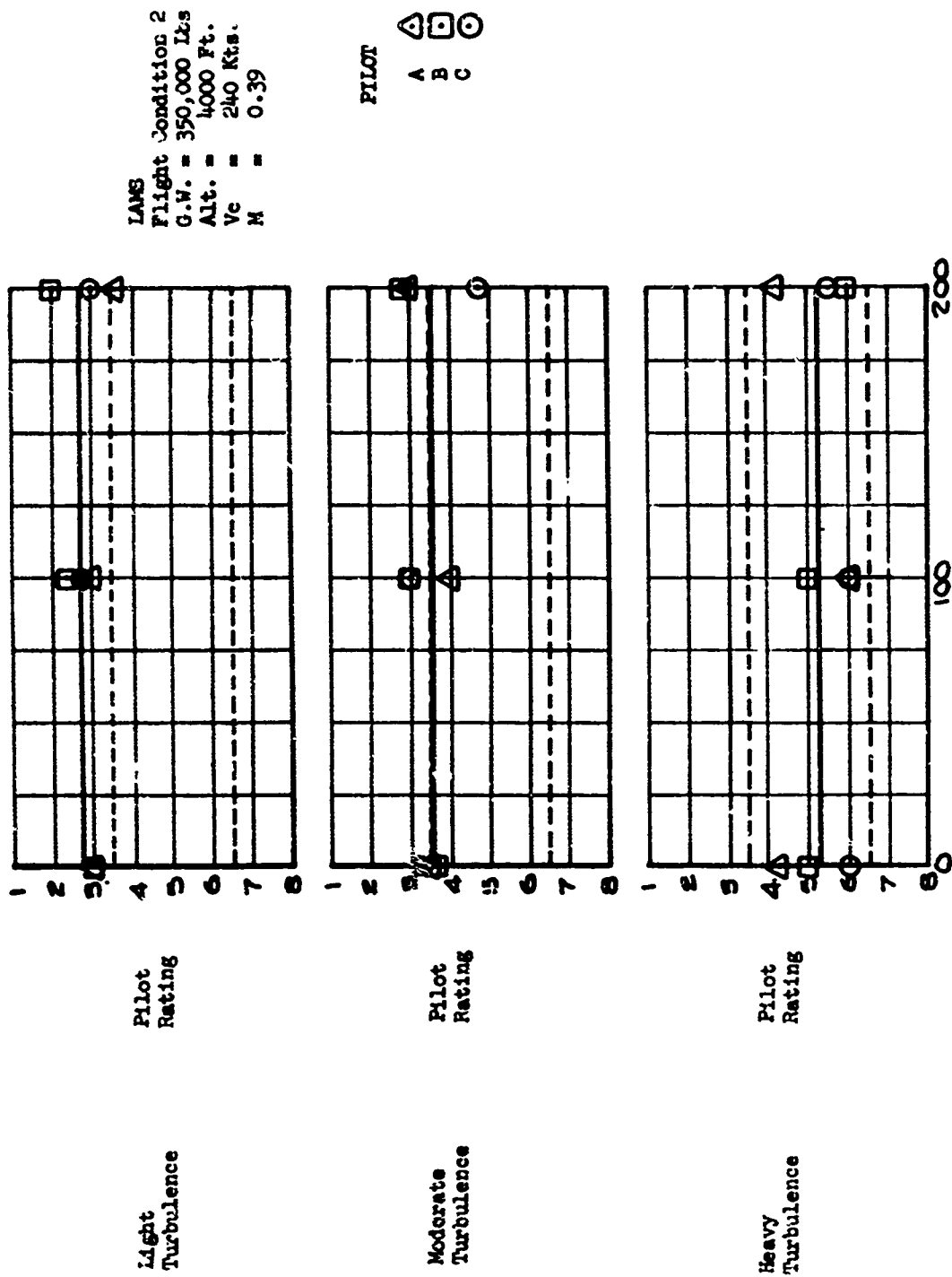


IAMS
Flight Condition 2
G.W. = 350,000 lbs.
Alt. = 4000 Ft.
Vc = 240 Kts.
M = 0.39

PILOT
A B C

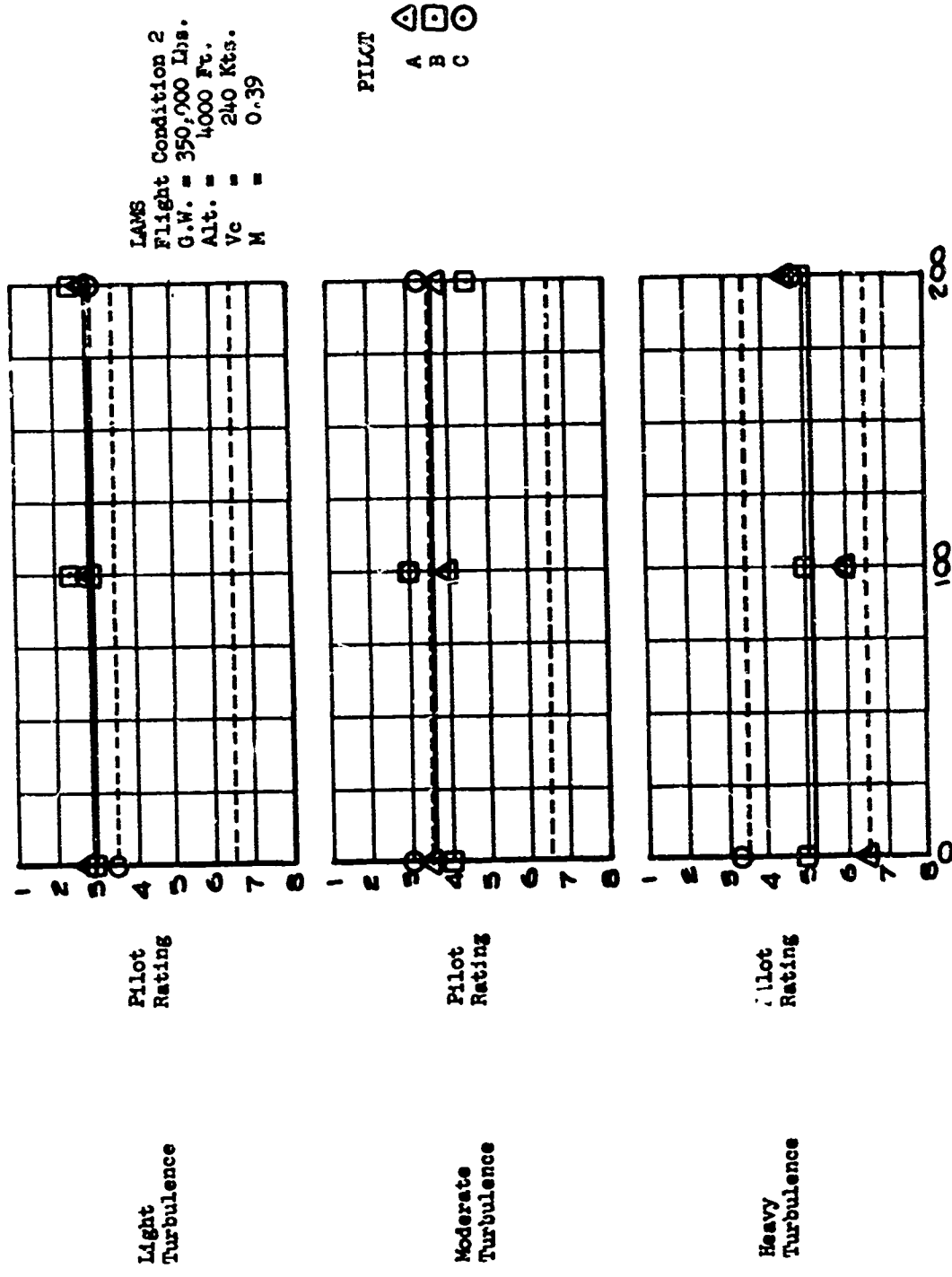
BASELINE SAS - DIRECTIONAL AXIS GAIN VARIATIONS

FIGURE 91



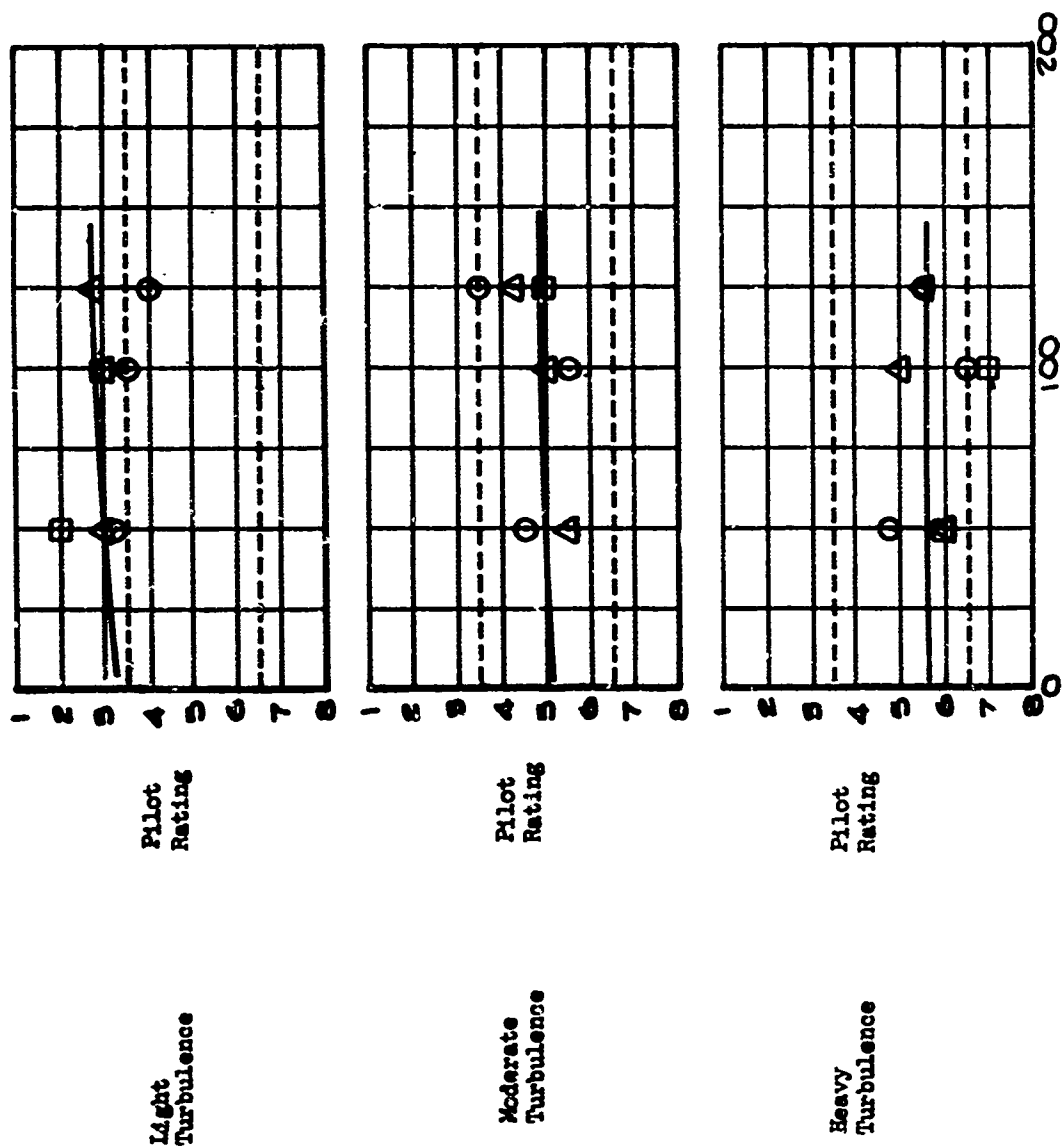
Percent Of Nominal Gain
 BASELINE SAS - LONGITUDINAL AXIS GAIN VARIATIONS

FIGURE 92



Percent of Nominal Gain
 BASELINE SAS - LATERAL AXIS GAIN VARIATIONS

FIGURE 93



Percent Of Nominal Gain

LAMS FCS - DIRECTIONAL AXIS GAIN VARIATIONS

FIGURE 94

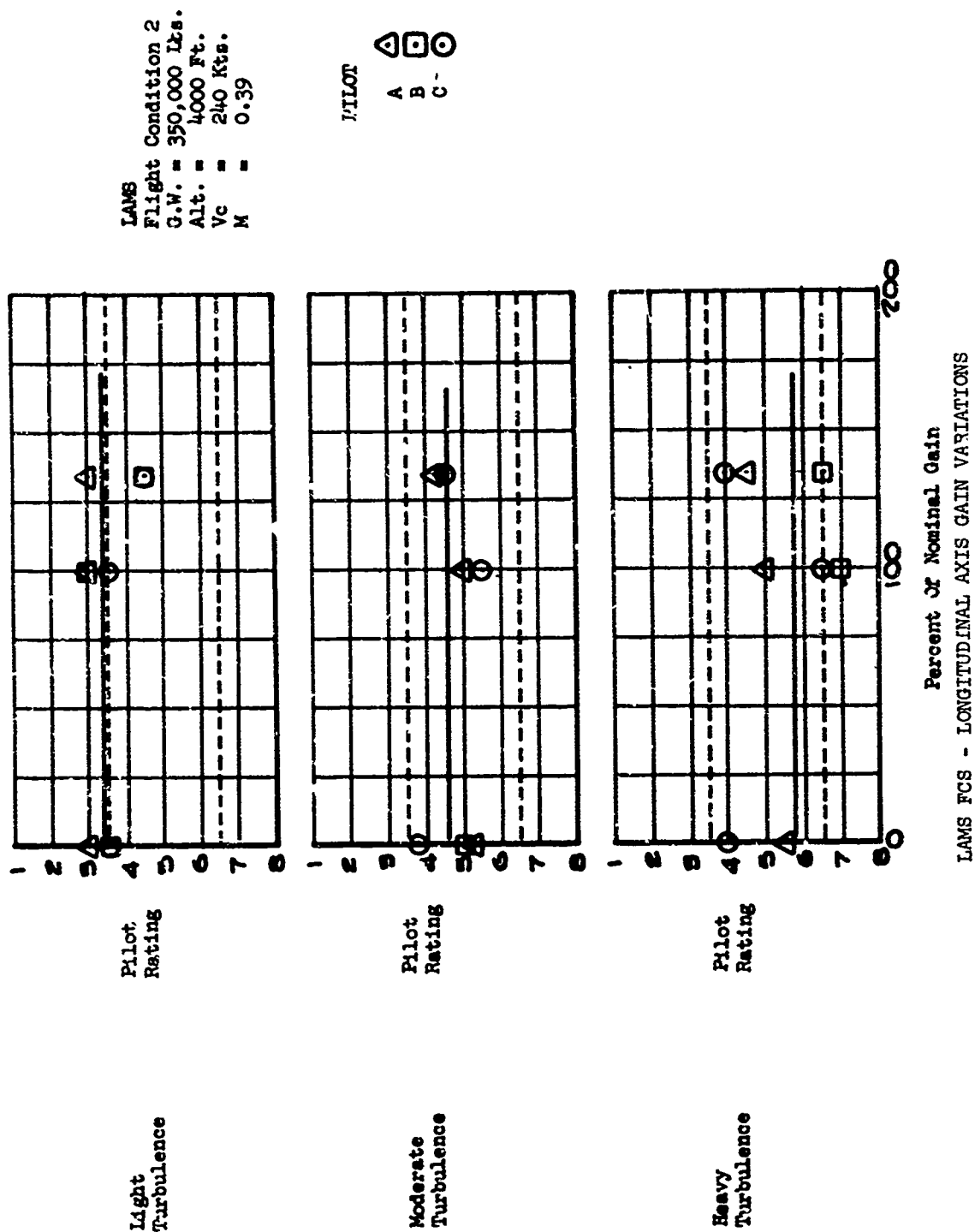
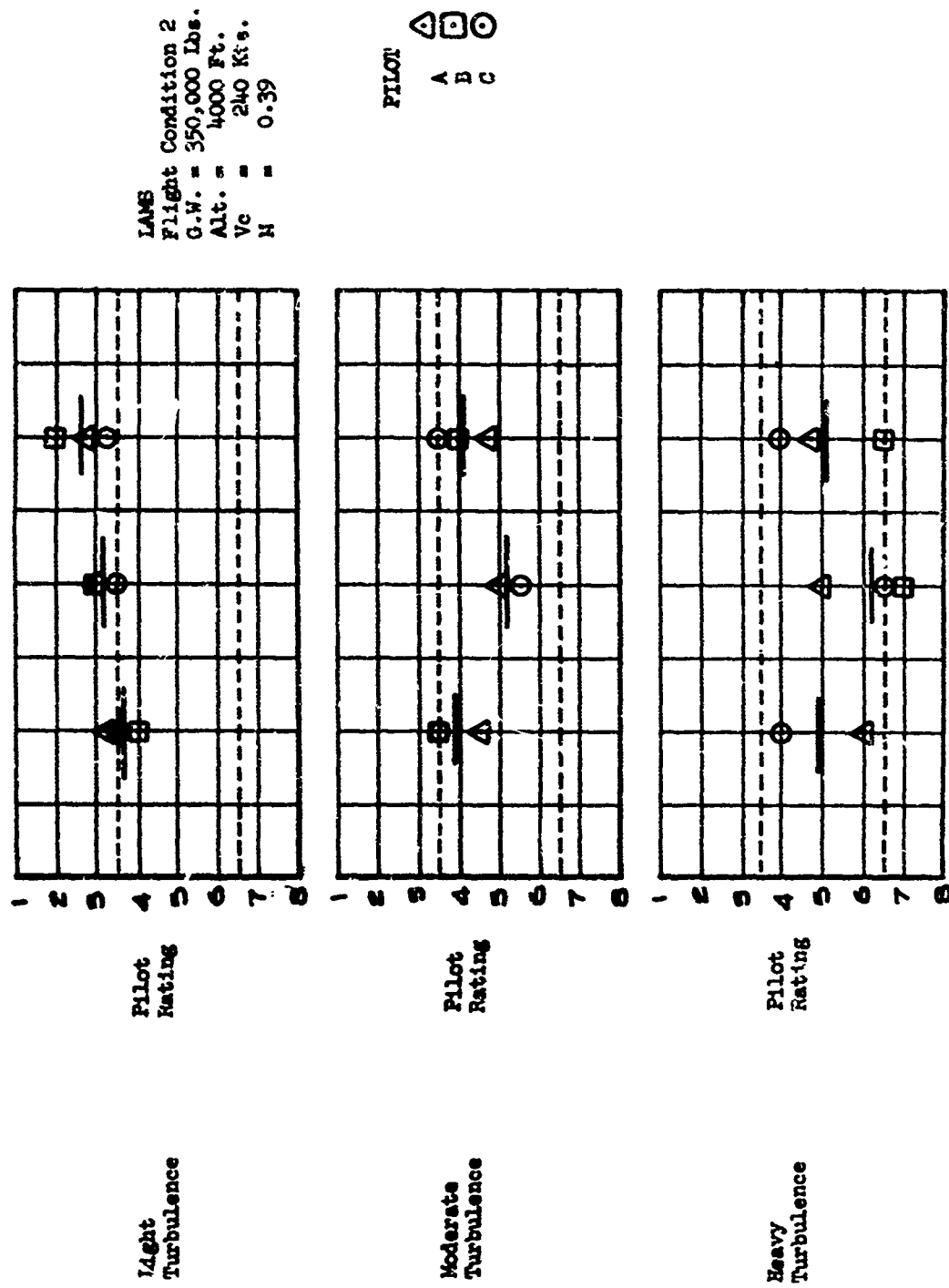
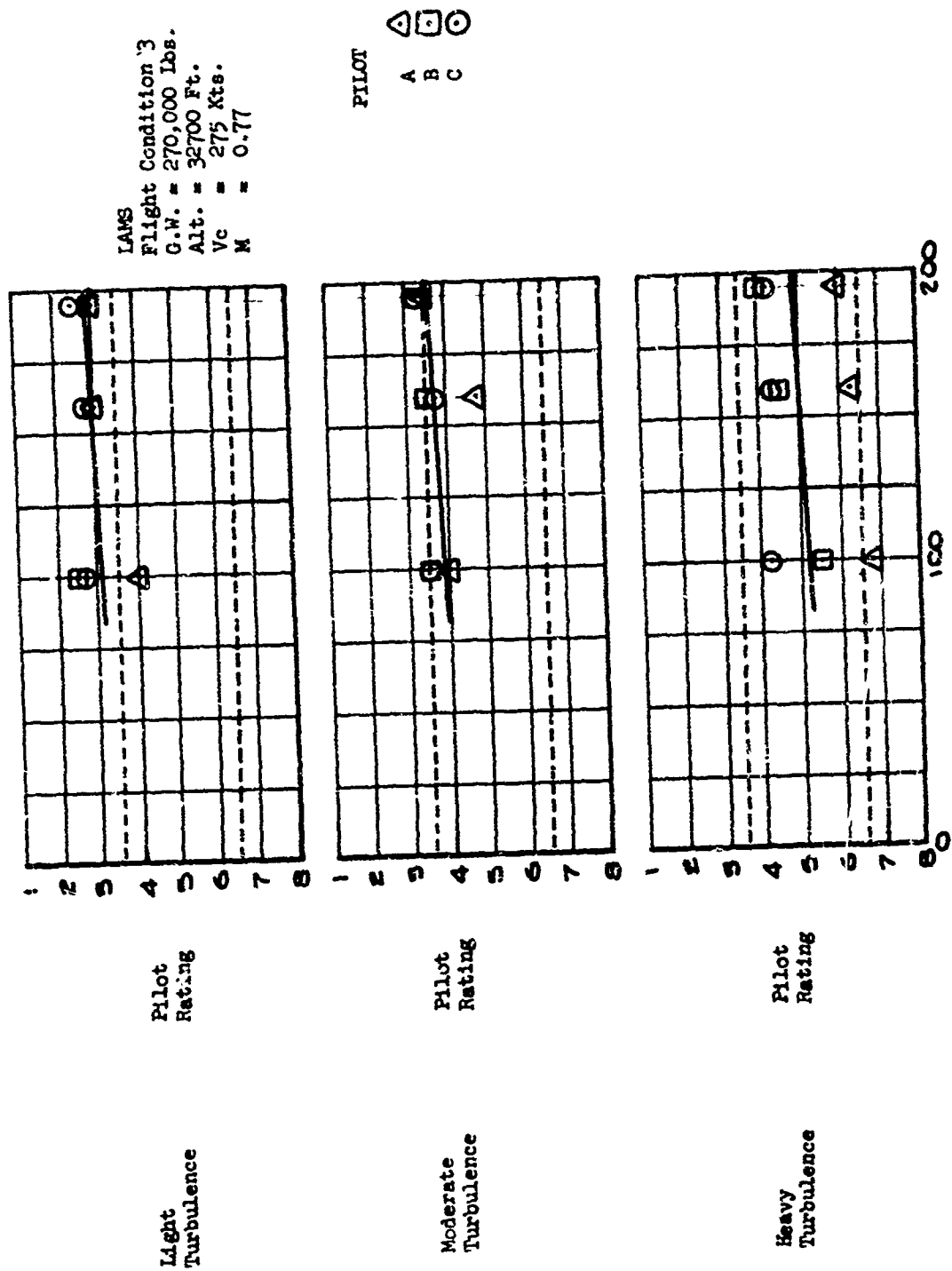


FIGURE 95



LAMS FCS - LATERAL AXIS GAIN VARIATIONS




FIGURE 96

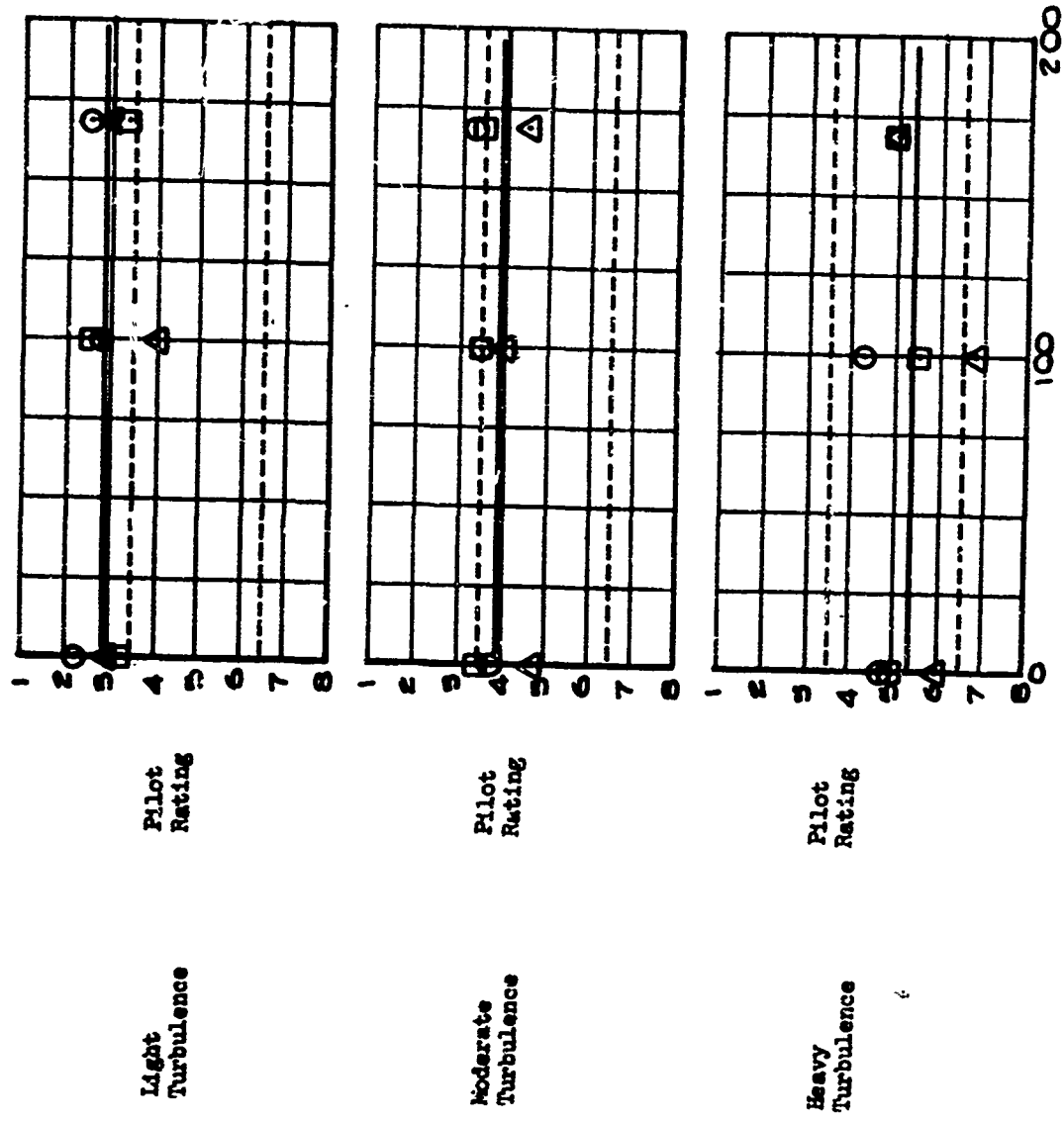


Percent Of Nominal Gain
BASELINE SAS - DIRECT . ONAL AXIS GAIN VARIATIONS

FIGURE 97

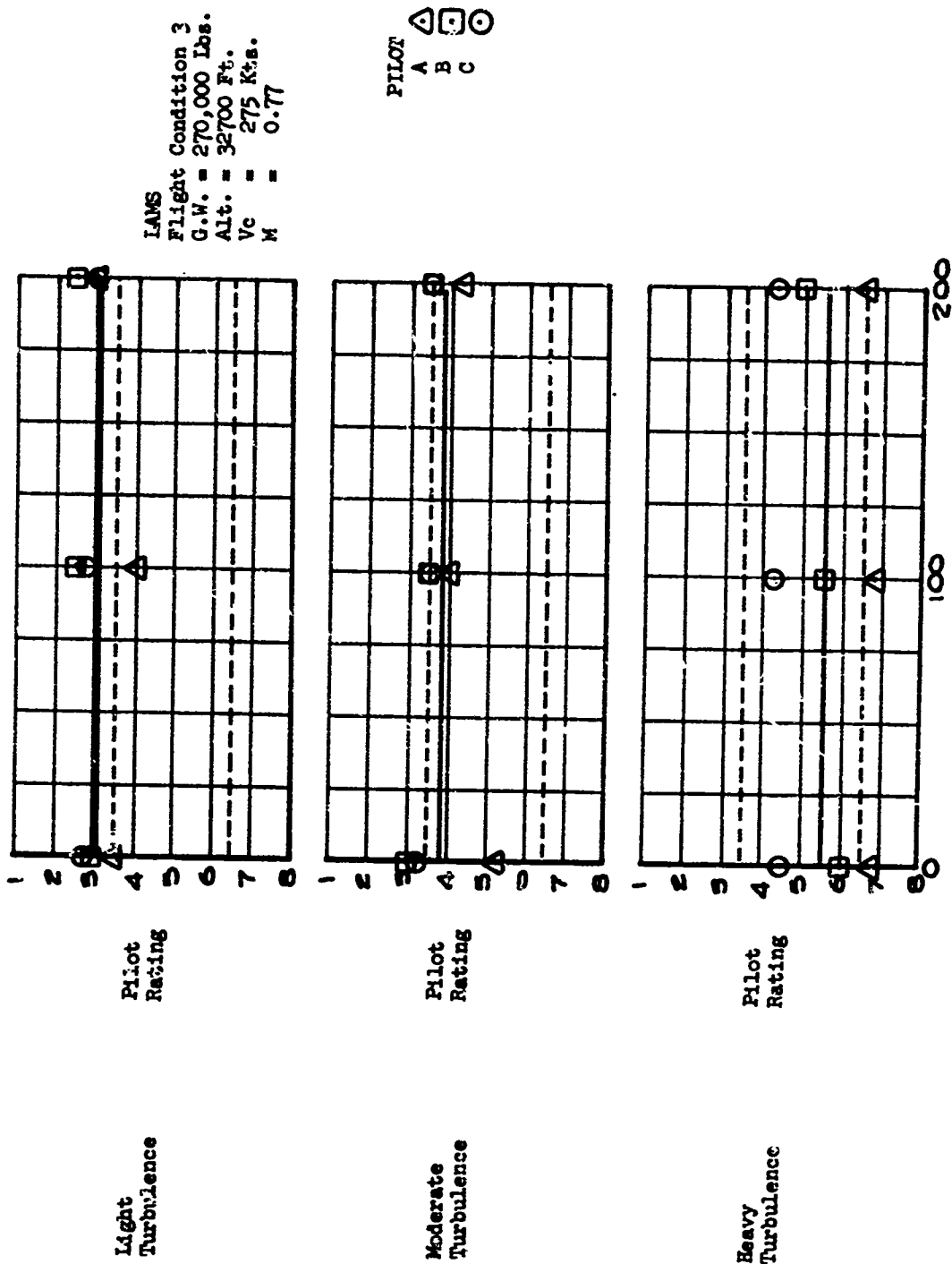
IAMS
 Flight Condition 3
 G.W. = 270,000 Lbs.
 Alt. = 32,700 Ft.
 Vc = 275 Kts.
 M = 0.77

PILOT
 A 
 B 
 C 



Percent of Nominal Gain
 BASELINE SAS - LONGITUDINAL AXIS GAIN VARIATIONS

FIGURE 98

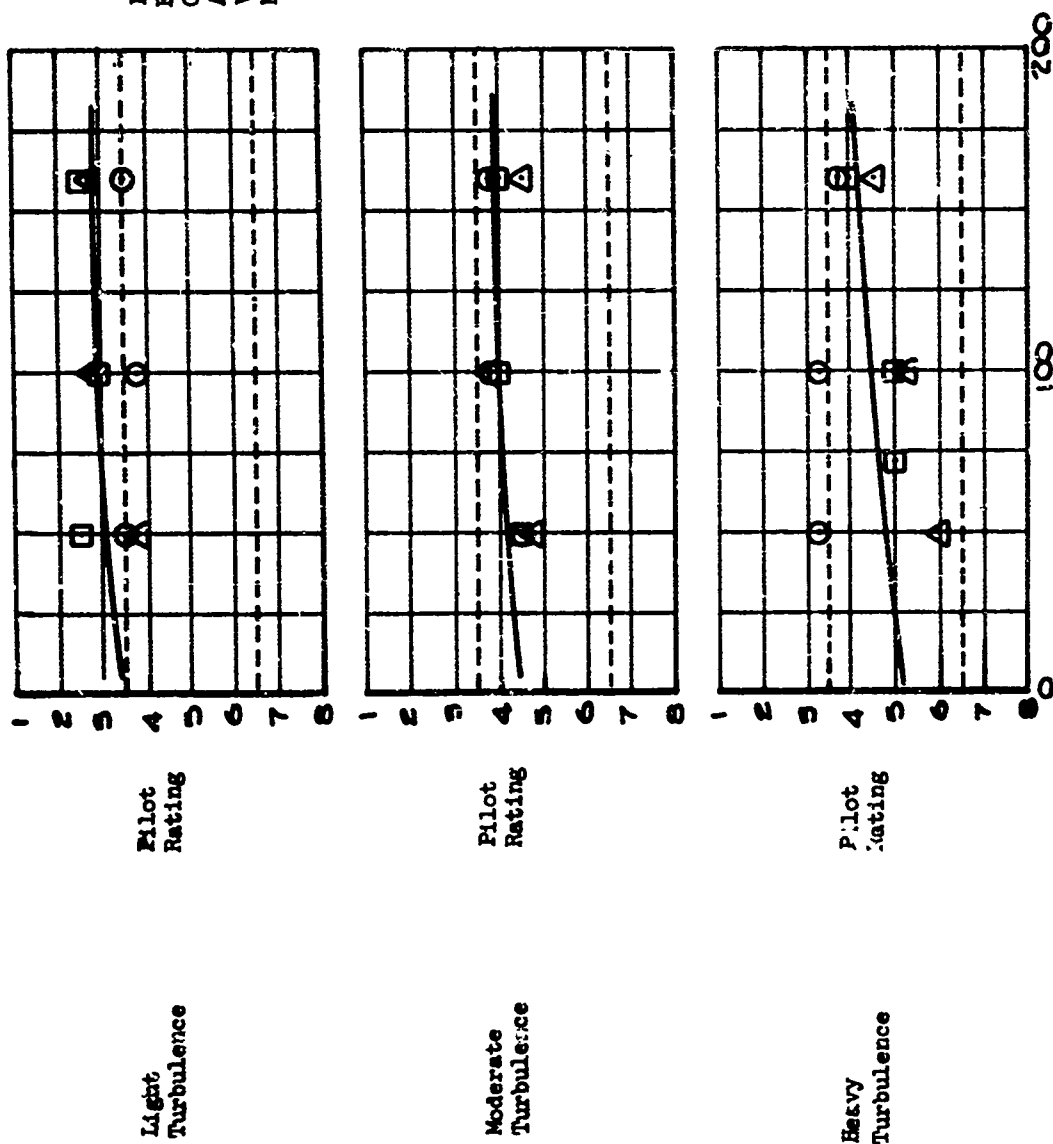


Percent Of Nominal Gain
 BASELINE SAS - LATERAL AXIS GAIN VARIATIONS

FIGURE 99

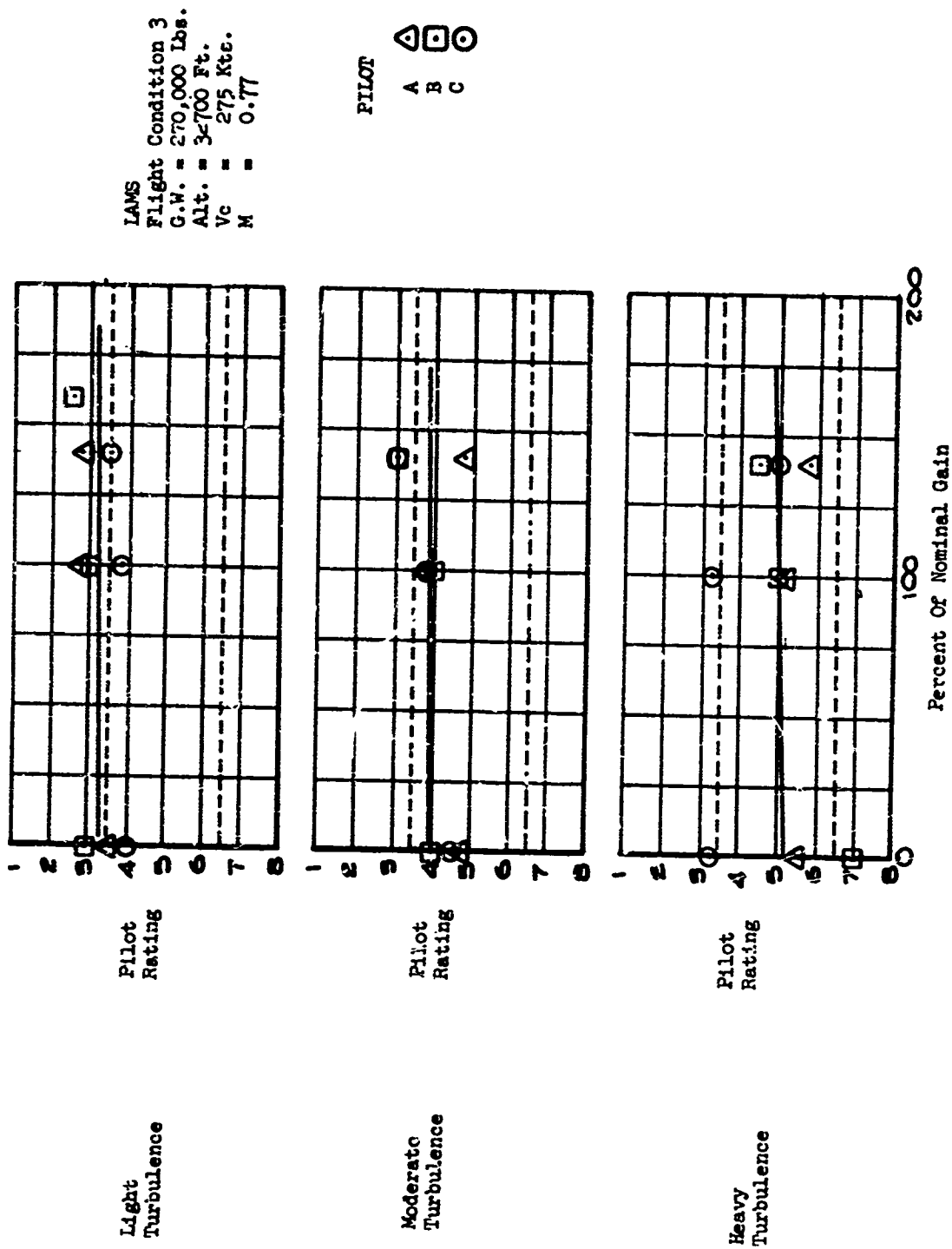
LAU'S
Flight Condition 3
G.W. = 270,000 Lbs.
Alt. = 32,700 Ft.
Vc = 275 Kts.
M = 0.77

PILOT
A Δ
B \square
C \circ



Percent of Nominal Gain
LAMS PCS - DIRECTIONAL AXIS GAIN VARIATIONS

FIGURE 100

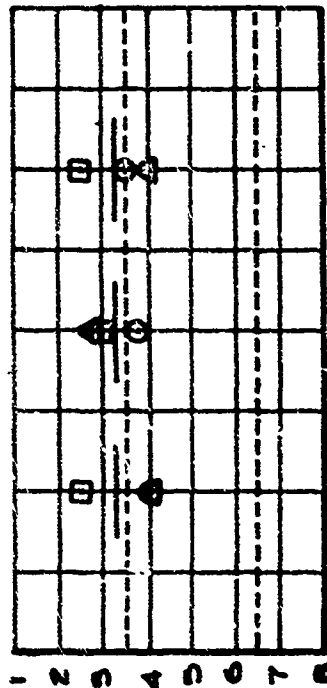


LAMS FCS - LONGITUDINAL AXIS GAIN VARIATIONS

FIGURE 101.

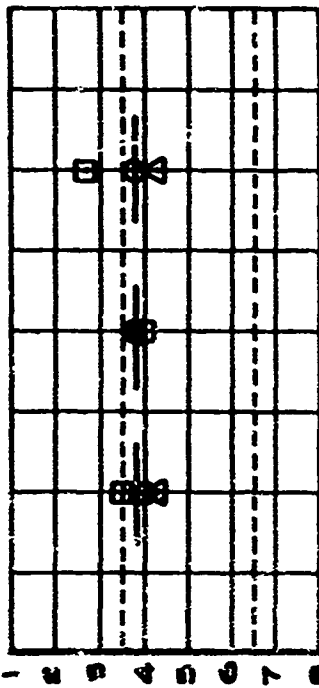
LAMS
Flight Condition 3
G.W. = 270,000 Lbs
Alt. = 32700 Ft.
Vc = 275 Kts.
M = 0.77

PILOT
A 
B 
C 



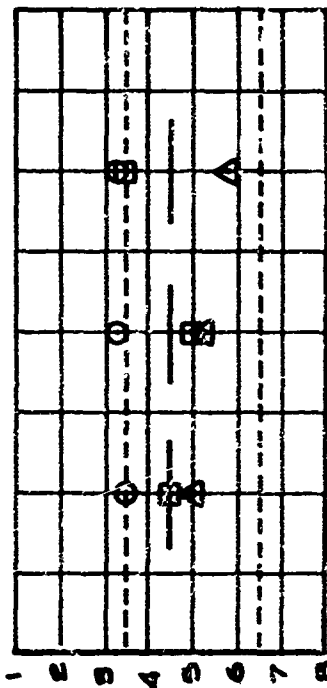
Pilot Rating

Light Turbulence



Pilot Rating

Moderate Turbulence



Pilot Rating

Heavy Turbulence

No Roll Forward Forward
SAS Gain = 1 Gain = 2
LAMS PCS - LATERAL AXIS GAIN VARIATIONS

FIGURE 102

UNCLASSIFIED

Security Classification

DOCUMENT CONTROL DATA - R & D

(Security classification of title, body of abstract and indexing annotation must be entered when the overall report is classified)

1. ORIGINATING ACTIVITY (Corporate author) The Boeing Company Wichita Division Wichita, Kansas 67210		2a. REPORT SECURITY CLASSIFICATION Unclassified	
		2b. GROUP N/A	
3. REPORT TITLE Aircraft Load Alleviation and Mode Stabilization (IAMS)			
4. DESCRIPTIVE NOTES (Type of report and inclusive dates) Final Technical Report			
5. AUTHOR(S) (First name, middle initial, last name) The Boeing Company and Honeywell, Inc.			
6. REPORT DATE November 1969		7a. TOTAL NO. OF PAGES 259	7b. NO. OF REFS 5
8a. CONTRACT OR GRANT NO. AF33(615)-3753 ✓		8b. ORIGINATOR'S REPORT NUMBER(S) AFFDL-TR-68-161	
a. PROJECT NO.		9b. OTHER REPORT NO(S) (Any other numbers that may be assigned this report)	
c.		D3-7901-1	
d.			
10. DISTRIBUTION STATEMENT This document is subject to special export controls and each transmittal to foreign governments or foreign nationals may be made only with prior approval of the Air Force Flight Dynamics Laboratory (FDCS), WPAFB, Ohio 45433			
11. SUPPLEMENTARY NOTES		12. SPONSORING MILITARY ACTIVITY Air Force Flight Dynamics Laboratory Wright-Patterson AFB, Ohio 45433	
13. ABSTRACT The Load Alleviation and Mode Stabilization (IAMS) program was conducted to demonstrate the capabilities of an advanced flight control system to alleviate gust loads and control structural modes on a large flexible aircraft using existing aerodynamic control surfaces as force producers. The analysis, design, and flight demonstration of the flight control system was directed toward three discrete flight conditions contained in a hypothetical mission profile of a B-52E aircraft. The FCS was designed to alleviate structural loads while flying through random atmospheric turbulence. The B-52 IAMS-FCS was produced as hardware and installed on B-52E, AF56-632. The test vehicle modification included the addition of hydraulically powered controls, a fly-by-wire (FBW) pilot station, associated electronics and analog computers at the bombardier-navigator station, instrumentation for system evaluation, and the IAMS flight controller. A flight demonstration of the B-52 IAMS-FCS was conducted to provide a comparison of experimental to analytical data. The results obtained during the IAMS program showed that the IAMS-FCS provided significant reduction in fatigue damage rates similar to that predicted. In addition to the above, a IAMS C-5A study was included in the program. This portion of the program was to analytically demonstrate that the technology developed for the B-52 would be applied to another aircraft. The C-5A study was conducted for one flight condition contained in the C-5A mission profile and predicted significant			

DD FORM 1473 NOV 65 reductions in fatigue damage rates and fuselage accelerations.

UNCLASSIFIED

Security Classification

UNCLASSIFIED

Security Classification

KEY WORDS	LINK A		LINK B		LINK C	
	ROLE	WT	ROLE	WT	ROLE	WT
LAMS Load Alleviation and Mode Stabilization Flight Control System (FCS) Stability Augmentation System Structural Mode Control Fly-By-Wire (FBW) LAMS B-52 LAMS C-5A Fatigue Damage Due to Turbulence Crew Ride Qualities Handling Qualities Structural Performance						

UNCLASSIFIED

Security Classification